Can Dincer

Electrochemical microfluidic multiplexed biosensor platform for point-of-care testing

Early and accurate diagnosis of a specific disease plays a decisive role for its effective treatment. However, in many cases the clinical findings, based on a single biomarker detection alone, are not sufficient for the appropriate diagnosis as well as monitoring of its treatment. Furthermore, it is highly desirable to screen multi-analytes (e.g. various diseases and drugs) at the same time enabling a low-cost, quick and reliable quantification. Thus, multiplexing, simultaneous detection of different analytes from a single sample, has become in recent years essential for diagnostics, especially for point-of-care testing (POCT).

This thesis focuses on the scientific issue regarding the sensitivity enhancement of microfluidic biosensor platforms. Simulations, design studies and experiments are employed to investigate the interplay between the immobilization area and the resulting sensitivity. Thereby, a novel concept comprising design rules for microfluidic biosensors using the stop-flow technique has been introduced. In combination with different technical measures it allows the realization of an electrochemical lab-on-a-chip (LOC) platform for the fast, sensitive and simultaneous POCT in clinically relevant samples.

This system employs a universally applicable, bioaffinity based biomolecule immobilization along with an amperometric readout. By means of the dry film photoresist technology, the fabrication of disposable microfluidic biosensors is enabled with high yield on wafer-level. The presented LOC platform offers three different biosensors with a microfluidic channel network of two, four or eight discrete immobilization sections, each with a volume of 680 nl. They can be actuated by individual channel inlets allowing a high flexibility in the assay design with respect to its format (e.g. competitive) and its technology (e.g. genomics).

The feasibility for multiplexing is successfully demonstrated with DNA-based antibiotic assays for tetracycline and streptogramin, both important growth promoters in livestock breeding. The extensive usage of antibiotics is one of the major causes of the multi-drug-resistant bacteria and so, it has to be kept under surveillance. This platform allows the simultaneous POCT of different antibiotics from human plasma along with a limit of detection of less than 10 ng ml^{-1}, a wide working range up to 1,600 ng ml^{-1} and inter-assay precisions of about 10 %. Moreover, the microfluidic LOC system provides a low consumption of reagent and sample, reduces the total assay time drastically with a sample-to-result time of only 10 min. The shelf-life of the biosensors is proven to be at least three months at +4 °C.

The introduced design concept with specific technical measures facilitates the implementation of microfluidic multiplexed biosensors in a low-cost, compact, and at the same time sensitive manner. This platform targets the point-of-care testing in the first place, yet, owing to its multiplexing approach it can be expanded for *in vitro* diagnostics.

Can Dincer

Electrochemical microfluidic multiplexed biosensor platform for point-of-care testing

Dissertation

A dissertation submitted in partial fulfillment of the requirements for the doctoral degree at the Faculty of Engineering, University of Freiburg

Electrochemical microfluidic multiplexed biosensor platform for point-of-care testing

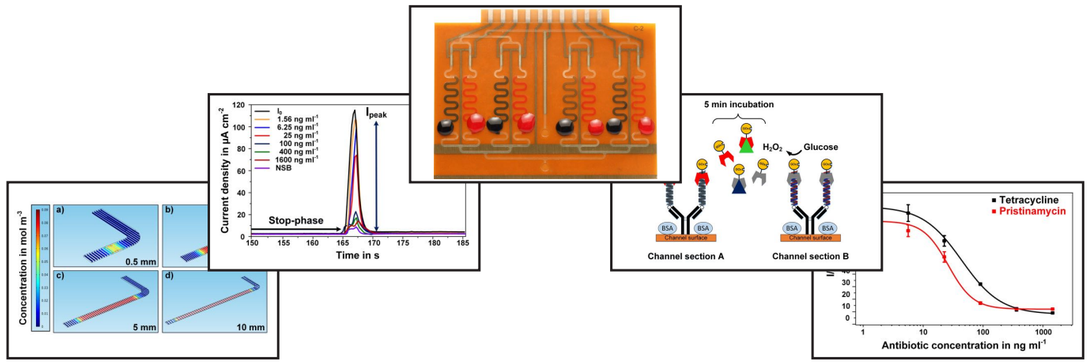

Can Dincer

25. Feb. 2016

Laboratory for Sensors
Department of Microsystems Engineering – IMTEK
Faculty of Engineering
University of Freiburg

A dissertation submitted in partial fulfillment of the requirements for the doctoral degree at the Faculty of Engineering, University of Freiburg

Electrochemical microfluidic multiplexed biosensor platform for point-of-care testing

Can Dincer

25. Feb. 2016

Laboratory for Sensors
Department of Microsystems Engineering - IMTEK
Faculty of Engineering
University of Freiburg

Dean: Prof. Dr. Georg Lausen

Doctoral committee

Chair: Prof. Dr. Jürgen Wilde, University of Freiburg, Germany
Co-chair: Prof. Dr. Jürgen Rühe, University of Freiburg, Germany
1^{st} **referee:** Prof. Dr. Gerald A. Urban, University of Freiburg, Germany
2^{nd} **referee:** Prof. Dr. Wilfried Weber, University of Freiburg, Germany

Date of submission: 25.02.2016

Date of disputation: 29.04.2016

"Our true mentor in life is science."
Mustafa Kemal Atatürk

Abstract

Early and accurate diagnosis of a specific disease plays a decisive role for its effective treatment. However, in many cases the clinical findings, based on a single biomarker detection alone, are not sufficient for the appropriate diagnosis as well as monitoring of its treatment. Furthermore, it is highly desirable to screen multi-analytes (e.g. various diseases and drugs) at the same time enabling a low-cost, quick and reliable quantification. Thus, multiplexing, simultaneous detection of different analytes from a single sample, has become in recent years essential for diagnostics, especially for point-of-care testing (POCT).

This thesis focuses on the scientific issue regarding the sensitivity enhancement of microfluidic biosensor platforms. Simulations, design studies and experiments are employed to investigate the interplay between the immobilization area and the resulting sensitivity. Thereby, a novel concept comprising design rules for microfluidic biosensors using the stop-flow technique has been introduced. In combination with different technical measures it allows the realization of an electrochemical lab-on-a-chip (LOC) platform for the fast, sensitive and simultaneous POCT in clinically relevant samples. This system employs a universally applicable, bioaffinity based biomolecule immobilization along with an amperometric readout. By means of the dry film photoresist technology, the fabrication of disposable microfluidic biosensors is enabled with high yield on wafer-level. The presented LOC platform offers three different biosensors with a microfluidic channel network of two, four or eight discrete immobilization sections, each with a volume of 680 nl. They can be actuated by individual channel inlets allowing a high flexibility in the assay design with respect to its format (e.g. competitive) and its technology (e.g. genomics).

The feasibility for multiplexing is successfully demonstrated with DNA-based antibiotic assays for tetracycline and streptogramin, both important growth promoters in livestock breeding. The extensive usage of antibiotics is one of the major causes of the multi-drug-resistant bacteria and so, it has to be kept under surveillance. This platform allows the simultaneous POCT of different antibiotics from human plasma along with a limit of detection of less than 10 $\mathrm{ng\,ml^{-1}}$, a wide working range up to 1,600 $\mathrm{ng\,ml^{-1}}$ and inter-assay precisions of about 10 %. Moreover, the microfluidic LOC system provides a low consumption of reagent and sample, reduces the total assay time drastically with a sample-to-result time of only 10 min. The shelf-life of the biosensors is proven to be at least 3 months at +4 °C. The introduced design concept with specific technical measures facilitates the implementation of microfluidic multiplexed biosensors in a low-cost, compact, and at the same time sensitive manner. This platform targets the POCT in the first place, yet, owing to its multiplexing approach it can be expanded for *in vitro* diagnostics.

Zusammenfassung

Frühe und präzise Diagnostik verschiedener Krankheiten spielt eine entscheidende Rolle für deren effektive Behandlung. In vielen Fällen basieren die Befunde allerdings nur auf einer einzelnen Biomarker-Detektion, was für die Diagnose und Überwachung der Behandlung nicht ausreichend ist. Außerdem ist die gleichzeitige Untersuchung von mehreren Analyten (z. B. unterschiedliche Krankheiten und Medikamente) äußerts wünschenswert, da dies eine günstige, schnelle und zuverlässige Quantifizierung ermöglicht. Wesentlich für die Diagnose, insbesondere bei der patientnahen Labordiagnostik (POCT), wurde in den letzten Jahren die simultane Detektion von verschiedenen Analyten, dem Multiplexing, aus einer einzelnen Probe.

Diese Arbeit konzentriert sich auf die wissenschaftliche Fragestellung bezüglich der Sensitivitätssteigerung von mikrofluidischen Biosensor-Plattformen. Das Zusammenspiel zwischen Immobilisierungsbereich und der entstehenden Sensitivität wird mittels Simulationen, Designstudien und Experimenten untersucht. Dabei wird ein neuartiger Entwurf mit Designregeln für mikrofluidische Biosensoren basierend auf Stop-Flow-Technik eingeführt, der in Verbindung mit unterschiedlichen technischen Maßnahmen die Realisierung einer elecktrochemischen Lab-on-a-chip-Plattform (LOC) für die schnelle, sensitive und gleichzeitige POCT in klinisch relevanten Proben erlaubt. Dieses System verwendet eine universell einsetzbare, auf Bioaffinität basierende Biomolekülimmobilisierung zusammen mit einer amperometrischen Messung. Durch die Trockenresisttechnologie wird die Herstellung der mikrofluidischen Einweg-Biosensoren mit hoher Ausbeute auf Wafer-Ebene ermöglicht. Die vorgestellte Plattform bietet drei verschiedene Biosensoren mit einem mikrofluidischen Netzwerk aus zwei, vier oder acht getrennten Immobilisierungsabschnitten, jeweils mit einem Volumen von 680 nl. Sie können durch verschiedene Kanaleinlässe angesprochen werden und erlauben damit eine hohe Flexibilität beim Entwurf des Assays bezüglich Format (z. B. kompetitiver Assay) und Technologie (z. B. Genomik).

Die Machbarkeit des Multiplexings wird erfolgreich mit DNA-basierten Antibiotika-Tests für Tetrazykline und Streptogramine, beides wichtige Wachstumsförderer für die Viehzucht, demonstriert. Die exzessive Verwendung von Antibiotika ist einer der Hauptursachen von multiresistenten Bakterien, weshalb deren Einsatz überwacht werden muss. Diese Plattform erlaubt gleichzeitige Vor-Ort-Tests von verschiedenen Antibiotika in menschlichem Plasma mit einem Detektionslimit von weniger als $10\,\mathrm{ng\,ml^{-1}}$, einem Arbeitsbereich bis $1.600\,\mathrm{ng\,ml^{-1}}$ und Inter-Assay-Präzision von etwa 10 %. Darüber hinaus ermöglicht die mikrofluidische Plattform einen geringen Verbrauch an Reagenzien und Proben. Sie reduziert die gesamte Dauer von der Probenentnahme bis zum Ergebnis auf zehn Minuten. Es wird gezeigt, dass die Haltbarkeit der Biosensoren bei +4 °C mindestens drei Monate beträgt. Das vorgestellte Designkonzept mit spezifischen technischen Maßnahmen ermöglicht die Implementierung von kostengünstigen, kompakten und gleichzeitig sensitiven Mikrofluidik-Multiplex-Biosensoren. Diese Plattform zielt in erster Linie auf die POCT, kann aber aufgrund seines Multiplexing-Ansatzes auch für die *in-vitro*-Diagnostik erweitert werden.

Contents

1 Introduction

Preface

Over the past two decades, diagnostic applications have become a matter of in-depth studies for the development of global public health. Remarkable improvements have already been achieved; yet there are still many challenges to come for the considerable application in various areas including point-of-care testing (POCT). This progress and studies are mostly driven by the scientific and technological advancements, such as improved diagnostics tools allowing high-throughput biomarker screening and DNA sequencing, combined with proteomics and RNA profiling [1–3].

Without a diagnostic test the medical decisions are made through the observation of clinical symptoms and the local spread of a disease. This may lead to mistaken identification of the disease and to an unnecessary treatment for the patient, because different diseases with local prevalence may appear with similar symptoms. Moreover, the patients cannot be treated accordingly and early enough, which slightly increases the risk of mortality and morbidity in some cases [1].

To prevent the drug resistance (e.g. misuse of antibiotics) and side effects caused by malpractice, a diagnostic test will be more profitable to detect a disease, condition, or infection. Thus it enables an appropriate and early diagnosis for the treatment. Diagnostic tests performed in an artificial environment using a specimen such as urine, blood and nasal are called in vitro diagnostics (IVDs). These tests are conducted mostly in healthcare settings and laboratories, which are capable of monitoring drug therapy and deliver correct diagnosis in more than 50 % of diseases [1, 4, 5].

1.1 Point-of-care testing - POCT

Even though traditional laboratory medicine plays a key role for the detection of diseases, point-of-care testing performed near the patient or by the patient himself has become increasingly commonplace in recent years. Especially in such cases that require immediate treatment as acute myocardial infarction or diabetes monitoring, the rapid confirmation of a clinical finding is vital. Hence, there has been a growing need for point-of-care testing devices which ensures in vitro diagnostic test results in a short time by a non-expert [4–7].

To cover the needs of POCT appropriately, the point-of-care systems must rigorously fulfill the following tasks: (i) uncomplicated operations acquiring minimized user interventions

by a non-trained personnel; (ii) rapid sample-to-result time enabling immediate treatment; and (iii) precise and quantitative test results in consistence with laboratory findings. Furthermore, equipment free diagnostics, i.e lowest-resource settings, are favorable in the developing world [1, 6, 7].

Due to these rigorous requirements, only POCT systems based on electrochemical detection (e.g. blood glucose test strips) or on lateral flow immunoassay (e.g. home pregnancy tests) have been successfully launched to the market so far. Yet, they both suffer from numerous disadvantages like poor performance causing inaccurate test results by blood glucose monitoring or qualitative (positive or negative) measurement by lateral flow assays along with other technical restrictions [1, 6].

These drawbacks of conventional POCT systems have led to an increasing demand on exploring new technologies, that offer fast, low-cost and quantitative point-of-care detection [2, 6].

1.1.1 Lab-on-a-chip & Microfluidics

In this sense, novel and carefully vetted technologies including the tailoring of lab-on-a-chip (LOC) devices with microfluidics have been adopted widespread as much as the conventional methods [2, 6, 8–17].

The contribution of microfluidics to science is the ability to manipulate fluids in microchannels and thus, enhances the fields of research in medicine and biology [9, 11]. Microfluidic systems facilitate to work with very small sample volumes and precise control of these liquids based on the microscopic behavior of fluids [17]. Here, as the impact of volume forces like inertia and gravity dominating at macroscopic levels reduces, surface related forces like surface tension and capillary forces play a decisive role [18].

Microfluidics has been advanced for the use with the microelectromechanical systems (MEMS), especially in Bio-MEMS applications. Lab-on-a-chip platforms or miniaturized total analysis systems (µTAS), introduced by Manz *et al.* [19] in 1990, are the most important outcome of microfluidics for meeting the needs of portable point-of-care (POC) medical diagnostic systems [6, 9, 12, 17, 20].

These POC systems bring many advantages together; (i) increased surface-to-volume ratio, accelerating biochemical reactions; (ii) low-consumption of sample volumes; (iii) reduced costs of used reagents; (iv) maximum information gathered from valuable specimens; (v) possibility for self-testing, resulting from automated fluid handling. These benefits improve the assay performance like speed, sensitivity and reproducibility, and reduce the total operating costs of conventional immunoassays [6, 9, 12, 17, 20]. Furthermore, LOC technology offers a high capability of integration, parallelization and multiplexing enabling further extensions of this approach such as multi-analyte detection [17].

1.2 Multi-analyte immunoassays

Immunoassays remain to be the most sensitive and selective detection technique for biomarkers in human body fluids and tissues. They have been applied for diagnostics as well as in various research areas including medicine, military, veterinary and environmental sciences. There are many different assay formats (e.g. competitive and sandwich) allowing extremely high sensitivities down to $fg\,ml^{-1}$ in genomics and proteomics [21, 22].

Although their first introduction by Ekins [23] dates back to the 1980s, the multi-analyte immunoassays (MAIs), simultaneous detection of multiple analytes, become more of an issue due to the technological advances in recent years. They offer a simple, fast and cost-efficient measurement of different biomarkers in the same specimen at the same time. Therefore, MAI devices have the potential to revolutionize the clinical diagnostics and to increase the life expectancy through early diagnosis of diseases, especially in case of POCT [4, 24–27].

1.2.1 Combating antimicrobial resistance

The prevalence and spread of multi-drug-resistant bacteria has recently been a serious issue worldwide [28, 29]. The antimicrobial resistance, or antibiotic resistance (in the case of bacteria), is the ability of microorganisms such as viruses, fungi, parasites and bacteria to withstand the effects of antimicrobial drugs (e.g. antibiotics) [30, 31]. In general, the evolution of resistant strains of microbes is a natural phenomenon. It results from erroneous mutations of new genes, or from transfer of genetic material between microbes. However, inappropriate human actions such as overuse, misuse or suboptimal use of antimicrobial drugs, as well as poor infection control and prevention practices accelerate further emergence and spread of multi-drug-resistant bacteria [30, 32].

Today, over one-tenth of the germs is rated as multi-resistant indicating that they could be more dangerous than cancer soon. The Federal Ministry of Health estimates that annually, at least 400,000 patients get infected by antibiotic-resistant bacteria which causes up to 15,000 deaths in Germany alone[1]. The current mortality rate is about 700,000 worldwide and it would boost to 10 million by 2050, if no global action across all country governments and society is undertaken [33]. To tackle this global challenge and to wake public interest, the World Health Organization (WHO) prepared a global action plan in May 2015[31]. Additionally, G7 countries[2] such as United States, Germany and England have also promulgated their national programs for fighting against the antimicrobial resistance.

One of the most important driving forces for the prevalence of multi-drug-resistant bacteria is the excessive use of antibiotics as growth promoters in livestock industry [28]. Hence, the WHO action plan regulates the judicious use of antibiotics in animal husbandry and promotes the development of novel antimicrobial drugs. In this context, there exists a

[1] Spiegel Online, 02.06.2015: Studie zu Todesursachen: Resistente Keime bald gefährlicher als Krebs
[2] Group of 7: The world's seven most powerful industrialized countries

strong demand for point-of-care devices enabling the multiparametric detection of different antibiotics in order to keep their application under surveillance, and to discover new antibiotics in a simple and highly sensitive manner [34].

In summary, this short survey about the point-of-care testing focusing on the microfluidic LOC devices for the multi-analyte detection indicates that there is still a great need for cost-efficient and easy-to-use POC systems providing quick, quantitative and reliable detection. Here, the main issue is not the technology itself, as the progress in immunoassays, microfluidics and detection techniques is sufficient enough to create an integrated miniaturized POC device [35]. Indeed, the main challenges are the standardization of the components and their smart integration [2, 13, 35].

Electrochemical immunosensors (EIS) are usually preferred because of their low-cost and easy fabrication, simple measurement setup, tunable selectivity and outstanding sensitivity. Moreover, it is possible to miniaturize their instrumentation and lower the power consumption. Owing to these advantages, EIS enables the development of hand-held POC devices for multi-analyte diagnostics using very small sample volumes [15, 26, 36].

1.3 Our approach

This work introduces the development and application of an electrochemical microfluidic platform for the simultaneous detection of multi-analyte assays in human body fluids, as well as a novel concept comprising design rules for microfluidic devices using the stop-flow technique. The presented LOC device targets the point-of-care diagnostics in the first place, however, due to its multiparametric approach it is possible to extend it for the conventional *in vitro* diagnostics. Furthermore, it associates low-cost and wafer-level fabrication via dry-film photoresists with fast, reproducible and sensitive electrochemical detection. Another tremendous advantage of the proposed platform in comparison to the state-of-the-art devices is the high flexibility in the assay design. DNA-based antibiotic assays for tetracycline and pristinamycin, both important growth promoters in livestock breeding, are employed for the validation of the multiparametric microfluidic platform.

The electrochemical multiparametric microfluidic sensor, as illustrated in Figure 1.1, used in this thesis relies on the amperometric detection. Amperometry is an electrochemical measurement technique with controlled-potential, where a constant potential is applied to the working electrode and thus the resulting current is recorded. In the case of a redox event at the electrode, this measured current is directly proportional to the concentration of the electroactive substances in the electrolyte [37, 38].

The claimed microfluidic chip consists of a microfluidic channel network of up to eight parallel channels for the immobilization of different biomolecules via individual channel inlets and an electrochemical measurement chamber for the amperometric detection. The electrochemical cell comprises up to eight (depending on the chip version used) platinum working (WE), short-circuited Ag/AgCl reference (RE) electrodes and a common Pt counter (CE) electrode. This sharp separation between different channel sectors is the

driving force behind the flexibility of this microfluidic chip. Thus, this biosensor system allows to combine not only different assay formats, such as competitive or sandwich, but also different advanced "omics" techniques like proteomics and genomics with each other simultaneously [39].

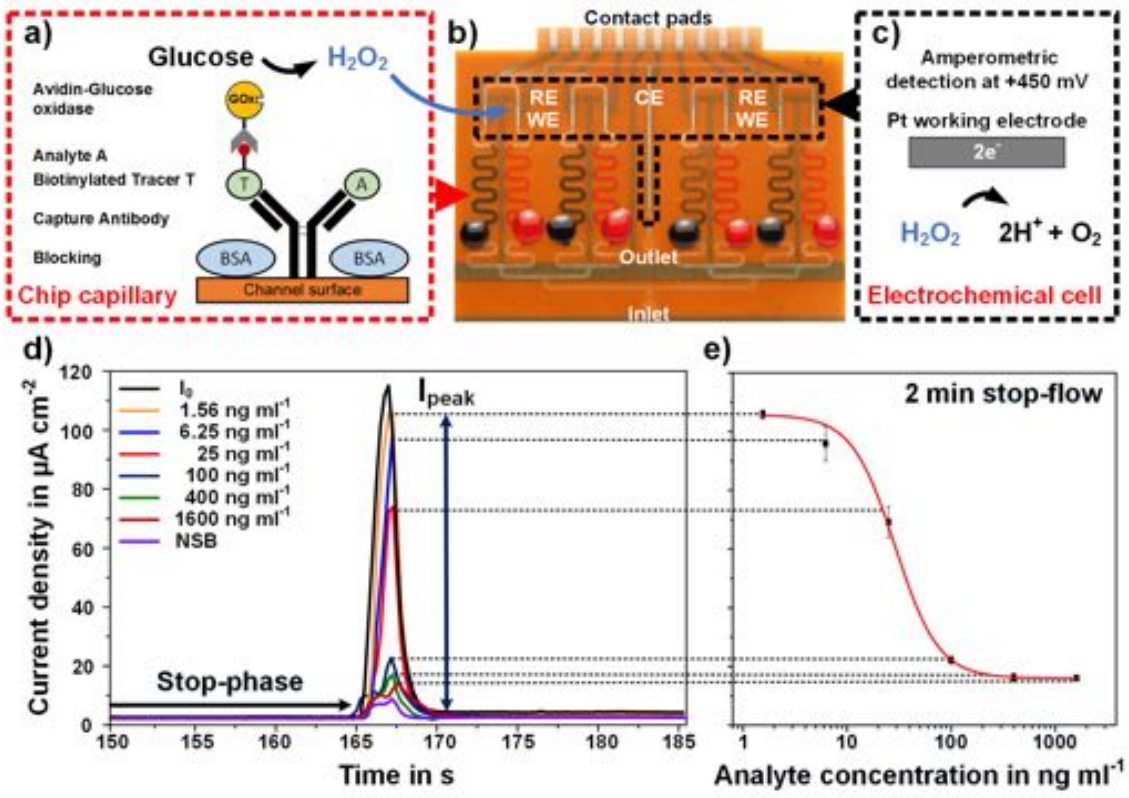

Figure 1.1: *Graphical abstract of the operation principle of microfluidic multiplexed chip presented in this thesis: a) Schematic diagram describing the working principle of a competitive ELISA. b) Photograph of the electrochemical biosensor. c) Schematics illustrating the subsequent electrochemical detection of hydrogen peroxide generated by the competitive ELISA. d) On single-chip calibration measurement represented by the peak height for 2 min stop-flow and the resulting calibration curve e) with a 4-parameter logistic fit.*

In this thesis, glucose oxidase (GOx) is used as the labeling enzyme with glucose for its appropriate substrate. The hydrogen peroxide (H_2O_2) produced by the bound enzyme GOx generates a transient signal at the WE polarized at 450 mV vs. the on-chip Ag/AgCl reference. Furthermore, a flow injection analysis (FIA) like measurement, the so called stop-flow measurement, is used to amplify the measured signals. Here, the flow is interrupted for a defined time interval (termed as stop-time), and thus, it leads to an increased H_2O_2 concentration in the immobilization section. This H_2O_2 cloud is subsequently flushed over the electrochemical cell by restarting the flow. The longer the stop-time is, the higher will be the signal response [39, 40].

The hypothesis presented in this work can be summarized as:

"In general, the area of immobilization section plays a decisive role on the performance and on the size of microfluidic biosensor platforms. This brings about technical and non-technical (e.g. cost) limitations on the design and fabrication of these systems. In this context, the quantification of the smallest possible immobilization capillary for microfluidic biosensors without any loss of the sensor sensitivity is the center of the research interest. Applying the stop-flow analysis in combination with technical measures enables a radical decrease in the sensor geometries, especially in the channel length, independent of the employed detection technique (e.g. optical or electrochemical).

Stop-flow method provides two different parameters, such as the height or the area of the signal peak, for the data analysis. Considering the peak height, measured signals depend on the concentration profile of the analyte over the channel cross-section. This occurs due to the diffusion of hydrogen peroxide in the stop-phase and allows for a dramatic decrease in the channel geometries (e.g. channel length) of the microfluidic biosensors maintaining their sensitivity. Therefore, the main limitations of the stop-flow technique in terms of the diffusion of the analyte as well as channel and electrode geometries has to be investigated with numerical simulations to derive design rules and to introduce a model system, which is universally applicable for the optimization of microfluidic platforms. Furthermore, the feasibility of the established design concept must be verified by proof-of-principle measurements."

A major highlight of this thesis, therefore, is that it makes use of the fundamentals of microfluidics along with indispensable technical measures to resolve this scientific issue. In the light of this knowledge, a multiparametric microfluidic platform for point-of-care diagnostics is possibly realized in a low-cost, compact, but still sensitive manner.

For the verification of this hypothesis, it is split up into four major goals:

1. Design rules for the microfluidic platforms via FEM simulations
2. Fabrication of the microfluidic chips by means of the introduced design concept
3. Proof-of-principle: Comparison between the miniaturized and the standard microfluidic biosensor as described in [40].
4. Application for the detection of multiple analytes in real samples

1.4 Outline of this thesis

In order to provide a better understanding of this multidisciplinary thesis, it is divided into eight main chapters, as shown in Figure 1.2. They are summarized as follows:

The **Introduction** chapter acts as a brief description of the point-of-care diagnostics particularly with regard to the microfluidic immunosensor platforms. Furthermore, the approach and the hypothesis followed in this thesis for the development of the microfluidic multiplexed electrochemical biosensors is introduced.

In the **State of the art** chapter, a survey of the existing diagnostics systems, mainly lab-on-a-chip platforms, for multi-analyte analysis is presented. Based on their detection techniques, such as electrochemical or optical (e.g. lateral flow assays), or their multiplexing methods like spatial or regional signal separation, or the use of different signal generating labels, different microfluidic devices are evaluated. Thereby, these systems are compared with each other in terms of their applicability for the point-of-care testing. This comparison includes their fabrication, handling, sample-to-result time, sensitivity, accuracy and potential for the miniaturization.

The **Theory** chapter resumes the underlying principles and methods of the electrochemical biosensor with multiplexed microfluidics. Thus, an overview about the basics of electrochemistry and microfluidics along with a detailed introduction to immunoassays are explained. In order to overcome the bottlenecks of the current point-of-care devices, it is very important to comprehend throughly the technical possibilities as well as the limitations of immunoassays.

In the **Design rules for LOC devices** chapter, a novel design concept for microfluidic biosensors has been introduced for the first time. In this context, simulations of different characteristics of the microfluidic platforms such as the channel and electrode geometries and their effect on the achieved sensor sensitivity through stop-flow detection are performed. Consequently, the simulation of the stop-flow analysis is demonstrated with the optimized design parameters and compared to the performance of the real system.

The development of the electrochemical multiparametric microfluidic platform is reported in the **Design and Fabrication** chapter. It begins with a brief outline of the dry film photoresist technology allowing a simple, high-throughput and low-cost sensor fabrication. Herein, the design and the wafer-level fabrication of the single-analyte versions, termed as “iLab” and “miLab”, as well as the multi-analyte version of the biosensors, called “MultiLab”, are described in detail. Furthermore, the system integration, which includes the production of a custom-made chip holder for the electrical and fluidic connections, is presented. This chapter covers from the design through both the fabrication and optimization of the sensors to the final platform.

The **Lab-on-a-chip performance** chapter is divided into two main parts: Electrochemical and biochemical characterization. The electrochemical characterization contains the investigation of the electrode material and the oxidation potentials of glucose (substrate) and hydrogen peroxide (analyte) as well as the performance parameters such as flow rate

dependency or stop-flow behavior of the microfluidic platform, whereas the biochemical characterization includes the examination of the immobilization and passivation strategy, the incubation time and the signal dependency on the substrate concentration.

In the **Chip-based antibiotic assay** chapter, the proposed microfluidic biosensing platform is evaluated for its assay performance as well as its applicability for the multi-analyte detection in serum samples. For this purpose, DNA-based antibiotic assays for tetracycline and pristinamycin are employed. Comprehensive optimization of the assay parameters including incubation time and concentration of each assay component is carried out and subsequently calibration curves of both antibiotics in human plasma are recorded. Additionally, the proof-of-principle measurements are provided in order to establish the claimed hypothesis. Finally, the simultaneous, fast and reliable detection of different antibiotics from a spiked sample is successfully demonstrated. Furthermore, to prove the long-term storage capability as a POC platform a 3-month study of the microfluidic chips immobilized with biomolecules is given.

The closing chapter, **Conclusions and outlook,** summarizes the major advantages and challenges of our approach in comparison with other point-of-care platforms, and presents an outlook for the future work. In the **Author's bibliography** the list of publications comprising also the results achieved in this work are stated on page 179.

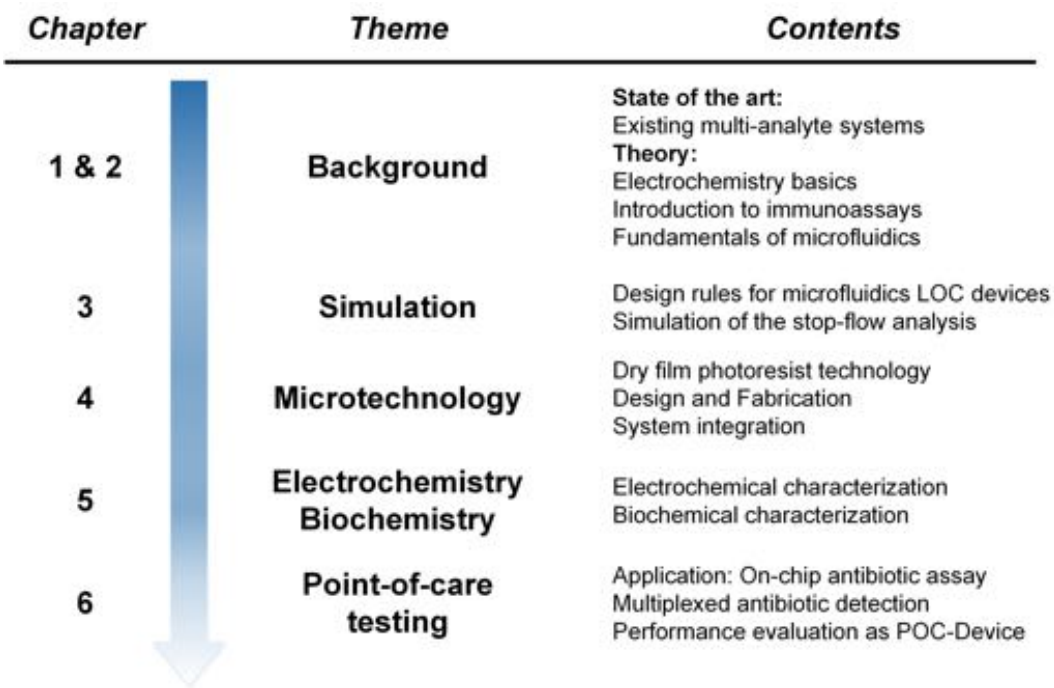

Figure 1.2: *Summary of the thesis outline.*

2 State of the art

Preface

This chapter provides a comprehensive overview of the present diagnostic systems in academia and industry for multi-analyte analysis. For the signal readout, optical and electrochemical methods are primarily employed [4, 41–45]. Here, our discussion will focus on the assets and drawbacks of these platforms as well as their applicability for point-of-care testing. At the end of the chapter a summary is given.

Furthermore, a particular attention is paid to lab-on-a-chip platforms. In recent years, the number of publications dealing with multiplexed LOC devices for point-of-care testing have been rapidly increased due to the remarkable technological advances [4, 41, 46]. The use of microfluidics enables the miniaturization of sophisticated laboratory techniques onto a small chip with various advantages such as low consumption of reagents and sample, and short turn-around times because of high surface-to-volume ratios [9, 12, 47].

A lab-on-a-chip platform should overcome the bottlenecks of the current POC devices and meet the urgent needs of multi-analyte diagnostics in order to be commercialized successfully. Therefore, it is very important to take a glance at the existing POC systems starting with the single-analyte approaches. At this point, the lateral flow assays (LFAs), such as the pregnancy tests, are the most successful POC products by far. Despite their simplicity in handling and production, they suffer mainly from highly reproducible, quantitative, and sensitive results. Over the last two decays there has been many efforts, especially by the industry, to improve the performance of LFAs but so far without any considerable success [1, 6, 47].

On the other hand, electrochemical detection empowers the realization of highly sensitive, low-cost and compact microfluidic devices compared to other techniques [10, 20, 46]. In this context, a remarkable example of an amperometric LOC platform based on dry-film photoresist (DFR) technology was introduced by Horák *et al.* [48–51] in our Laboratory for Sensors at IMTEK, University of Freiburg. This approach combines different materials, fabrication methods and design features and thus, it (i) facilitates simple and low-cost fabrication allowing mass-production, (ii) provides easy handling, (iii) enables simple reagent filling by capillary forces, (iv) allows low sample consumption and (v) is compatible with different "omics" techniques such as genomics and proteomics. These outstanding advantages favor this immunosensor platform for point-of-care diagnostics.

Here, the integrated microfluidic chip is fabricated by the lamination of DFR, Vacrel® 8100 (Dupont™, USA), onto a platinum (Pt) deposited polyimide wafer, followed by the

formation of channels by standard photolithography. The material composition of Vacrel® 8100 includes numerous carboxylate groups which can be directly accessed for the fast and high yield immobilization of biomolecules by the stable amide formation [48]. The microfluidic immunochip, as shown in Figure 2.1, comprises a meandering immobilization section, defined by the hydrophobic stop barrier, and an electrochemical measurement cell consisting of a Pt working, counter and silver/silver chloride reference electrode. The working electrode has a surface area of 2.2 mm^2 given by the channel structures.

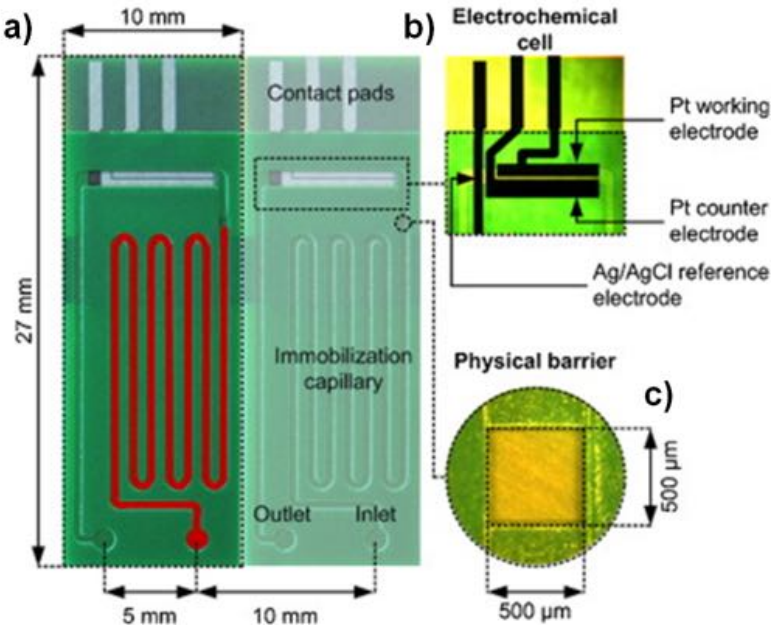

Figure 2.1: *a) Image of the electrochemical microfluidic chip including the main features such as the immobilization section (highlighted in red), the electrochemical measurement cell b), and the stop barrier c) improved with Teflon® AF (Dupont™, USA) (reprinted from [48], copyright 2014, with permission from Elsevier).*

The immobilization capillary has an area of 112 mm^2 and a volume of 3.6 µl resulting in a surface-to-volume (S/V) ratio of 310 cm^{-1}. The high S/V ratios imply faster reaction kinetics of the biomolecules and thus, shortens the total assay times. Different reagents and samples into the microfluidic chip are delivered spontaneously by the capillary forces. For the signal transduction, glucose oxidase (GOx) is employed as enzyme label with its appropriate substrate glucose. The latter converted by GOx into hydrogen peroxide (H_2O_2) which is detected amperometrically at the working electrode. Moreover, in order to achieve an amplification of the enzyme-mediated signal a stop-flow protocol is used.

For almost a decade, this DFR-based microfluidic immunochip has been developed and investigated for different ELISA applications with various surface modifications and assay formats. The proof-of-concept of this platform is first demonstrated by the quantification of the Epstein-Barr virus in a direct ELISA format [48]. Later, substance P, a potential

biomarker for acute neuroinflammation, is detected with a LOD of 15.4 pg ml^{-1} using a competitive ELISA [49].

Furthermore, the cardiac troponin I (cTnI) [50], a biomarker for acute myocardial infarction, and chemokine[1] (C-C motif) ligand 18 (CCL18), which plays a key role in various diseases including inflammatory joint, lung and skin diseases, were both measured using the sandwich ELISA format. For the fast and sensitive cTnI detection, the channel surface is modified with linear (LPEI) as well as branched polyethylenimine (BPEI) and their performance is compared with the classical immobilization technique. In the case of BPEI modification, a limit of detection of 25 pg ml^{-1} for cTnI together with a CV of 10 % is reached with stop-flow detection in 4 min [50].

The fundamentals of the electrochemical multiparametric microfluidic platform proposed in this thesis underlie our extensive experience in the DFR-based immunosensors [48–51]. Although there was a great expectation from microfluidics to revolutionize the clinical diagnostics, surprisingly a low number of LOC devices have managed to take place in the market. Therefore, for the development of a LOC device aiming a commercial success it is crucial to study the existing commercial POC systems and thereby, to identify the arising challenges [9, 47].

One of the most successful commercial products for point-of-care testing is the i-STAT® platform (Abbott Point of Care Inc., USA), as illustrated in Figure 2.2. It combines capillary-driven microfluidics and electrochemical detection on a single LOC handheld device. This platform is capable of performing clinical measurements like a range of blood chemistries (blood gas, electrolytes and hematology) and limited number of single-analyte immunoassays including cardiac (e.g. troponin I) and coagulation markers [47, 52–54].

The i-STAT® platform is a cartridge-based system with a battery-powered handheld analyzer. The disposable plastic test cartridges consist of a silicon microchip with a thin-film deposited electrode array, integrated microfluidics with a pre-loaded calibration solution, and contact pads for the electrical connection to the handheld reader. Depending on the application for different analytes, the electrode arrays are coated either with specific ion selective membranes, ionophores, or enzymes. The handheld reader allows to perform different electrochemical techniques such as amperometry (e.g. for glucose, pO_2 and immunoassays), potentiometry (e.g. for sodium, potassium, pH and pCO_2) and conductometry (e.g. for hematocrit).

In order to determine the analytical characteristics of the i-STAT cTnI assay as a 10 min POC assay, Apple *et al.* presented a study showing very high precision along with a limit of detection of 20 ng ml^{-1} [53]. For the immunoassay detection, the capture antibodies are immobilized on the electrodes. Nearby, the secondary antibodies conjugated with the enzyme alkaline phosphatase (AP) are located in freeze-dried form. If a sample (e.g. blood) is introduced into the channel, the secondary antibodies will dissolve and bind to its analyte. These are then captured by primary antibodies on the electrodes. After the

[1] Bachelor thesis of Edvina Qelibari with the titel "Development and Integration of CCL18 Immunoassay on a Disposable Microfluidic Platform" in 2013.

washing step, the substrate solution is introduced into the biosensing area, which allows the amperometric ELISA detection.

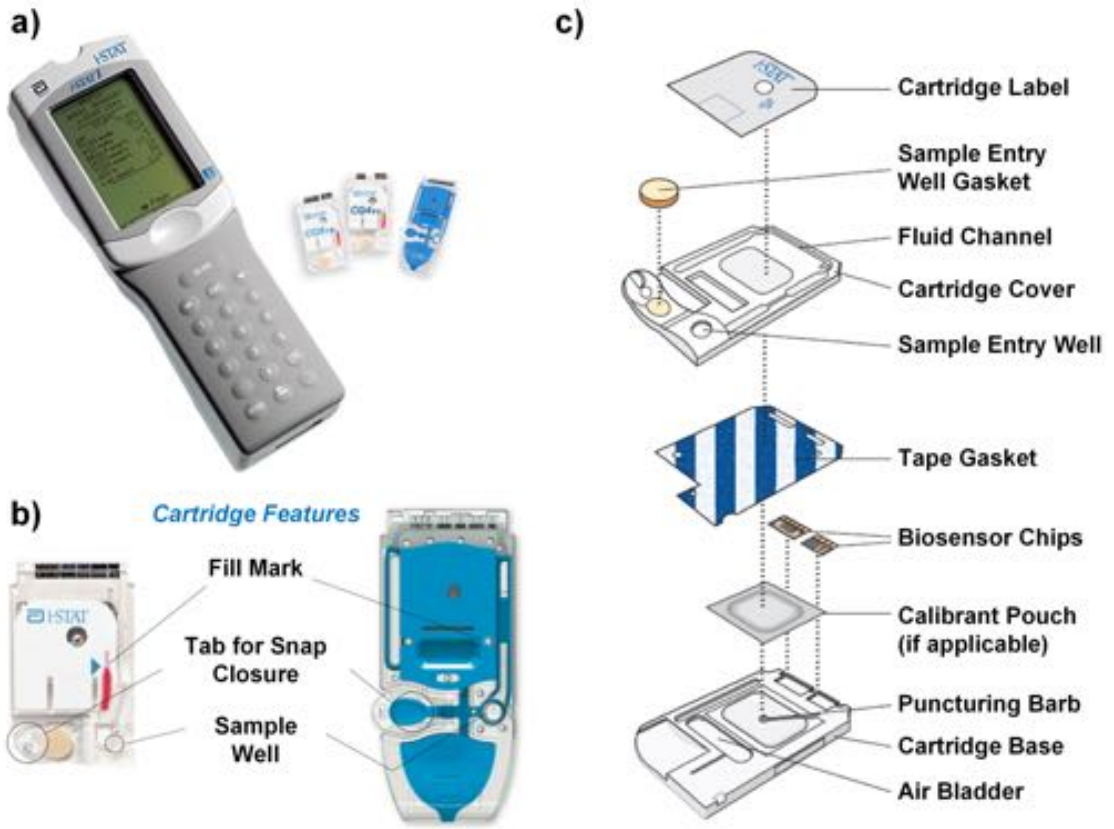

Figure 2.2: *i-STAT® system: a) i-STAT® handheld device, b) Photograph of two different i-STAT® cartridges including their features, c) Schematic explosion view of the i-STAT® cartridge (reprinted with permission Abbott Point of Care Inc., USA).*

In spite of its valuable clinical sensitivity for a commercial device, there exist some drawbacks such as the complexity and running costs of the i-STAT® platform, which limits its further use for resource-limited settings. Besides, there are no claims of multiplexing ability for immunosensors [55].

Multi-analyte systems

Multiplexing, simultaneous detection of various analytes from a single sample, has become more important for clinical diagnostics, as the single biomarker detection of a specific disease cannot supply adequate clinical findings for the diagnosis as well as the monitoring of its treatment [4, 56]. Multiplexing is usually realized through three different approaches; (i) spatial separation (e.g. different spots or wells), (ii) regional separation (e.g. different channels or electrode arrays), or (iii) the use of various labels (e.g. enzymes, redox molecules, beads and dyes).

So far, spatial separation of analytes in different wells or spots is the most preferred technique for multi-analyte detection. However, they mostly suffer from the complexity of the system, such as fabrication procedure and assay preparation, and/or of the consecutive readout. Another frequently used method is the employment of different labels, but generally results in an increased readout complexity. Contrary to other approaches the regional separation is rarely utilized due to a possible cross-sensitivity between single detection-sites caused by diffusion [4, 41, 45, 46, 55, 57]. The next section highlights recent advances in clinical diagnostics including LOC technology as well as commercially available platforms for multiplexed bioanalyses.

2.1 Lateral flow assays

As previously mentioned, lateral flow assays are by far the best-established commercial products in the field of point-of-care testing. A remarkable contribution of LFAs to simultaneous quantitative multi-analyte detection was introduced by the Alere Triage® platform (Alere Inc., USA) combining the simple LFA test panels with a portable fluorometer, as shown in Figure 2.3 [55, 58].

The working principle of this sophisticated system is comparable to the classical LFA and described in Figure 2.3a. First, the sample including whole blood, plasma or urine passes through a blood filter, where the red blood cells are separated out, into the reaction chamber with freeze-dried fluorescent-labeled antibodies. Here, the sample remains for a defined incubation time given by the stop barrier. Subsequently, the fluid containing the sample and the secondary antibodies is driven slowly by capillary forces over the capture antibodies into a waste reservoir. Thereby, the formation of sandwich immunoassay happens at the capture antibodies immobilized on distinct sites and the excess secondary antibodies are flushed out by capillary flow automatically. The quantitative readout is executed by an automatic fluorometer [55, 58].

Currently, the Alere Triage® platform offers up to 20 different single-analyte but only a limited number of multiplex immunoassays (e.g. for drug screening [59] and cardiac biomarkers [60]). The point-of-care tests deliver results within approximately 15 minutes after the sample introduction. Depending on the targeted analyte, either whole blood and plasma for the diagnosis of myocardial infarction or urine for drug testing can be

analyzed. Overall, this platform combines the simplicity of LFAs with quantitative multi-analyte immunoassays. However, the internal complexity and the high cost of the Triage® test panel are the main disadvantages [55].

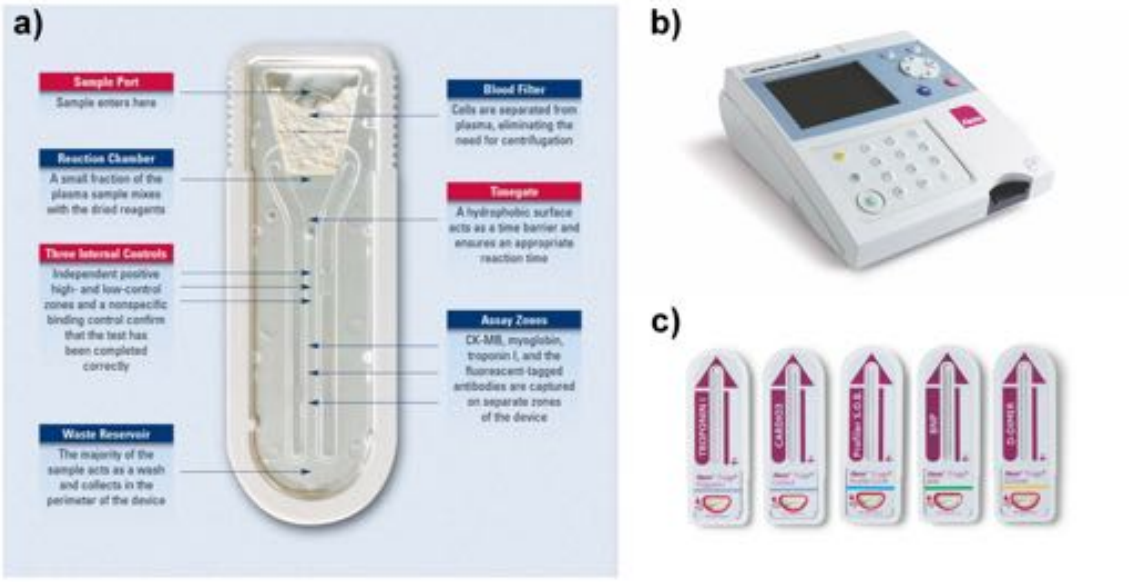

Figure 2.3: *Alere Triage® System: a) Photograph of the Alere Triage® Cardiac Panel describing its working principle (reprinted from [58], copyright 2002, with permission from Wolters Kluwer Health). b) Portable Alere Triage® MeterPro fluorometer together with different test panels c) for cardiac markers. Further panels are available. (reprinted with permission from Alere Inc., USA).*

Another multi-analyte LFA application was introduced by Taranova *et al.* [61] using multicolor quantum dots (QDs) for the simultaneous detection of different antibiotics in diluted milk samples. The term "traffic light" assay refers to the three QDs with different emission peaks resulting in red, yellow and green colors. This LFA is based on the principle of competitive assays: The presence and the concentration of each antibiotic are simultaneously determined by the absence or decrease in intensity of the appropriate color line. The qualitative analysis can be made above a specific threshold by naked eye with the help of the "traffic light" design, whereas the quantitative readout of fluorescence intensities, as a result of the different emission peaks of QDs, is performed by a fluorometer. Using this approach, different antibiotics such as ofloxacin (OFL), chloramphenicol (CAP), and streptomycin (STM) were reproducibly detected in diluted milk samples within 10 min resulting in limits of detection of 0.3, 0.12, and 0.2 $\mathrm{ng\,ml^{-1}}$, respectively.

In general, LFAs are still the best way to perform qualitative POC analysis of multi-analytes because of their notable advantages like (i) sample loading by capillarity, (ii) 'instrumentless' detection with the naked eye, and (iii) capability of self-testing by a non-expert. Yet, there is still a need for a readout device in case of a quantitative detection with high sensitivity. The main drawback of LFAs is their inflexibility for different assay formats

including competitive or direct, assay technologies like genomics and the combination of those on the same platform.

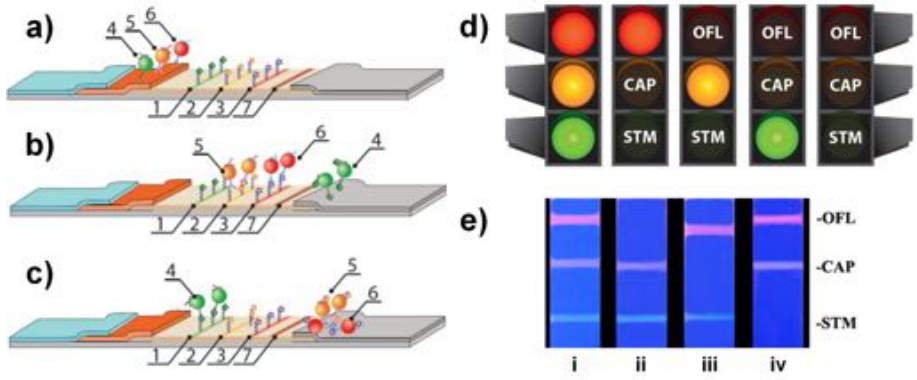

Figure 2.4: *"Traffic light" LFA for the simultaneous measurement of multiplex antibiotics. a-c) Schematics of detection principle: Three multicolor quantum dots 4, 5, 6 can be competitively detected at the appropriate capture sites 1, 2, 3 in case of absence of the antibiotics, respectively. 7 serves as a control line. d) Schematic overview of "Traffic light" principle. e) LFA results for different samples: (i) In the absence of antibiotics and in the presence of (ii) 200 ng ml^{-1} OFL, (iii) 10 ng ml^{-1} CAP, and (iv) 500 ng ml^{-1} STM (reprinted from [61], copyright 2015, with permission from Elsevier).*

2.2 Microfluidic paper-based analytical devices - µPADs

The demand for paper-based microfluidics has recently been increased for low-cost diagnostic devices due to their outstanding ability to control fluids at a high level. Patterning various design elements in 3D paper-based microfluidics enables the implementation of different fluidic operations including mixing, splitting, separation and filtration [62, 63].

Paper-based devices provide many benefits such as easy handling, portability, low fabrication costs and no need for instrumentation (e.g. external pump). They mostly underlie the colorimetric readout, the visual comparison of the color intensity of the reaction spots by naked eye or mobile phones and portable scanners [64, 65].

Microfluidic paper-based analytical devices can be employed for: (i) POC diagnostics in the developing world together with telemedicine [66], (ii) low-cost array-based platforms in pharmaceutical sector and scientific research [67], and (iii) other analytical application areas including military, veterinary and food sciences [62].

In contrast to the conventional paper-based POC devices like lateral flow assays, that allow the detection of single- or multi-analytes in series with a certain degree of assay flexibility. µPADs are capable of high degree multiplexing in parallel along with increased assay performance and higher assay diversity. With this approach, both crosstalk and cross-reactivity between assays are completely eliminated [68].

Moving beyond proof-of-concept, Pollock and colleagues [68] presented a multiplexed µPAD for POC liver function testing by measuring the levels of two liver enzymes in whole blood: Aspartate aminotransferase (AST) and alanine aminotransferase (ALT). Liver injury is a common side effect of the HIV treatment comprising antiretroviral drugs. Therefore, low-cost POC solutions draw great interest for hepatotoxicity screening in the developing world. In this context, this multiplexed µPAD was extended from an earlier prototype [69]. The schematics of its fabrication and measurement procedure, and data analysis is summarized in Figure 2.5. This multi-analyte device offers a colorimetric read-out with both qualitative and quantitative data evaluation within 15 min after sample introduction (less than 35 µl blood) [68].

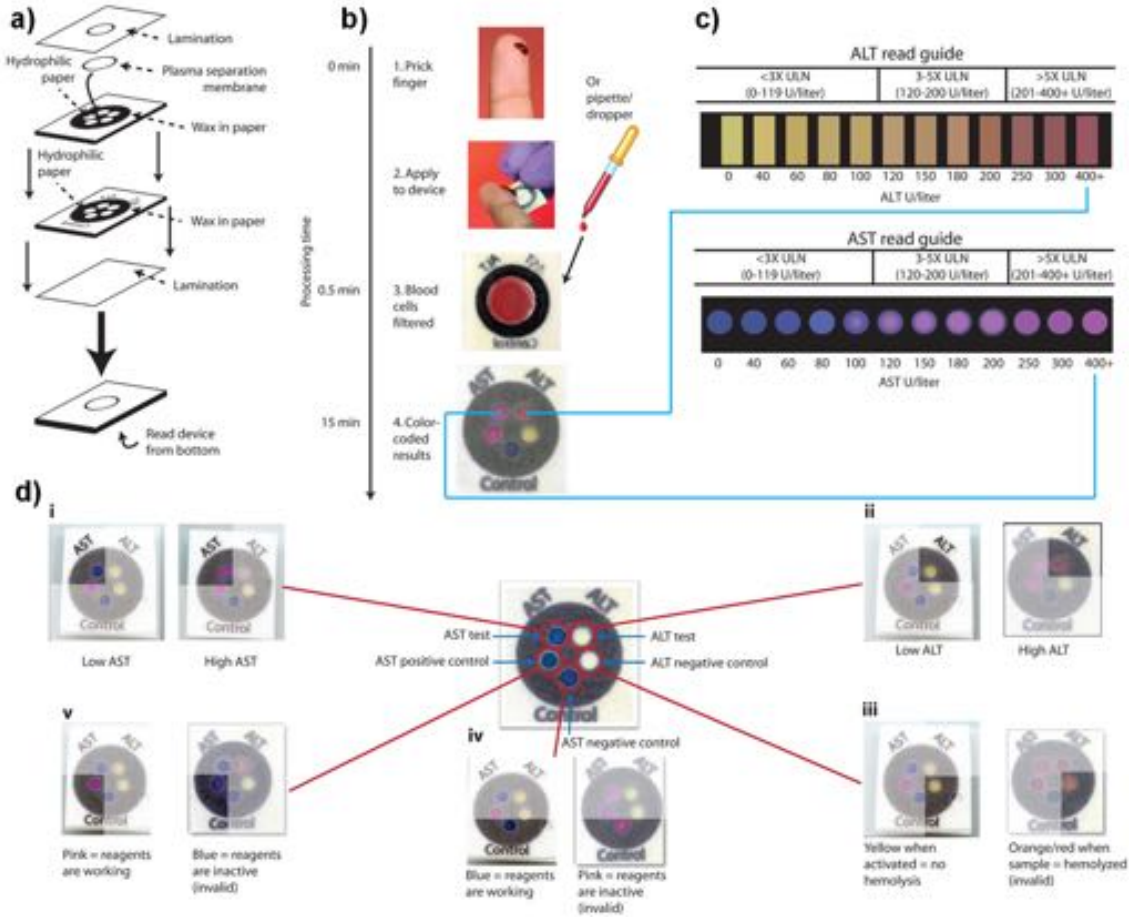

Figure 2.5: *Schematics of the paper-based multiplexed POC liver function testing: a) Fabrication and b) measurement procedure, c) ALT/AST color read guides, and d) Detailed schema of the transaminase measurement including possible colorimetric readouts (from [68], reprinted with permission from AAAS).*

However, µPADs using colorimetric detection are mostly limited to a qualitative or a semi-quantitative data analysis due to the lack of sensitivity and selectivity on mobile phones and portable scanners. For example, ambient light conditions could interfere with the color intensities of digital images taken by a camera. Hence, for a quantitative analysis of low-level analyte concentrations a bulky instrument comprising a detector with sensitivity and selectivity is still necessary [64, 65].

As an attractive alternative to optical detection platforms, electrochemical approaches present many advantages such as low-cost, easy miniaturization, high sensitivity and selectivity by appropriate choice of measurement techniques (e.g. amperometry, fast scan cyclic voltammetry or differential pulse voltammetry) as well as electrode materials. The electrochemical µPADs was introduced for the first time by Dungchai *et al.* [65] for the investigation of multiple metabolites (glucose, lactate, and uric acid) in human plasma using the respective oxidase enzymes (glucose oxidase, lactate oxidase, and uricase). The microfluidic channels were fabricated by photolithography, while the electrodes were patterned by screen-printing on a filter paper.

Only three years later, Ge *et al.* [64] presented the electrochemiluminescence (ECL) µPADs for multiplex detection of four tumor markers, r-fetoprotein (AFP), carcinoma antigen 125 (CA125), carcinoma antigen 199 (CA199) and carcinoembryonic antigen (CEA), in human serum samples within 30 min. This more sophisticated paper-based ECL immunochip consists of two stacked cellulose paper sheets with eight carbon working electrodes on one piece, and a common Ag/AgCl reference and carbon counter electrodes on the other one. The device was fabricated first by patterning of the microfluidics using a wax printer, and subsequently by screen-printing of electrodes on cellulose paper sheets. Finally, these paper sheets are "easily" aligned with the help of a device-holder.

The electrochemical paper-based platforms are still at research and development stage. The presented approaches are either too complex or cannot fulfill requirements of the point-of-care systems, in terms of sample-to-result times.

2.3 Array-based systems

One of the most popular methods for high throughput multiplexing in clinical diagnostics is array-based assays on planar surfaces [44, 45, 70]. Under the favor of the recent huge technological progress in mainly genomics, microarray manufacturing (e.g. inkjet printing) and detection devices are appeared to be among the standard equipments at laboratories [45, 70, 71]. For example, a high dense array of microspots[2] (down to pl) is easily realized by inkjet printing and subsequently analyzed for diagnostic purposes [44]. The signal readout of array-based platforms is primarily performed by optical or electrochemical detection techniques [71, 72]. These methods are discussed briefly in the following section.

[2]Microspot is the position of the targeted analyte immobilized on a planar microarray.

2.3.1 Optical systems

Most of the optical microarray platforms are based on chemiluminescence or fluorescence detection and have a similar measurement setup with automatic sample incubation and washing. The signal readout of bound fluorescent or chemiluminescent labeled biomolecules is achieved with the intensity measurement via laser scanning or imaging with a scanning charge coupled device (CCD) camera [45, 73].

In this context, the IMPACT (Immunological Multi-Parameter Chip Technology) platform is demonstrated by Roche Diagnostics for proteomics [74]. The working principle of the fully automated system is presented in Figure 2.6.

The IMPACT chip consists of a polystyrene substrate coated with streptavidin on which biotinylated capture antibodies are printed in spots. For the measurement, digoxin labeled secondary antibodies are mixed with the sample (e.g. serum) to capture the analyte and subsequently added to the multiplex chip. After sandwich formation, using anti-digoxin antibodies tagged with fluorescent beads the signal readout is realized by a CCD camera. Hence, it is possible to measure up to 20 different analytes in a 20 µl sample with a total assay time of less than 30 min. The IMPACT platform was employed in clinical studies to measure different biomarkers for osteoporosis [75] and rheumatoid arthritis [76].

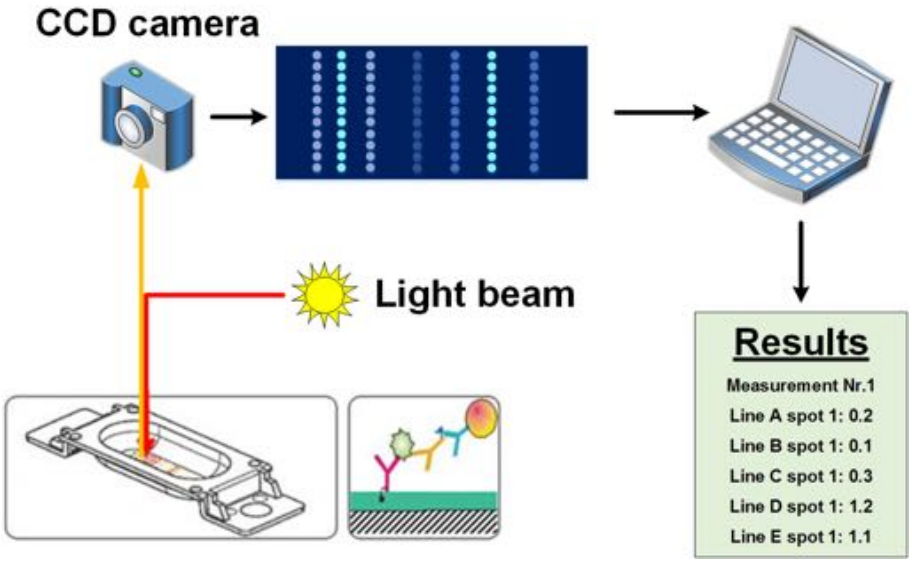

Figure 2.6: *IMPACT platform including the imaging/analysis unit from Roche Diagnostics GmbH, Switzerland (adapted from [74], with permission from Springer Verlag Heidelberg). Here, the test-specific biomolecules containing biotinylated antibodies or antigens are spotted by piezo-inkjet printing in lines with up to 20 identical drops with a volume of 250 pl. The optical readout of bound analytes with fluorescent markers is performed by a CCD camera.*

Micromosaic immunoassays (MIAs) was introduced by Bernard and colleagues [77] as an interesting alternative to the classical microarray platforms for the quantification of the

specific interaction between protein A and eight IgGs from different species. Additional to its multiplexing capability with high sensitivity and reliability, MIAs allow the use of ELISA technique for signal readout.

The immobilization of MIAs were performed on PDMS substrates using different microfluidic networks (µFNs). First, various antigens were patterned by a µFN along single lines on PDMS. Secondly, the whole substrate was blocked with BSA to prevent nonspecific protein binding in following steps. Thirdly, the sample (here, FITC labeled anti-rabbit IgGs) was delivered by a second µFN across the patterned antigens, which resulted in a mosaic of antigen-antibody complexes on the surface. Depending on the assay format, additional immobilization steps are required. By means of a fluorescence microscope, the MIAs were visualized.

Later, a similar approach was presented by Ligler *et al.* for the rapid and simultaneous analysis of a variety of toxins, including staphylococcal enterotoxin B, ricin, cholera toxin, botulinum toxoids, trinitrotoluene, and the mycotoxin fumonisin, on the surface of a single waveguide [78].

Furthermore, there exist a few examples of label-free detection of multiarrays based on metallic nanoparticles supporting localized surface plasmon resonances (LSPR). Besides their distinguished detection properties, shown in literature [79, 80], these systems are too complex and too expensive to be adopted in the POC diagnostics.

2.3.2 Electrochemical systems

Array-based electrochemical platforms for multiplexing rely mostly on addressable microelectrode arrays (MEAs) [46]. They are simple and cheap to fabricate by applying standard lithographic techniques and are usually disposable. Furthermore, microelectrodes feature fast response times and increased signal-to-noise ratios because of their small dimensions [81].

Compared to microspots in optical array-based systems, the immobilization of biomolecules such as antibodies, antigens or DNAs are directly performed on the single electrodes. Therefore, the choice of the electrode material plays a decisive role on the assay performance and is to be considered by the device design. To date, various electrode arrays including screen-printed thick-film carbon electrode arrays (SPCEs) [42, 82], or thin-film platinum [83], gold [84, 85] and iridium oxide [86, 87] electrode arrays have been presented for the multi-analyte detection. In general, thin-film deposition of electrodes offers many benefits such as (i) easy miniaturization, (ii) simple, fast and effective immobilization procedure (especially for gold electrodes) (iii) high throughput fabrication, and (iv) high-dense arrays for multiplexing [46]. Hence, electrochemical signal readout can be obtained through a label [88] or label-free [89].

One of the pioneers in the field of electrochemical array-based multiplexing, AJ eBiochip GmbH, a spin-off of the Fraunhofer Institute for Silicon Technology (ISIT, Germany), has released silicon biochips comprising 16 gold interdigitated electrode arrays (IDA) [90].

They have been employed for the simultaneous amperometric detection of both proteins and nucleic acids by means of enzymatic labels [91]. Therewith, ISIT has carried this commercialized technology one step further to "Fraunhofer ivD-platform", along with other six Fraunhofer Institutes [92]. This platform is built on a cartridge system. A cyclic olefin copolymer (COC) top cartridge includes microfluidics and the total internal reflectance fluorescence (TIRF) sensor. A bottom cartridge is equipped with an electrochemical sensor and a printed circuit board (PCB) to control the integrated and disposable pumps. This device incorporates both optical and electrochemical detection. The applicability of this system for electrochemical multiplexed measurements has been demonstrated for the simultaneous detection of C-reactive protein (CRP) and prostate-specific antigen (PSA).

An impressive example for commercialized array-based systems is the ElectraSense® platform from CustomArray (previously known as CombiMatrix) with an handheld reader, as shown in Figure 2.7. The CustomArray 12K™ chips employ a complementary metal oxide semiconductor (CMOS) circuitry to address VLSI (56×224) arrays of 40 µm diameter Pt electrodes individually.

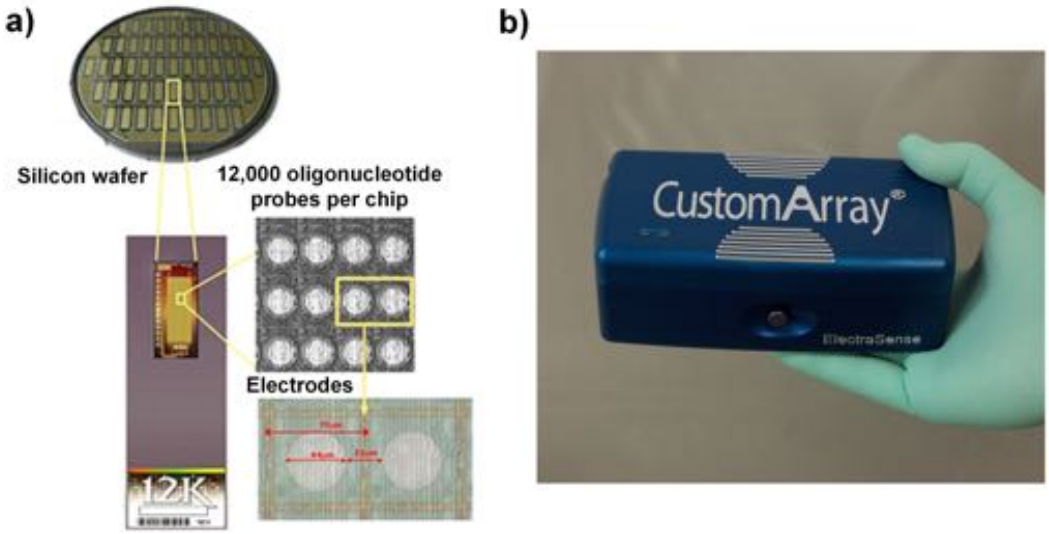

Figure 2.7: *ElectraSense® platform: a) General scheme of 12K™ microarray chips, b) Photograph of the handheld reader (adapted with permission from CustomArray Inc., USA).*

The high throughput ElectraSense® platform provides both electrochemical and fluorescent detection. It is likely to be applied for different applications including genomics, proteomics as well as the combination of both [71, 72]. This wide assay diversity comes from the universal immobilization protocol of biomolecules (e.g. DNA, antibodies, proteins) on each electrode via hybridization of oligonucleotides. In the case of proteomics, the capture antibodies are tagged with complimentary oligonucleotides to bind probes attached directly on the electrodes. The assay signal is obtained by the enzyme HRP electrochemically, while by fluorescent dyes optically, both coupled via biotin–avidin in-

teraction. Furthermore, the CustomArray 12K™ chips are reusable up to four times through the combination of stripping and rehybridization of oligonucleotides [71, 72].

The signal readout is executed with the handheld ElectraSense® reader, that consecutively measures steady state currents of 12,544 electrodes in approximately 40 s, or a fluorescent scanner for electrochemical or optical detection, respectively [93]. Moreover, the performance of CustomArray 12K™ microarray chips was evaluated by Ghindilis *et al.* in spike-in experiments with both detection techniques available [73]. Using the electrochemical detection with the portable ElectraSense® reader a lower limit of detection of 0.75 pM was determined, whereas a detection limit of 1.5 pM was measured with fluorescence detection. Beyond this, the electrochemical approach offers low-cost and quick measurements with less complex and miniaturized diagnostic devices [93].

Array-based platforms facilitate simple, fast and high throughput (more than thousand parameters) measurements of different assay technologies for clinical diagnostics. However, they have still several drawbacks, which limit their use in POCT, such as (i) high sample consumption to prevent evaporation, denaturation and inactivation of proteins [70], (ii) complex assay preparation using inkjet printers or array synthesizers, (iii) expensive and complex fabrication (in the case of the CustomArray platform), and (iii) bulky instrumentation for the signal readout (especially in optical systems).

2.4 Bead-based systems

The use of beads as a flexible substrate material for assay design is an important cornerstone of biotechnology. There exist a vast variety of beads including different sizes, materials (e.g. magnetic beads for easy manipulation) and surface coatings. To overcome the above-mentioned bottlenecks of array-based methods, bead-based systems, mostly with optical readout, have been developed for multiplexing in recent years. In this context, there are mainly two conceptual approaches preferred: (i) Functionalization of different beads, which can be distinguished from either their size/shape or internal color barcodes, with various analytes, and (ii) spatial separation of beads in different channel sections [4, 41, 45].

2.4.1 Optical systems

Sato *et al.* [94] presented a microfluidic chip, as illustrated in Figure 2.8, including four branching multichannels for spatial encapsulation of microbeads. Individual channel inlets allow the introduction of the beads into the different compartments of the microfluidic network. The assay immobilization can be performed both inside or outside the channel. For the measurement the reagents are delivered by a common channel inlet using an external pump and the signal is read out by a thermal lens microscope. The multiplexing applicability of this microfluidic system was demonstrated by the simultaneous detection of the cytokine interferon-γ in different concentrations.

In bead-based multiplexing there are two commercialized optical platforms such as flow cytometry and compact discs for centrifugal microfluidics [4, 8, 41]. In the following they will be briefly discussed.

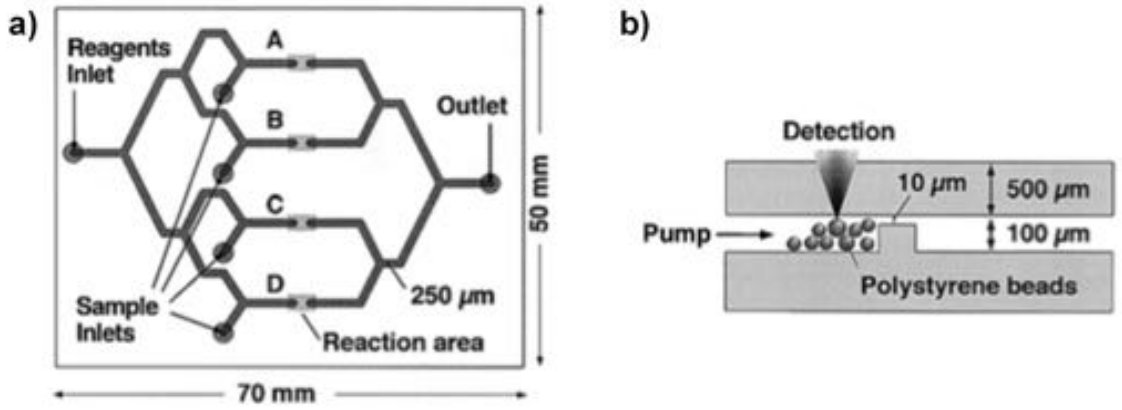

Figure 2.8: *a) Overview of the microfluidic chip for the simultaneous interferon-γ detection and b) cross-sectional schematics of its working principle (reprinted from [94], copyright 2002, with permission from John Wiley & Sons).*

Flow cytometry

In the flow cytometry, optically tagged, mostly with fluorescence labels, particles like cells or beads containing biological information are gauged individually through a small laser beam in a fluid flow. For the multiplexing, different beads with either different size/shape or internal color barcodes are employed. A basic flow cytometer consists of (i) a microfluidic system, (ii) an optical excitation system and (iii) an optical light collection system with high-speed digital signal processing [95, 96].

Currently, there are many commercial platforms available for bead-based flow cytometry allowing multi-analyte detection in clinical diagnostics [4]. One of them is the Luminex xMAP® system (Luminex Corp., USA), as illustrated in Figure 2.9. Here, the multiplexing technology, that enables the simultaneous analysis of a great amount of different analytes in the same sample, is achieved by the use of 5.6 µm color barcoded polystyrene beads with two different fluorescent dyes. Using a reporter biomolecule, like DNA, antibody or protein, tagged with a third fluorochrome, multiplexed bioassays on microbeads can be measured one at a time [97, 98].

In general, bead-based multiplexed flow cytometry provides fast, accurate and sensitive measurements with low running costs for clinical diagnostics at central laboratories. Nevertheless, the size and the cost of instruments for the signal readout limit their application in point-of-care testing [95, 96]. For this purpose, microflow cytometers with small optical components and lab-on-a-chip flow cytometers were developed and evaluated for different

approaches such as characterization of the variations in marine algae populations [99] as well as simultaneous detection of bacteria and toxins in clinical samples [100].

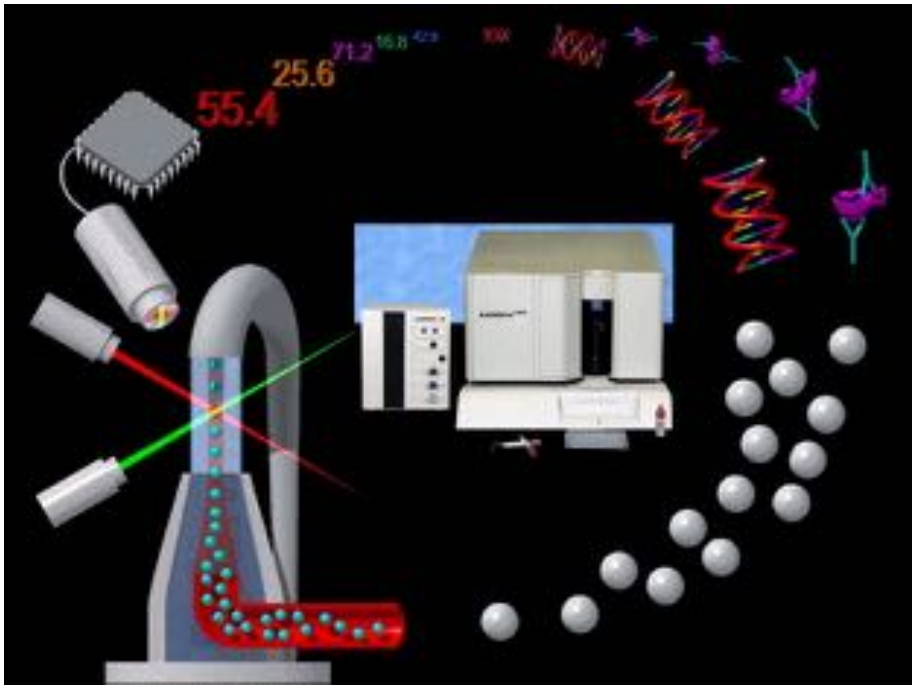

Figure 2.9: *Luminex xMAP® system including four main components describing its working principle: Fluorescently color-coded beads for multi-analyte measurement interact first with the sample and subsequently pass through a laser beam in a fluid stream. The signal readout as well as the bead classification are achieved by a single detector along with the high-speed signal processing (reprinted from [97], copyright 2006, with permission from Elsevier).*

Compact discs for centrifugal microfluidics

CD-based microfluidic platforms, also called "lab-on-a-disc", employ centrifugal forces to route fluids in microchannel networks without the need for an external pump. Thus, this enables an automated assay procedure realized only by the rotation of the compact discs [41, 101]. Except a few electrochemical approaches [102, 103], the analyte detection relies mainly on the optical readout in CD-based microfluidic systems.

Lab-on-a-disc applications are capable of multiplexing by the use of spatial separation of different analytes. For instance, the Gyrolab Bioaffy compact disc (Gyros AB, Sweden), introduced by Honda *et al.* [104], enables analysis of a high number of samples in parallel on Gyrolab™ workstation.

The microfluidic cartridge, as shown in Figure 2.10, is fabricated by injection molding using a cycloolefin polymer. It includes 112 200 nl microstructures each comprising a reaction

chamber pre-loaded with streptavidin coated beads as a solid phase. Covering the CD with a lid, containing individual and common inlets for the filling of microcolumns, prevents a possible evaporation of the sample and reagents. The fluid manipulation is realized by a combination of different techniques based on centrifugal and capillary forces along with hydrophobic barriers located in the microstructures. Furthermore, this system offers full flexibility in assay design owing to the ability to address each microstructure by its individual inlet [104, 105]. The simultaneous detection of alpha-fetoprotein, interleukin-6 and carcinoembryonic antigen in human plasma was presented by Honda *et al.* [104] to specify the device performance characteristics for multiplexing.

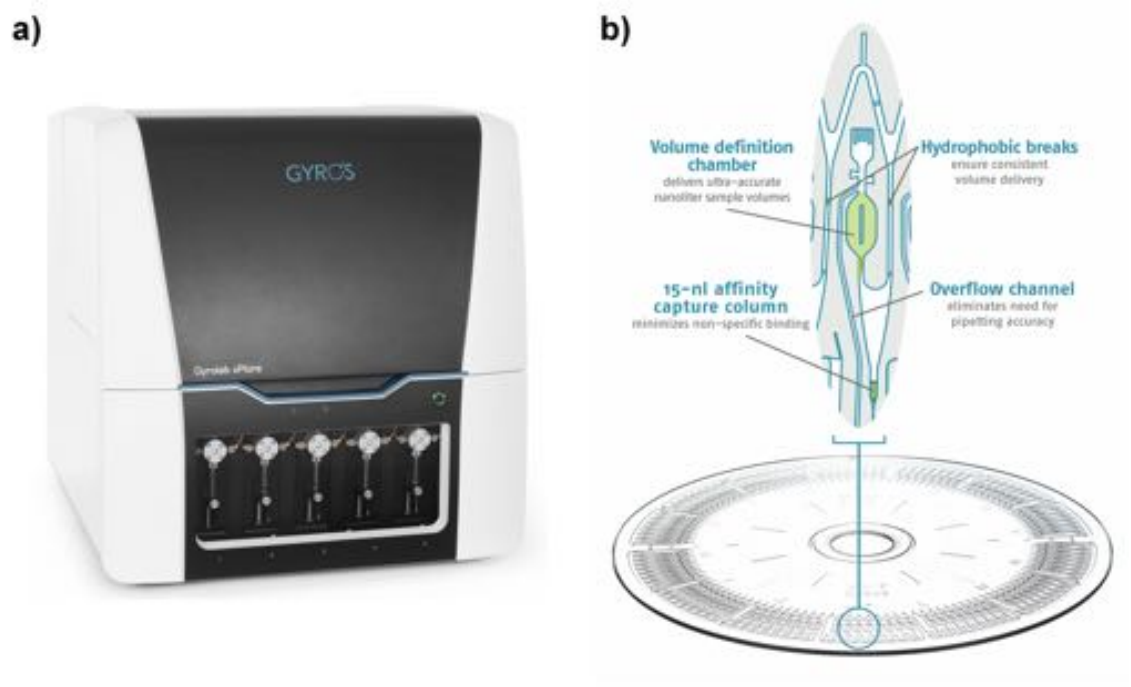

Figure 2.10: *Photograph of the Gyrolab xPlore™ single-CD platform. a) Gyrolab Bioaffy CD b) with expanded view (inset) of the main elements describing their function (adapted with permission from Gyros AB, Sweden).*

The bead-based CD platforms have many advantages including (i) short turnaround times, (ii) low sample consumption, (iii) rapid assay development, (iv) high flexibility in assay design, and (v) easier assay transfer. Thus, they meet specific needs for in vitro diagnostic applications [105]. Yet, they are supposed to be improved further for the application in point-of-care testing due to their complexity and bulky instrumentation.

2.4.2 Electrochemical systems

Bead-based electrochemical platforms for multiplexing are based almost exclusively on multilabeling of micro- or nanobeads [106]. Different labeling methods like enzymes (e.g.

HRP, laccase and Glucose-6-phosphate dehydrogenase) [107], metal ions (e.g. Cd^{2+} and Zn^{2+}) [108], redox tags (e.g. thionine and ferrocene) [109], and QDs (ZnS, CdS and PbS) [110, 111] are shown in the literature for multi-analyte applications. Among them, QDs are the most promising tags for the electrochemical coding due to their outstanding advantages. They are robust, at the same size like proteins, and flexible in surface coating. Besides they have narrowband emission and broad excitation spectra for multicolor detection [106]. Here, stripping voltammetry is employed as signal transduction technique for its powerful performance in the detection of trace metals. The electrochemical coding by QDs is limited by the discrimination of their stripping potentials [106, 110].

On the other hand, bead-based electrochemical systems using spatial encapsulation are rather rarely. Ko *et al.* [56] presented a similar approach for bead capture with PDMS micro pillars, as shown in [94], to detect simultaneously three different cancer markers in real time. The microfluidic chip comprising four parallel channels was fabricated on glass with an integrated Pt interdigitated electrode array. PDMS was employed for the microfluidics and micropillars. The polystyrene beads immobilized with different capture antibodies are introduced through separate inlets into different sections of the microfluidic channel and trapped by the pillar-type microfilters on top of the IDAs. The electrical signal readout of the immunoreaction is achieved by the resistance measurement between single IDA fingers by means of gold nanoparticles and silver enhancer.

Similar to their other competitors, bead-based platforms provide fast and high throughput (especially in the flow cytometry) multi-analyte analysis along with low sample consumption and high assay flexibility for clinical diagnostics. Nevertheless, they are still not suitable for the use in POC testing mainly because of the complex handling of beads, and their bulky and expensive measurement devices.

2.5 Microfluidic multiplexed systems

Microfluidic multiplexing of different analytes has been realized in spatially distinct sections of microfluidic channel networks. For this purpose, various reagents and samples have to be addressed precisely to the detection sites under the favor of valves or individual inlets [41, 112, 113]. For fluid distribution (e.g. sample or reagents) in microfluidic arrays, Y- [114] or T- junctions [115] are used to produce branched channel sections. In most of the microfluidic multiplexed approaches described in literature [11, 112, 116, 117], fluid handling is provided by a number of pneumatic valves integrated into PDMS-based devices.

Indeed simple microfluidic networks can be designed with an individual valve control path for each fluid channel [118]. Nevertheless, such an uneconomic approach limits its capacity for scale-up and is not suitable for POC testing, because it needs a bulky instrumentation. To overcome this issue, similar to transistors in VLSI technology microfluidic large-scale integration (mLSI) makes use of microfluidic multiplexors, combinatorial arrays of binary valves [112, 113]. Thus, this allows to control a microfluidic network including N channels with only $2 \log_2 N$ valve channels. This approach combines simple and rapid fabrication with high throughput multiplexing of fluids using a minimum number of inputs.

The feasibility of mLSI technology has been demonstrated for the simultaneous multi-analyte detection in proteomics [119, 120] and genomics [121, 122]. Despite their great potential for high level multiplexing they are not applicable yet for the POC testing due to their complexity compared with other diagnostic platforms (e.g. paper-based) and their bulky instrumentation for the pneumatic control and signal readout.

2.5.1 Optical systems

Regarding high mortality rates caused by infectious diseases in developing world, there is a great and urgent demand for multiplexed POC devices to differ diseases with similar symptoms in low-resource settings. If the diagnosis occurs early and correct, it is possible to treat infectious diseases by applying available medicines. Furthermore, low-cost and easy-to-use systems are likely desired which motivate the untrained personnel or patients themselves to operate with minimum user input.

In this context, Chin and colleagues [123] demonstrated an microfluidic integrated strategy the “mChip” for multiplexed immunoassays. It combines the POC testing in resource limited settings with the early diagnosis of different infectious diseases. The low-cost plastic cassettes, as displayed in Figure 2.11, are fabricated with injection molding. Each channel comprises four meandering sections located in series. Assay preparation including the functionalization of meandering areas with different capture and blocking reagents is done manually or automatically by dispensing. To achieve a signal amplification using a compact readout device, the reduction of silver ions onto gold nanoparticles coupled to the detection antibodies in a sandwich assay format. The optical signal density is read

out by a compact and low-cost device employing light-emitting diodes and photodetectors. The multiplexing performance in the simultaneous POC diagnosis of HIV and syphilis was presented with only 1 µl blood obtained by a finger prick and showed similar sensitivities and specificities to reference assay systems [123].

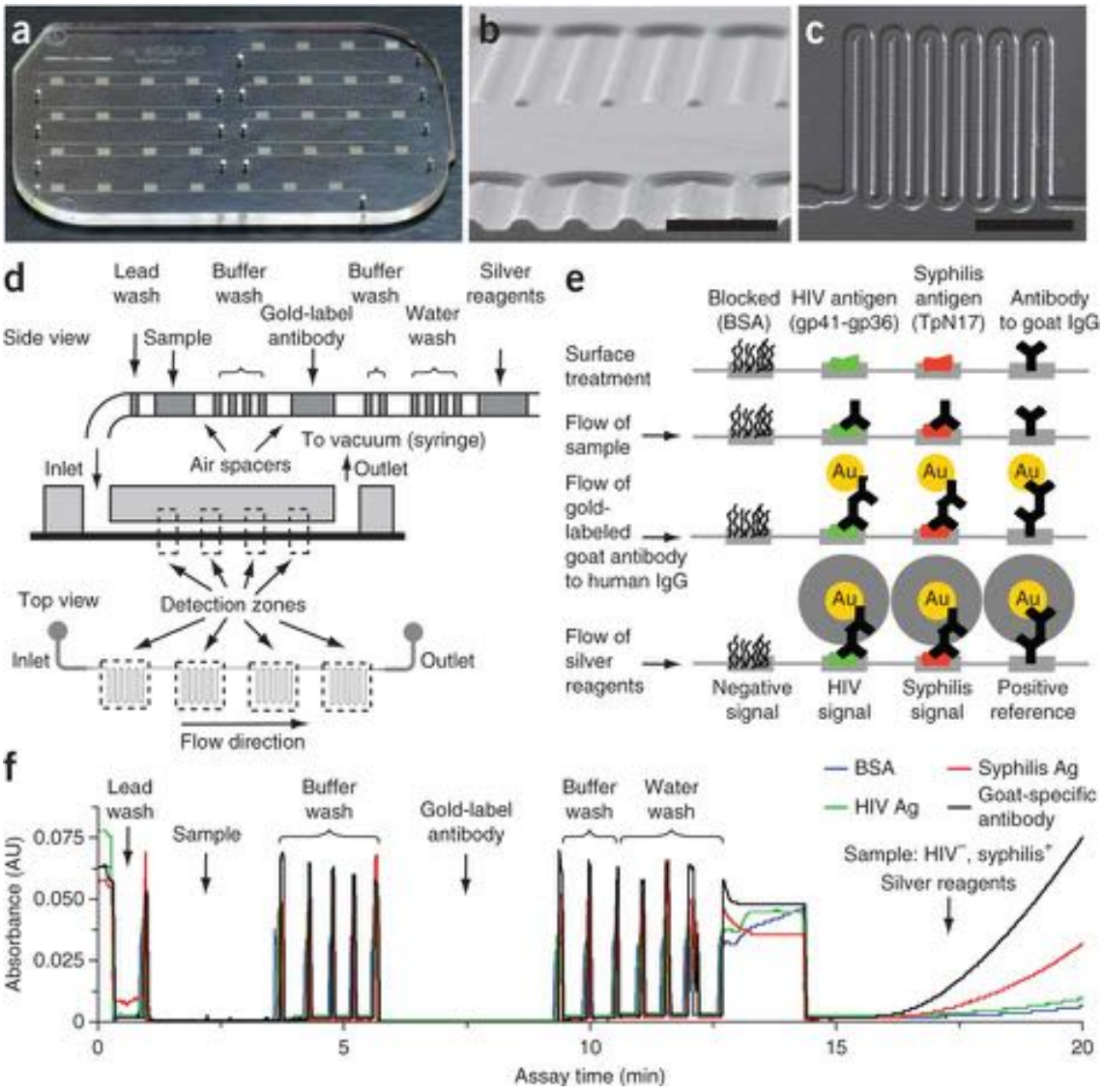

Figure 2.11: *mChip system for multiplexed POC testing: a) Photograph of the microfluidic polystrene chip comprising seven measurement units. b) SEM image of channel cross-section (scale bar: 500 µm). c) Transmitted light micrograph of the microchannel (scale bar: 1 mm). d) Passive delivery of preloaded sequence of different reagents. e) Schematics of the on-chip detection by reduction of silver ions on secondary antibodies tagged with gold nanoparticles. f) Optical density (OD) plot of a HIV-syphilis duplex test (reprinted by permission from Macmillan Publishers Ltd: Nature medicine [123], copyright 2011).*

Two years later the same group reported a completely automated system, which includes a cartridge with pre-loaded reagents and custom-made analyzer. An integrated micropump, signal detection and data communication modules minimize the user intervention [124]. The main drawbacks of this system are its limited flexibility in assay design and complex sample handling (by a capillary tube) despite automatization.

With a similar objective, Lafleur *et al.* [125] introduced an microfluidic multiplexed cartridge "DxBox", shown in Figure 2.12, with a paper-based detection unit for the simultaneous measurement of malaria pfHRPII antigen and IgM antibodies to Salmonella typhi in whole blood. The dried reagents stored on-chip, according to the procedure shown in [126], were delivered by pneumatic actuation through the detection zones to waste reservoir. Here, the same signal amplification strategy, as described in [123], was employed for the optical detection. The images of each detection spot was captured by a flatbed scanner and the obtained optical intensities were measured for the quantitative analysis. The DxBox system showed assay performances comparable with laboratory ELISAs. Nevertheless, there are several disadvantages for high level multiplexing including (i) the complexity in device fabrication, (ii) comparable high costs, (iii) poor management of air bubbles, and (iv) limited assay diversity.

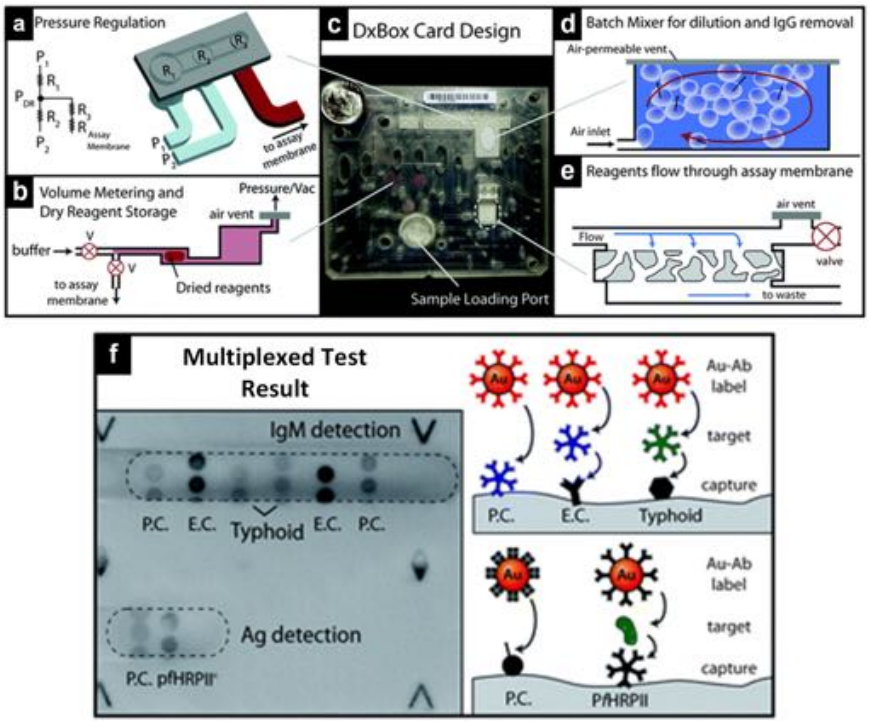

Figure 2.12: *DxBox integrated microfluidic cartridge with the main features (a–e) describing its working principle. f) On-chip simultaneous multiplexed detection of IgM antibodies against typhoid infection and malaria pfHRPII antigen in human plasma (reproduced from [125] with permission of The Royal Society of Chemistry).*

As an alternative approach, Hu *et al.* [127] reported a fluorescence-based flow-through LOC device using a number of serially plugged glass capillaries, coated inside with zinc oxide (ZnO) nanorods as solid substrate, for the multi-analyte detection. The ZnO nanorods offer a large surface area for increased biomolecule attachment as well as a higher sensitivity by enhancing the fluorescent signals. The signal detection was conducted by a custom-made analyzer comprising a pump and a fluorescence readout module. Here, the multiplexed detection of PSA , AFP and CEA in human plasma with a detection limit of 1-5 ng ml^{-1} within 30 min. However, many academic examples are far away from the POC reality due to its drawbacks especially in terms of handling and device performance (e.g. sample-to-result time).

2.5.2 Electrochemical systems

Electrochemical microfluidic multiplexed systems are mostly preferred to realize compact analytical devices along with automated assay procedures by combining the fast and sensitive electrochemical detection with the powerful microfluidic technologies. For the design of multi-analyte platforms the use of a single electrochemical cell with multiple working electrodes is favorable owing to the needs for the application in resource limited settings [128]. However, most of the systems, described recently in literature [115, 129], employ distinct electrochemical measurement cells within a microfluidic network. As a result, the signal readout can be conducted either consecutively or by using multichannel potentiostats.

Rossier *et al.* introduced a novel technology using plasma etching for the high throughput fabrication of polymer microfluidic sensors in 2002 [130]. Based on this technology, the same group presented and commercialized later an automated microfluidics-based platform immuSpeed™ (DiagnoSwiss S. A., Switzerland), formerly known as GRAVI [129, 131]. The amperometric microfluidic "immuSpeed" chip consists of eight microchannels, each with a volume of only 65 nl and an electrochemical cell. Each measurement chamber comprises 42 gold microelectrodes as working electrode, a counter and a Ag/AgCl reference electrode and is operated by a custom-made workstation and software in parallel and automatically. The multi-analyte measurement was first shown by the detection of different concentrations of folic acid in infant formula [131]. Currently, the immuSpeed™ platform employs magnetic beads as solid surface for the biomolecule immobilization, as described earlier in [129] for the measurement of immunoglobulin G in a competitive ELISA format. Magnetic beads enable the regeneration and thus, the reuse of the expensive microfluidic chips up to 12 times. This system is not suitable for the POC detection mainly due to its size and complexity.

In another example, the Asklepios POC platform was developed by Lawi *et al.* [115] using amperometric detection and later commercialized by Genefluids, Inc. (USA), as displayed in Figure 2.13. The disposable microfluidic cartridge offers six electrochemical cells, located in parallel channels, with individually addressable gold working electrodes for multiplexing. Furthermore, it combines a hydraulically operated reagent storage module and

a pneumatically actuated fluid handling module. The feasibility of the Asklepios system for the simultaneous detection of different cytokines such as IL-8 protein in proteomics and IL-8 RNA in genomics was proved [115]. The main drawbacks of this platform for high throughput multiplexed POCT are (i) the complexity in cartridge fabrication, (ii) comparable high costs, and (iii) high sample consumption.

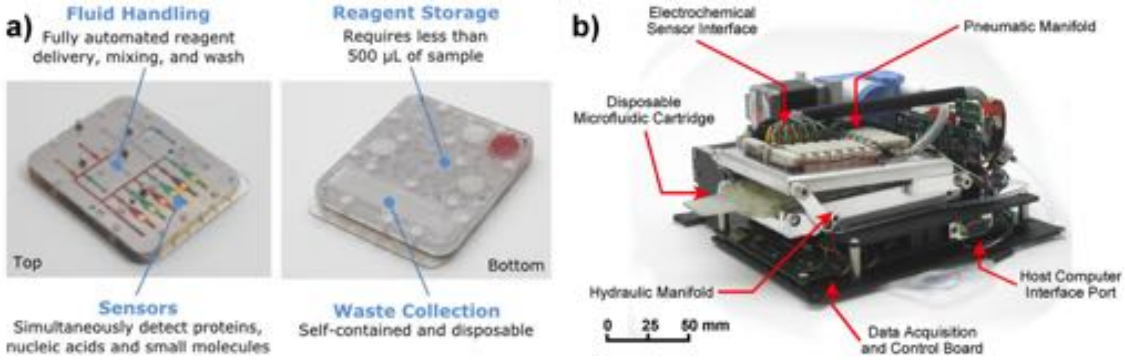

Figure 2.13: *Asklepios POC system: a) Self-contained, disposable microfluidic cartridge including six electrochemical cells for the simultaneous detection (reprinted with permission from GeneFluidics Inc., USA), and b) Cartridge control system comprising different modules (reprinted from [115]).*

2.6 Summary

In conclusion, the multiplex diagnostic platforms which are capable of high throughput screening (more than 100 parameters) including array-based (e.g. CustomArray) or bead-based (e.g. xMAP® and Gyrolab™) systems have lately had their place in central laboratories as part of standard equipment. In the near future these methods will have the greatest impact, above all in biomarker discovery and validation. Despite their numerous advantages they are not suitable for point-of-care testing.

Currently, there is a great and urgent demand for multiplexed POC testing, chiefly in resource-limited settings, for example in developing countries, directly at the bedside or in doctor's offices [41]. In general, an ideal multiplex POC device must offer a high performance, such as high sensitivity and multiplexing capability, at low complexity including simple fabrication and minimized user input. Therefore, the state of the art platforms presented in this work are summarized in Figure 2.14 regarding their complexity and multiplexing performance. According to Figure 2.14 it is obvious that the challenges remain for the POCT, since most multiplexed platforms are still at the proof-of-principle stage or limited by their multiplexing capability (e.g. paper- or microfluidic-based devices).

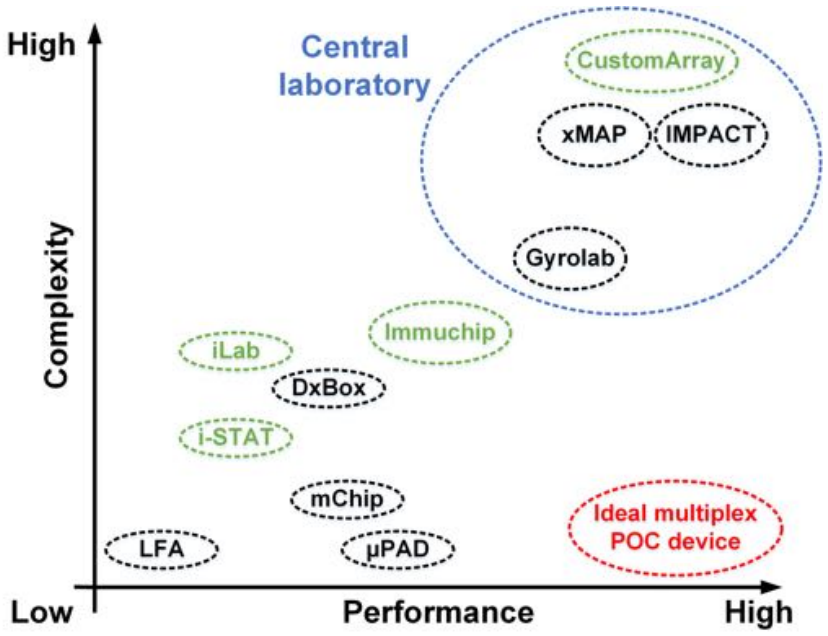

Figure 2.14: *Diagram of two important conceptual approaches, complexity versus performance, for an ideal multiplexed POC device including the presented state of the art platforms. Electrochemical systems are marked in green (adapted from [47]).*

In this context, microfluidic technologies play a decisive role and offer many benefits (e.g. capillary filling). Here, the design of LOC devices has to be considered particularly to

limit its complexity due to unnecessary features [15]. Thereby, it is desirable to combine a cheap fabrication with a highly sensitive platform requiring minimum user intervention. Besides, for the successful commercialization a great effort is essential to integrate all parts on disposable and low-cost microfluidic cartridges or cassettes of POC device [20].

Electrochemical microfluidic multiplexed systems have the potential to cover the needs for POC diagnostics, especially in low-resource settings, due to its superior features compared to optical systems. These are (i) high sensitivity and selectivity using a palette of analytical methods, (ii) capacity for scale up using a single electrochemical cell with multiple working electrodes, (iii) fast, low-cost and high degree multiplexing with a miniaturized analyzer, (iv) design flexibility in combination with various other techniques such as microfluidics or beads, and (v) no influence of the matrix opacity on the measured signals [128, 132]. Furthermore, the use of polymer-based materials allows (i) the realization of biocompatible and cost effective diagnostic devices, (ii) the construction of 3D microfluidics leading to a high flexibility in device design with a (iii) fast and high throughput fabrication [48, 50].

The goal of this thesis is the development of a polymer-based electrochemical multiplexed LOC platform for the fast, sensitive and simultaneous point-of-care testing. Additionally, the proposed system should offer a high flexibility in the assay design including format (e.g. competitive) or technology (e.g. genomics). To prove the feasibility of such a device, this work focuses mainly on an simple and easy-to-use platform rather than on high degree multiplexing.

3 Theory

Preface

To understand the working principle of the electrochemical immunosensor combined with multiplexed microfluidics proposed in this work, it is important to get an overview of the basics of electrochemistry, microfluidics and immunoassays.

This chapter provides a brief introduction into the electrochemical fundamentals, from basics towards applications, the different formats of the immunoassays and their immobilization and detection strategies for biosensor applications, as well as the microfluidics theory. The electrochemistry section contains also a specific part about the platinum electrochemistry.

3.1 Electrochemistry: From basics towards applications

This section gives an overview about the fundamentals of electrode reactions and the principles of electrochemical methods used in this work. All information descend from the following references [37, 38, 133–137] or otherwise as stated in the text.

3.1.1 Electrochemical cell

The electrochemical cell is the smallest constituent unit of electrochemistry. It combines two half-cells each with an electrode and an electrolyte (e.g. a salt or weak acid solution). Electrochemical cells are classified as either electrolytic or galvanic cells. In galvanic cells the reactions occur spontaneously, whereas in electrolytic cells an external source (a current or potential) has to be applied to induce a chemical reaction.

In an electrochemical cell the electrode, at which the reaction of interest takes place, is the working electrode (WE). They should not be involved in the electrochemical reactions itself in sensor applications. Therefore, mostly inert electrodes, such as platinum (Pt), gold (Au) or carbon-based materials, are employed. The second electrode is the reference electrode (RE), which provides a well-defined and stable potential independent of electrolyte properties, and completes the electrical circuit. When a potential is applied to this system, the resulting current is measured as a function of this potential. Such an arrangement is referred to as two-electrode measurement setup.

However, this setup has several disadvantages. The current flow through the reference electrode polarizes the electrode itself and thus, an overpotential occurs. Hence, it can not provide a stable potential. Other problems encountered in such a system are the material consumption of the reference electrode and the contamination of the solution by release of the electrode material.

To avoid these problems, the active area of the reference electrode must be kept huge in comparison to the working electrode area. This leads again to a minimized electrode resistance and so the voltage drop at the reference electrode can be neglected. The two-electrode setup is normally utilized for the energy storage or conversion systems like batteries, fuel cells, etc.. On the other hand, for biomedical applications the geometries of electrodes are crucial, especially for *in vivo* measurements.

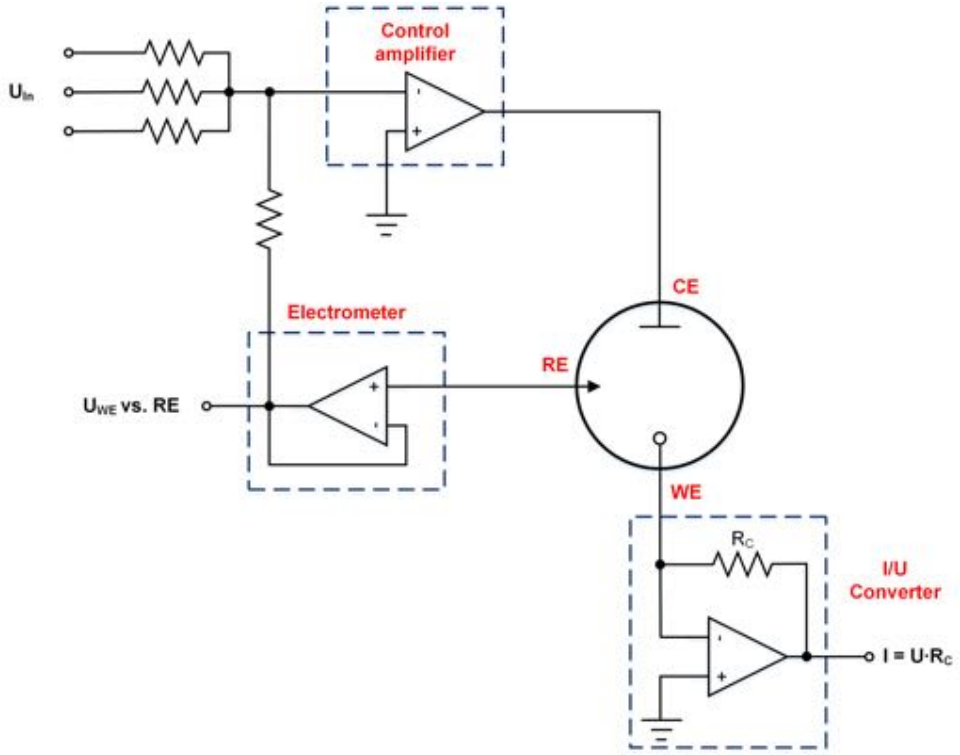

Figure 3.1: *Three-electrode setup in a potentiostatic configuration using working (WE), counter (CE) and reference electrode (RE). A potentiostat determines the cell voltage between the working and reference electrodes, regulates the current at the counter electrode to keep the cell voltage at the desired value constant, and measures the cell current indirectly by measuring the voltage drop U across an internal resistance R_C.*

A better approach to overcome these issues with the reference electrodes is the introduction of a third electrode in a potentiostatic configuration, counter electrode (CE). The so called three-electrode setup is the most commonly used cell setup in electrochemistry. Here, the working electrode potential is kept constant with respect to the reference electrode by

adjusting the current at the counter electrode in a close-loop system. This is realized in practice by a potentiostat as shown in Figure 3.1.

Potentiostats measure the cell voltage, the potential between the working and reference electrodes, by using an electrometer amplifier. Its output is the feedback signal for the control amplifier in the potentiostat circuit. The control amplifier compares the cell voltage with the set value continuously and regulates the current at the counter electrode to keep the cell voltage constant. The current/voltage converter measures the cell current I indirectly over the voltage drop U across an internal resistance R_C. Additionally, the input terminals of this operational amplifier link the working electrode to virtual ground. Cell currents can vary generally by several orders of magnitude. Therefore, it is not possible to measure the current over a wide range with a single resistance. Each current range needs to be gauged with an adequate resistance. Potentiostats can distinguish between the different current ranges during the measurement and select the appropriate resistance R_C by using different algorithms.

3.1.2 Electrochemistry at equilibrium

At the electrode/electrolyte interface, transfer of electrons or ions occurs from an analyte in electrolyte to the electrode, or vice versa. The overall reaction in an electrochemical cell is also known as redox reaction (see Equation 3.1). At the anode the oxidation appears and it is defined by the loss of electrons by a molecule, atom, or ion. The reduction takes place at the cathode and is the uptake of electrons, respectively.

$$Ox + n \cdot e^{-} \rightleftharpoons Red \tag{3.1}$$

where Ox is the oxidized and Red is the reduced form of the redox couple, and n is the number of electrons.

Redox reactions will occur only in a defined potential range, in which the electron transfer is either kinetically limited or in thermodynamic equilibrium. In the case of thermodynamically equilibrated systems, the Nernst equation gives the relationship between the working electrode potential and the concentration of the redox couple:

$$E = E_0 + \frac{RT}{nF} \ln\left\{\left(\frac{a_{Ox}}{a_{Red}}\right)\right\} \tag{3.2}$$

where E_0 is the standard potential of the electrode, R is the universal gas constant, T is the Kelvin temperature, $F$is the Faraday constant and a_{Ox} and a_{Red} are the activities of the oxidized and reduced forms of the redox couple. At low concentrations of the electroactive species, the activities are nearly equal to the concentrations. Therefore, the Nernst equation is often simplified by replacing them with the concentrations of the redox couple.

3.1.3 Reference electrodes: Theory and practice

As mentioned in Section 3.1.1, reference electrodes have a well-known and stable potential independent of the electrolyte. They are used to refer the potential of the working electrode to the electrolyte in a potentiostatic cell setup. The most prominent reference electrodes are the normal hydrogen electrodes (NHE) and the standard hydrogen electrodes (SHE). They consist of a half cell with a platinum electrode immersed in a hydrogen chloride (HCl) solution as electrolyte and constantly flushed with hydrogen gas (H_2). The normal hydrogen electrodes are internationally accepted as the zero point for the electrochemical standard potentials E_0 at all temperatures [138].

As the hydrogen reference electrodes prove to be poor to handle and do not meet the need for the miniaturization in various applications, the electrodes of the second kind are mostly chosen as reference electrodes. These are metal electrodes covered by their hardly soluble salt. The connection to the electrochemical cell is via an inner electrolyte, containing a common anion. The potential of these reference electrodes depends on the concentrations of both the salt and the anion in the electrolyte. Therefore, their saturated salt solutions are utilized as inner electrolyte.

Nowadays, silver/silver chloride ($Ag/AgCl/Cl^-$) reference electrodes are mostly used. It consists of a silver electrode coated with a silver chloride layer in an inner electrolyte with a defined chloride ion concentration (e.g. 3 M sodium chloride NaCl). The redox reaction for silver/silver chloride is given as

$$AgCl + e^- \rightleftharpoons Ag + Cl^-. \tag{3.3}$$

In alkaline solutions the saturated calomel electrodes (SCE) are favorable as a reference due to their stability against the hydroxide ions. Their standard potential E_0 is $+0.241\,V$ vs. NHE.

For disposable lab-on-a-chip applications, not only further miniaturization but also a facile fabrication of the reference electrodes are crucial [139]. In this context, the so called pseudo-reference electrodes are employed, where the sample solution is used as reference electrolyte. Hence, they can provide a stable but unknown potential which depends on the chloride concentration of the sample solution. The potential of such an electrode can be calculated by the Nernst equation (see Equation 3.2) with unit activity for the solid silver and silver chloride under standard conditions:

$$E = E_0 - \frac{RT}{F} \ln\left(a_{Cl}\right) \tag{3.4}$$

Furthermore, the pseudo-reference electrodes can be implemented easily by thin-film technology or by screen printing. The advantages of pseudo-reference electrodes are their low impedance and comparably simple fabrication process [139, 140].

3.1.4 Faradaic and Non-Faradaic processes

There are two different types of processes which can occur during an electrochemical reaction. In the so called faradaic processes, a charge transfer will happen across the electrochemical cell as a result of redox reactions. They are governed by the Faraday's law:

$$Q = N \cdot F \cdot z \tag{3.5}$$

In a redox reaction, the amount of oxidized or reduced substances N is proportional to the charge Q and the valency of the ions z. On the other hand, charge-related processes such as adsorption and desorption at the electrode-electrolyte interface can also induce a change of the electrode potential. These processes are termed non-faradaic processes. The faradaic processes mostly arouse the interest of the electrochemical investigations. In voltammetric measurements, the total current is the sum of not only the faradaic currents for the sample and blank measurements, but also the non-faradaic currents as background signal.

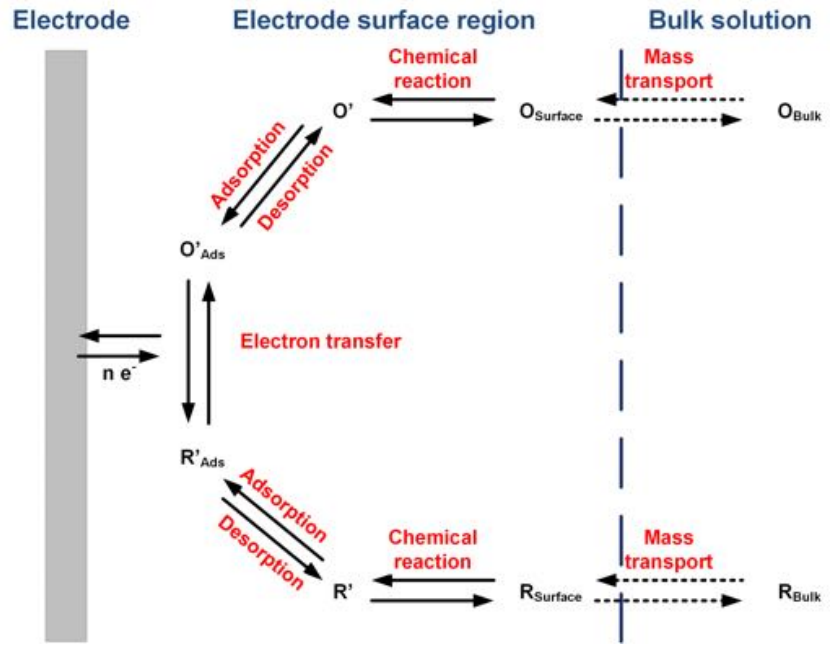

Figure 3.2: *Schematic pathway of the electrode reactions. The rate of the electrode reactions is given by the slowest step in this sequence (adapted from [38]).*

The schematic pathway of the redox reactions at an electrode is shown in Figure 3.2. In general, it consists of many different processes and can be very complicated depending on the number and complexity of these reactions. The reaction rate is defined by the slowest step in this sequence. The overall speed of the redox reactions and so, the measured current is limited by either mass transport of electroactive species to the electrode or ki-

netically through the rate of the electron transfer at the electrode. In this work, platinum, known for sufficiently high electron transfer rates, is used as the electrode material for the biosensors. Therefore, only the mass transport controlled reactions will be discussed in the next section.

3.1.4.1 Mass-Transport-Controlled-Reactions

The rate of the mass transport through a plane with a certain area is described by the flow J and has the unit of $\mathrm{mol\,cm^{-2}\,s^{-1}}$. The mass transport of electroactive species to the electrode can appear in three different manners:

- **Diffusion:** A spontaneous fluctuation of molecules driven by concentration gradients tends to eliminate or minimize these gradients.
- **Convection:** Transport of molecules takes place via an external mechanical energy (e.g. stirring) or density gradients of the electroactive species to the electrode (e.g. by local warming).
- **Migration:** Charged species move along an electrical field. Besides, the charged particles can drag neutral particles and thereby, can cause a flow.

In general, all these processes of the mass transport exist at the electrode simultaneously.

In microfluidics the flow is almost always in laminar regime. Additionally, electrolytes containing high concentrations of an inert salt as a supporting electrolyte will eliminate the migrational limitation by increasing the solution conductivity, which causes a reduction of the electric field inside the electrolyte. In the following part, only the diffusion-limited mass transport of electroactive species will be considered and its basic equations will be introduced.

For diffusion-limited systems, the measured current is direct proportional to the flux J of electroactive species and electrode area A, and can be derived from Faraday‘s law (Equation 3.5):

$$i(t) = -n \cdot F \cdot A \cdot J(t). \tag{3.6}$$

Fick‘s first law describes the directly proportional relationship between the flux J and the slope of the concentration gradient $\frac{\partial C(x,t)}{\partial x}$ and can be described as

$$J(x,t) = -D \cdot \frac{\partial C(x,t)}{\partial x}. \tag{3.7}$$

The diffusion coefficient D is the proportionality factor of a substance and has typically values between 10^{-5} and $10^{-6}\,\mathrm{cm^2\,s^{-1}}$ in aqueous media.

A general term for the faradaic current response depending on the concentration gradients is given by combining the Equation 3.6 and Equation 3.7:

$$i(t) = n \cdot F \cdot A \cdot D \cdot \frac{\partial C(x,t)}{\partial x}. \tag{3.8}$$

According to the equations above, the flux of electroactive species is time-dependent and the concentration change with time can be expressed with Fick's second law for the linear diffusion:

$$\frac{\partial C(x,t)}{\partial t} = D \cdot \frac{\partial^2 C(x,t)}{\partial x^2}. \tag{3.9}$$

3.1.5 Electrochemical methods

Electroanalysis deals with the interaction between chemical processes and electrical quantities (e.g. potential, current or charge). Since the fundamental developments including voltammetry and low-signal techniques in the 1950s and 1960s, electroanalytical methods became more and more popular as detection principles of chemical sensor applications [81]. This section features an overview of the electrochemical methods applied in this work including their theoretical basics.

3.1.5.1 Cyclic voltammetry

The cyclic voltammetry is the most commonly used electroanalytical measurement technique for the qualitative study of electrochemical processes. Thus, reliable information about the kinetics of the reactions, the electron transfer, and the chemical as well as physical properties of the electrodes and the electrolytes (analyte solution) can be obtained quickly.

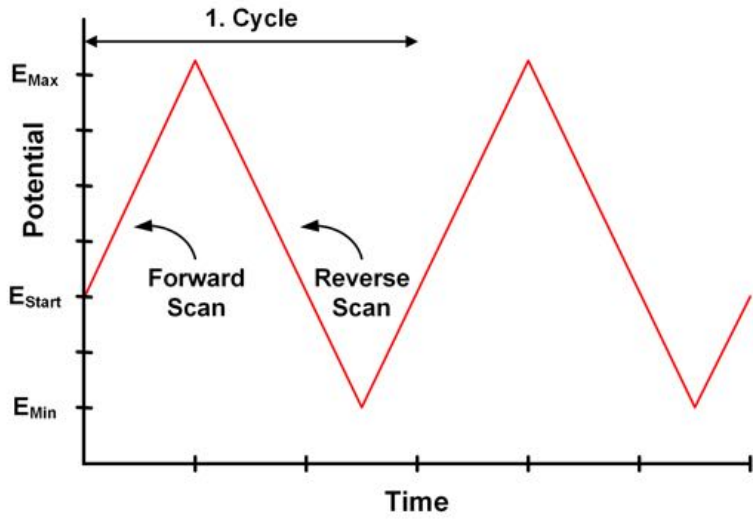

Figure 3.3: *Typical triangular excitation signal for cyclic voltammetry.*

By applying a triangular excitation shown in Figure 3.3, the potential at the working electrode is scanned linearly and the resulting current is measured by a potentiostat. The resulting typical current-potential plot is the so called cyclic voltammogram. The

most important parameters of the cyclic voltammetry are the scan rate ($V\,s^{-1}$), the slope of the applied potential, and the potential extrema. The start potential can be chosen independently from the potential extrema. The potential range defined by the potential extrema should be within the potential range of the oxygen- and hydrogen evolution, in other words, "water window".

3.1.5.2 Amperometry

Amperometry is a controlled-potential measurement method for the quantitative detection of redox active species. A constant (in case of single-potential amperometry) or varying potential over time in a certain manner (in case of pulsed amperometry or chronoamperometry) is applied to the working electrode and the resulting current is recorded. In the case of diffusion limitation, the measured faradaic current at the working electrode is ideally direct proportional to the analyte concentration in the electrolyte.

Chronoamperometry is used most widely for sensor applications aiming long term measurements to prevent electrode fouling. Here, a specific protocol containing of one or more potential steps will be applied. An amperometric measurement begins generally with the preconditioning of the working electrode using different potentials, at which no reaction of the analyte takes place. After polarization of the working electrode to the redox potential, analytes will start to oxidize or reduce, depending on the applied potential. In this work, chronoamperometry is used as the measurement principle for the microfluidic multiplexed biosensor platform.

In an amperometric experiment, the current response can be derived from the Fick´s second law (Equation 3.9) for linear diffusion solved by using adequate initial and boundary conditions:

At $t = 0$, the concentration is uniform over the whole system and equal to the electrolyte concentration $C_O(x, 0) = C_O(Elektrolyte)$. Directly after the beginning of the experiment $t > 0$, the analytes next to the electrode are completely consumed by the electrode reactions and so, the concentration at the electrode $C_O(0, t)$ is zero. This causes a concentration gradient towards the electrode. This depletion region is termed as diffusion layer. The analyte concentration increases with the increasing distance from the electrode $C_O(x, t) \rightarrow C_O(Elektrolyte)$ for $x \rightarrow \infty$. Under these circumstances the time-dependent concentration profile for planar electrodes is described by:

$$C_O(x,t) = C_O(Elektrolyte)\left\{1 - \mathrm{erf}\left[\frac{x}{\sqrt{4D_O \cdot t}}\right]\right\} \tag{3.10}$$

The concentration gradient at the electrode surface is given then:

$$\frac{\partial C}{\partial x} = \frac{C_O(Elektrolyte)}{\sqrt{\pi \cdot D_O \cdot t}} \tag{3.11}$$

The substitution of Equation 3.11 into Equation 3.8 leads to the well-known Cottrell equation:

$$i(t) = \frac{n \cdot F \cdot A \cdot D_O . C_O(Elektrolyte)}{\sqrt{\pi \cdot D_O \cdot t}} \tag{3.12}$$

The diffusion layer grows over time, whereas the concentration gradient decreases. According to the Cottrell equation, the faradaic current response decays directly proportional to the square root of the diffusion coefficient D and $1/t$.

3.1.6 Platinum electrochemistry

This section studies the electrochemical characteristics of platinum electrodes by means of cyclic voltammetry and the hydrogen peroxide (H_2O_2) oxidation at platinum electrodes.

3.1.6.1 Characteristics of the platinum electrodes

Noble metals are the most widely employed electrode materials in electrochemistry. Amongst others, platinum is favorable due to its high chemical inertness and its electroactive properties like high electron transfer kinetics. The multiplexed biosensor platform proposed in this work deals with platinum as basic electrode material. Therefore, it is important to study the material characteristics as well as its catalytic behavior in relevant electrolytes. The cyclic voltammetric analysis at platinum electrodes, shown in Figure 3.4, will be discussed in more detail here.

A typical cyclic voltammogram starts with the open circuit potential (OCP)[1]. In this double layer region (R1) no faradaic processes occur. There exists a nearly zero current density j_C, which can be linked to the charging of an electrolytic double layer at the working electrode. The so called double layer capacity C_D is assumed to be:

$$i_c = C_D \cdot \frac{\partial E}{\partial t} \tag{3.13}$$

At cell potentials of above 0.55 V vs. Ag/AgCl, the chemisorption of oxygen begins. First, the adsorption of water (R2) occurs at the bare platinum electrodes leading to platinum hydroxide. According to Angerstein-Kozlowska *et al.* [141], there are three successively formation stages depending on the platinum lattice occupation for three resulting anodic current peaks:

$$4Pt + H_2O \rightarrow Pt_4OH + H^+ + e^- \tag{3.14}$$

$$Pt_4OH + H_2O \rightarrow 2Pt_2OH + H^+ + e^- \tag{3.15}$$

$$2Pt_2OH + H_2O \rightarrow 2PtOH + H^+ + e^- \tag{3.16}$$

[1] The equilibrium potential of a working electrode measured versus a reference electrode under zero current and no-load conditions

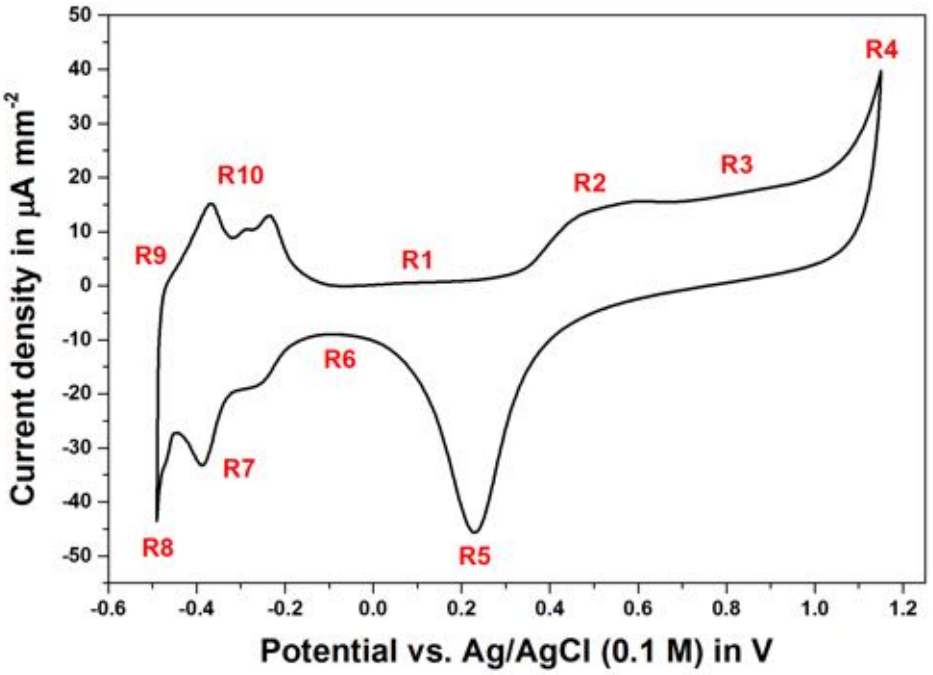

Figure 3.4: *Cyclic voltammogram at a polycrystalline platinum on-chip electrode (without cover) in 1 N sulfric acid (H_2SO_4), scan rate of 100 mV s^{-1}.*

Further, the platinum hydroxide is oxidized to platinum oxide at higher potentials, in the so called broad region (R3):

$$\mathrm{PtOH} \rightarrow \mathrm{PtO} + \mathrm{H^+} + \mathrm{e^-} \tag{3.17}$$

At a potential of approximately 1.35 V vs. Ag/AgCl, the anodic oxygen evolution starts at the Pt electrode (R4):

$$\mathrm{H_2O} \rightarrow \mathrm{O_2} + 4\mathrm{H^+} + 4\mathrm{e^-} \tag{3.18}$$

In the reverse scan, first the formed platinum oxide layer (R5) is reduced, which is followed again by a short double layer region (R6).

At a potential of approximately -0.2 V vs. Ag/AgCl a monolayer of hydrogen atoms adsorbs at the Pt electrode (R7) resulting in two current peaks due to the reduction of adsorbed protons. The reaction can be described as

$$\mathrm{Pt} + H^+ + \mathrm{e^-} \rightarrow \mathrm{Pt\text{-}H}. \tag{3.19}$$

Subsequently, the cathodic evolution of the molecular hydrogen begins at the platinum electrode (R8). In the forward scan, first the formed molecular hydrogen (R9) and then the in step R7 adsorbed hydrogen monolayer can be oxidized again (R10).

The hydrogen desorption at platinum electrodes proves three typical peaks in sulfuric acid, among which the smallest one is a sensitive indicator for the material quality. It can

be observed only when dealing with residue-free electrode surfaces. Furthermore, both hydrogen adsorption and desorption can be employed to determine the surface roughness and thus, the real surface area. This will be discussed extensively in the next section.

Determination of surface roughness

The electrode surface roughness plays a crucial role in the sensitivity of the electrochemical bio- and immunosensors. The higher the active electrode area is, the higher is the electrocatalytic activity and the resulting current response [142, 143].

As mentioned in the previous section, both hydrogen adsorption and desorption regions of cyclic voltammograms at platinum electrodes can be studied to estimate their surface roughness [144, 145]. The charge density Q_H transferred during the adsorption, respectively desorption, of the hydrogen monolayer is directly proportional to the amount of hydrogen atoms. It can be determined by integrating the current density over time. The nominal value for the charge density of hydrogen monolayer at a smooth platinum electrode is given as $210\,\mu C\,cm^{-2}$ [144]. The surface roughness factor, and thus, the real surface area can be determined by comparing the calculated value with the theoretical one.

3.1.6.2 Hydrogen peroxide oxidation

Amperometric biosensors, based on the electrochemical oxidation of hydrogen peroxide, are employed frequently for electrochemical immunosensors (EIS) nowadays. In these systems, hydrogen peroxide is generated by an enzyme reaction (e.g. glucose oxidase, horseradish peroxidase - HRP, etc.). Its concentration is directly proportional to the analyte concentration. Therefore, it is important to understand the reaction mechanism of H_2O_2 oxidation at platinum working electrodes [146].

The oxidation of H_2O_2 is favored at the oxidized platinum electrodes [147, 148]. Hickling and Wilson [149] demonstrated for the first time that there is a good agreement between the potentials of platinum oxide formation and H_2O_2 oxidation. Therefore, they strongly suggest that the platinum oxide PtO may play a role as an intermediate step by the H_2O_2 oxidation. Later, the findings of Lingane and Lingane [147] supported this argument. They proved that the primary electron transfer takes place by the re-oxidation of platinum to platinum oxide after the reduction of the former oxide layer by the decomposition of hydrogen peroxide. Hall *et al.* [146] extended the earlier findings to a complete reaction mechanism for the H_2O_2 oxidation at platinum surfaces. H_2O_2 adsorbs onto Pt(II) binding site, $Pt(OH)_2$, considering a Langmuir isotherm:

$$H_2O_2 + Pt(OH)_2 \rightleftharpoons Pt(OH)_2H_2O_2 \tag{3.20}$$

It should be noted that there exists many different models for the platinum oxide evolution. In contrast to Section 3.1.6.1, here another model is used which represents the hydrogen peroxide oxidation better.

Subsequently, this complex breaks down into the zero oxidation state of platinum, H_2O and O_2 which is caused by an internal electron transfer:

$$Pt(OH)_2H_2O_2 \rightarrow Pt+2H_2O \tag{3.21}$$

Finally, the electrochemical regeneration of the platinum oxide layer results in a current signal:

$$Pt+2H_2O \rightarrow Pt(OH)_2+2H^+ +2e^- \tag{3.22}$$

3.2 Introduction to immunoassays

Immunoassays are analytical methods employing antibody-antigen interactions for the detection and the quantification of biomolecules in various research areas and applications, primarily in medical diagnostics [23, 25, 150–152]. Comparing with the chromatography (e.g. high-performance liquid chromatography - HPLC or gas chromatography) and the mass spectroscopy, immunoassays are the most frequently used measurement technique due to their speed, simplicity, and comparatively low costs [153–155]. Nowadays, the application area of immunoassays ranges from pharmaceutical, veterinary, environmental, forensic, and food sciences to medical diagnostics, and military [25].

As already mentioned, immunoassays are based on the employment of antibodies which can recognize and bind to their specific antigens[2], the analyte of interest, even in the presence of hundreds of other substances in a sample solution [25, 156]. Antigens range from larger substances like cells and macro-biomolecules to smaller molecules such as haptens (e.g. fluorescein, biotin and digoxigenin), hormones and low-molecular weight analytes (e.g. drugs and pesticides). Antibodies, also known as immunoglobulins (Igs), are large glycoproteins. They are synthesized by some white blood cells and play an important role in immune recognition as well as in the immune response system. The structure and properties of antibodies and the antibody-antigen interaction will be briefly summarized in Section 3.2.4.

The monitoring of these antibody-antigen interactions is another key issue. This is realized either label-free (e.g. surface plasmon resonance (SPR) [150, 155] or by conductimetric and capacitive immunosensors [150] using a huge number of different labels including enzymes, fluorophors, redox molecules, radioactive isotopes, fluorescence quenchers, and luminescent compounds. Among all, SPR is the most powerful technique for studying real-time kinetics of immunoassays such as association, dissociation and equilibrium constants. However, it requires expensive and bulky instruments, and the analysis may last longer due to the needed sample preparation. Therefore, nearly all commercial immunoassays rely on labels which are typically chemically attached or conjugated to either the antigen or the antibody, depending on the immunoassay format [154, 156].

The basic idea of employing labeled antibodies for the antigen detection dates back to 1941 [157]. Albert H. Coons and his co-workers studied fluorescently (fluorescein isothiocyanate - FITC) labeled antibodies for the antigen screening in tissues and demonstrated for the first time, that the labeled antibodies can still bind to their antigens. Almost 20 years later, the principles of immunoassays (radioimmunoassay - RIA) were first presented by Yalow and Berson for the detection of plasma insulin levels in men [158, 159] and subsequently, by Ekins for the estimation of thyroxine in human plasma [160].

In the RIAs, a known concentration of the radioisotopically labeled antigen (tracer) and a variable number of unlabeled antigens, the analyte, from the sample such as blood, plasma, or urine compete with each other to bind to limited amount of antibodies. Ra-

[2] Abbreviation of antibody generator.

dioimmunoassays are extremely sensitive owing to the combination of the high detectability of radioisotopes with the extraordinary specificity of antibody-antigen interactions [23, 150, 161]. Yet there are several drawbacks: (i) Short lifetime of radioisotopic labels, (ii) need for a specialized equipment, (iii) special precautions due to health hazard of radioactive substances and (iv) requirement for radioactive waste management [154].

To overcome these bottlenecks, Engvall and Perlmann [162] presented the enzyme linked immunosorbent assay (ELISA) for the first time in 1971. They combined the technical advances in three different research areas of immunohistochemistry, serology and RIA [163].

First, they came up with the idea to substitute the radioactive isotopes in RIAs with enzymes in the light of the new developments for labeling antibodies with enzymes in the immunohistochemistry. As mentioned previously, the labeling of antibodies with fluorescent quenchers by Coons *et al.* in 1941 was a huge milestone in the histochemistry. Despite of the high sensitivity and specificity of this technique, there exist some critical issues such as the naturally arising autofluorescence. In 1966, two different research groups, Avrameas [164] and Nakane and Pierce [165], described simultaneously the employment of enzyme labeled antibodies in immunohistochemistry.

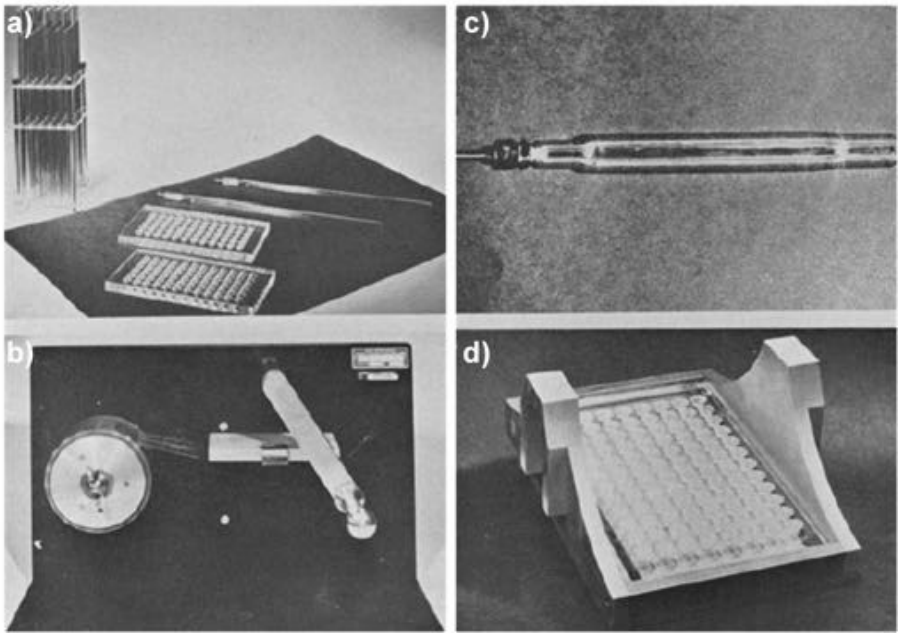

Figure 3.5: *a) Basic microtitrator system containing microtiter plates, modified pipette-dropper b), tape dispenser c) and special centrifuge carrier d) [166] (reprinted by permission from The American Association of Immunologists, Inc., Copyright 1962).*

Second, Engvall and Perlmann took the advantages of the employment of microtiter plates to perform large numbers of assays concurrently. The microtiter plate was invented in the early 1950‘s by Dr. Gyula Takatsy in Hungary to carry out serological investigations in

virology [167]. The early microtiter plates, shown in Figure 3.5, consisted of 6 rows of 12 "wells" with a diameter of 6 mm and each well had a volume of 75 µl. Later, John L. Sever and his colleagues modified it further and introduced a molded version [166].

Finally, Engvall and Perlmann made the decision to unify these different approaches by combining them with the solid phase assay concept, already known from radioimmunoassays. In 1967, Catt and Tregear introduced the solid phase RIAs by coating polymeric surfaces (e.g. disposable tubes) with antibodies via adsorption for the first time. This method offers outstanding advantages such as simplicity, speed, low costs and suitability for automation [168]. As a proof-of-concept assay, Engvall and Perlmann applied an ELISA to investigate IgG concentrations in rabbit serum using the enzyme alkaline phosphatase (AP). Almost simultaneously, Van Weemen and Schuurs [169] showed a similar approach to measure human chorionic gonadotropin[3] (HCG) in the urine by employing the enzyme HRP. Nowadays, the ELISA is applied in different fields and has became a standard tool in analytical research and medical diagnostics. In the next section, the ELISA method will be discussed in detailed.

3.2.1 Enzyme linked immunosorbent assay - ELISA

> "After all this time, it is surprising that ELISA has not been replaced by something more modern, such as the PCR, chemiluminescence, or something else. The reason? Few assay systems are as simple as the ELISA and require so little in terms of automation and equipment. There is beauty in simplicity."

Almost 40 years later, Eva Engvall describes the reason for the tremendous success of the ELISA technique with these words [170].

ELISA is a solid phase enzyme immunoassay (EIA). The basic principle is the detection of the antibody-antigen interaction bound to a solid phase (e.g. microtiter plate or sensor surface) using an enzyme as label. Many different enzymes can be employed as a label in ELISA, i.e. glucose oxidase (used in this work), horseradish peroxidase, alkaline phosphatase, beta-galactosidase (ß-gal) and urease. Each enzyme catalyzes a different chemical reaction that converts a substrate into a measurable product [150, 154, 171]. There exist four different detection techniques for ELISA: (i) Electrochemical, (ii) optical, (iii) microgravimetric, and (iv) thermometric. The commonly used ELISA detection strategies will be briefly explained in Section 3.2.6.

The ELISA technique owes its great success to its numerous advantages such as (i) high sensitivity and specificity comparable with RIA, (ii) low costs, (iii) requirement for small sample volumes, (iv) fast assay times, (v) easy detection using automated and high throughput systems without any need for special equipment or radioactive labels, (vi) very versatile, (vi) offering a possibility for point-of-care devices. Besides these advantages some problems may also occur when dealing with the ELISA technique including (i) non-specific binding of antibodies or antigens, (ii) the efficiency of wash procedure, (iii)

[3] HCG is a hormone and its presence in urine indicates most likely the pregnancy.

yield and purity of enzyme-labeled antibodies or antigens, (iii) effect of enzyme labeling on the antibody-antigen binding characteristics, (iv) enzyme stability, (v) low reliability compared with RIA [171, 172].

3.2.2 Classification of enzyme immunoassays

Various types of different enzyme immunoassay systems are reported in the literature. Depending on their underlying working principle, they can be categorized. In Figure 3.6, the common types of ELISA are illustrated schematically.

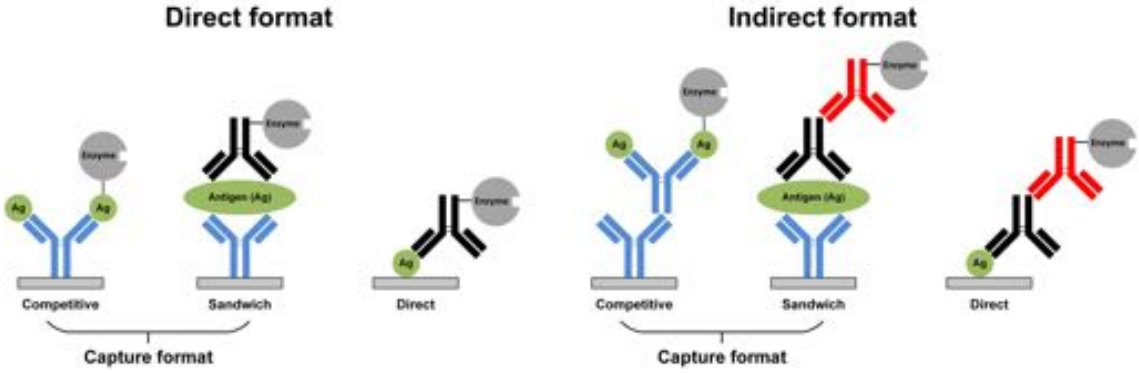

Figure 3.6: *Schematics of different ELISA formats for antigen detection.*

3.2.2.1 Heterogeneous vs. homogenous

Enzyme immunoassays are divided into two major categories: Heterogeneous and homogeneous assays. In the homogenous EIAs, the activity of the enzyme label will be modified (or even inactivated) by the antibody-antigen interaction. Therefore, no separation step such as washing of bound and free label is required prior to detection. This change in the enzyme activity is a proportional measure of the analyte concentration. Homogenous EIAs, owing to their procedural simplicity which is the result of any required separation step, offer generally a cheap and fast detection as well as monitoring of small analytes (e.g. therapeutic and abused drugs). On the other hand, they usually suffer from their low sensitivity because of non-specific interactions with the interferents in the specimen (matrix effect).

In the heterogeneous EIAs, the bound analyte is to be separated from the free analyte through different washing procedures. This separation is applied after the antibody-antigen reaction in order to impede any interference of any other molecules in the sample solution. Therefore, the assay procedure is more complex than the homogenous EIAs comprising one or more washing step(s) and mostly an immobilization process (solid phase EIAs). Nevertheless, heterogeneous EIA formats are more often used because of their high sensitivity and specificity [25, 152, 171, 172].

3.2.2.2 Direct vs. indirect

Solid phase enzyme immunoassays can be split up again into two different formats based on the signaling method of the employed label, direct or indirect. As already reported, the direct ELISA method was the first ELISA technique and thus, pioneered other ELISA formats [162, 169]. This method can be used for the antigen detection only.

At first, the antibody or antigen is bound directly to the solid phase. Depending on the preferred capture format (see Section 3.2.2.3), further steps will be followed. Finally, an enzyme labeled antigen or antibody facilitates the detection [172].

The indirect ELISA technique was introduced in 1978 by Lindström and Wager [173]. In this format, the antigen-antibody binding is visualized by the employment of an another antibody tagged with enzyme. Comparing to the direct format, this method offers more flexibility and high sensitivity due to the universal applicability of the enzyme labeled antibody, and the binding of more than one enzyme conjugated antibody to a single antigen, respectively. However, it needs an additional incubation and washing step resulting in longer assay preparation times. The achieved high sensitivity compensates for this minor drawback. Therefore, the indirect method is the most commonly utilized ELISA format nowadays [171, 172].

3.2.2.3 Capture format

Heterogeneous EIAs can be distinguished also with their format to capture the analyte, competitive and non-competitive (mostly sandwich) assays.

In the competitive ELISA, the milestone of the analyte detection is the competition between the enzyme labeled (tracer) and unlabeled (analyte) antigen or antibody, respectively. This technique was first described in 1976 by Yorde *et al.* [174] for the HCG measurement. Herein, the solid phase is coated with a specific antigen/antibody depending on the analyte of interest. The tagged and untagged antibody or antigen then compete with each other for the limited number of specific binding sites coated on the solid surface. The lower the analyte concentration in the specimen is, the higher amount of tracer interacts with the antibody or antigen, thus the higher is the signal, or vice versa [154, 172]. Hence, the measured signals are inversely proportional to the analyte concentration and usually given as B/B_0 by the ratio of the number of bound labels in the presence B and in the absence of the sample B_0 [175]. This favors the competitive ELISA for the quantification of antibodies or antigens in sample at very low concentrations.

Standard calibration curve of a competitive ELISA is illustrated in Figure 3.7a and exhibits a characteristic sigmoid shape with a negative slope [25]. This assay format is often used for the detection of low-molecular weight analytes with only one epitope, or antibody binding site (e.g. drugs and hormones), and biomacromolecules including DNAs and proteins, mostly antibodies against disease-causing organisms (e.g. HIV virus in AIDS) [152, 171].

In non-competitive assays, an excess of antibodies is employed for the antigen detection. There are many different methods to visualize the antibody-antigen interactions [156].

The sandwich ELISA, most widely used non-competitive assay format, was introduced in 1997 by Kato and his co-workers for the first time [176].

In the sandwich format, the analyte is caught in between two antibodies and so, this is called "sandwich ELISA". The first antibody, the capture antibody, is immobilized on a solid phase followed by subsequent blocking. After adding the sample, the analyte is trapped by the capture antibody. The presence of bound analyte is detected using a secondary antibody coupled to an enzyme. Washing steps after each incubation allow the removal of unbound compounds and prevent eventual non-specific interaction. Depending on the amount of the antibody-antigen-antibody complexes, the measured signals are directly proportional to the analyte levels in samples. A typical calibration curve is shown in Figure 3.7b [25, 171, 172].

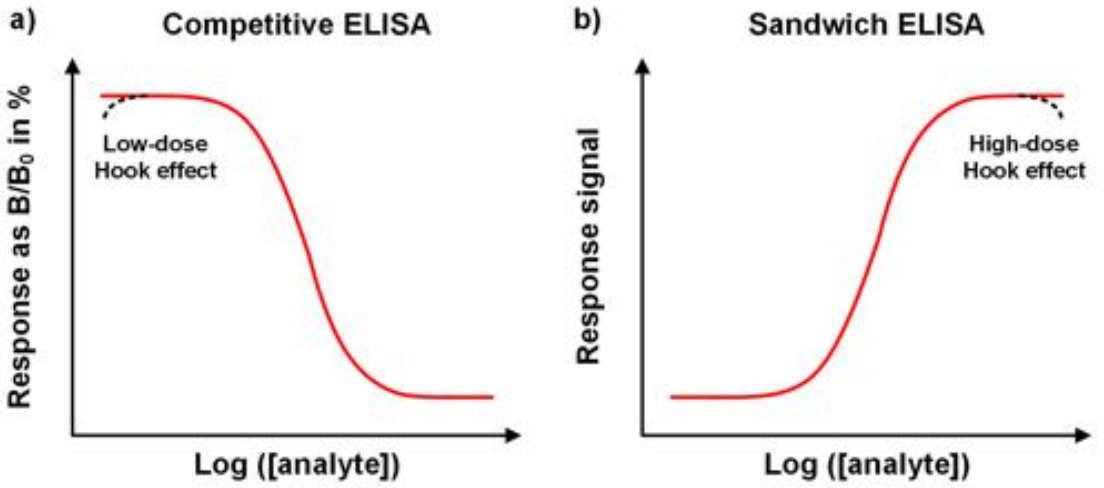

Figure 3.7: *Schematics of the response signals for the calibration curves of the a) competitive and b) sandwich ELISA. In both formats, a low-dose or high-dose Hook effect can occur at very high or very low concentrations, respectively (adapted from [25]).*

The sandwich ELISA is widespread for the quantification of high molecular weight analytes with two or more different binding sites, epitopes. Comparing with competitive assays, this format offers higher sensitivity and selectivity due to the two recognition steps employed for the detection [152].

In both ELISA formats, a decrease in the measured signals, also referred to as Hook effect, may occur at very low or very high concentrations of analyte, respectively. In competitive ELISA, the low-dose Hook effect can be noted at very low analyte concentrations. Here, the number of the antibody-antigen bindings can exceed the number found at zero concentration, resulting in lower signals. On the other hand, the high-dose Hook effect can be observed at very high concentrations of analyte in sandwich ELISA. In this case, an excessively high number of analytes saturates simultaneously not only the capture but also the secondary antibodies and thus, prevents the formation of the sandwich complexes.

It is possible to avoid the high-dose Hook effect by the employment of sufficiently high concentrations of capture and secondary antibodies [25].

3.2.2.4 Multi-analyte immunoassays

The concept of the "multi-analyte" immunoassays (MAIs) was first described in 1989 by Ekins [23] to allow the simultaneous detection of multiple analytes in the same low-volume sample. MAIs represent a simple, fast and low-cost alternative method for the detection of multiple analytes on-site.

There are many different approaches for the realization of MAIs including the application of immunoassays with either different enzyme- or fluorescence-labeling, or various single-analyte immunoassays combined with diverse sensor technologies by parallelization. Overcoming their current bottlenecks such as their complexity, sensitivity and selectivity, MAI platforms will have a great impact on medical diagnosis, especially on point-of-care diagnostics, in foreseeable future [24, 25].

3.2.3 Immobilization strategies for biomolecules

The immobilization of biomolecules is a key issue for the immunosensor performance characteristics like sensitivity, selectivity, and reproducibility. Thereby, the quality of the chosen immobilization method and surface passivation technique have a huge impact [177].

The attachment of biomolecules onto the surface with a very high density is generally desired in sensor applications. The non-specific adsorption of proteins should be avoided or at least diminished to stimulate the immunoassay performance. Furthermore, the active binding sites of the biomolecules should ideally be accessible for the coupling of other assay components (e.g. antibodies, enzymes, etc.). Any steric hindrance of these binding sites, caused by the applied immobilization technique, or by neighboring proteins, may lead to partial or complete loss of protein activity. Usually, the uncoated surface should be passivated by a so called blocking agent[4] (e.g. bovine serum albumin - BSA and ethanolamine - EA) after the protein immobilization in order to minimize non-specific adsorption of other biomolecules [177, 178].

There is a wide variety of protein immobilization methods, as shown in Figure 3.8, which differ largely from each other depending on various factors like immobilization surface, biomolecule properties, and assay performance characteristics. They can be categorized into (i) physical, (ii) covalent, (iii) bioaffinity immobilization and also (iv) different combinations of them. Usually, the immobilization methods are employed in combination with a spacer to maintain protein functionality. In the following, the specific aspects of these immobilization strategies will be presented.

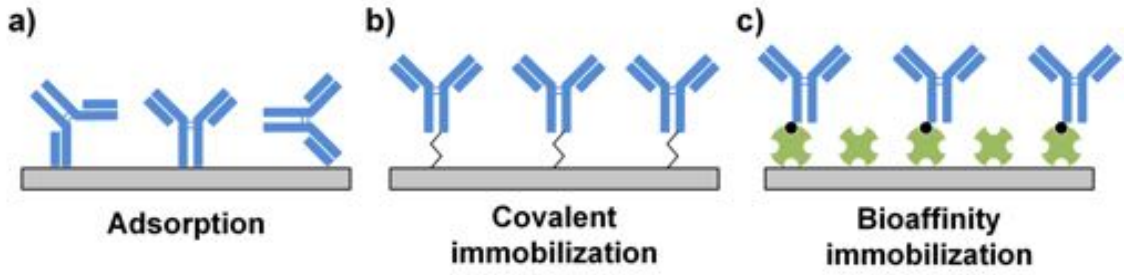

Figure 3.8: *Schematics of the common immobilization strategies for biomolecules: a) Adsorption, b) covalent, and c) bioaffinity immobilization (adapted from [178]).*

3.2.3.1 Physical immobilization

The easiest way to couple biomolecules onto a surface is adsorption (i.e. physical immobilization). In general, adsorption of proteins to diverse surfaces occurs via intermolecular forces including hydrophobic, electrostatic, van der Waals forces, or the combination of

[4]Blocking agents are proteins or chemical compounds which show no binding affinity for the assay component.

them. Therefore, environmental factors like pH, ionic strength and temperature of the reagents play a crucial role.

Compared with the other crosslinking methods, adsorption offers a weak protein attachment together with a heterogeneous and random orientation. The adsorption density of proteins relies on their geometric sizes, as well as the physicochemical surface characteristics. In the case of an immobilization with high-density packing the active sites of proteins could be sterically blocked. This may be again overcome by the introduction of a spacer molecule.

Mostly, the adsorption occurs spontaneously and quickly resulting in short incubation times and simple assay protocols. Thus, it can be applied as an intermediate immobilization step (e.g. for the spacer attachment) of an immunoassay in combination with another immobilization technique. Drawbacks of the adsorption are the steric hindrance of proteins, in case of a high-dense attachment, random and unstable non-covalent binding and mostly high non-specific interactions compared to other strategies [177, 178].

3.2.3.2 Covalent immobilization

There are various functional groups in proteins, especially in the amino acid side chains, which are well-suited for the covalent immobilization of proteins to different surfaces using a wide range of conjugation chemistry. Thereby, amino acids, which exist already at the surface of the protein, react via their side chain residues with the activated surface. So that, an irreversible binding with a high surface coverage is formed.

The covalent bonds through the side chains of amino acids (non-specific immobilization) are usually random. If an oriented and reproducible immobilization of proteins is desired, then the so called site-specific immobilization should be used. This method includes biomolecules as spacer, conjugation of the biomolecules with functional groups, or tailoring of the surface, or both. The well-defined attachment of proteins results in a covalent immobilization with a high reproducibility and conformational stability. Thus, the partial or complete loss (denaturation) of the protein activity is avoided.

Disadvantages of the covalent immobilization are (i) the denaturation of proteins (in case of the non-specific immobilization), and (ii) the use of toxic and complicated linkage chemistry, which requires long activation and incubation times of the surface and proteins, respectively [177, 178].

Carbodiimide crosslinker chemistry

Carbodiimide chemistry is the most widely employed and versatile method for labeling or immobilization of biomolecules containing primary amines (-NH_2) to carboxylic acids (-COOH) through covalent amide bond. The most popular carbodiimide for aqueous crosslinking chemistry is the water-soluble N-ethyl-N´-(3-(dimethylamino)propyl)carbodiimide, also known as EDC. In general, carbodiimides are regarded as zero-length carboxyl-to-amine crosslinkers, because there exist no additional spacer arm between two conjugated

molecules. To obtain high efficiency for the activation reaction, EDC chemistry must be performed in buffer solutions, excluding carboxyls and amines, under acidic conditions (pH around 4.5). Usually, the MES buffer (4-morpholinoethanesulfonic acid) is used for the carbodiimide chemistry [179, 180].

EDC catalyzes the formation of amide bonds between carboxylic acid and amine groups, whereas its by-product is released as a soluble urea derivative. First, an O-acylurea intermediate is formed by activating the carboxylic acids with carbodiimide. This active intermediate can further react pursuant to four competitive ways: (i) Directly by a nucleophilic attack of amine groups, or (ii) indirectly through the formation of an anhydride, which occurs by dehydration of the O-acylurea with a neighboring carboxyl group, followed by a nucleophilic attack of amines to form amide, and (iii) by a N-acylurea, its unreactive side product, via an intramolecular acyl transfer, and (iv) by the regeneration of the O-acylurea intermediate back to carboxylic acids by the hydrolysis. The achieved activation yield suffers from the use of the O-acylurea as amine reactive intermediate [179–182].

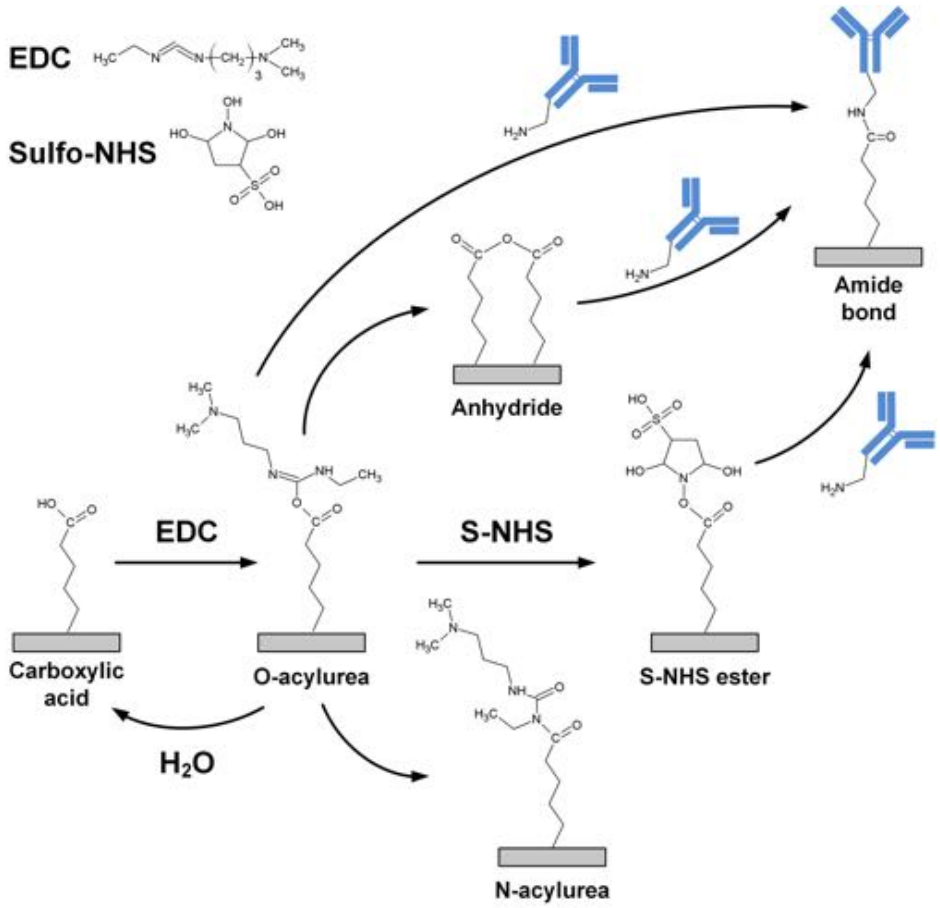

Figure 3.9: *Schematics of the activation mechanisms involving probably in the EDC/Sulfo-NHS chemistry (adapted from [179–181, 183]).*

N-hydroxysuccinimide (NHS) and water-soluble Sulfo-NHS are often employed as activating reagent together with EDC to form NHS esters of carboxyl acids. These amine-reactive esters provide a higher stability than the O-acylurea intermediate and react with the primary amines of biomolecules further to form amide bonds. Overall, EDC chemistry in combination with NHS highly enhances the coupling efficiency at physiological pH and allows to run a two-step activation [180–183]. The schematics of molecular activation mechanisms, which are thought to play a part in the EDC/Sulfo-NHS chemistry, is presented in Figure 3.9.

3.2.3.3 Bioaffinity immobilization

Bioaffinity interactions allow a quite strong and oriented immobilization of proteins using specific binding natural phenomena. This leads to a minimization of the effects caused by the non-specific adsorption as well as the steric hindrance of the protein binding sites in comparison to other immobilization techniques (e.g. adsorption and non-specific immobilization) with random orientation. Furthermore, due to the reversibility of the bioaffinity reactions using heat, chemical treatment, or pH change it is possible to detach the biomolecules and use the same surface repeatedly.

Usually, the bioaffinity interaction is employed for the immobilization of the biomolecules of interest in combination with the capture molecules attached by one of the previously described methods on the sensor surface. The most commonly used bioaffinity interactions in immunoassays are (i) avidin-biotin binding, (ii) protein A/G-antibody (iii) tagged protein-antibody (e.g. His-tag), (iv) aptamer, (v) DNA hybridization, and (vi) affinity capture ligand systems [177, 178].

Avidin-biotin system

The interaction of avidin and biotin is the strongest known non-covalent interaction with a dissociation constant $K_D = 10^{-15}$. Avidin is a tetrameric glycoprotein (69 kDa) containing four biotin-binding sites. On the other hand, biotin, also known as vitamin B, is a small molecule which allows an easy and effective conjugation to proteins without effecting their activity or conformation. Due to its specificity, fast kinetics and stability against pH and temperature changes, or denaturing agents, the avidin-biotin system is one of the most used bioaffinity interaction [177, 178].

3.2.4 Antibody

Antibodies are flexible Y-shaped glycoproteins produced by white blood cells, also called B-lymphocytes, of the immune system in response to its specific antigen. Despite their different physicochemical characteristics and functionalities, antibodies have the same basic structure of a heterodimer comprising four polypeptide chains: two heavy chains H_C (50-70 kDa) and two light chains L_C ($\approx$ 25 kDa) attached together by disulfide bridges and non-covalent bonds. Each chain has a constant domain C (C_{H1}, C_{H2}, C_{H3} and C_L,

respectively), which defines its isotype, and a variable region V (V_H and V_L, respectively) acting as the antigen-binding site.

The class and functionality of the antibodies are given by the structure of the constant region of its heavy chains. There exist five different main classes of immunoglobulins based on their isotopes: immunoglobulin G (IgG), immunoglobulin D (IgD), immunoglobulin M (IgM), immunoglobulin A (IgA), and immunoglobulin E (IgE). Among them, IgG is the most abundant one in the human serum and is usually employed for the immunoassay design. They can be divided into different subclasses such as IgG1, IgG2, IgG3, and IgG4 according to the carboxy-terminal part of their heavy chain. The molecular weight of IgG antibodies are about 150 kDa.

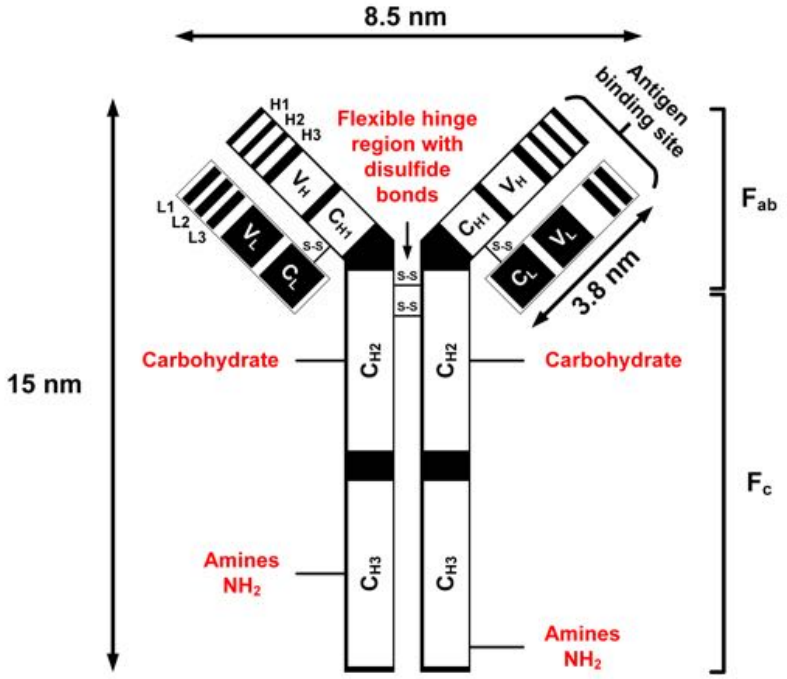

Figure 3.10: *Structure of an IgG antibody and its labeling sites (adapted from [25, 184, 185]).*

The antigen specificity of antibodies is defined by their variable regions which differ from each other. Each variable region includes three different hypervariable segments (L1, L2, L3 and H1, H2, H3, respectively), also called complementarity-determining regions (CDRs). The CDRs from both, the heavy and the light chains, constitute the very selective antigen-binding sites, so-called paratopes, at the tip of each arm of IgG antibodies. Different combinations of heavy- and light-chain V regions contribute to antibodies the ability to bind a specific antigen, thus arising the well-known and outstanding antibody diversity [25, 152, 184].

All immunoglobulins can be cleaved at their polypeptide sequences by different proteolytic enzymes (proteases). This allows the study of the activity and stability of a specific

antibody fragment without any interferences from the other parts. The most widespread used enzymes are papain and pepsin. Papain cleaves the antibody in one F_c (fragment crystallisable) fragment and two identical F_{ab} (fragment antigen binding) fragments by cutting its disulphide bonds on the amino-terminal side. In the case of the protease pepsin, the immunogloblin is cleaved on the carboxy-terminal side of its disulphide bridges to generate one $F_{(ab')_2}$ fragment and several small F_c fragments. The $F_{(ab')_2}$ and F_{ab} fragments show the exact same antigen-binding characteristics as the antibody itself. Thus, they are employed for the therapeutic and diagnostic applications in medicine [184].

Traditionally, the production of antibodies can be realized by the immunization; exposing (most commonly vaccination) an animal (e.g. mouse, sheep, goat, rabbit and rat) with an antigen in a controlled manner. In this case, the serum of these animals includes antibodies with different features showing idiosyncratic affinity and specificity to a different epitope of the given antigen. Such antibodies are termed as polyclonal, and are relatively easy and cost-effective to produce. However, their given properties may differ if hosted in different animals. On the other hand, César Milstein and Georges J. F. Köhler introduced the so called monoclonal antibodies in 1975 [186]. They are produced by the hybridoma technique, where antibody-producing B cells fused with immortal myeloma cells. Monoclonal antibodies feature the single specificity and affinity towards its antigen [25, 152].

3.2.4.1 Labeling and immobilization sites

For the decision of the appropriate conjugation strategy, it is important to understand the functional groups available on an antibody [187]. In general, three reactive targets, as illustrated in Figure 3.10, on antibodies are mainly favored for the immobilization and labeling strategies:

Amines (-NH_2)

Antibodies are frequently crosslinked via amino groups because of their large quantity in antibodies as well as the simplicity, speed, ease handling, high yield and low cost of their conjugation reaction. Amines can be found mainly on lysine residues. The most popular and efficient amine-based conjugation technique is the use of N-hydroxysuccinimide esters (NHS esters) resulting in a stable amide bond. The only drawback of this strategy is the risk of a significant decrease in the antigen-binding capacity of the antibody.

Thiol groups (-SH)

Besides the amines, sulfhydryl groups can also be chosen as labeling target of antibodies due to their specificity and higher reactivity towards maleimide-activated crosslinkers and reagents. But there exist a small number of thiol groups on antibodies which makes the labeling very specific. These thiol residues are crucial for the stabilization of the antibody structure as they are involved in disulfide bonds either in the hinge region, or between the heavy and light chains. Therefore they are not directly available for cross linking. The disulfides in the hinge region can be selectively reduced to obtain free thiol groups

available for the antibody conjugation, whereas the antibody is cleaved into monovalent halves without effecting its antigen-binding capacity. In contrast to amine-based strategies, sulfhydryl labeling offers many advantages including high labeling specificity, low non-specific binding and preservation of antibody functionality.

Carbohydrates (sugars)

Glycosylation sites of antibodies are mainly located in the F_c part. Modification of carbohydrates is more complicated than other techniques because their hydroxyl groups have to be first oxidized to generate the reactive aldehydes (-CHO) which can then be used for the covalent binding. However, carbohydrate targeted method shows hardly ever considerable effects on their antigen-binding activity.

3.2.4.2 Antibody-antigen interaction

The centerpiece of every immunoassay, independent of its detection technique, is the interaction between the antibody and the antigen. Therefore, in order to design and/or to optimize an immunoassay, it is very important to understand the basic mechanism and the reaction kinetics behind it.

The forces, or bonds, participating in the antibody-antigen interaction are non-covalent forces including hydrophobic, electrostatic and van der Waals forces, and hydrogen bonds. Thus, the binding reaction is reversible. Different parameters such as temperature, pH and ionic strength of the specimen and the presence of detergents or organic solvents play an important role on the reaction kinetics by promoting either the association or dissociation of antibody-antigen complexes. There exist no covalent bonds between antigens and naturally produced antibodies [25, 184].

Depending on the involved antibody and its antigen, the contribution of these different forces to the overall reaction varies. Nevertheless, the hydrophobic and van der Waals forces are valid at very short distances and help to contract two specific complementary shapes which fit exactly into each other. On the other hand, hydrogen bonds, bridging oxygen and/or nitrogen atoms, and electrostatic forces between the oppositely charged side chains of the epitopes and the paratopes enhance the strength of the overall interaction. Additionally, they accommodate reactive sites or distinctive features [184].

The antigen-antibody interaction can be expressed with the Law of Mass Action as follows:

$$[\text{Ag}] + [\text{Ab}] \underset{k_d}{\overset{k_a}{\rightleftharpoons}} [\text{Ag-Ab}] \tag{3.23}$$

where [Ag-Ab] is the antigen-antibody complex and k_a and k_d are the association and dissociation rate constants, respectively.

The ratio of the association and dissociation rate constants presents the bound strength of the antigen-antibody complex and is known as the affinity constant. It is a key property about the functionality of an antibody in an immunoassay.

At equilibrium $\left(\frac{d[\text{Ag-Ab}]}{dt} = 0\right)$, the affinity constant, also called the equilibrium constant K_{eq} , can be described as

$$K_{eq} = \frac{k_a}{k_d} = \frac{[\text{Ag-Ab}]}{[Ag] \cdot [Ab]}. \tag{3.24}$$

3.2.5 DNAs as biomarkers

Deoxyribonucleic acid (DNA) is the most important biomolecule storing the genetic informations of all known living organisms. It is a nucleic acid comprising one or two biopolymer strand(s) which are again polynucleotides. Each nucleotide consists of a sugar phosphate backbone[5] as well as one of the four different bases: Adenine (A), cytosine (C), guanine (G) and thymine (T). These nitrogenous bases can bind two single DNA strands specifically to each other, adenine with thymine and cytosine with guanine, via hydrogen bonds and thus, form the double-stranded DNA, also known as double-helix [188].

DNAs play not only a key role for genetics but they are also of great interest in analytical and technical use. For example, DNA-protein interactions are an essential component of almost all cellular functions including DNA replication, translation and transcription as well as DNA damage recognition and repair. Therefore, the modification of proteins with certain DNA-binding and/or labeling sites, or the direct application of DNAs as biomarkers have became more of an issue for life sciences in recent years. DNA markers have profited highly from the blooming DNA sequencing techniques and from many excellent results in biological and medical research. In general, DNA can also be considered as a very robust material thanks to other outstanding physical and physico-chemical properties favoring it as a versatile tool for the nano-biotechnology [188, 189].

3.2.5.1 DNA-based antibiotic assay

In this thesis, DNA-based antibiotic assays for tetracycline and pristinamycin were gauged to prove the applicability of the microfluidic multiplexed biosensor platform for the simultaneous multi-analyte detection in clinically relevant samples. A brief description of their assay principle will be given in this subsection.

Some prokaryotes possess a characteristic resistance mechanism against various classes of antibiotics such as tetracyclines, macrolides or streptogramins. This mechanism involves an antibiotic-dependent DNA-binding protein, also called repressor, (e.g. TetR, PIP, MpHR(A) protein), which specifically binds to its corresponding operator DNA (e.g. tetO, pir, etr) and is released in a dose-dependent fashion in the presence of antibiotics. The repressor proteins recognize a specific core structure of the antibiotic, that is common in a whole class of antibiotic. This makes them not only suitable for the detection of

[5]The sugar phosphate backbone comprises alternating deoxyribose sugars and phosphate groups, and determines the directionality of the DNA.

a single antibiotic but also for the entire antibiotic family including a pallet of different antibiotics (e.g., tetracycline, chlorotetracycline, demeclocycline, etc.). Another advantage of these systems is the high specificity and sensitivity of the repressor to its antibiotics (e.g. $K_A = 10^9\,\mathrm{M}^{-1}$ in the case of TetR and tetracycline [190]). Such a prokaryotic antibiotic response mechanism can be engineered and transferred in a cell-free environment to be employed as recognition element in a biosensor platform enabling the dosing of various classes of antibiotics, for example [28, 34, 191].

The working principle of a DNA-based antibiotic assay is illustrated in Figure 3.11. The substrate surface is coated first with the biotinylated operator DNA by avidin or streptavidin and subsequently blocked to prevent any unspecific binding. Secondly, the His-tagged antibiotic repressor is added and binds to its operator DNA. In the presence of the class-specific antibiotics, it is released from the DNA depending on the antibiotic concentration in the sample. The signal readout is usually performed optically by a primary anti His-tag antibody followed by a secondary antibody labeled with an enzyme, e.g. HRP or GOx. Please note that the common DNA-based antibiotic assays require two separate incubation steps for the sample and immunoassay-based labeling [28, 34].

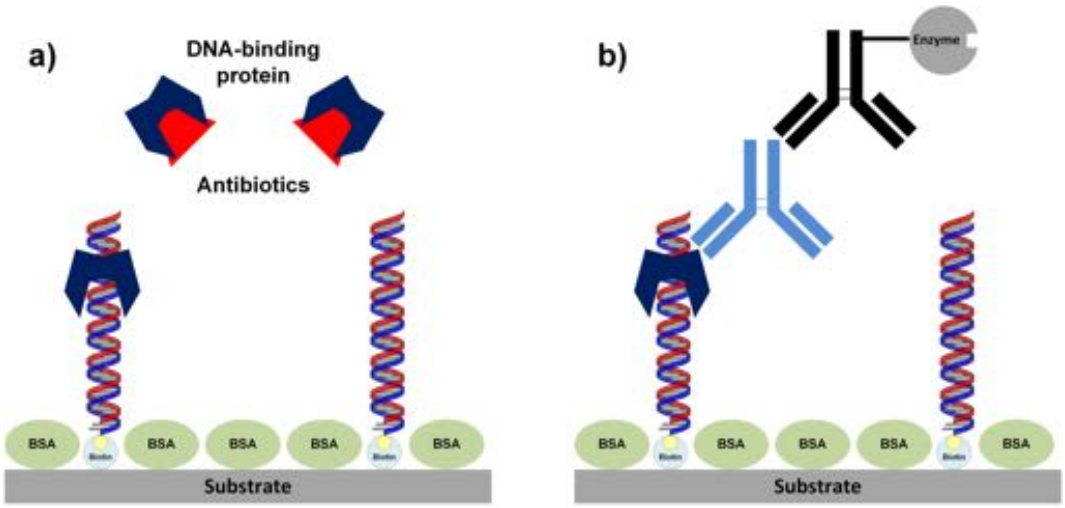

Figure 3.11: *Working principle of a DNA-based antibiotic assay: a) The biotinylated operator DNA is immobilized via avidin on the substrate. After blocking, the His-tagged antibiotic repressor is introduced and bind to its operator DNA. In the presence of the class-specific antibiotics, it is released from the DNA. b) The His-tagged proteins remaining bound to the operator DNAs are detected via anti-His antibodies followed by an incubation with secondary antibodies coupled to an enzyme (adapted from [28, 34]).*

3.2.6 ELISA detection strategies

Nowadays, the integration of enzymes into the conventional immunosensor design as presented in Figure 3.12 is frequently used. Each enzyme catalyzes a different chemical reaction and thereby, produces a measurable product which can easily be measured by different methods including (i) optical, (ii) electrochemical, (iii) microgravimetric, and (iv) thermometric detection. Additionally, due to their high catalytic activity the application of enzymes in immunoassays enhances the measured signal levels resulting in a better sensitivity with detection limits down to the attomolar range.

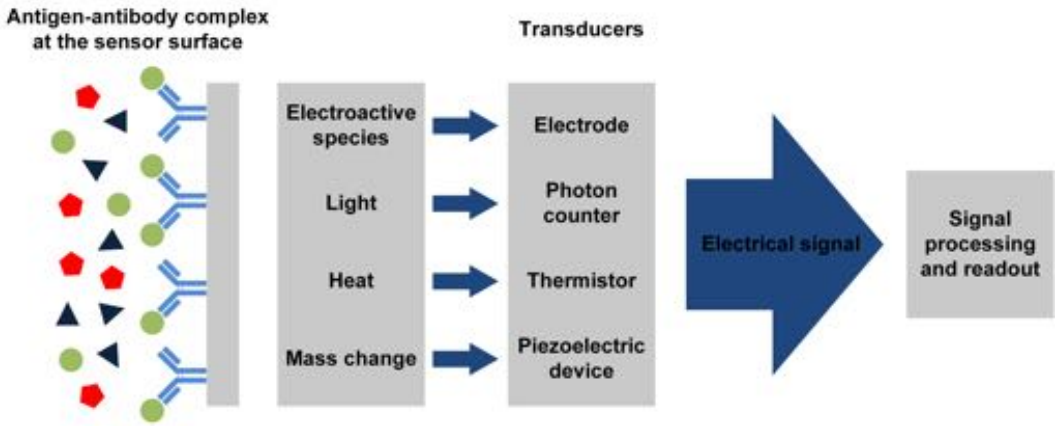

Figure 3.12: *Schematic representation of the conventional immunosensor design illustrating the interaction between the immunological recognition element at the sensor surface and the signal transduction (adapted from [150]).*

The optical and electrochemical readout are the most commonly used detection techniques for ELISA and will be explained shortly in the following [13, 150, 152, 156].

3.2.6.1 Optical detection

In optical immunosensors, the formation of the antibody-antigen complex produces either an optical signal (e.g. color or fluorescence), or a change in optical attributes of the environment like absorption, emission, reflectance, emission, optical path, or refractive index. Later, the optical readout is usually achieved by photodiodes or photomultipliers. Owing to their outstanding advantages such as the use of visible radiation, the non-destructive operating mode as well as the fast signal generation and readout, optical immunosensors are the most commonly used tool for the clinical analysis by far [13, 150, 192].

3.2.6.2 Electrochemical detection

Electrochemical methods are one of the most sensitive detection techniques for ELISAs. Here, the immune reactions (e.g. antibody-antigen complex) are measured by recording the changes in electrical activity. Furthermore, the electrochemical techniques are well suited for the miniaturization of the measurement devices as the electrochemical detection of the analyte takes place at the electrode/electrolyte interface. In comparison to the optical detection, the electrochemical immunosensors do not need transparent solutions and therefore, are theoretically able to execute measurements direct in real samples including whole blood, hemoglobin and fat globules.

There exist five major detection methods for electrochemical ELISA platforms depending on the measured electrical parameter: (i) voltammetric, (ii) potentiometric, (iii) conductometric, (iv) capacitive and (v) impedimetric. Some of the above-mentioned techniques, such as potentiometric, capacitive, impedimetric and in some cases also voltammetric, can be also applied as direct (label-free) immunosensors. These are capable to measure the physical changes during the formation of the antibody-antigen complex. In contrast, indirect immunosensors using labels as signal generators, facilitate a versatile detection with higher sensitivity despite their complexity. The electrochemical immunosensor platform proposed in this work is premised on the voltammetric detection (i.e. amperometric detection of hydrogen peroxide) which is mentioned detailed in Section 3.1.6.2.

An enzyme label for ELISA should fulfill the following properties:

- High catalytic activity
- Good overall stability (during the measurement and storage)
- Electrochemical detection of the enzyme activity
- Limited cross-reaction of the enzyme products
- Good compatibility under optimal conditions, such as pH, ionic strength and buffer composition, for the enzyme and immuno reaction

The most commonly applied enzymes for ELISA are alkaline phosphatase, peroxidases (e.g. HRP), glucose oxidase and ß-galactosidase [13, 152, 156].

3.2.7 ELISA data analysis

There exist a wide range of models and algorithms for the evaluation of the calibration data for ligand binding assays (LBAs). In comparison with chromatographic assays, the LBAs such as RIA and ELISA feature generally a non-linear behavior between the analyte concentration and the corresponding signal. Therefore, the choice of an appropriate calibration model is a crucial issue for the analysis of LBAs [193, 194].

3.2.7.1 Choice of the appropriate calibration model

The characteristic shape of the calibration curves for LBAs is sigmoidal including a minimum asymptote close to the background signal (non-specific binding) and a maximum asymptote around the infinite standard concentration. To evaluate such sigmoid-shaped calibration curves, the 4-parameter logistic (4-PL) model, as shown in Figure 3.13, is commonly applied as the reference model. The equation for the 4-PL fit can be described as follows:

$$y = \frac{A - D}{1 + \left(\frac{x}{C}\right)^B} + D \tag{3.25}$$

where y is the response signal, A is the zero concentration response, D is the infinite concentration response, x is the analyte concentration, C is the inflection point at IC_{50}, and B is the slope factor.

The 4-PL equation is a monotonic function which means it is either always increasing ($A < D$) or decreasing ($A > D$) with the analyte concentration. A perfect symmetry for the calibration curve around the inflection point IC_{50} appears at the concentration $C = \frac{(A+D)}{2}$ where the direction or the sign of the calibration curve changes. The slope factor B gives the steepness of the calibration curve.

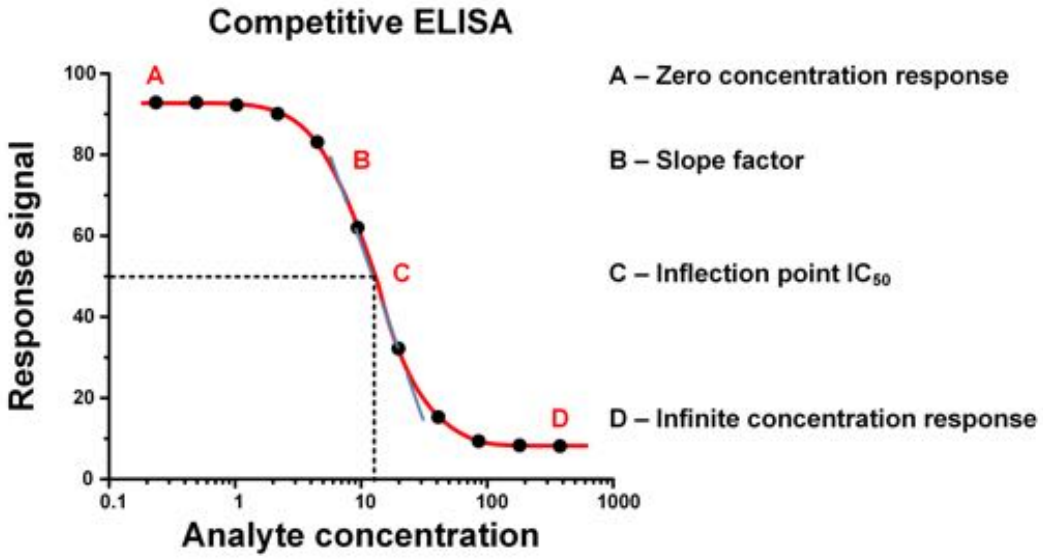

Figure 3.13: *Typical sigmoidal calibration curve for a competitive ELISA using the 4-parameter logistic model (adapted from [193, 194]).*

In general, the 4-PL function is not sufficient enough for the evaluation of the asymmetric concentration-response curve and so, additional modeling flexibility is needed. The use of the 5-parameter logistic (5-PL) model easily overcomes such a problem with asymmetry.

It includes a fifth parameter G which allows for the efficient fitting of an asymmetric calibration curve [193, 195]. The equation of a 5-PL function is given by

$$y = \frac{A - D}{\left(1 + \left(\frac{x}{C}\right)^B\right)^G} + D. \tag{3.26}$$

The 5-PL model should be used only when the calibration data proves clearly an asymmetric behavior. Otherwise, the addition of the fifth parameter can lead to the instability of the fitting algorithm [193].

Another popular choice due to its simplicity is a linear model using the transformed calibration curve data. Basically, this includes the transformation (often log or ln) of either one or both variables. In this case, the fit quality depends largely on the investigated assay range. Because of the imperfect linearization of this model, there exist some discrepancies mainly at the maximum of the calibration curve.

3.2.7.2 Optimal design for assay calibration

The model and fitting algorithms as well as the assay design with the number and the dilution of calibrator concentrations play a key role in the quality of the calibration [193, 194]. The recommendations for the 4-parameter logistic model are:

- At least 5 and not more than 8 calibration concentrations should be measured.
- The calibration solutions should be prepared and studied in duplicate or triplicate.
- The concentration row for the calibration curve should be logarithmic, typically of the power of 2 or 3.
- The middle calibrator concentration should be slightly higher than the inflection point IC_{50}.
- For the optimization of curve fitting, the so called anchor concentrations outside the range of quantification can be included in the calibration curve.

3.2.7.3 Assay performance characteristics

The most important characteristics of the assay performance are briefly introduced below:

Signal-to-noise ratio

Signal-to-noise ratio (SNR) is the ratio of the signal height of a specimen containing the analyte to the noise level. Noise is defined as the standard deviation (SD) of the signal if a sample without analyte (zero calibrator or control) is repeatedly measured. By increasing the signal level at a defined analyte concentration, and/or reducing the noise, an increased SNR can be achieved [25].

Signal-to-background ratio

Signal-to-background ratio (SBR) is the ratio of the signal height of a sample comprising the analyte to the control signal. Similar to SNR, an increase in the SBR can be obtained by enhancing the signal height at a defined analyte concentration.

Limit of detection

Limit of detection (LOD) is the smallest measured concentration of an analyte which can be determined in the specimen with reasonable reliability. In general, there are two approaches for the determination of LOD which are based on either (i) signal-to-noise ratio, or (ii) the standard deviation of the signal and the slope of the calibration curve. In case of the SNR-based method, the LOD is mostly defined as the analyte concentration which delivers signal levels equal to the control signal plus three times the SNR. For the second method using the calibration curve and standard deviation, LOD can be expressed as:

$$\mathrm{LOD} = \frac{3.3\,\sigma}{B} \tag{3.27}$$

where σ is the standard deviation of the control and B is the slope factor of the calibration curve [196].

Limit of quantification

Limit of quantification (LOQ) is the smallest measured concentration of an analyte, at which the analyte is quantified in the sample with acceptable accuracy and precision. Similar to the LOD measurement, there are also two approaches for the determination of LOQ which are again based on either (i) the signal-to-noise ratio, or (ii) the standard deviation of the signal and the slope of the calibration curve. For the SNR-based method, LOQ is usually defined as the analyte concentration which is necessary to obtain signal levels equal to the control signal plus ten times the SNR [196]. In case of the second method using the calibration curve and standard deviation, LOQ is given by

$$\mathrm{LOQ} = \frac{10\,\sigma}{B}. \tag{3.28}$$

Precision

The precision of an immunoassay shows the reproducibility of its results within (intra-assay precision) and between assays (inter-assay precision). The coefficient of variation (CV) is its measure and can be calculated as:

$$\mathrm{CV} = \frac{\sigma}{\text{mean value}}. \tag{3.29}$$

For clinical applications, the CV values used in testing are commonly less than 15 %. Intra-assay precision gives the reproducibility between wells within an assay and allows

to obtain similar results for the multiple replicates. The reproducibility between assays is called inter-assay precision and ensures the repeatability of the results using multiple assay kits over a specific time period [25, 196, 197].

Spike and recovery

In the so-called "spike-and-recovery" experiments, a known concentration of the analyte is added (spiked) into a specimen and the corresponding response is measured (recovered) by comparison to the calibration curve. The influence of the interfering substances on the immunoassay signals is usually determined by the "spike and recovery" measurements. Analyte concentrations of three different regions (low, medium and high) are spiked into the sample solution and then investigated for recovery [198].

3.3 Microfluidics

Recently, lab-on-a-chip systems with integrated microfluidics serve not only for analysis purposes but also for clinical applications including point-of-care testing. Therefore, it is very important to understand the fundamental laws of nature in microscopic dimensions. For example, surface related forces, such as surface tension or capillary forces, which are negligible at the macroscopic scale, play a key role in microfluidics. On the other hand, volume forces like inertia and gravity decisive for the macrofluidics become increasingly insignificant in LOC systems as the size shrinks [18, 199].

This section briefly summarizes the basics of microfluidics as well as the principles of the pressure-driven flow and the capillarity.

3.3.1 Fundamentals

In general, a material, which is continuously deformed under the application of external forces, such as shear stress, and does not return to its initial form after the cease of these forces, is defined as a fluid. They is likely to categorize them in two main classes, as liquids and gases, regarding the intensity of the dominant inter-molecular forces. The molecule densities of liquids and solids are comparable, and so liquids are usually considered as incompressible whereas gases as compressible. However, a clear distinction between solids and fluids cannot be made all the time. For example, there exist some solids such as hand cream or play-dough showing fluid behavior as soon as the exerted force reaches a threshold level [18, 200, 201].

3.3.1.1 Surface tension

As mentioned previously, the surface forces like surface tension or viscosity dominates the fluid behavior in microfluidic systems [18, 202]. To describe and understand the working principles of these forces, the Gibbs free energy G has to be studied. In thermodynamics, the Gibbs free energy is a measure for the energy of thermodynamic systems at a fixed pressure p and temperature T. In most instances, systems in equilibrium or quasi-equilibrium are of importance, where the Gibbs free energy is by definition at a minimum ($\Delta G = 0$).

The surface tension is a characteristic of fluids and occurs only at the interface between the fluids and the gases [18, 202]. In the bulk of a liquid, the intermolecular forces, such as van der Waals forces, applied to molecules are equal and distributed symmetrically. On the other hand, at the fluid-gas interface there is an imbalance of intermolecular forces towards the bulk of the liquid due to large intermolecular distances in the gases. To compensate these forces, the amount of the molecules in the interfacial region decreases, and thus causes an increase in the intermolecular distance. The energy, also known as surface tension, needed by the system for the reduction of this increased intermolecular distance

leads the surface molecules to contract and form an energetically favorable surface. The surface tension γ in $\mathrm{N\,m^{-1}}$ is given as the change of the Gibbs free energy per area at a constant pressure and temperature: $\gamma = \left(\partial G/\partial A\right)_{p,T}$.

3.3.1.2 Contact angle

Another basic concept belonging to the theory of the surface effects in microfluidics is the so-called contact angle. A liquid droplet placed on a solid surface, as illustrated in Figure 3.14a, forms in a characteristic shape depending on the three surface tensions acting at the liquid/solid/air interfaces. The resulting contact angle between the solid-liquid and the liquid-gas interface at the contact line is the measure of the wettability of fluids on a solid surface [18, 202, 203].

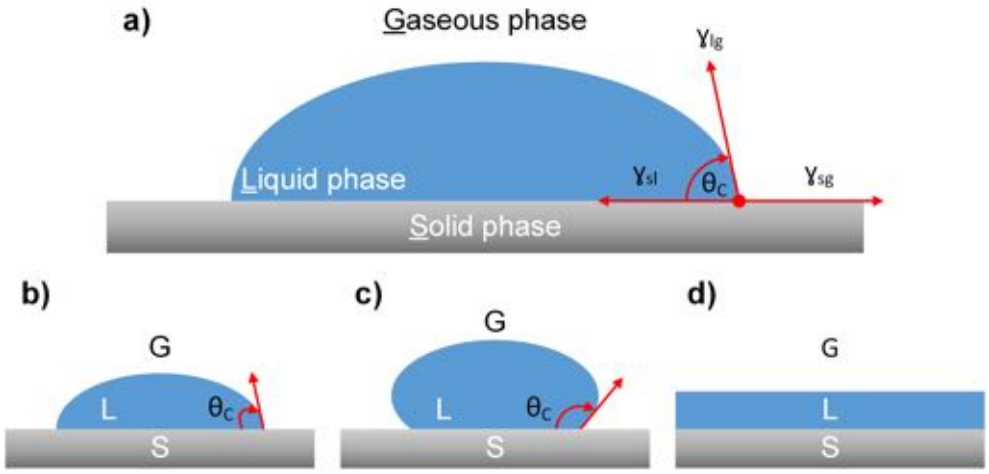

Figure 3.14: *a) Schematics of the contact angle θ_C and the surface tension γ_{ij} between the different interfaces (Liquid/Solid/Gaseous) i and j for a resting drop on a solid surface. b-d) The wettability of a fluid on a solid surface depends on the contact angle θ_C: The surface in b) shows high wettability ($\theta_c < 90\,°$, hydrophilic), in c) low wettability ($\theta_c > 90\,°$, hydrophobic), and in d) perfect wetting ($\theta_c = 0\,°$).*

Young's Law describes the relation between contact angle θ_C and surface tension γ as

$$\gamma_{sa} = \gamma_{sl} + \gamma_{la}\cos\theta_C \tag{3.30}$$

where γ_{ij} is the surface tension between the different interfaces (Liquid/Solid/Gaseous) i and j for a resting drop on a solid surface.

The wettability of a fluid on a solid depends on the contact angle θ_C. According to this, solid surfaces are mainly classified in three different groups, as shown in Figure 3.14b-d. A surface is termed as wettable to a given fluid if the contact angle $\theta_C = 0$, or partially wettable for $\theta_C < 90°$, while for fluids with $\theta_C > 90°$ is the surface described

as non-wettable. In the special case of water, wettable surfaces are also often called hydrophilic (water loving) and non-wettable surfaces hydrophobic (water fearing).

3.3.2 Principles of pressure-driven flow in microfluidic networks

To fathom the basics of microfluidics in lab-on-a-chip systems using pressure-driven flow (PDF), the hydrodynamic behavior of fluids in a conduit must be studied first [18, 199–201]. The solution of this hydrodynamic behavior can be deduced from the so called Navier-Stokes equation for incompressible (Newtonian) fluids excluding the body forces (gravitational and electrical forces):

$$\underbrace{\rho\frac{\partial\vec{\nu}}{\partial t}}_{\text{Rate of change momentum}} = \underbrace{-\rho\vec{\nu}\nabla\vec{\nu}}_{\text{convective force}} + \underbrace{-\nabla \mathrm{p}}_{\text{pressure force}} + \underbrace{\eta\nabla^2\vec{\nu}}_{\text{viscous force}} \tag{3.31}$$

where p is the pressure in Pa, ρ is the fluid density in $\mathrm{kg\,m^{-3}}$, η is the viscosity in Pa s (µ is also often used) and $\vec{\nu}$ is velocity vector in $\mathrm{m\,s^{-1}}$.

For the characterization of the flow regime (either turbulent or laminar flow) the dimensionless Reynolds number Re, which equals to the ratio between inertial forces and viscous forces, is used and can be calculated by

$$Re = \frac{\text{inertial forces}}{\text{viscous forces}} = \frac{\rho\nu D_H}{\eta} \tag{3.32}$$

where ν is the average velocity over the cross-section in $\mathrm{m\,s^{-1}}$ and D_H is the hydraulic diameter of the channel in m. The hydraulic diameter D_H is a geometric constant and given by

$$D_H = 4\frac{A}{P} \tag{3.33}$$

with the cross-sectional area A in $\mathrm{m^2}$ and P is the perimeter of the channel in m. Nowadays, the most popular channel geometries in microfluidic systems are rectangular defined mostly by technical limitations of the employed fabrication methods. In this case, the hydraulic diameter becomes

$$D_H = 2\frac{wh}{(w+h)} \text{ for } w \approx h \tag{3.34}$$

where w and h are the width and the height of the channel, respectively.

At low Reynolds numbers ($Re < 2300$) laminar flow will usually appear, whereas turbulent flow occurs at higher Re. For the microfluidic devices, Reynolds numbers are typically $Re \leq 1$ due to slow average velocities and small hydraulic diameters, and thus the inertial forces (e.g. gravitation) are negligible. For microfluidic immunosensor proposed in this work a Reynolds number of 1.18 was calculated by using a D_H of 0.113 mm, an average flow rate of $10.4\,\mathrm{mm\,s^{-1}}$ and typical values for ρ about $10^3\,\mathrm{kg\,m^{-3}}$ and η about $10^{-3}\,\mathrm{Pa\,s}$.

After the classification of the flow profile as laminar, analytical solutions to the Navier-Stokes equation is calculated by considering a steady-state PDF (fully developed laminar flow with unidirectional velocity field) in a long, solid and straight conduit. According to this, the rate of change momentum and the convection term can be neglected, and the Navier-Stokes equation is simplified to

$$\nabla p = \eta \nabla^2 \vec{\nu}. \tag{3.35}$$

Equation 3.35 gives the equilibrium between the net pressure force and the net viscous force. The flow velocity of the steady-state PDFs in microchannels, also known as Poiseuille flow, has a characteristic parabolic profile with the highest velocity in the center and zero velocity (no-slip condition) at the channel walls. Using these boundary conditions together with the geometric simplifications the area-averaged flow velocity at a particular point in a cylindrical conduit with a radius R is defined as

$$\nu(r) = \frac{R^2 - r^2}{4\eta} \left(-\frac{dp}{dx} \right) = \nu_{max}\,(r)\,(1 - \frac{r^2}{R^2}) \tag{3.36}$$

where the maximum velocity $\nu_{max}(r) = \frac{R^2}{4\eta}(-\frac{dp}{dx})$ at $r = 0$.

The volumetric flow rate[6] Q in a microchannel is the spatial integral of the area-averaged flow velocity, as given in Equation 3.36, and is expressed with the Hagen-Poiseuille's law for the pressure-driven steady-state laminar flow in a circular conduit

$$Q = \frac{\pi R^4 \triangle \rho}{8\eta L}. \tag{3.37}$$

For the most pressure-driven microfluidic networks the pressure drop along the channel length L is uniform and thus, the term $-dp/dx$ can be approximated to $\triangle p/L$.

Unexpectedly, there is not any analytical solution to the Navier-Stokes equation, as given in Equation 3.35, for the rectangular microchannels. Therefore, it is possible to calculate only as the summation of a Fourier series representing a solution for the Poiseuille equation. The volumetric flow Q for a rectangular duct with a channel width w and height h becomes simply

$$Q \approx \frac{h^3 w \triangle \rho}{12\eta L} \left[1 - 0.63 \frac{h}{w} \right], \text{ for } w > h. \tag{3.38}$$

This approximation for the volumetric flow rate Q shows unexpected good results with error values about 13 % even for the worst case ($h = w$) [18].

[6] The volumetric flow rate Q has a positive sign for a flow from the channel inlet to the outlet.

3.3.2.1 Electric circuit analogy

In order to describe the flow-pressure relation in complex microfluidic networks, comprising multiple channels connected via junctions, the well-known analogy between the hydraulic and electric circuits is used [18, 199, 201]. As aforementioned, the Hagen-Poiseuille's law (Equation 3.37) describes this flow-pressure relation in PDF systems and is analog to Ohm's law, $U = R \cdot I$. The equivalent circuit symbols for the electrical and fluidic resistors are illustrated in Figure 3.15. For this purpose, Hagen-Poiseuille's equation may be simplified as

$$\triangle p = Q \cdot R_H \tag{3.39}$$

where R_H is the hydraulic resistance in $\mathrm{Pa\,s\,m^{-3}}$ and is described with the so called geometric coefficient $C_{geometry}$

$$R_H = C_{geometry}\,\eta\,\frac{L}{A^2} \tag{3.40}$$

where $C_{geometry} = 12\,{}^{w}/_{h}\,({}^{w}/_{w-0.63\,h})$ for the rectangular and $C_{geometry} = 8\pi$ for the circular channels [18, 199, 201].

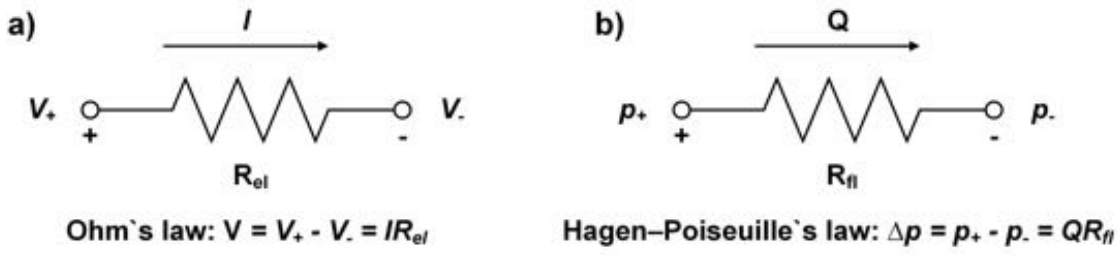

Figure 3.15: *Equivalent circuit symbol of a resistor a) for the electric resistance and Ohm's law, b) for the hydraulic resistance and Hagen-Poiseuille's law (adapted from [199, 201]).*

Compared to the electric circuitry, the applied pressure difference $\triangle p$ (e.g. by a syringe pump) between the inlet and outlet of the channel results in a volume flow Q through the hydraulic resistance R_H. Furthermore, this analogy is used to estimate the total hydraulic resistance $R_{H,total}$ of a complex microfluidic network with N hydraulic resistors connected in parallel or serial. In case of the serial addition of N resistances, the total hydraulic resistance is equal to the sum of these resistances: $R_{H,total} = R_{H,1} + R_{H,2} + \ldots + R_{H,N}$.

On the other hand, in a fluidic network comprising parallel located N resistances, the reciprocal of total hydraulic resistance is calculated by the sum of reciprocals of these hydraulic resistances: ${}^{1}/_{R_{H,total}} = {}^{1}/_{R_{H,1}} + {}^{1}/_{R_{H,2}} + \ldots + {}^{1}/_{R_{H,N}}$. This analogy in its simple form has a crucial drawback regarding the capacitive compliances resulting from air bubbles trapped in microfluidic networks, or the elasticity of the employed channel materials [18, 199, 201]. However, it can be expanded by the implementation of the appropriate capacitive elements.

3.3.3 Dynamics of capillary filling

One of the most important characteristics of microfluidics is the capillarity which occurs because of the dominance of the surface effects, such as surface tension and contact angle, at the microscale. In microfluidic lab-on-a-chip systems, the "power-less" capillary flow is usually used to introduce biomolecules and other reagents into a well-defined channel section for the assay immobilization, the measurement, or both [18, 203].

Capillarity, also referred to as capillary rise in case of vertically standing microchannels or capillaries, are observed: If a capillary is immersed in a liquid, the liquid will rise inside the conduit up to the so called capillary rise height H until the gravitational force is compensated by the surface tension of the liquid-air interface. The capillary rise height is given as $H = {}^{2\gamma}/_{\rho g R} = {}^{2}/_{\rho g R} \cdot (\gamma_{sa} - \gamma_{sl})$ and is often employed for the measurement of the surface tension with high accuracy[18].

On the other hand, the gravitational force has no influence to the capillary flow, if a microchannel is located horizontally. In this case the liquid flows continuously through the capillary, which is also known as capillary pump. The schematics of the capillary flow in a microchannel with the channel height h is depicted in Figure 3.16. The driving force for the capillary filling is the pressure drop Δp_{surf} across the liquid–air interface. The channel inlet at the fluid container, where the pressure is almost equal to the atmospheric pressure p_0, is assigned as the position $L(t) = 0$ in this model [18, 203].

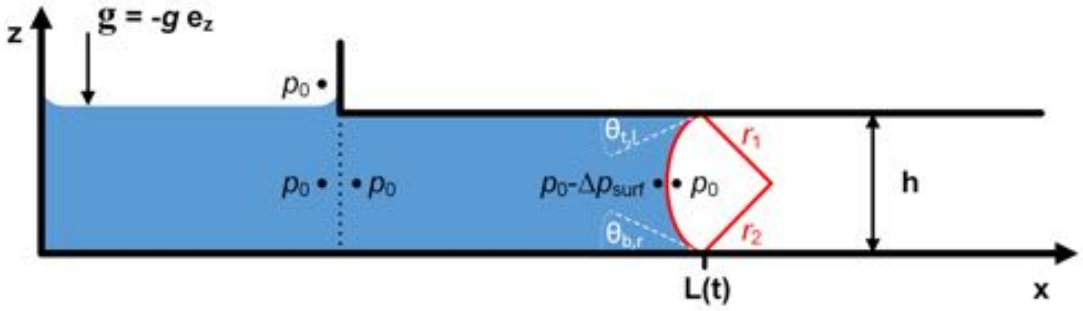

Figure 3.16: *Schematics of the capillary flow (capillary pump) in a microchannel with the channel height h. The capillary flow occurs due to the unbalanced Young–Laplace under pressure $-\Delta p_{surf}$ caused by the concave meniscus of the filling front at position $L(t)$. Please note that all the points where the pressure is approximately identically to the atmospheric pressure p_0 (adapted from [18, 203]).*

The time-dependent position $L(t)$ of the filling front in rectangular microchannels with high aspect ratio $h \ll w$ is determined by using the results of the Hagen-Poiseuille equation (Equation 3.38) for the volumetric flow $Q \approx {}^{h^3 w \triangle \rho}/_{12\eta L}$. The so called Young-Laplace pressure drop Δp_{surf} between the channel inlet ($x = 0$) and the marching meniscus ($x = L(t)$)

stays constant and is expressed as

$$\Delta p_{surf} = \frac{2\gamma}{h} \cos\theta_C. \tag{3.41}$$

Using the known pressure drop at the meniscus front, the incompressible Navier-Stokes equation is solved to derive the time-dependent position $L(t)$ of the capillary meniscus as

$$L(t) = h\sqrt{\frac{t}{\tau_{adv}}}. \tag{3.42}$$

with the time t and the characteristic time $\tau_{adv} = \frac{6\eta}{\Delta p_{surf}} = \frac{3\eta h}{\gamma \cos\theta_C}$ of a parallel-plate channel ($h \ll w$) [18].

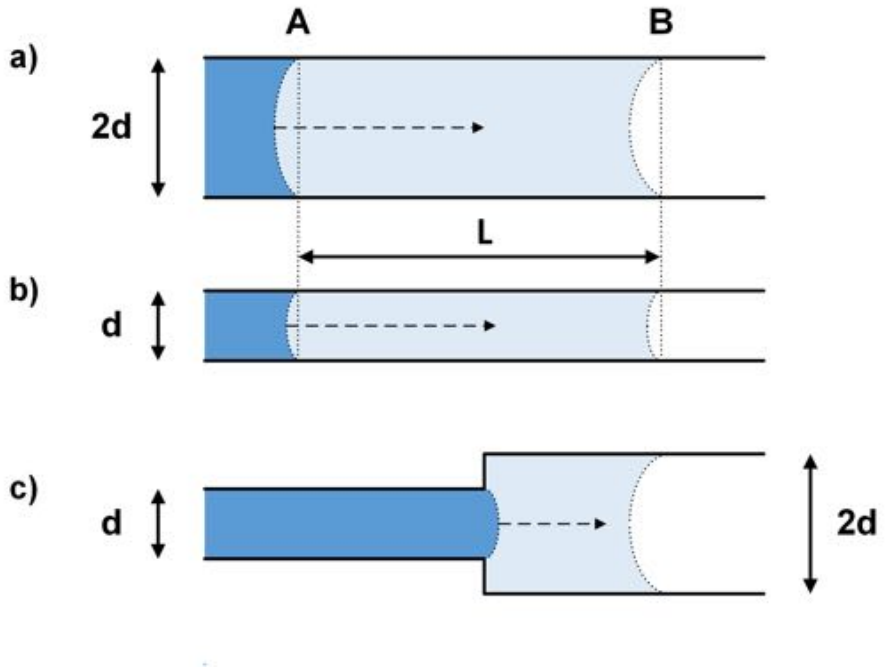

Figure 3.17: *Capillary filling in microchannels with different cross-sections.*

In Figure 3.17 capillary filling in two-dimensional microchannels with different cross-sections are illustrated. Although the capillary in Figure 3.17b has the half diameter of the capillary in Figure 3.17a, they both show similar conditions for the spontaneous capillary filling. The only difference is that for the same fluid volume, the conduit with half diameter is filled up by the capillary forces to a length of twice more than the wider one. Thus, it indicates that the Gibbs free energy per volume is doubled for the narrow conduit. Such a relation is given by $\Delta G \propto 1/d$ and is the expression of the surface-to-volume ratio.

Using this “geometric tool”, capillary effects such as capillary pump can be regulated, i.e. enhanced or reduced depending on the application, by the cross-sectional variations of the purposely designed microchannels.

A good example for the manipulation power of this “geometric tool” is displayed in Figure 3.17c. The microchannel has a sharp increase in its cross-section with two channel walls being at 180° to each other resulting in a superhydrophobic surface. Therefore, it is likely to apply such a geometry as a passive fluid control element, also known as a geometric stopping barrier, for the capillary filling of microfluidic systems. In this thesis, a similar approach is also used to define the channel sections for assay immobilization on the biosensor with multiplexed microfluidics.

4 Design rules for LOC devices

Preface

This chapter introduces a novel design concept for microfluidic biosensors using the stop-flow technique which can be employed in any enzyme-mediated detection for the signal amplification. Here, the fluid flow through the microfluidic channel or channel network is stopped for defined time intervals and thus, leads to an accumulation of the by-products of enzymatic reactions (e.g. H_2O_2 molecules in the case of glucose oxidase) in the immobilization capillary. By restarting the flow, these molecules are subsequently delivered to the measurement cell for the detection (e.g. in this work electrochemical cell). The obtained short signal peak is directly proportional to the duration of the stop-time.

This technique allows fast and sensitive electrochemical detection of various analytes independent of the assay format, as presented in [48–50]. For the data analysis both the maximum signal height or the integral of the signal peak can be employed [40, 204]. For a signal evaluation based on the peak height, the concentration profile of the signal molecule, here H_2O_2, over the channel cross-section is decisive for the gauged signals. H_2O_2 concentration profile is again dependent on the diffusion coefficient of hydrogen peroxide in the stop-time only. This special feature of the stop-flow method allows a dramatic decrease in the channel dimensions. Especially the channel length of microfluidic biosensors can be reduced, while maintaining its benefits such as high sensitivity and fast detection.

For the verification of the hypothesis proposed in this work, different numerical simulations and proof-of-principle measurements are carried out. This chapter gives an overview about the simulation results and presents new design rules for microfluidic LOC devices. In this context, firstly the evolution of H_2O_2 concentration profile over the channel cross-section is simulated under no-flow conditions. By varying the size of the channel, the minimal length of the channel is determined. This ensures a homogenous and saturated H_2O_2 concentration profile. In the second place, time-dependent simulations are performed by increasing the channel length, beginning with the optimum value obtained from the no-flow investigation. Here, the goal is to find out the minimal channel length which enables the analyte detection without a loss in the sensitivity under flow conditions. Consequently, the simulation of a stop-flow measurement is demonstrated with the optimized design parameters to compare its characteristics with those of a real measurement by the existing system.

In this thesis, the numerical resolution of the differential equations has been performed through a finite element method (FEM) with COMSOL Multiphysics 5.1 (COMSOL Inc.,

Sweden). Thus, a simulation model including different geometries and features is developed and combined with appropriate initial and boundary conditions. Subsequently, this model is solved on a Mac OS X platform using an Intel 3.06 GHz Core 2 Duo processor with 12 GB RAM.

4.1 Simulation model

This section presents the model geometry of the microfluidic channel considered for the numerical analysis of the stop-flow technique. The basic geometry, as depicted in Figure 4.1, is a L-shaped microchannel. It includes an immobilization section with a $500 \times 64\,\mu m^2$ rectangle cross-section and a variable channel length $l_{channel}$, a working electrode having an active area of $19.7 \times 10^{-2}\,\mu m^2$, and a 5 µm deep well as a stop barrier to specify the immobilization area. The height of the channel is defined by the thickness of the utilized dry film photoresist, in this work 64 µm given by Pyralux® PC1025 (DuPont™, USA). The fluid flow occurs from the inlet to the outlet of the microfluidics channel, as highlighted in Figure 4.1. Having employed this 3D simulation model along with the stop-flow technique, the effects of the immobilization capillary and electrode geometry on the performance of microfluidic biosensors are studied numerically.

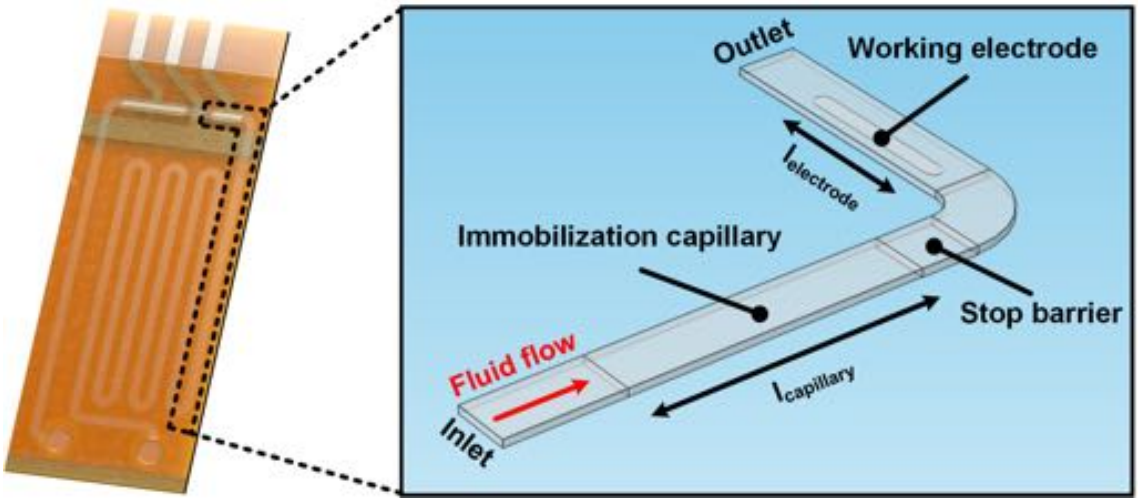

Figure 4.1: *Photograph of the standard biosensor chip with the inset illustrating the COMSOL simulation model and its main features: Immobilization capillary, stop barrier and working electrode.*

4.2 Boundary conditions

Boundary conditions are inputs of a simulation model and connect the simulation model to its environment. Therefore, the appropriate definition of the initial and boundary conditions is crucial. The values of different parameters employed in the simulation model are given in Table 4.1.

Table 4.1: *Constants applied to the simulation model.*

Constants	Value	Unit	Remark
Temperature T	298	K	
Density ρ	1×10^{3}	$\mathrm{kg\,m^{-3}}$	Water
Dynamic viscosity μ	0.001	$\mathrm{Pa\,s}$	Water
Diffusion coefficient D	1×10^{-9}	$\mathrm{m^2\,s^{-1}}$	H_2O_2 [146]
Flow rate	10.4×10^{-3}	$\mathrm{m\,s^{-1}}$	
Enzyme unit per area n_{enzyme}	4.2725	$\mathrm{m^{-2}}$	experimentally derived
Enzyme activity per unit a_{enzyme}	0.166×10^{-7}	$\mathrm{mol\,s^{-1}}$	GOx @ 25 °C [205]

4.2.1 Fluid flow

For microfluidic channels and channel networks, the Reynolds numbers are low (typically $Re \leq 1$) because of low fluid velocities and small channel dimensions. Therefore, the surface forces (e.g. viscous shear stress) become dominant over the body forces (e.g. gravitation) [18, 199–201]. Since the microfluidic flow is far in the laminar regime, it is assumed to be incompressible. As described earlier in Section 3.3.2, neglecting the terms of mass (e.g. convection) and momentum conservation the flow velocity field in microchannels is given simply by the Navier-Stokes and continuity equations as:

$$\nabla\vec{\nu} = 0 \tag{4.1}$$

$$\nabla p = \eta\nabla^2\vec{\nu}. \tag{4.2}$$

The resulting flow velocity of the Poiseuille flow shows a typical parabolic profile with the maximum velocity in the channel center and zero velocity (no-slip condition) at the channel walls. Hence, the no-slip boundary condition is conducted for all of the channel walls. Additionally, a constant flow velocity is applied to the inlet and outlet of the channel to discharge atmospheric pressure. To put the stop-flow technique in practice, the fluid flow is interrupted for a defined stop-time with the help of rectangle step functions.

4.2.2 Mass transport

To mimic a stop-flow measurement, the mass transport phenomena of diluted species has to be combined with the fluid flow. Having calculated the velocity field by the Navier–Stokes equation, the determined velocity is likely to be employed for the simulation of the mass transport phenomena. In microfluidic systems, the electroactive molecules are transported along the channel by controlled convection (e.g. using an external pump). However, the mass transport transverse to the flow direction is dominated by diffusion to compensate the concentration gradient which occurs due to the electrochemical reaction at the working electrode. The flux of the electroactive species is time-dependent and their concentration change with time is described by Fick's second law for linear diffusion as

$$\frac{\partial c}{\partial t} + \nabla \cdot (-D\nabla c + c\nu) = 0. \tag{4.3}$$

Furthermore, insulation (no flux) boundary conditions are applied to the capillary walls except those of the immobilization section, as no mass transport is possible in or out of the channel walls. In the immobilization capillary, the channel walls (except the bottom side owing to the inactivity of SU-8) are defined as inward flux boundaries with a time-dependent function $f(t) = n_{enzyme} \cdot a_{enzyme} \cdot t$ to imitate the ELISA-based H_2O_2 generation by the glucose oxidase. Consequently, the outflow boundary is assigned to the channel outlet, where the electroactive species are carried away out of the simulation model by the fluid flow. For the implementation of the electrochemical reaction, the H_2O_2 concentration is assumed to be zero at the working electrode. It is to be implied that we assume sufficiently fast electron transfer kinetics at the Pt working electrode.

In summary, the equations and assumptions, discussed in this section, can be implemented using the steady-state or time-dependent, laminar "Incompressible Flow" module along with the "Transport of Diluted Species " interface of COMSOL Multiphysics to run simulations with the stop-flow technique in a 3D environment. The following initial and boundary conditions are applied to the simulation model:

- $C_{H_2O_2\,@\,\text{Electrode}}(t) = 0$
- $C_{H_2O_2\,@\,\text{Channel}}(\text{initial}) = 0$
- $C_{H_2O_2\,@\,\text{Immobilization area}}(t) = n_{enzyme} \cdot a_{enzyme} \cdot t$
- $\nu_{\frac{1}{2}\,\text{channel height}}(t) = v_{max}$ (laminar flow)
- $v_{\text{channel walls}}(t) = 0$ (no-slip)
- $v(t) = \begin{cases} 10.4{\times}10^{-3}\,\text{m s}^{-1} & \text{for } 0 < \text{t} < 15 \text{ (flow-phase)} \\ 0 & \text{for } 15 \leq \text{t} \leq 75 \text{ (stop-phase)} \\ 10.4{\times}10^{-3}\,\text{m s}^{-1} & \text{for } 75 < \text{t} < 90 \text{ (flow-phase)} \end{cases}$

4.3 Optimization of the immobilization capillary under no-flow conditions

Firstly, 3D simulations of the simulation model, explained in the previous section, are executed under no-flow conditions in order to find the optimal channel length, at which the H_2O_2 concentration profile over the channel cross-section reaches its maximum with a homogenous distribution. In this regard, the different channel lengths, starting from 0.5 mm up to 10 mm increasing with 0.5 mm steps, are applied to the simulation model. The results of this study are given in Figure 4.2. Different 3D simulation models illustrate the H_2O_2 concentration profiles of different immobilization capillaries following 1 min stop-time under no-flow conditions. It is clearly shown that the hydrogen peroxide concentration cannot reach its maximum at very small channel geometries, e.g. by a channel length of 0.5 mm. This brings about the diffusion of H_2O_2 away into its environment owing to the resulting concentration gradient.

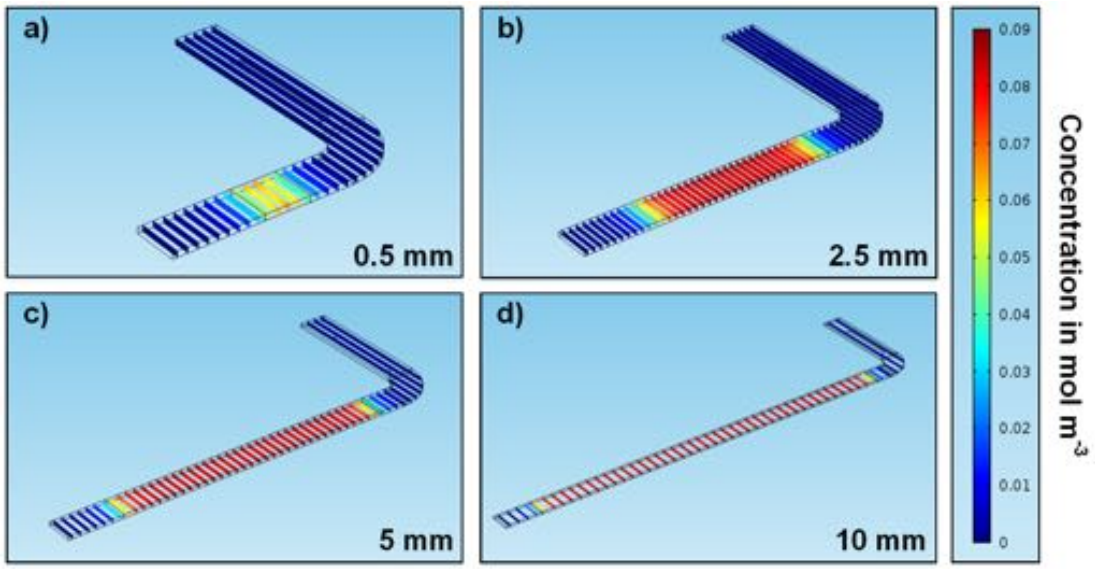

Figure 4.2: *3D simulation models with different lengths of the immobilization capillary a)-d) depicts the evolution of H_2O_2 and its subsequent diffusion through the microfluidic channel after 1 min stop-time under no-flow conditions.*

The correlation between the length of the immobilization channel and the attained H_2O_2 concentration at the half height of the channel is represented in Figure 4.3 to study diffusive effects on the concentration profile. It is found out, that a channel length of longer than 2 mm is essential for the immobilization capillary to obtain a homogenous and saturated H_2O_2 concentration profile without flow conditions. In the light of these findings, a minimum channel length of 2.5 mm is chosen as the initial length of the channel geometry for further simulations combining the stop-flow technique with the laminar flow.

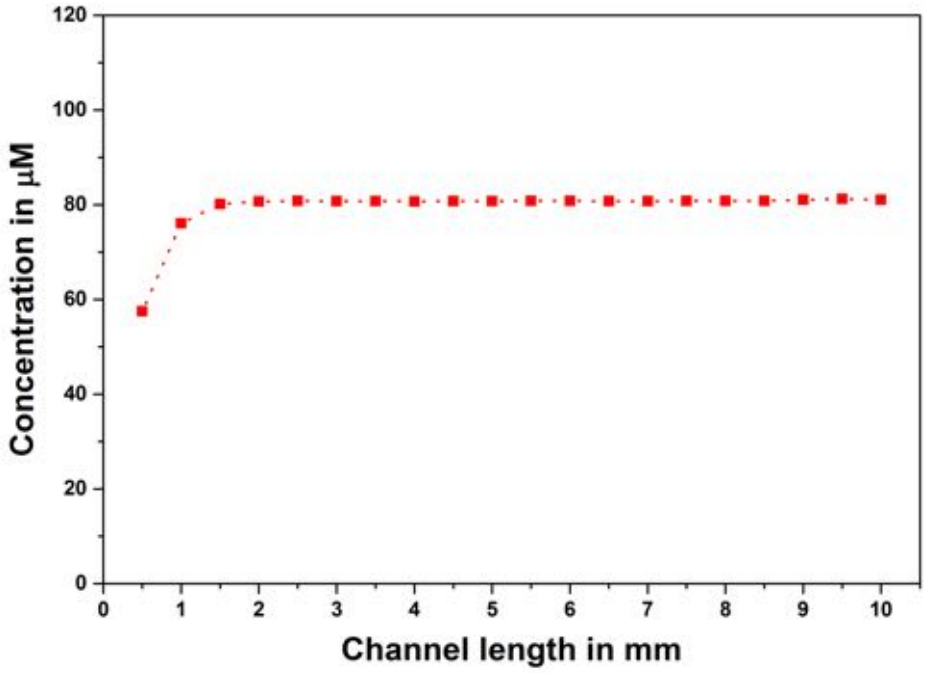

Figure 4.3: *1D point plot of simulated values describing the correlation between the channel length of the immobilization section and the analyte concentration determined in the middle of the channel cross-section. A saturation of the H_2O_2 concentration profile is observed at a channel length of more than 2 mm.*

4.4 Simulation of stop-flow measurements

In this section, the effect of the immobilization channel and electrode geometry on the performance of microfluidic biosensors is investigated numerically under flow conditions. For this purpose, the stop-flow-technique is implemented to the simulation model examined previously. At the end of this section, a comparison between the simulated and measured stop-flow signals is presented.

4.4.1 Effect of the channel geometry on the sensor performance

The channel geometries play a key role for the performance (e.g. the sensitivity) of the traditional microfluidic LOC systems. In this work we assume, that the effect of the channel geometry on system sensitivity becomes less important, if the stop-flow technique is examined. In this sense, time-dependent 3D simulations are performed by dint of increasing the immobilization area. The aim is to achieve the minimum value required for its length without any significant effect on the sensor sensitivity.

To mimic the electrochemical detection, the boundary flow ($\mathrm{mol\,s^{-1}}$), comparable with the

current values, at the working electrode is calculated for different channel geometries and compared with each other. Beginning with the initial value of 2.5 mm, calculated by the previous simulation without fluid flow, different sizes up to 15 mm increased with a step of 2.5 mm for the channel lengths are applied to the microfluidic model. A fully developed laminar flow (data not shown) with a maximum velocity at the center is observed and no-slip behavior is noted on the walls of the microfluidic channel.

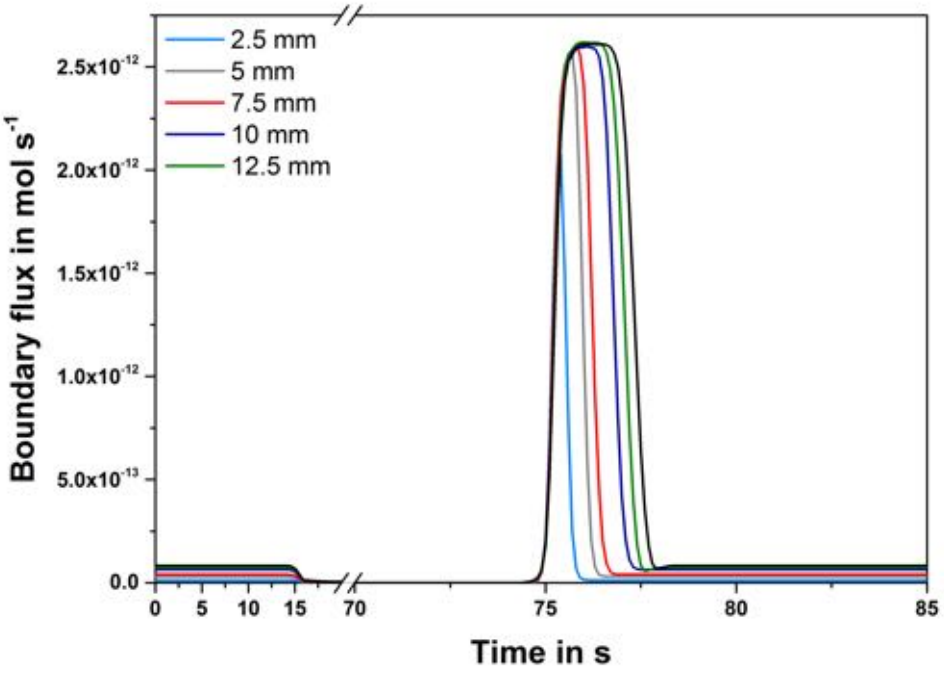

Figure 4.4: *Characteristic signal peaks of different immobilization capillary geometries for 1 min stop-flow measurement depicting its effect on the sensor performance. A length of 5 mm is adequate for the channel geometries used in this thesis to ensure a full sensor performance.*

After the interruption of the fluid flow, the analyte concentration near the working electrode sinks drastically to a minimum value, which is given by the diffusion of the analyte to the electrode. At the meantime, the analyte concentration increases linearly in the immobilization capillary. As the flow is restarted, this enhanced analyte concentration is flushed over the electrode and causes the experimentally confirmed signal behavior of stop-flow technique. The characteristic stop-flow signal peaks for different channel geometries are displayed in Figure 4.4. The calculated stop-flow signals of different channel geometries indicate clearly that the total analyte concentration, the integral of the signal peak, increase with the channel length. In contrast, the maximum peak values of the concentration are saturated sufficiently at an immobilization channel length of 5 mm. So, a channel length of 5 mm is employed for the immobilization capillary to examine the effect of the electrode length on the sensor sensitivity.

4.4.2 Effect of electrode area on the sensor sensitivity

In order to specify the role of the electrode size on the sensor sensitivity 3D simulations of stop-flow measurements are carried out by varying the length of the working electrode. For the realization of the concentration-dependent electrochemical signals, here the total flux magnitude at the electrode ($\mathrm{mol\,m^{-2}\,s^{-1}}$), comparable with the current density, is monitored for different electrode areas and their relation to the system performance is studied. Applied electrode lengths are 0.4, 0.8, 1.2 and 1.6 mm with the respective electrode areas of 0.065, 0.131, 0.197 and 0.262 $\mathrm{mm^{-2}}$.

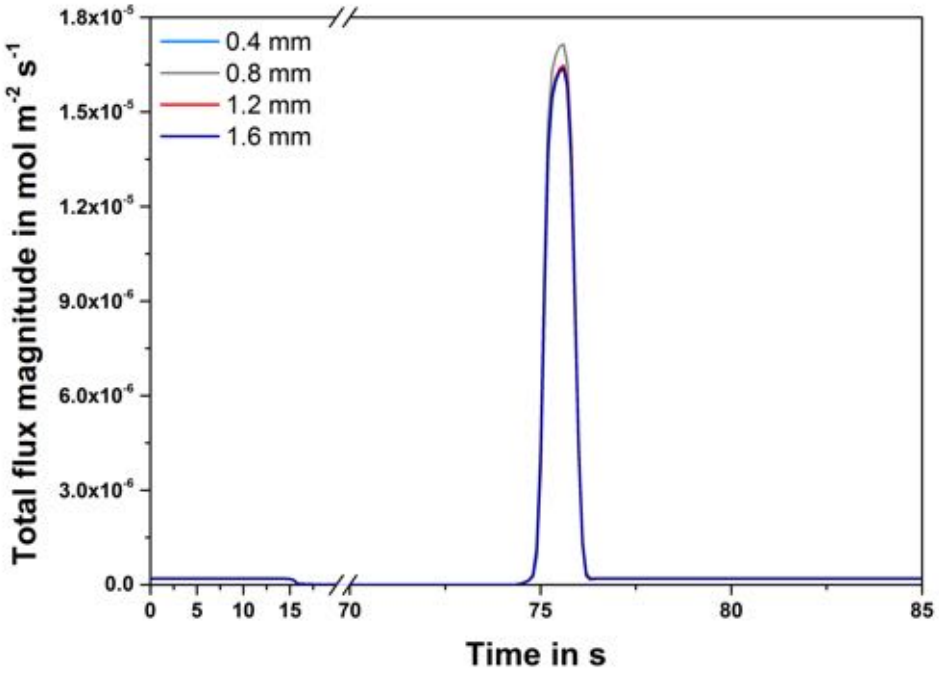

Figure 4.5: *Simulation of stop-flow measurements using different electrode areas to study its effect on the sensor performance. The electrode size plays no significant role for the sensitivity.*

Pursuant to Figure 4.5, there are no remarkable differences in the sensor sensitivity between the employed electrode sizes, although the respective boundary flow values are growing by increasing the electrode area. However, it is favorable to obtain sufficiently high signals along with a low signal-to-noise ratio for the electrochemical detection.

4.4.3 Simulation vs. measurement utilizing the stop-flow technique

After studying the effect of the channel and electrode geometry on the performance of microfluidic biosensors using the stop-flow method numerically, the comparison between the simulation and real measurement is realized. For this purpose, the simulation of a

stop-flow measurement is performed with a channel length of 15 mm and an electrode area of 0.197 mm^2. Its characteristics are compared with the available LOC system. The microfluidic chip "miLab", which will be explained detailed in the following section, employed in this measurement has an immobilization capillary of approximately 15 mm along with the same electrode size as given in the simulation model.

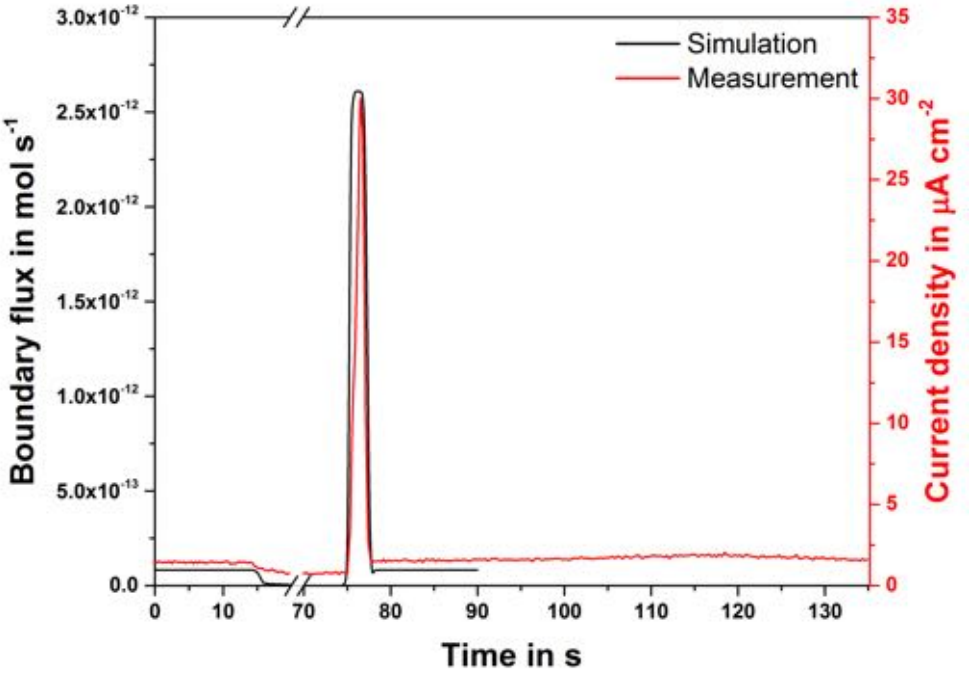

Figure 4.6: *Simulation vs. measurement of stop-flow technique. Compared to each other, both signal responses show very similar behavior.*

In Figure 4.6 the results of this study are presented. The signal responses of both simulation and measurement of the stop-flow method match with each other and exhibit a rectangular pulse shape, as expected. Furthermore, it is beyond doubt, that the peak widths resulting from the length of the immobilization capillary are close to equal. There exist only two main differences: Higher signals of the real measurement due to the background currents and the second small "peak" between 100 and 125 seconds, which is most probably caused by the compliance of the used silicon tubes for the fluid delivery.

4.5 Design rules

In summary, different design rules are derived numerically from the 3D simulations and constitute a novel design concept, presented in this work for the first time, for optimized microfluidic LOC systems using the stop-flow technique. Such an approach facilitates the minimization of microfluidic biosensors maintaining their performance, including the high sensitivity and fast quantification, independent from the employed detection technique (e.g. optical or electrochemical).

The proposed design rules are outlined as follows:

- The length of the immobilization capillary is a key feature for a high sensitivity of microfluidic LOC systems. Applying the stop-flow technique results in a drastic decrease in the channel geometry. It is possible to determine the optimal length of the immobilization capillary for different channel cross-sections, measurement conditions (e.g. flow rate or stop-time) or even materials by means of the simulation model introduced in this work.
- To achieve the rectangular-shaped signals of stop-flow measurements, the length of the immobilization section is to be at least equal to the size of the working electrode in the case of electrochemical detection.
- The electrode area plays no significant role on the sensor sensitivity of electrochemical LOC platforms adopting stop-flow technique. Nevertheless, it should be designed aiming sufficiently high currents for the signal detection in consideration of the signal-to-noise ratio.

5 Design and fabrication

Preface

This chapter describes the design through both the production and optimization of the electrochemical sensors to the final platform for multi-analyte detection. The iLab platform offers both single-analyte, a conventional "iLab" and a miniaturized "miLab" format, as well as a multi-analyte "MultiLab" versions of the biosensors. The single-analyte sensor formats are employed later for the verification of the presented design concept and thus, this enables the advanced development of the multiplexed version of iLab platform.

At the beginning, a short description of the dry film photoresist technology is given. On the basis of this advantageous technology, the design and wafer-level fabrication of the iLab platform is described in detail. Furthermore, the design and production of a custom-made chip holder is presented, which allows a fast and easy fluidic and electrical connection of the biosensor to its environment. Finally, the measurement setup used for the electrochemical detection is introduced.

5.1 Dry film photoresist technology

Compared to soft-lithographic materials like PDMS or SU-8, dry film photoresists offer a low-cost and high-speed fabrication alternative for microfluidic sensors and therefore, has become more of an issue in recent years. They are supplied in sandwiched layer format between a polyester support film and a protective polyolefin release sheet to protect them from ambient oxygen. Instead of complex processing by spin coating, DFRs are laminated onto the substrate and subsequently manufactured further with standard photolithography.

From material perspective, DFRs present many advantages: They (i) are available in a variety of compositions and thicknesses (from a few microns to several millimeters); (ii) facilitate the fluid flow via capillary forces; (iii) own a very high surface area owing to its roughness, which ensure excellent adhesion to many different materials; (iv) feature excellent thickness uniformity over the whole wafer; (v) offer low-cost, simple and high-throughput fabrication; (vi) are easy to cut by means of various low-cost tools and standard techniques; and (vii) allow for the generation of 3D structures such as microfluidic channels by stacking due to their tenting ability [206, 207].

The main drawback of DFRs is their relatively poor resolution in contrast to liquid photoresists, which is mainly caused by their high film thicknesses and the increased gap between the mask and the DFR due to the protective cover film. However, they are highly convenient for the continuous, low-cost mass production of sensors and microfluidic integrated devices.

Pyralux® PC1000 flexible circuit materials (DuPont™, USA) are acrylic-based negative working dry-film photoresists [207]. They have an optimal exposure conditions in the 350 - 450 nm wavelength range in the ultraviolet (UV) spectrum. As water-soluble negative resist, unexposed areas will be removed by a mild alkaline carbonate solution as developer. The resolution limit of Pyralux® PC dry-film photoresists is in the range of 35 µm using standard photolithography techniques, as described detailed in [208]. The digits in the name of DFRs refer to its composition and thickness. For example, Pyralux® PC1025 used in this work for the microfluidics holds a thickness of 64 µm (2.5 mil).

5.2 Chip design

Under the favor of the elegant combination of diverse fabrication strategies along with technical measures and various design elements regarding aforementioned design rules, three different chip designs of this microfluidic platform have been created. Therewith, this approach enables to overcome technical and non-technical limitations of LOC platforms in corporation with new functional features. Thus, it offers (i) simple and low-cost fabrication allowing mass-production, (ii) easy handling, (iii) reagent loading by capillary actions, (iv) low sample/reagent consumption, (v) adequacy with various biomolecules immobilization, and (vi) the possibility for simultaneous multi-analyte detection [39, 40].

The design of different microfluidic biosensors is performed with Clewin layout editor (WieWeb software, Netherlands) for the wafer-scale fabrication on polyimide foils with a diameter of 150 mm. To enable a time-efficient processing, critical fabrication steps such as electrodeposition of silver and silver chloride on reference electrodes as well as electrochemical cleaning of the working electrodes are considered on wafer-level. For this purpose, all reference electrodes are connected to a common bulk contact pad on the left side, while the common bulk contact pad for the working electrodes is located on the right side of the wafer.

The interested reader may find further information about the development and properties of the old versions of this biosensor in our previous publications [48–50].

5.2.1 iLab & miLab

The design and fabrication of the DFR-based microfluidic sensor platform described by Horak *et al.* and others [48, 49, 51] are here further optimized to the “iLab” chip, as shown in Figure 5.1a. Consequently, the minimized version of this optimized biosensors,

"miLab" chip in Figure 5.1b, is introduced to verify the design rules established in this thesis. Both microfluidic chip designs comprise three main sections: Contact pads for electrical connection, a meandering microcapillary for biomolecule immobilization, and an electrochemical cell. The dimensions of all chip versions used in this work as well as their immobilization capillaries and electrodes are summarized in Table 5.2 at the end of the "Chip Design" section.

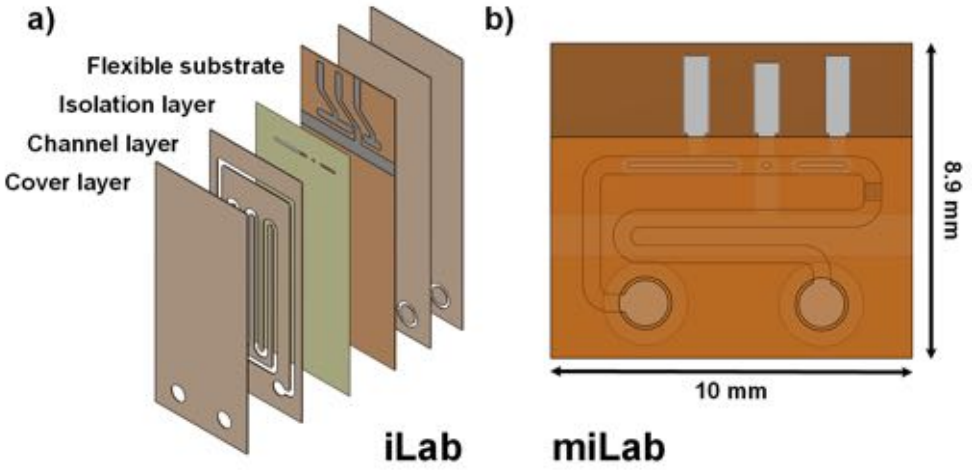

Figure 5.1: *CAD drawings of the different single-analyte chip versions depicting a) the different layers of the iLab chip, and b) the miLab chip with its main dimensions.*

The meandering microchannel for the biomolecule immobilization is 500 µm wide, 64 µm high, given by the thickness of the used DFR, and 100.8 mm long and 16.4 mm long in the case of iLab and miLab, respectively. These channel dimensions give the possibility to work with high viscosity solutions (e.g. serum or blood). The delivery of different reagents and samples into the immobilization capillary is achieved easily by capillary forces. The area of the immobilization section is defined by a hydrophobic stop barrier, which inhibits the spreading of the liquid and prevents the contamination of the electrochemical cell with the reagent used for the coating. This barrier is realized by an additional $700 \times 500\,\mathrm{mm}^2$ long spacer across the channel in the isolation layer and subsequently by dispensing 1 % Teflon AF (DuPont™, USA) solution into this predefined wells. This passive system for the capillary filling combined with a physical barrier does not require any external instrumentation (e.g syringe pump). Additionally, it provides an increased reproducibility by multiple incubation steps needed for the assay preparation [48, 49].

In both chip designs, the electrochemical measurement cell is placed next to the immobilization capillary. It consists of Pt working, counter and Ag/AgCl reference electrodes. The reference electrode is located between the working and counter electrode to prevent any potential drop between WE and RE. Furthermore, the working electrode is situated to the upstream flow direction, as the counter to the downstream, in order to avoid any measurement errors caused by the silver ions [40, 204].

On a single six inch wafer, there exist 38 sensors, each with a dimension of $10\times25.5\,\mathrm{mm}^2$, in the standard format, whereas 120 sensors, each with a size of $10\times8.9\,\mathrm{mm}^2$, in the miniaturized version.

5.2.2 MultiLab

The main objective of this work is the development of an electrochemical microfluidic multiplexed biosensor for the simultaneous detection of multi-analytes. To achieve this, first a design concept for microfluidic biosensors is introduced. Later, this is verified by the proof-of-principle measurements using both single-analyte versions of the iLab platform. Thereafter, further technical considerations are made in combination with these design rules to realize a felicitous chip design.

Technical measures

In the first place, a model for the channel network containing the electrochemical cell(s) and several immobilization sections is to be designed. Regarding the fundamentals of microfluidics, the flow velocity decreases, if the total channel cross-section increases. Therefore, the fluidic resistances has to be designed uniform in order to achieve identical flow velocities in parallel channel sections. The schematic illustration of the channel network proposed in this thesis for multi-analyte detection is displayed in Figure 5.2.

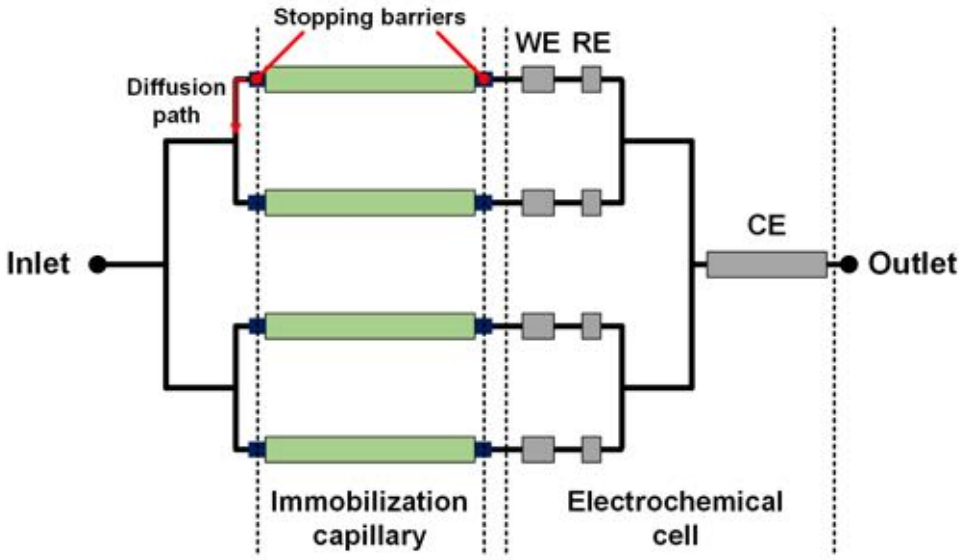

Figure 5.2: *Schematics of the proposed channel network for multi-analyte detection illustrating four immobilization capillaries, the diffusion path, and the single electrochemical cell. Each immobilization area is defined by two stop barriers. The electrochemical cell consists of a common counter electrode and multiple working as well as short-circuited reference electrodes.*

Within this microfluidic network, each channel requires a particular zone for the assay immobilization and a working and reference electrode for signal transduction, as shown in Figure 5.2. In this regard, the microfluidic biosensor should give the possibility to address each immobilization capillary by individual channel inlets. To prevent any contamination between the neighboring channels and thus, any cross-sensitivity, two hydrophobic stopping barriers are employed to define single immobilization areas. The utilization of discrete channel inlets facilitates high flexibility in the assay design.

Moreover, for a comfortable handling and facile measurement setup (e.g. using only one syringe) the different channel sections shall own a common inlet and outlet for the fluid flow during the measurements. Similar to the single-analyte versions, the fluidic ports and the electrical contact pads are located contrarily to each other in the chip layout to obviate any interferences. Again, the reagent filling for the assay incubation is realized by the capillary action.

For the electrochemical signal readout by a facile and low-cost measurement configuration, the use of a single electrochemical cell with multiple working, and a common counter and reference electrodes is highly desirable. For example, a low-priced and compact potentiostat with a multiplexer module can be used in such a setup. In this work, a three-electrode setup is applied to the chip design. The multiple working and short-circuited reference electrodes are juxtaposed in each immobilization section to prevent any potential drop, whereas the common counter electrode is located downstream in the outlet channel.

As mentioned before, individual immobilization areas of each channel are delimited by two hydrophobic stop barriers. In order to avoid any cross-sensitivity between different sections arising from the diffusion of the analyte (here H_2O_2) at the stop-phase, there is to be a particular distance among these immobilization capillaries and previous crossing point. This critical path is termed here as diffusion path d and is approximated by:

$$d = \sqrt{D \cdot t} \tag{5.1}$$

where t is the stop-time and D is the diffusion coefficient of H_2O_2.

To calculate the minimum diffusion path, the highest value of $1.4 \times 10^{-9}\,m^2\,s^{-1}$, is chosen for the diffusion coefficient of H_2O_2, found in literature [146]. The relation between the length of the diffusion path and the stop-time is presented in Table 5.1.

Table 5.1: *Calculated values of the diffusion path length for different stop-times.*

Stop-time t	1 min	2 min	5 min	10 min	30 min
Diffusion path length d **in mm**	0.29	0.41	0.65	0.92	1.59

The major technical measures and design considerations are summarized as follows:

- The application of single electrochemical cell comprising multiple working and short-circuited reference electrodes, and a common counter electrode
- One common inlet and outlet for the fluid flow
- Individual inlets for the discrete immobilization sections allowing a high assay flexibility
- The use of diffusion paths to prevent the crosstalk between individual channels
- The definition of single immobilization areas by two hydrophobic stop barriers

Chip layout

Following these approaches, the chip layout is designed for the wafer-level fabrication of the microfluidic multiplexed chip. The final mask design includes three different biosensor formats with a microfluidic network of 2-, 4- and 8-channels. The number of the employed channels are limited by the multiplexing capability of the used potentiostat. A single six inch wafer consists of nine 2-channel, five 4-channel as well as five 8-channel sensors.

Furthermore, it is planned to utilize a universal custom-made chip holder independent from the chip format. Hence, the length of the different chip versions and the configuration of the electrical contacts are identical. As for the dimensions of the designed biosensor chips, they are 27.5 mm in length and 11.5, 20.5, 35.5 mm in width, for the different versions, respectively.

The main features of the microfluidic network are discrete immobilization zones and the electrochemical cell. The individual immobilization capillaries, defined by two hydrophobic barriers, are 2.1 cm in length and have a volume of 680 nl resulting in a surface-to-volume ratio of 155 cm^{-1}. Moreover, a diffusion length of 6.3 mm is selected to avoid any cross-sensitivity between the neighboring channels as well as to achieve a simple handling for the pipetting.

The dimensions of the fluidic ports like the common in- and outlet with a distance of 5.5 mm are designed in the same way as the electrical connections to enable an easy and universally applicable connection. In order to exclude any undesired fluid flow by capillary filling, additional stop barriers are integrated into the common inlet channel. In the layout, all channel sections are connected in a set of T-junctions to the common in- and outlet for the fluid flow, induced by a syringe pump, through the common in- and outlet. For the measurement process, the individual channel inlets are permanently sealed with a PMMA adapter prior to connect the chip to the custom-made holder.

5.2.3 iLab platform

The chip characteristics of the different versions of the iLab platform are outlined briefly in Table 5.2. It includes their chip dimensions, electrochemical and biochemical attributes of individual designs, as well as the technical measures like diffusion path length to prevent a possible crosstalk between discrete channels.

Table 5.2: *Chip characteristics of the different formats of the iLab platform.*

	iLab	**miLab**	**MultiLab**		
			2-Channel	**4-Channel**	**8-Channel**
Width [mm]	10	10	11.5	20.5	35.5
Length [mm]	25.5	8.9		27.5	
Immobilization capillary length per channel [mm]	100.8	16.4		21	
Immobilization capillary area per channel [cm^2]	63.5	10.34		13.23	
Immobilization capillary volume per channel [µl]	3.27	0.53		0.68	
Surface-to-volume ratio [cm^{-1}]			155		
Total channel volume [µl]	4.39	1.03	3.37	6.47	13.07
Diffusion path [mm]		-		6.3	
Working electrode [mm^2]	0.31	0.2		0.227	
Counter electrode [mm^2]	0.69	0.45	1.12		3.3
Reference electrode [mm^2]	0.05	0.03		0.09	

5.3 Chip fabrication

In the first part of this chapter, the optimization of the chip fabrication is briefly discussed. Next, the wafer-level fabrication of the microfluidic biosensors is described. Here, please note that all different chip designs of the iLab platform are produced on wafer-level by dry-film resist technology using the same fabrication protocol. Finally, a short estimation of cost and time-to-fabrication is given.

5.3.1 Optimization of the fabrication

The former fabrication of the DFR-based microfluidic sensor platform, presented in [48, 49, 51], are further optimized employing the following modifications:

At first, SU-8, a negative-working photoresist, is introduced as isolation material instead of the dry-film photoresists owing to its chemical and physical stability together with its high resolution. Thus, the active electrode surface is defined with a high precision. Besides, for the reduction of the diffusion length of the analytes to the working electrodes, the thickness of the isolation layer was reduced to 5 µm.

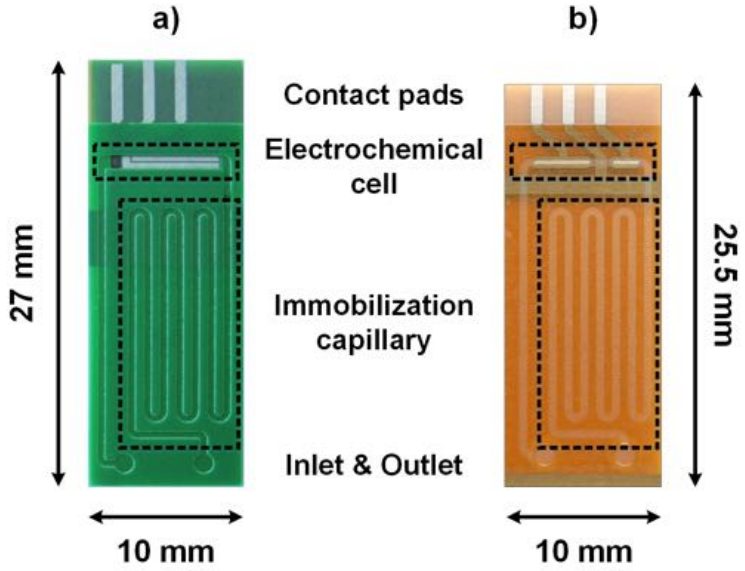

Figure 5.3: *Picture of the two generations of the iLab platform: a) Vacrel® 8100-based presented by Horak et al. [48], b) Pyralux® PC1025-based introduced by Armbrecht et al. [40] highlighting their dimensions and main features: Immobilization capillary, electrochemical cell, contact pads and fluidic ports.*

Electrochemical evaluation of the DFR Vacrel® 8100 used for microfluidics with respect to its longtime stability proved that electroactive substances dissolving from the DFR itself could lead to the mistaken results. Regarding this, Vacrel® 8100 is at the following step

replaced by Pyralux® PC1025 (DuPont, USA), which is more appropriate for the chip fabrication due to not only its faster and cleaner development but also its higher chemical stability. Additionally, it was observed that the composition of Pyralux® PC1025 is more compatible with the different immobilization techniques.

In the former chip fabrication, a 100 nm thin titanium (Ti), served as a protective layer during the DFR processes, was evaporated onto the platinum electrodes. Having created the microfluidics, this protection layer must be etched in highly hazardous hydrofluoric acid. Our studies regarding the necessity of this layer have led us to adopt a new approach without the Ti evaporation. Thus, the chip fabrication process is quite facilitated.

Apart from all these aforementioned improvements, the DFR-based microfluidic chip has been redesigned. In this context, the working electrode area was reduced from 2.2 to 0.31 mm^2 without a change in its sensitivity, as predicted by the established design rules. The both generations of the iLab platform are displayed in Figure 5.3.

5.3.2 Wafer-level fabrication

The entire fabrication of the microfluidic biosensor chips presented in this thesis is performed on wafer-level and in a non-cleanroom setting except the metal deposition. For all lithographic processes of DFRs, masks printed on low-cost transparent foils are used with a vacuum UV-exposure unit instead of chromium masks and a mask aligner.

Pyralux® AP 8525R (DuPont™, USA) with a thickness of 50 µm is employed as the substrate material. This rough polyimide (PI) foil is embedded in double-sided copper clad in order to realize flexible PCBs for electronics. The copper layers are cut in a 6 inch format using a cylindrical cutting tool. They are then etched for one hour in a heated etch bath PA104 (MEGA Electronics, UK) containing 20 % sodium persulfate at 45 °C. The wafers are rinsed with deionized water (DI-water) and dried in a conventional oven (Binder, Germany) for one hour at 160 °C.

For the electrode patterning, the negative photoresist ma-N 1420 (Micro resist technology GmbH, Germany) is spin-coated onto the PI substrates. In order to achieve a layer thickness of 2 µm a rotation speed of 3,000 rpm is applied for 30 s. A soft bake step of the photoresist, performed on a hotplate at 100 °C for 2 min, is followed by a UV exposure for 4 min through an appropriate foil mask on a vacuum UV-exposure unit BEL Hellas (Bungard Electronic, Germany). Subsequently, the photoresist is developed for 1 min in an alkaline developer ma-D 533s (Micro resist technology GmbH, Germany) bath on a platform shaker. After the removal of the non cross-linked photoresist, a controlled under-etching of the resist occurs depending on the exposure and development duration, which allows a good lift-off process.

Consequently, 200 nm thick platinum is deposited on the PI wafer by physical vapor deposition (PVD) at an evaporation rate of 0.1 $nm\,s^{-1}$ in the sole cleanroom step. Metal patterns are released through a following lift-off process by exposing the wafer to a remover mA-R 404S (Micro resist technology GmbH, Germany) bath. Here, the metal

deposited remains directly on the substrate, whereas the metal on the resist is lifted off after the removal of the photoresist. At the next step, SU-8 3005 resist (MicroChem Corp., USA) is spin-coated as isolation layer with a rotation speed of 4,000 rpm for 30 s resulting in a film thickness of 5 µm. After a 3 min soft bake on a hotplate at 95 °C, the wafer is kept in the wafer box for half an hour to reduce the risk of sticking of the resist to the mask. The wafer is UV exposed for 1 min through the adequate foil mask, which is followed by a 2 min post-exposure bake on a hotplate at 95 °C. At the final step, the SU-8 development is realized in 1-methoxy-2-propyl acetate solution (Merck KGaA, Germany) on the platform shaker for 1 min. Thus, this releases the elements of the isolation layer which defines the active electrodes areas, the contact pads as well as the physical barrier wells. After a rinse-and-dry step with isopropanol and DI-water for the removal of the resist residues, the wafer is hard baked in an oven for 1 h at 150 °C.

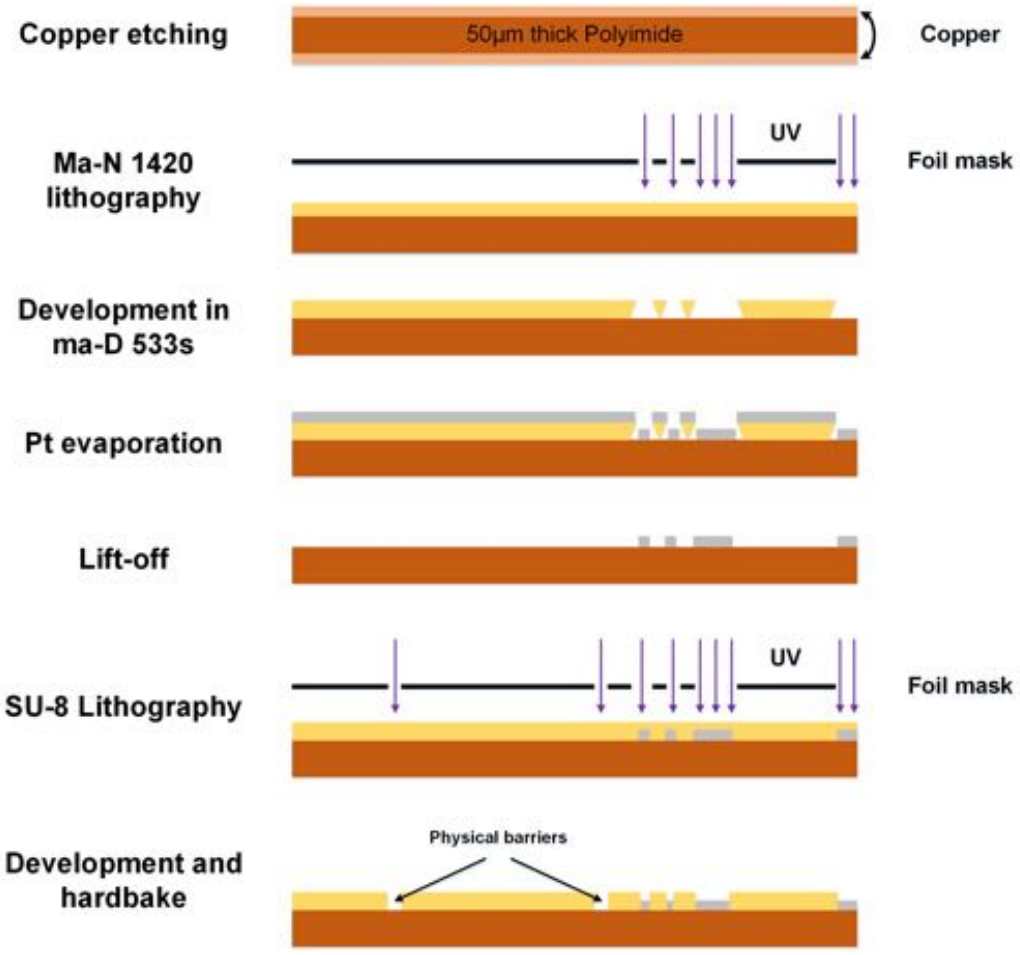

Figure 5.4: *First part of the fabrication process illustrating the electrode patterning and realization of the SU-8 isolation.*

For the realization of the microfluidics, the different layers of Pyralux® PC1025 are laminated and structured onto the wafer. Having removed the dim protective polyolefin foil from the DFR, it is partially attached to a transparent foil. Subsequently, the wafer is placed between the DFR and the transparent foil and laminated with an office laminator MyJoy 12 (GMP Prographics, Germany) at room temperature. Each lamination step is followed by a UV exposure for 2 min 30 s with the appropriate mask. The remaining polyethyene terephtalate (PET) support film has to be removed prior to different lamination steps and the final development of the DFR layers.

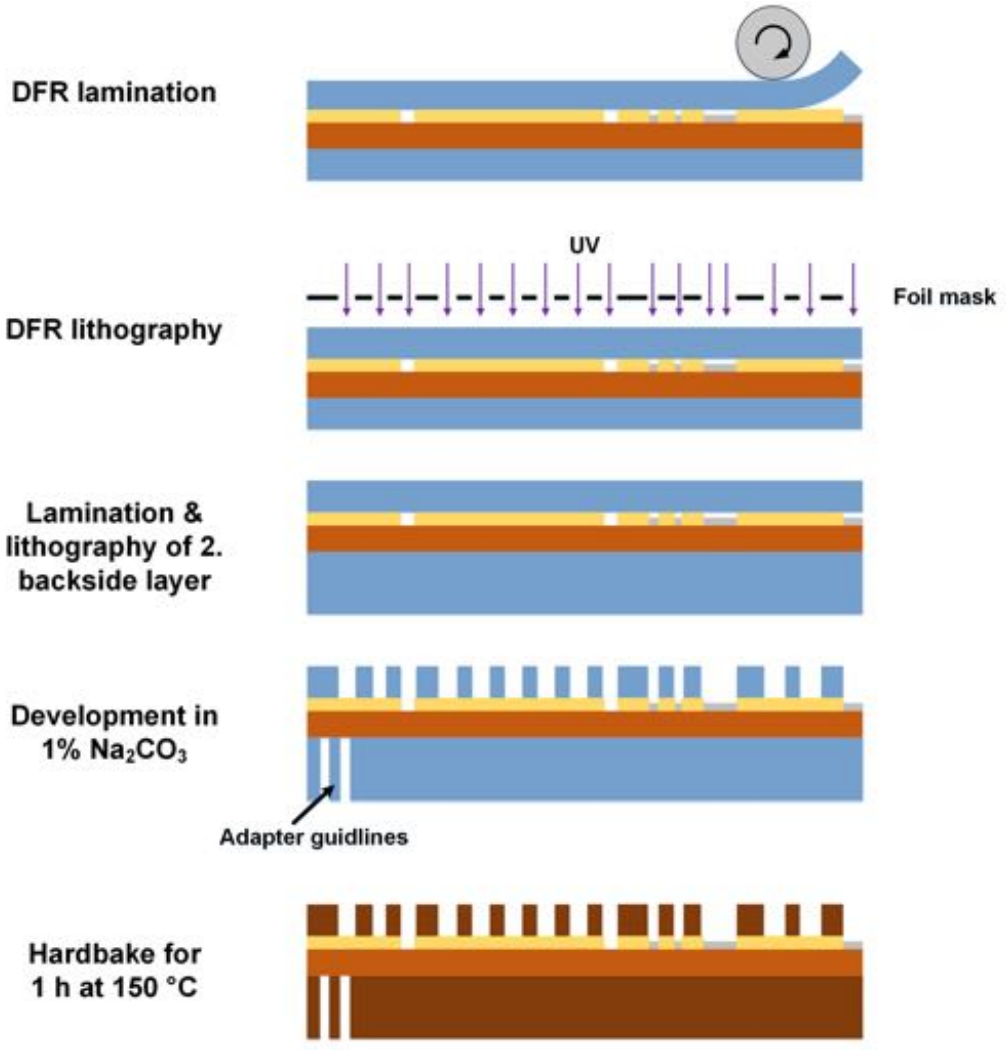

Figure 5.5: *Second part of the fabrication process depicting the structuring of the DFR-based microfluidics.*

Repeating the lamination and exposure steps for different DFR layers, one onto the front- and two onto the backside of the wafer, the microfluidic channels are created. The DFR

layers on the backside of the substrate minimize the thermal expansion, that occurs in the final hard bake step, and thus, prevent the bending of the microfluidic chips. Consequently, the wafer is developed for 2 min in an ultrasonic bath with 1 % sodium carbonate (Na_2CO_3) solution at 42 °C. To stop the development process, the wafer is first dipped in 1 % HCl bath and then rinsed with DI-water. The wafer is first air dried to diminish the swelling of the DFRs during the hard bake for 1 h at 150 °C. Here, a hard bake is required for further fabrication steps in order to improve the chemical resistance of DFRs against different chemicals like Arguna S utilized for silver deposition.

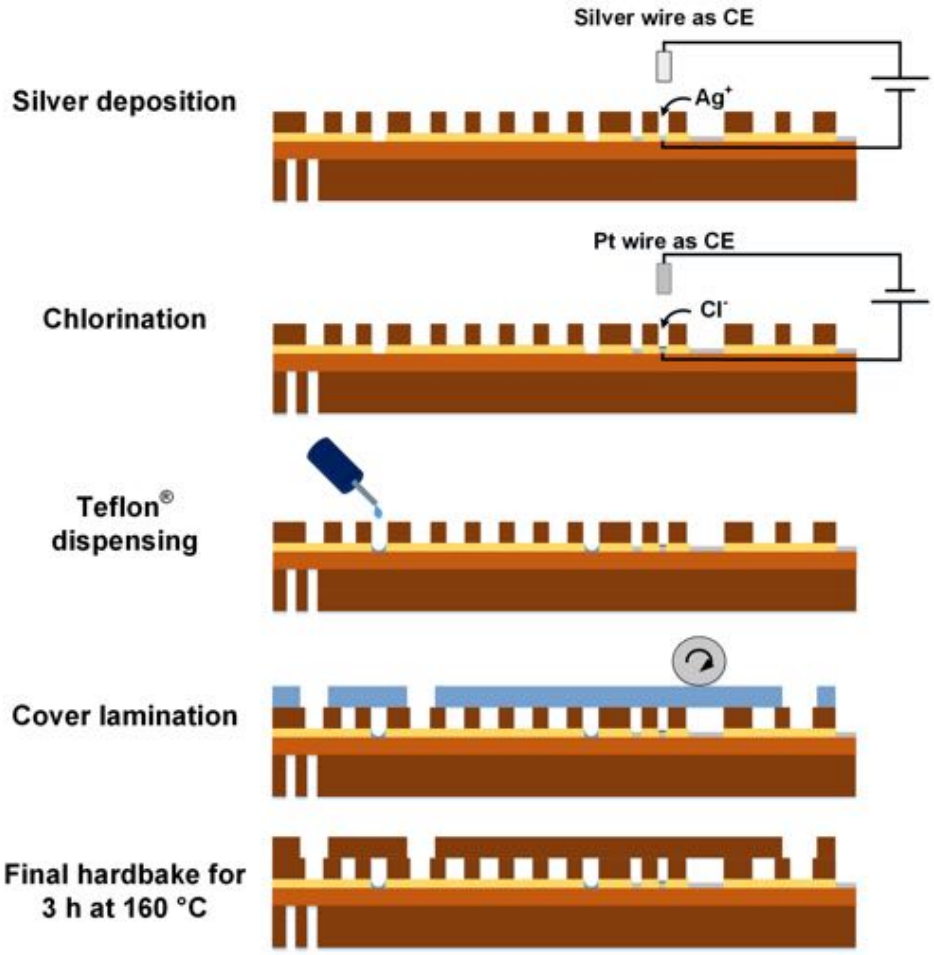

Figure 5.6: *Final part of the chip fabrication illustrating the electrodeposition of reference electrodes and the preparation of the hydrophobic stop barriers.*

The wafer-level fabrication of the on-chip Ag/AgCl reference electrodes is a two step galvanic process: Silver deposition and chlorination. At the first step, all contact pads on the wafer (except the bulk RE contact) are passivated by laminating with an UV adhesive tape 1020R (Ultron Systems Inc., USA), which can be removed afterward easily. This, i.e.

the reduction of the target area for the silver deposition, enhances the process quality such as the uniformity of the deposited layer. Subsequently, the electrodeposition of silver onto the Pt reference electrodes from an Arguna S (Umicore Galvanotechnik GmbH, Germany) solution is performed in an ultrasonic bath to avoid any bubble formation at the electrodes. For this purpose, a current density of -16 mA cm^{-2}, resulting in a deposition rate of approx. 1 µm min^{-1}, is applied for 5 min with a silver wire as counter electrode using a current source (Agilent, USA). At the final step of the galvanization, the silver layer is chlorinated in a 0.1 M KCl solution to Ag/AgCl at +1.6 mA cm^{-2} (approx. 0.1 µm min^{-1}) for 10 min with a platinum wire as counter electrode.

Additionally, a small drop of 1 % Teflon® 1600 in FC-75 (DuPont, USA) is dispensed into the physical stopping barriers by a hand dispenser with the aim of improving their functionality. To seal the microfluidic channels, a cover layer, a sheet of Pyralux® PC1025, is illuminated with an appropriate foil mask and developed with aforementioned process parameters. Subsequently, it is laminated onto the wafer, which is followed by an UV exposure for 10 min to improve the adhesion of the cover layer by polymerization. Finally, the wafer is singularized into individual microfluidic chips by scissors and is hard baked for three hours at 160 °C by means of a linear temperature ramp.

The DFR-based microfluidic iLab platform including two different single-analyte and three multi-analyte approaches is presented in Figure 5.7.

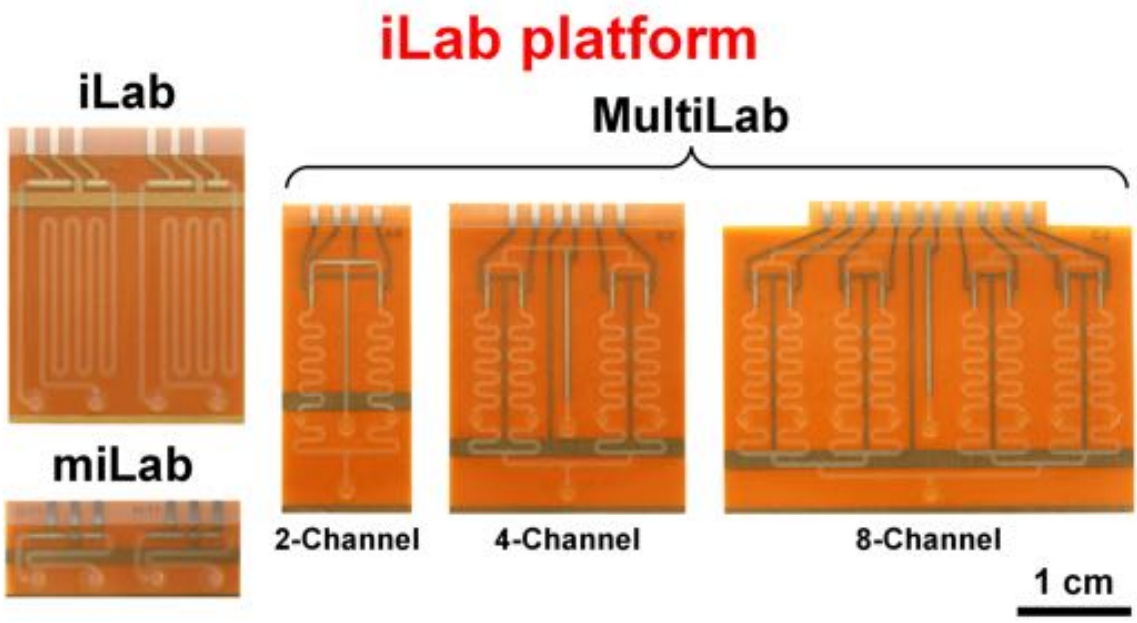

Figure 5.7: *Photograph of the iLab platform comprising two different single-analyte and three multi-analyte approaches.*

5.3.3 Estimation of cost and time-to-fabrication

The fabrication costs[1] of the different microfluidic sensor devices presented here are 1.57, 0.49 and 0.77 € for iLab, miLab and a channel of MultiLab, or vice versa. The cost of a single chip is quoted considering the substrate and DFR materials, the Pt evaporation for the electrode patterning, and the chemical reagents like SU-8, silver and silver chloride electrolytes as well as developer and remover solutions. The material costs of a single chip are detailed in Table 5.3.

Table 5.3: *Calculation of fabrication costs of different iLab platform devices.*

	iLab	**miLab**	**MultiLab**
Costs in €	**single device**		**per channel**
Substrate - Pyralux® AP	0.32	0.1	0.16
DFR - Pyralux® PC	0.11	0.03	0.05
Pt Evaporation	0.79	0.25	0.39
Chemical reagents	0.35	0.11	0.17
Total device	**1.57**	**0.49**	**0.77**

Due to the low reagent consumption of the iLab platform the volumes of the reagents and samples required for a measurement is less than 5 µl independent from the chip version. In the case of miLab and MultiLab this is even below 1 µl per channel. We presume, given that 1 µl of anti-fluorescein antibody at a concentration of 50 µg ml^{-1} is essential for functionalization of the immobilization capillary, that the number of tests is about 600, which can be executed with a stock antibody solution of 125 µl (at 2 mg ml^{-1}). Since the antibody solution is prized about 75 € per mg, the anti-fluorescein antibody cost per measurement is estimated to be between 0.20 € and 0.30 €. Using similar calculations, the operator DNAs tagged with fluorescein, and biotinylated TetR and PIP for tetracycline and pristinamycin detection, respectively, costs per test are 0.01 € each. 1 % BSA blocking, assay preparation and wash buffers are estimated to be less than 0.01 € in total. Adding the costs of all reagents amounts to an estimated total assay cost of 0.29 € per DNA-based multiplexed antibiotic test, which is mainly dictated by the price of the anti-fluorescein antibodies used for the chip functionalization.

The entire fabrication process of the DFR-based biosensors takes a work time of approximately 10 hours (except the hard bake steps and the platinum evaporation) and can be easily scaled-up by means of the automatization. Furthermore, the assay preparation, for example DNA-based antibiotic detection, is about 2 hours and 15 minutes (1 hour of anti-fluorescein antibody coating, 1 hour for BSA blocking, and 15 minutes for the fluorescein tagged DNA binding). Many sensor chips can be processed in parallel. In this work we used manual pipetting for the different incubation steps. However, it is possible to

[1] Based on the fabrication of 460 wafers.

combine our system with robotic techniques for spotting biomolecules on individual chip inlets in parallel, which increases further the throughput of the chip preparation.

5.4 System integration

Besides the design and fabrication of the sensors, the system integration is also crucial for the development of microfluidic chip platforms. For this purpose, a reliable and simple measurement setup is to be realized. In this section, different custom-made chip holders enabling the fluidic and electrical connection of the fabricated biosensors to its environment as well as the final measurement setup are described and discussed briefly.

5.4.1 Chip holder

Different custom-made chip holders are implemented for the single-analyte and multiple analyte versions of the iLab platform. In the next two sections they will be explained in detail.

iLab & miLab

For iLab and miLab biosensor chips custom-made chip holders are designed and fabricated using the same approach. The only difference between them is their dimension stemming from the chip size. Therefore, in this part, the main strategy behind the realization will be described merely.

Above all, the custom-made chip holder is to be capable of providing an easy connection between the biosensor chip and the electrical and fluidic periphery for the signal readout as well as fluid flow. To achieve the electrical connection, a PCB is designed with EAGLE PCB Design Software (CadSoft Computer GmbH, Germany). It comprises a rotary back lock connector XF2M (Omron Corp., Japan) for fast and reliable chip mounting and a 16-way micro-match connector (Tyco Electronics Amp, Germany) for the communication with the bipotentiostat (Jobst Technologies GmbH, Germany). For the fluidic flow, a reversible connection between the microfluidic chip and the syringe pump is obtained by means of vacuum cups (Nordson EFD, Germany).

The custom-made chip holder allows the measurement of four sensors at the same time and consists basically of milled PMMA parts. At the bottom part, the PCB takes place for the electrical connection, whereas the fluidic connection blocks, two upper parts, are embedded with the vacuum cups. After chip loading, the upper parts are mounted to the bottom block via screws and thus, provide the fluidic connection, as shown in Figure 5.8. This design allows a tight chip connection, achieved by vacuum cups with low pressure, without an effect to the fluid flow in the chip capillary. The distinctive features of such a setup are reliability, re-usability and quick chip mounting.

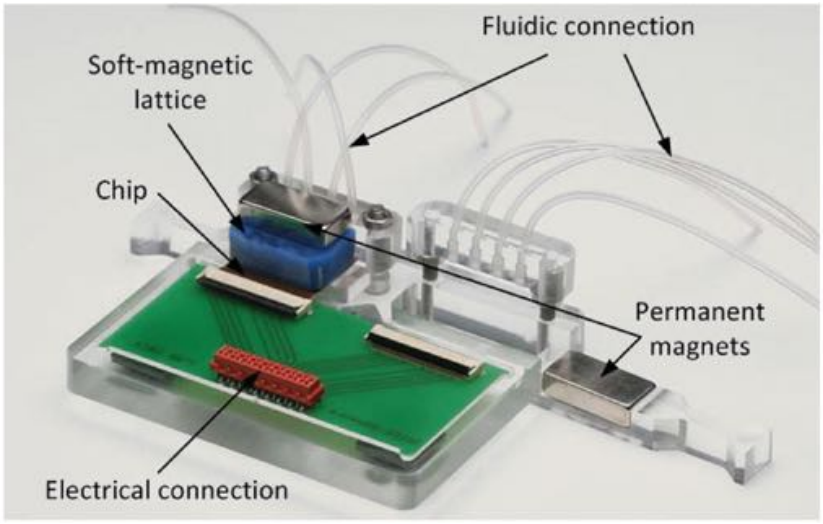

Figure 5.8: *Photograph of the custom-made chip adapter illustrating its key features. This particular chip holder is designed for the manipulation of magnetic beads in the chip capillary (reprinted from [204]).*

MultiLab

On account of our experience from the single-analyte versions of the iLab platform, a superior custom-made chip holder with a magnetic fluidic connection system is adopted for the microfluidic multiplexed biosensors.

Similar to the previous versions, a PCB is designed for the electrical connection with the same lock connector aiming easy chip loading and a 37-pin D-sub connector as well as a ground contact for the potentiostat, as shown in Figure 5.9. The application of a ground contact offers a sufficient shielding for low currents, in the nA range, and eliminates the need for a Faraday cage. As aforementioned, vacuum cups require a low pressure to connect the fluidic ports of the sensors with the periphery. Here, the same manner is chosen to seal the individual channel inlets. Hence, the vacuum caps are filled to a mid-level with PDMS and embedded in the fluidic connection block.

The custom-made chip holder comprises two main parts: The fluidic connection block and the bottom plate. The single parts are milled out of 8 mm thick PMMA. To supply the electrical connection, the designed PCB is fixed into the bottom plate with UV-curable adhesive Loctite 3201 (Henkel Ltd., UK). The magnetic-actuated fluidic connection is realized by means of cylindrical neodymium magnets with a holding-force of 2.2 kg, which are buried in the PMMA blocks. The outer diameter of the employed magnets is 10 mm, whereas the inner diameter is 4 mm. In the locked mode, the distance between two magnets is 2 mm. To enable a simple handling, the fluidic connection block is guided by two screws and attached to the magnets on top of the screws during the chip loading, as displayed in Figure 5.9a.

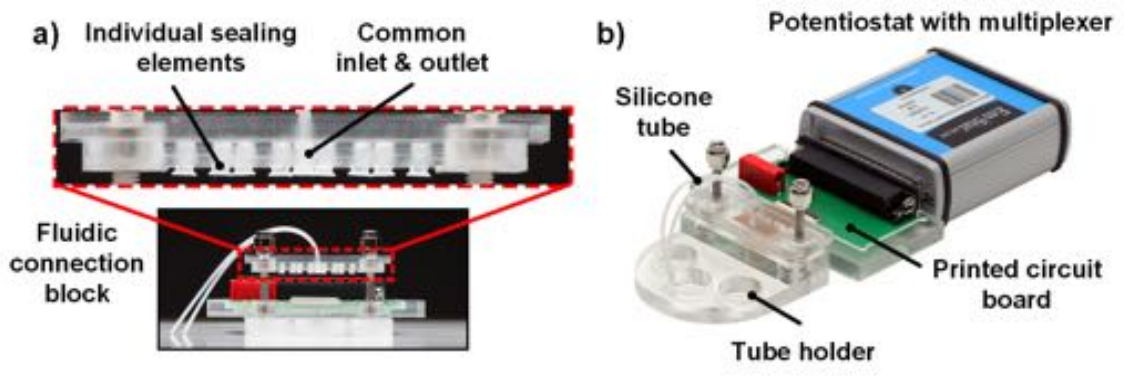

Figure 5.9: *a) Cross-sectional image of the custom-made chip holder depicting its main elements. It allows for a simple and fast chip loading using magnetic actuation. b) Photograph of the compact potentiostat with multiplexer mounted with the custom-made chip holder. (adapted from [39]).*

5.4.2 Measurement setup

For the single-analyte versions of the iLab platform, the same measurement setup is utilized as presented previously in [40, 204]. It includes the custom-made chip holder and provides facile chip connection and simultaneous measurement of up to four microfluidic chips. The amperometric signal readout is performed with a four-channel bipotentiostat (Jobst Technologies GmbH, Germany) and visualized by a personal computer using the BioMON software (Jobst Technologies GmbH, Germany). To establish a constant fluid flow as well as the stop-flow protocols, a syringe pump PHD2000 (Harvard Apparatus, USA) is used in withdrawal mode with four individual 2.5 ml syringes (Hamilton Gastight, USA) and silicone tubes.

As for the microfluidic multiplexed biosensor, the whole measurement setup is depicted in Figure 5.10. Here, all electrochemical measurements are conducted by the application of a compact potentiostat EmSTAT3 integrated with an eight channel multiplexer MUX8 (PalmSens BV, The Netherlands). For the simultaneous multiplexed detection, the following potentiostat specifications are chosen: An auto current range (CR) between 1 nA and 1 µA is set, which offers a signal resolution of one tenth of the actual CR. Further, the integrated multiplexer is configured for a constant polarization of all working electrodes connected to the system by the use of a common reference and counter electrode.

The measured signals are recorded by a personal computer with the PSTrace 4.6 software (PalmSens BV, The Netherlands). To regulate the fluid flow a similar approach to the single-analyte measurement is followed. To ensure a bubble-free filling, the microfluidic channel network is filled by hand prior to the measurements.

Figure 5.10: *Photograph of the whole measurement setup illustrating a 8-channel microfluidic chip fastened into the chip holder, connected to the syringe pump and potentiostat.*

6 Results: Lab-on-a-chip performance

Preface

This chapter reports the performance evaluation of the microfluidic multiplexed biosensor platform with regard to its electrochemical and biochemical characteristics. It starts with an electrochemical characterization to obtain the optimal measurement conditions for the amperometric detection of hydrogen peroxide.

In the first place, basic electrochemical studies of the employed electrode material (e.g. determination of the surface roughness, and of the preconditioning method) and of the oxidation potentials of glucose (substrate) and hydrogen peroxide (analyte) are conducted. Later, the investigation of the performance parameters such as hydrogen peroxide sensitivity and flow rate dependency the iLab platform is presented.

After the electrochemical characterization, the surface properties of the DFR Pyralux® PC1025, employed here as solid phase material for the immunoassays, is examined using an biotin-avidin GOx model assay. This biochemical survey contains the investigation of the different surface functionalization and passivation strategies, including their incubation times and concentrations, as well as the glucose concentration dependency of the measured assay signals. Consequently, a cross-sensitivity test is examined with the microfluidic multiplexed biosensors in order to exclude any crosstalk between the neighboring channels.

6.1 Electrochemical characterization

In this section, the electrochemical characterization of the iLab platform is discussed. All electrochemical measurements are performed in 0.1 M phosphate buffer saline (PBS) as supporting electrolyte containing 0.1 M NaCl at physiological pH of 7.4. The buffer solution is prepared with ultra pure water HPLC grade (Alfa Aesar GmbH & Co KG, Germany). For the electrochemical experiments, D-(+)-Glucose (99.5 %) and hydrogen peroxide (30 % wt) are purchased from Sigma-Aldrich, Germany.

6.1.1 Investigation of the electrochemical cell

The electrochemical study begins with an investigation of the single electrochemical cell with multiple working and short-circuited reference electrodes, and a common counter electrode. In order to examine the cleanliness and the surface roughness of microrough

Pt electrode surface, as well as the electrochemical behavior of such a measurement cell setup, cyclic voltammetric analysis are performed.

For this purpose, cyclic voltammograms at single working electrodes of different MultiLab versions are recorded under steady-state conditions (no fluid flow) in 0.1 M PBS with a scan rate of 50 mV s^{-1}. Cyclic voltammograms, as shown in Figure 6.1, depict all of the platinum specific features, which are explained detailed in Section 3.1.6.1. This is an indication for clean and residue-free electrodes after the chip fabrication. Please note that to provide a better understanding of the curve characteristics only cyclic voltammograms of single working electrodes of different MultiLab versions are illustrated in Figure 6.1.

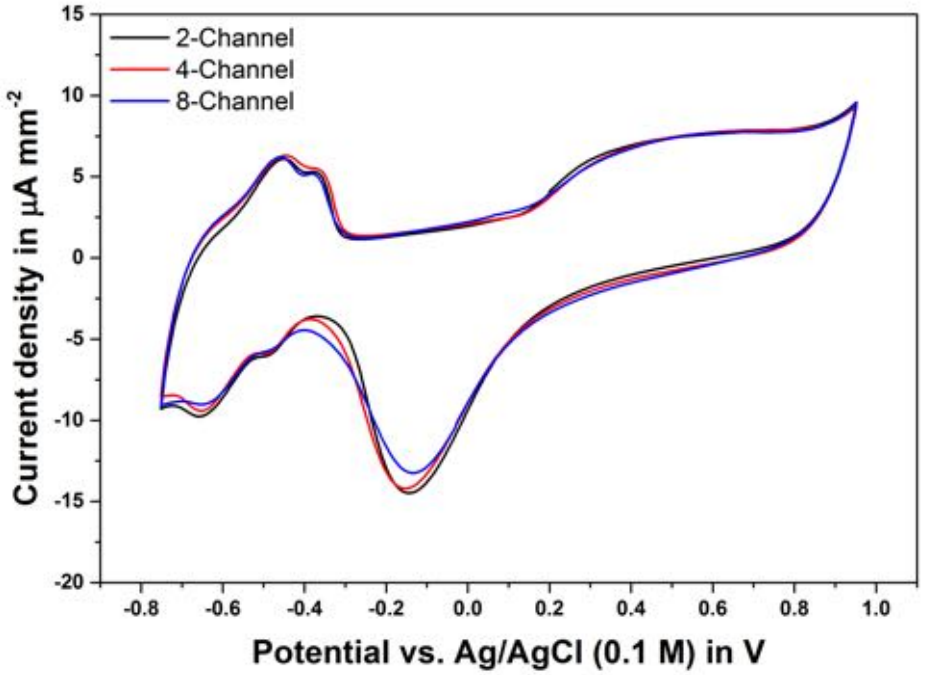

Figure 6.1: *Cyclic voltammograms at a single microrough Pt working electrode of the different MultiLab versions in 0.1 M PBS using an scan rate of 50 mV s^{-1} with 2 mV potential step vs. the on-chip Ag/AgCl reference electrode.*

Furthermore, cyclic voltammograms of the different MultiLab designs prove almost the same electrochemical behavior independent of the size of the microfluidic network and the number of working electrodes. Thus, a potential drop at the electrochemical cell in the microfluidic channel can be excluded. This is most likely because of the application of multiple short-circuited reference electrode next to each working electrode.

6.1.2 Determination of the surface roughness

For the sensitivity of the electrochemical sensors, the roughness of the electrode surface is crucial. The higher the electrode area is, the higher is its catalytic activity and resulting current signals [142, 143]. Hence, the polyimide substrate Pyralux AP 8525R known for its high surface roughness is used for chip fabrication [209]. The hydrogen adsorption and desorption regions of cyclic voltammograms at platinum electrodes are a measure for the electrode surface roughness. The underlying theory is previously described in Section 3.1.6.1.

In this regard, the active electrode area is determined by a cyclic voltammogram with a scan rate of $100\,\mathrm{mV\,s^{-1}}$ (see Figure 3.4). The integration of the current density over time in the hydrogen region is illustrated in Figure 6.2 and thus, the charge transfer for hydrogen adsorption and desorption can be calculated. Comparing the resulting charge of $2{,}959.3\,\mu\mathrm{C\,cm^{-2}}$, for the hydrogen desorption area with the experimentally derived value of $210\,\mu\mathrm{C\,cm^{-2}}$ at the smooth polycrystalline platinum electrodes [144], a surface roughness factor of 14.1 can be estimated.

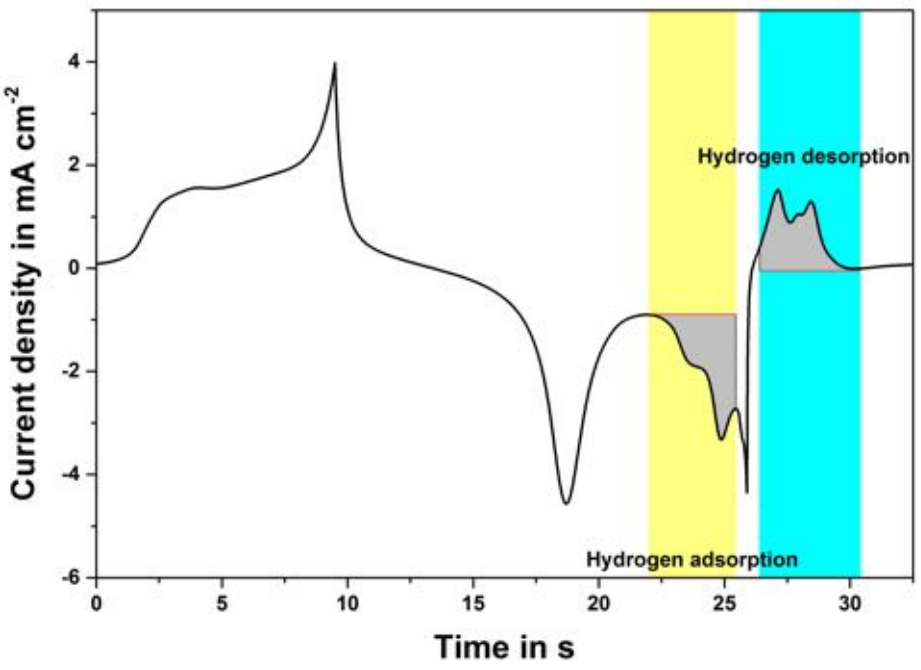

Figure 6.2: *The current density at the microrough platinum on-chip working electrode (without cover) over time of a cyclic voltammogram in 1 N H_2SO_4 at scan rate of $100\,mV\,s^{-1}$. The integration of the hydrogen desorption area gives a total charge transfer of $2{,}959.3\,\mu C\,cm^{-2}$, resulting in a surface roughness factor of 14.1.*

This result proves the high surface roughness of the polyimide substrate in contrast to the classical substrates applied for the thin-film technology such as glass [210] or silicon [211],

where surface roughness factors of less than 2 were reported for both. In direct comparison with the values of the surface roughness factor of about 7 presented by Weltin *et al.* [208] with a similar approach, the calculated values are twofold higher. The optimization of the fabrication process may cause this difference, in other words by the elimination of the titanium layer and its subsequent etching in hydrofluoric acid. The etching step could limit the electrode area in case of an insufficient process. This may occur due to a highly oxidized titanium layer or blocked sites on the microrough polyimide surface, where the etch solution cannot access to the titanium layer.

6.1.3 Investigation of the oxidation potentials

The working principle of the electrochemical microfluidic biosensor relies on the amperometric detection of hydrogen peroxide, a measure of the ELISA reaction. Hence, the oxidation of the hydrogen peroxide at the platinum electrodes is to be investigated by cyclic voltammetric analysis for the determination of the optimal working potential. Furthermore, the electrooxidation of the glucose direct at working electrode should be also studied in order to exclude any side effects.

Different cyclic voltammograms at the on-chip working electrodes are conducted in 40 mM glucose and 195 µM hydrogen peroxide and compared with a cyclic voltammogram performed in pure PBS. Here, an appropriate working potential needs to be determined for the oxidation of hydrogen peroxide in the presence of glucose.

According to Figure 6.3, hydrogen peroxide is oxidized, whereas oxygen resulted from H_2O_2 oxidation is reduced again at the platinum electrodes. These processes lead to increased current densities positively by oxidization or negatively by reduction. In the case of the glucose oxidation, the recorded cyclic voltammogram shows distinct current peaks that can be related with different reactions according to [212, 213] as follows:

- Peak 1 takes place in the potential region, where hydrogen adsorption at the platinum electrodes arises, and corresponds to the adsorption and dehydrogenation of glucose. Thereby, the generation of an adsorbed residue poisons the electrode surface.
- The second peak is associated with the oxidation of these residues produced in the potential region of Peak 1.
- Peak 3 represents the direct reaction of glucose at the oxidized platinum electrode.
- Directly after the removal of the platinum oxide during the cathodic scan, in the region of Peak 4 the oxidation of glucose occurs.

For the hydrogen peroxide detection, Peak 3 is likely to play a decisive role. Herein, the glucose reacts quickly with chemisorbed oxygen at the platinum working electrode (PtO) in a non-faradaic process to generate gluconic acid [214] as follows:

$$\text{glucose} + \frac{1}{2}\,O_2 \rightarrow \text{gluconic acid}. \tag{6.1}$$

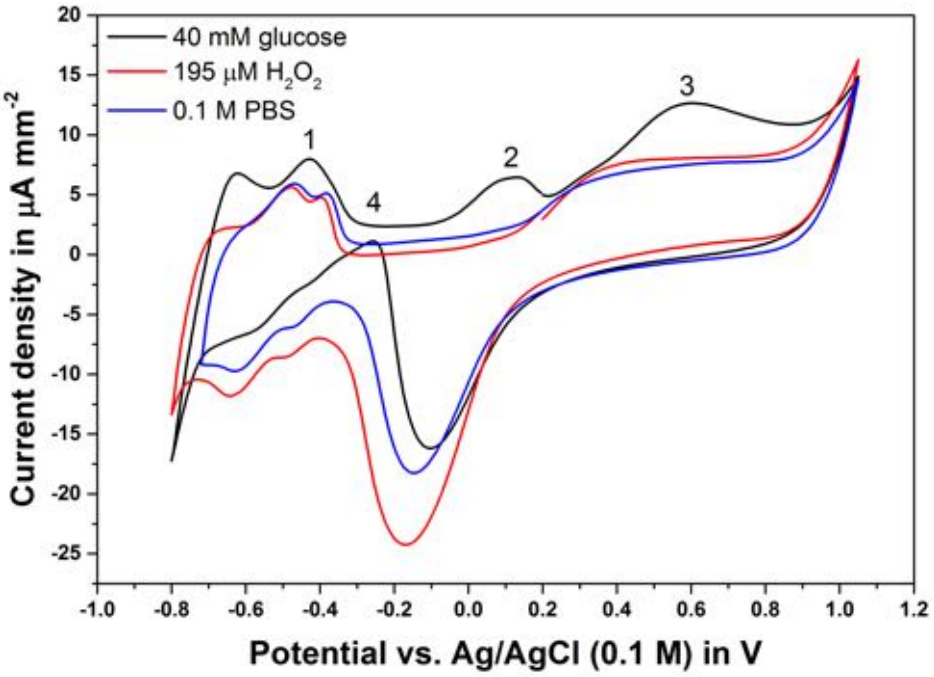

Figure 6.3: *Cyclic voltammograms at a microrough platinum working electrode in pure (blue), PBS containing either 40 mM glucose (black) and 195 µM hydrogen peroxide (red) with a scan rate of 50 mV s^{-1} vs. the on-chip Ag/AgCl reference.*

This leads to a strong deactivation of the working electrodes by the reversible formation of platinum oxide (PtO_2) as well as increased background currents [215]. Therefore, the oxidation potentials of glucose should also be taken into account for the final decision of the working potential. The influence of glucose on the measured signal is examined at every step of the electrochemical characterization and optimization.

In order to take a close look at the oxidation potentials of hydrogen peroxide under real measurement conditions, cyclic voltammograms at the on-chip Pt electrode in hydrogen peroxide and in pure PBS are performed using a flow rate of 20 µl min^{-1}. The resulting curve for H_2O_2 is shown in Figure 6.4 by the subtraction with the pure PBS curve. On the cathodic (reverse) scan, the measured current densities prove a diffusion-limited behavior at potentials between ca. 0.45 V and 0.8 V. On the other hand, the signal saturation occurs first at a potential of about 0.65 V in the anodic (forward) scan, 0.2 V higher than in the reverse scan.

Figure 6.4 clearly demonstrates, that for the oxidation of hydrogen peroxide at platinum electrodes first the platinum oxide layer has to be formed, which is already constituted in the case of the cathodic scan. These results support strongly the theory described in Section 3.1.6.2. To exclude any signal effect caused by glucose oxidation on the one hand and to provide a diffusion-limited reaction of H_2O_2 at the platinum electrodes on

the other hand, a working potential of 0.45 V vs. the on-chip Ag/AgCl reference is chosen for the presented platform. Prior to the amperometric measurements, the electrodes are preconditioned with a potential of 0.8 V for 1 min in order to form a stable platinum oxide layer.

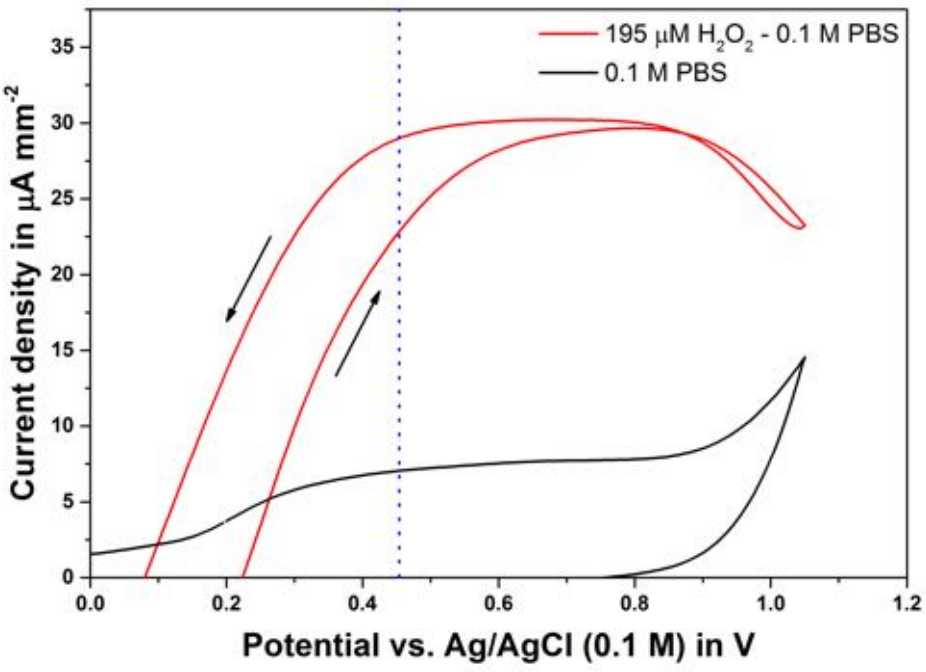

Figure 6.4: *Cyclic voltammogram at the on-chip Pt electrode of 195 µM H_2O_2 (red) using a scan rate of 50 mV s^{-1} and flow rate of 20 µl min^{-1} with pure PBS curve (black) subtracted. The dashed line indicates the chosen measurement potential of 450 mV, while the arrows show the scan direction.*

6.1.4 Preconditioning

The chip fabrication consist of many different steps such as DFR processing for the realization of microfluidics and several hardbake procedures. These processes could effect the electroactive surface of the electrode, and thus the sensor sensitivity and reproducibility.

As a result, an electrochemical pretreatment protocol of the working electrodes is investigated in addition to the initial oxidation of the platinum electrodes at 0.8 V for 1 min. It is mainly based on a two-step choronoamperometric protocol, where the electrode surface is oxidized to platinum oxide and reduced back to platinum. To achieve a residue-free electrode surface and thus, reproducible results, the applied protocol is repeated for a specific number of cycles. Therefore, the appropriate oxidation and reduction potentials for the preconditioning as well as an optimized number of repetition is to be determined. All preconditioning tests are performed in 0.1 M PBS with a defined cycle time of 5 s.

Firstly, different preconditioning procedures with a fixed number of cycles (N = 100) are performed and evaluated by the determination of the current densities for 39.2 µM H_2O_2 and 40 mM glucose by amperometric detection at 0.45 V. Herein, the oxidation potential is hold at 0.8 V, while the reduction potential is varied between 0.2 and -0.3 V. The H_2O_2 sensitivity strongly increases and reaches a plateau at a reduction potential of above -0.05 V, as can be seen in Figure 6.5a, while the glucose sensitivity stays constant up to a potential of -0.3 V. In order to maximize the H_2O_2 sensitivity in the presence of glucose, 0.8 V and -0.1 V are selected as oxidation and reduction potentials for the optimized pretreatment protocol, respectively.

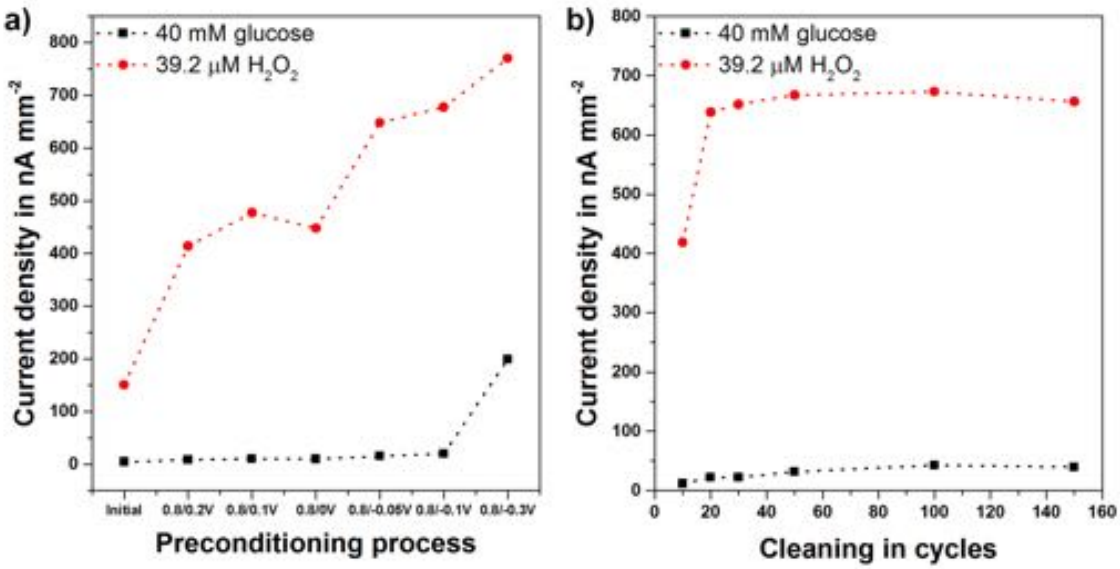

Figure 6.5: *The current densities measured in 39.2 µM H_2O_2 and 40 mM glucose for different preconditioning procedures a) with 100 cycles, and for different number of cleaning cycles using the optimized preconditioning procedure b) with 0.8 and -0.1 V vs. the on-chip Ag/AgCl reference. All preconditioning tests are executed in PBS with a cycle time of 5 s.*

Secondly, the required number of cleaning cycles is tested with the chosen preconditioning. The achieved signals in both cases indicate almost no difference after 20 cycles, as shown in Figure 6.5b. To guarantee a good reproducibility, the number of the cleaning cycles is set to 50 for the following experiments. The final measurement protocol is given in Table 6.1.

Table 6.1: *Chronoamperometric protocol used in stop-flow measurements.*

	Applied potential(s)		**Duration**
Electrode cleaning	0.8 V	-0.1 V	50 cycles each for 5 s
Oxide layer formation	0.8 V		60 s
Amperometric detection	0.45 V		

6.1.5 Flow rate dependency

After the quantification of the working potential and preconditioning method, the flow rate dependency of the iLab platform is evaluated to determine the optimal flow rate for the electrochemical detection of hydrogen peroxide in the presence of glucose. For this purpose, different flow rates up to 50 µl min^{-1} are applied to the microfluidic chip and the resulting steady-state currents in pure PBS, in PBS with 39.2 µM H_2O_2 and with 40 mM glucose are recorded, as illustrated in Figure 6.6.

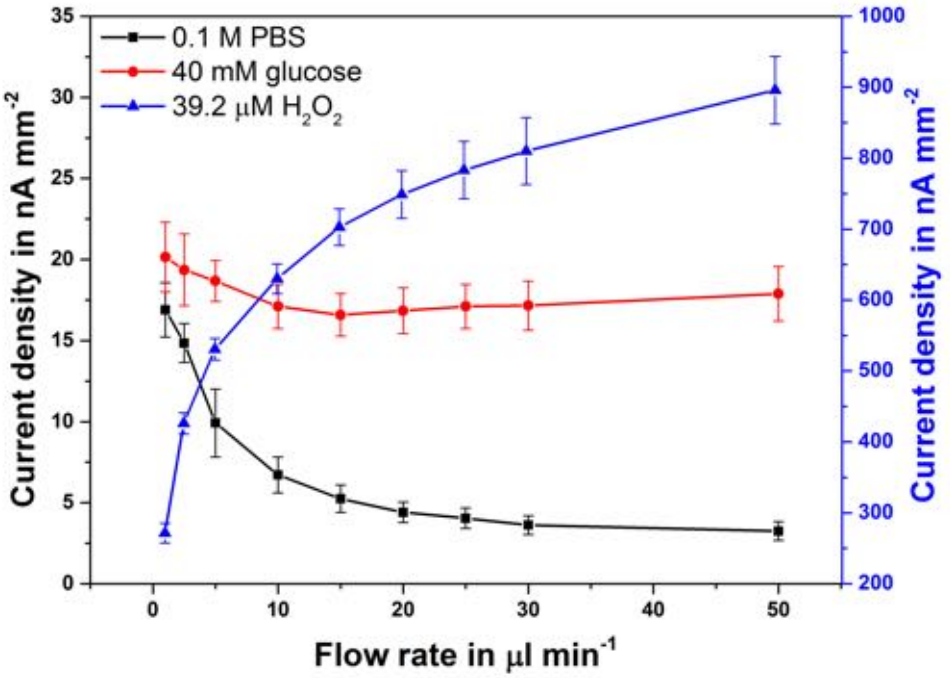

Figure 6.6: *Flow rate dependencies of the biosensor chips (presented data of $N = 8$ from different fabrication batches) for 0.1 M PBS (black), 40 mM glucose (red) and 39.2 µM hydrogen peroxide (blue). As for H_2O_2, the measured current signals increase with the application of higher flow rates due to enhanced analyte transport to the working electrode.*

In the case of PBS and glucose there is only a small flow rate dependence of the measured signals. On the other hand, the signal response to the hydrogen peroxide is highly contingent on the applied flow rates. Although the signal curve indicates a typical saturation behavior, beginning with a flow rate of 20 µl min^{-1}, this is not achieved by the investigated flow rate range. This means, that the highest current response is recorded at the maximum tested flow rate.

In order to constitute a good compromise between the signal sensitivity and other important system parameters such as reagent consumption during the amperometric measurement and stability (e.g. of the multichannel networks), an adequate flow rate of 20 µl min^{-1} is chosen for the iLab platform. Please note that the given flow rate here is defined per

channel and has to be adapted to 40, 80 and 160 µl min^{-1} for the 2-, 4- and 8-channel MultiLab designs, respectively.

6.1.6 Hydrogen peroxide calibration and performance characteristics

At the final step of the electrochemical characterization, the hydrogen peroxide sensitivity using the optimized system parameters from the previous experiments is to be determined. For the calibration measurement, a 2-fold dilution series of H_2O_2, from 345 nM up to 195 µM, is introduced into the microfluidic chip at a flow rate of 20 µl min^{-1} per channel and a working potential of 0.45 V vs. the on-chip Ag/AgCl reference.

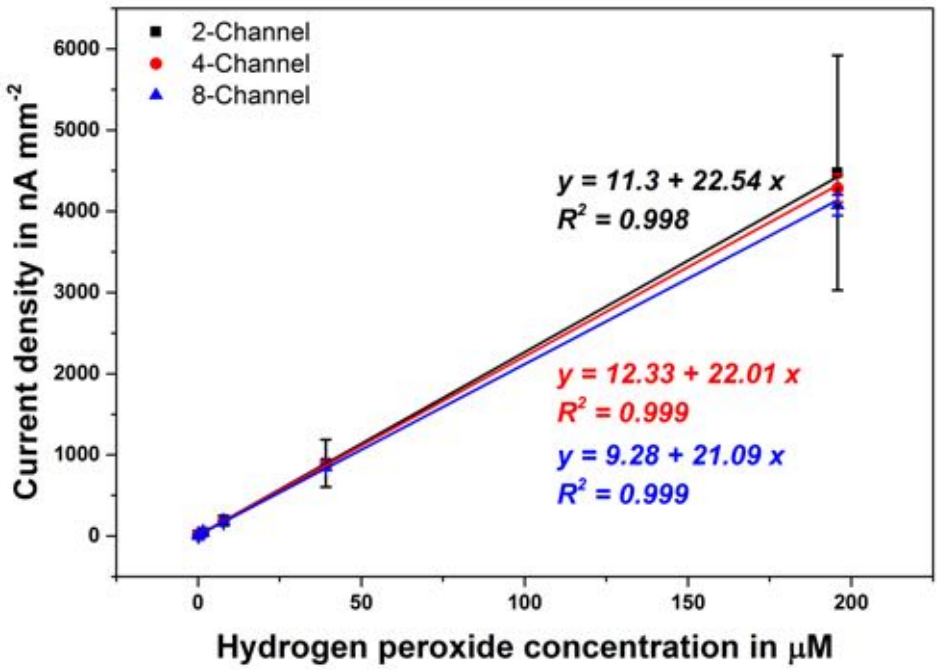

Figure 6.7: *Calibration curves for the amperometric hydrogen peroxide measurement using the different MultiLab versions (N=2× channel number) under the optimized conditions. A flow rate of 20 µl min^{-1} is applied per channel and a working potential of 0.45 V vs. the on-chip Ag/AgCl reference.*

The calibration curves of hydrogen peroxide obtained with the different MultiLab formats are depicted in Figure 6.7. To show the degree of batch-to-batch variability each curve presents a duplicate measurements using 2 individual sensors from different fabrication batches (N=2×channel number). The microfluidic platform clearly exhibits a linear signal behavior over the whole measurement range of 345 nM up to 195 µM H_2O_2. The resulting hydrogen peroxide sensitivities (slope of the fit) for the 2-, 4- and 8-channel chip are 22.54, 22.01 and 21.09 nA mm^{-2} µM^{-1}, respectively. Please notice that comparable average

H_2O_2 sensitivities of 20.03 nA mm^{-2} µM^{-1} are obtained from the calibration with different single-analyte versions of the iLab platform (data not shown).

For different MultiLab versions, the average hydrogen peroxide sensitivity is found to be 21.4 nA mm^{-2} µM^{-1} with a coefficient of variation below 5 %. In comparison with the 2-channel chip, the 4- and 8-channel formats supplies 97.7 % and 93.5 % of the particular current densities. These results prove only very slight differences because of the ohmic drop in the case of increasing the channel number. Therefore, this effect can be excluded here for the further applications. Yet, it should be kept in mind that this may limit the system and should be deeper investigated in case of a scaling up design (e.g. more than 10 channels).

6.2 Biochemical characterization

The second part of the characterization, i.e. biochemical characterization, deals mainly with the investigation of the immobilization characteristics of the Pyralux® PC 1025 utilized for the microfluidics and the optimization of the assay conditions. For this, a biotin-avidin model assay with glucose oxidase as enzyme label is employed. This simplified assay system accommodates an easier control over the biochemical performance of the developed platform compared to the conventional immunoassays.

The biochemical characterization begins with the comparison of different immobilization strategies. This is followed by the assay optimization of the chosen method including its concentration and incubation times. Furthermore, different blocking strategies are studied to minimize the background signals caused by the non-specific binding of biomolecules.

After the optimization of the individual assay components, the glucose concentration is investigated to obtain a kinetic limitation of the analyte generation by the immobilized enzymes, so called "Michaelis-Menten kinetics". Finally, a cross-sensitivity test, only for the MultiLab sensors, is carried out to exclude any crosstalk between the neighboring channels owing to the diffusion of hydrogen peroxide during the stop-phase.

6.2.1 Chemicals and methods

Both GOx–avidin and biotinylated glucose oxidase (bGOx) conjugates are purchased from Biomol, Germany. All other chemicals are obtained from Sigma-Aldrich, Germany or otherwise as stated in the text. The following reagents are used for the assay preparation and the electrochemical measurements:

- Physiological PBS: 0.01 M phosphate buffer, 0.137 M NaCl and 2.7 mM potassium chloride (KCl) , pH 7.4, at 25 °C.
- Wash buffer: 0.01 M phosphate buffer, 0.137 M NaCl, 2.7 mM KCl and 0.05 % Tween® 20, pH 7.4.
- Blocking solution: 1 % BSA in physiological PBS, pH 7.4.
- Activation buffer: 0.1 M MES buffer containing 0.9 % NaCl, pH 6.0.
- Glucose substrate: 40 mM D-(+)-Glucose in 0.1 M PBS containing 0.1 M NaCl, pH 7.4.

The stock solution of 1 M glucose is prepared and stored overnight at 4 °C prior to use. A standard volume of 6, 3 and 2 µl reagent per channel is used for the incubation processes of iLab, miLab and MultiLab chips, respectively. To prevent any contamination of the electrochemical cell, all reagents (except the wash buffer) and samples are introduced and sucked out through the channel outlet. The wash buffer is introduced by the channel outlet. Each incubation is followed by a washing step to remove unbound biomolecules and a drying step using a custom-made vacuum pen. This step mimics the washing procedure of

the conventional ELISA. For the incubation of the different MultiLab versions, individual channel inlets are temporarily sealed with an adhesive tape during the washing steps.

For signal evaluation of the amperometric stop-flow measurements, either the peak charge or peak height can be employed. Our previous studies demonstrate that there is a linear correlation between the peak charge and peak height of the stop-flow signals [40, 204]. For this reason, only the peak height is utilized for the data analysis in this thesis to allow an easy signal processing.

6.2.2 Adsorption vs. Immobilization

The first step of the biochemical characterization is the comparison of different immobilization strategies regarding their feasibility to the employed channel material. For this purpose, adsorption and covalent immobilization by means of carboxyl-to-amine crosslinking of biomolecules are performed with the model assay. The theoretical background of these techniques is given in Section 3.2.3.

For the covalent immobilization of avidin, the biosensor chips are pretreated with the EDC/NHS-linker chemistry to activate the carboxyl groups on the Pyralux® PC 1025. The immobilization capillaries are activated for 1 h with 100 mM EDC and 200 mM SNHS in activation buffer at RT in the dark. After a subsequent washing step with 200 µl of 100 mM MES buffer, 100 µg ml^{-1} avidin in physiological PBS is incubated in the activated channels for one hour. In the case of the adsorption test, the microfluidic chips are directly incubated with avidin. This is followed by the introduction of the blocking solution, 1 % BSA in physiological PBS, in all biosensor chips for another hour. In the last step, 1 µg ml^{-1} of biotinylated glucose oxidase is incubated for 15 min to all channels. Prior to the amperometric detection chips are rinsed with 300 µl of wash buffer and dried. The control chips are prepared with the same assay protocol, except the avidin immobilization.

The electrochemical measurements are performed in duplicates with a 40 mM glucose substrate using different stop-flow times. The 2 min stop-flow readout of avidin-bGOx model assay for different immobilization techniques are depicted in Figure 6.8. For the covalent immobilization, 32 % higher signals than for the adsorption along with an improved signal-to-background ratio are observed. Nevertheless, the peak current densities of both strategies are sufficiently high enough to ensure a reasonable assay performance. Because of the easier assay procedure, adsorption has been chosen as standard immobilization method for the iLab platform.

In contrast to Vacrel® 8100, utilized as channel material in the former chip version [48–51], Pyralux® PC offers the possibility of not only covalent immobilization, but also adsorption of biomolecules. In general, adsorption contributes short incubation times and facile assay protocols without the application of toxic and complicated linker chemistry. Its main drawbacks are steric hindrance of biomolecules in the case of a high-dense attachment and high non-specific interactions compared to the covalent coupling method.

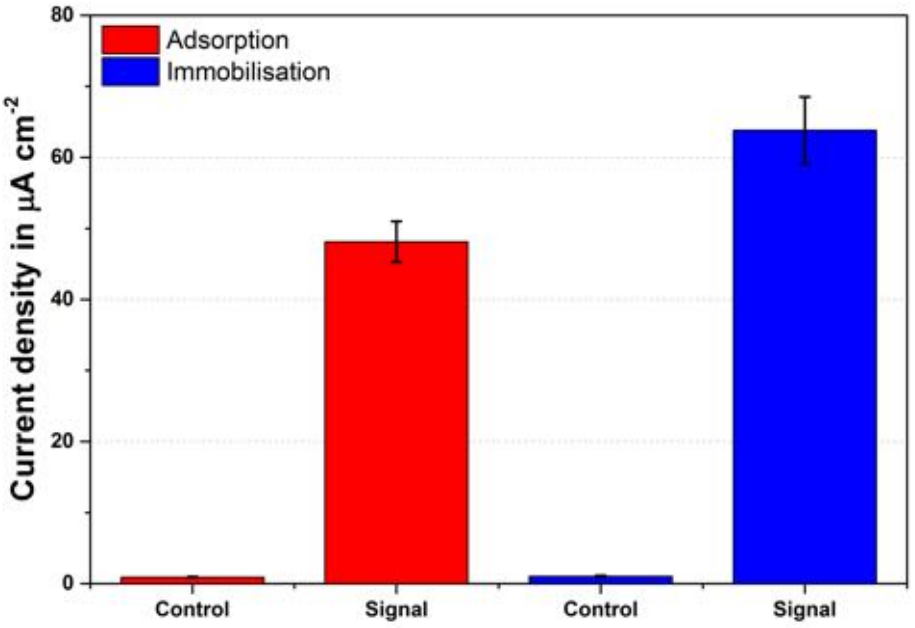

Figure 6.8: *Comparison of the different immobilization techniques for the detection of the avidin-bGOx model assay: Adsorption (red) and covalent immobilization (blue). The current density signals represent 2 min stop-flow. Error bars show the standard deviation of two parallel measurements.*

To overcome a possible steric hindrance of proteins, an intermediate step, i.e. adsorption of a universally applicable spacer, is performed in combination with bioaffinity immobilization. Furthermore, such an approach enables to adapt various bioassays to the iLab platform, without a need for an extensive optimization. In this thesis, anti-fluorescein antibodies are employed as spacer along with fluorescein-tagged DNAs for the realization of the on-chip DNA-based antibiotic assay. In addition, the different blocking strategies are intensively studied to diminish the non-specific binding.

6.2.3 Optimization of the physical immobilization

After choosing adsorption as standard for surface functionalization, its optimal parameters such as the incubation time and required minimum biomolecule concentration have to be determined. Firstly, the influence of the adsorption time on the measured amperometric signals is investigated. For this purpose, the same assay protocol, given in the previous section, is applied with different incubation times of 30, 60, 90 and 120 min for avidin.

Figure 6.9 shows the influence of different adsorption times on the amperometric signal measured with different stop-flow times. The resulting peak currents of the avidin-bGOx

model assay indicate a saturation profile after an incubation duration of 30 min for avidin. Such an adsorption behavior can be explained by the physical adsorption isotherm, the so-called Langmuir isotherm, which is typical for microporous adsorbents [216] and matches well with the highly porous surface of the Pyralux® PC 1025. For an optimal adsorption of biomolecules, an incubation time of 1 h has been selected for further measurements.

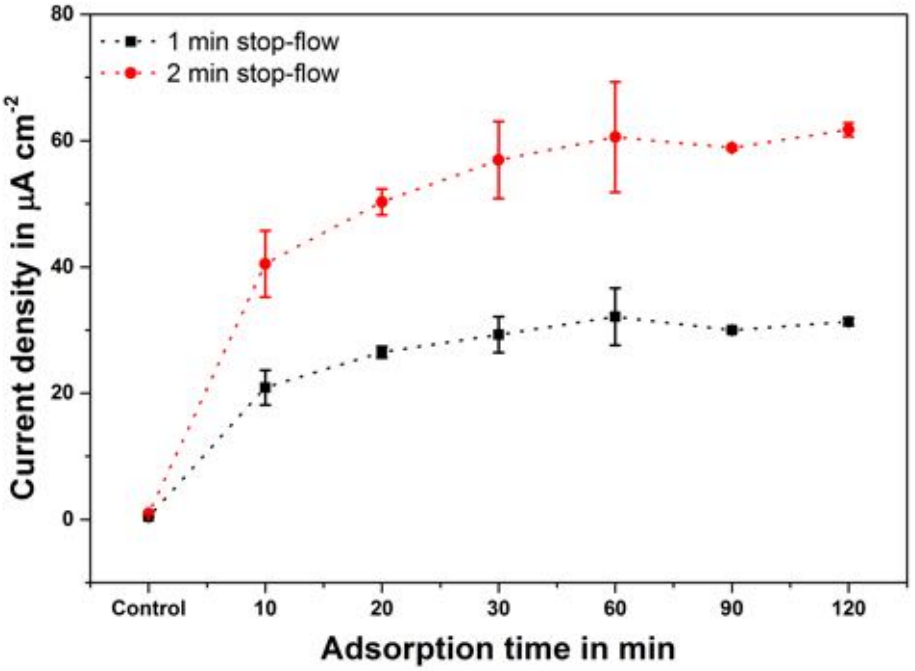

Figure 6.9: *Influence of adsorption times on the amperometric signal for different stop-flow durations. The current densities prove a signal saturation after an incubation time of 30 min for the avidin adsorption. Error bars show the standard deviation of two parallel measurements.*

Additionally, the coating concentration of biomolecules has a great influence on the assay response. Therefore, the effect of the biomolecule concentration on the on-chip assay performance is evaluated by means of a calibration curve for avidin. Herein, 5, 10, 20, 50 and 100 µg ml^{-1} of avidin are coated on the biosensor chips to functionalize the capillary surface for the subsequent measurement with 1 µg ml^{-1} biotinylated GOx.

The obtained calibration curves of avidin for different stop-flow intervals are illustrated in Figure 6.10. The amperometric results prove again a typical adsorption isotherm with a saturation starting from an avidin concentration of 50 µg ml^{-1}. Besides, there can be no difference between the measured control and signal values observed up to avidin concentration of 20 µg ml^{-1}. To achieve a sufficient surface coating as well as protein activity, 100 µg ml^{-1}, the relatively high concentration of avidin, is further utilized for the adsorption of the model assay.

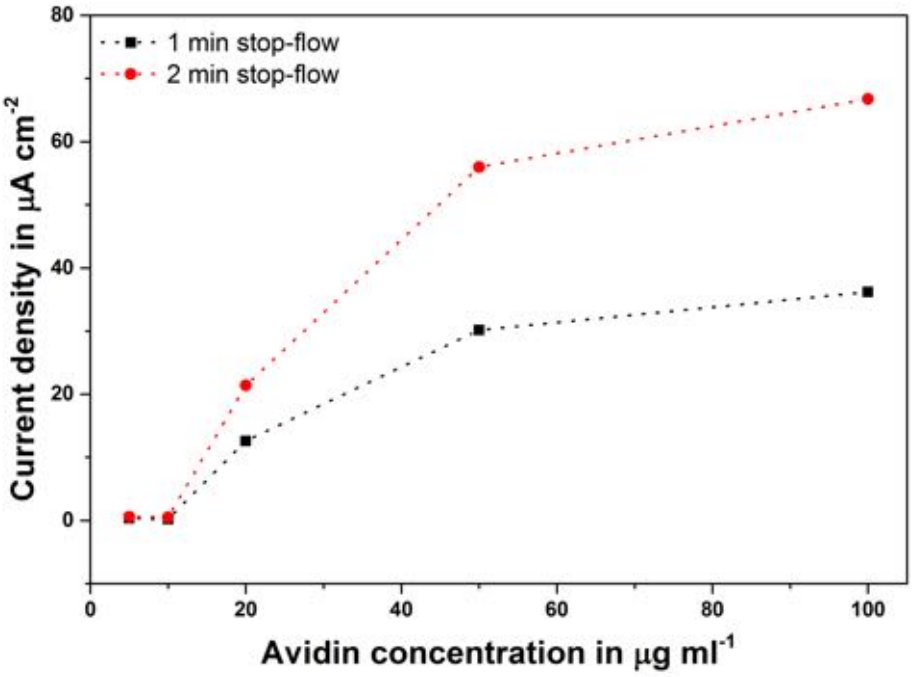

Figure 6.10: *Amperometric response of the bGOx model assay depending on the avidin concentrations (5, 10, 20, 50 and 100 µg ml^{-1}) used for the functionalization of the capillary surface.*

6.2.4 Blocking strategies

As previously mentioned, one of the main drawbacks of adsorption is the high non-specific interactions of off-target biomolecules compared to the other immobilization techniques. Therefore, different blocking strategies have to be investigated to increase the blocking efficiency of the channel surface.

An ideal blocking buffer is expected to improve the assay sensitivity by minimizing the background interferences and so that, it increases the signal-to-noise ratio. The assay components such as the antigen itself and the signal label play a crucial role on the appropriate choice of the blocking buffer. In this regard, different blocking agents including 3 % and 1 % BSA in PBS as well as SuperBlock™ blocking buffer[1] (Thermo Fisher Scientific, Germany) are applied for 1 h to the biosensor chip capillaries. Subsequently, 1 µg ml^{-1} avidin-GOx, the enzyme label used in the iLab platform for the assay detection, is incubated for 15 min in the biosensor chips.

The results of different blocking strategies for 1 min stop-flow readout are compared with each other and control chip coated with only avidin-GOx for 15 min. According to Figure 6.11, the best blocking efficiency for avidin-GOx is reached by using 1 % BSA as

[1]The SuperBlock™ blocking buffer contains a proprietary protein in physiological PBS.

blocking solution. Overnight blocking with 1 % BSA performed at 4 °C is tested as well, nevertheless, without any significant improvement of the blocking efficiency. Finally, a blocking step with 1 % BSA for 1 h is set as standard for the assay protocol.

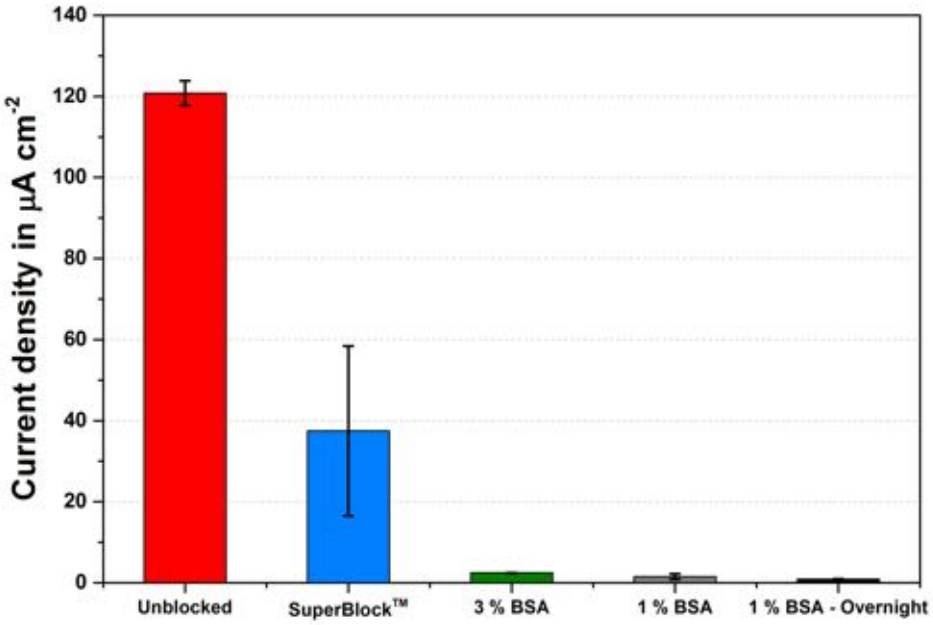

Figure 6.11: *Comparison of different blocking strategies for avidin-GOx by 1 min amperometric stop-flow readout. The best blocking efficiency for glucose oxidase label is achieved with 1 % BSA solution. Error bars show the standard deviation of two parallel measurements.*

6.2.5 Substrate concentration dependency of stop-flow signals

The employment of avidin-GOx as assay label for the on-chip amperometric readout requires a glucose solution as the substrate of the enzymatic reaction. Thereby, it is important to have an excessive amount of glucose during the measurement in the microcapillary to limit this reaction only by the enzyme kinetics. On the other hand, glucose solutions have an increased viscosity depending on its concentration and thus, it can rise difficulties for the fluid handling as well as for pressure-driven flow in the microfluidics.

To determine the optimum glucose concentration for the real application, chips are immobilized with the avidin-bGOx model assay and measured electrochemically with different concentrations of glucose at a flow rate of 20 µl min^{-1}. The substrate solution contains a defined concentration of glucose solved in 0.1 M ultra pure PBS to minimize the contamination risk. Figure 6.12 displays the resulting 2 min stop-flow peak signals in dependence with the glucose concentration. A kinetic limitation of the enzymatic reaction is almost

accomplished at a concentration of 40 mM glucose and thus, it is selected as the optimal substrate concentration for further experiments.

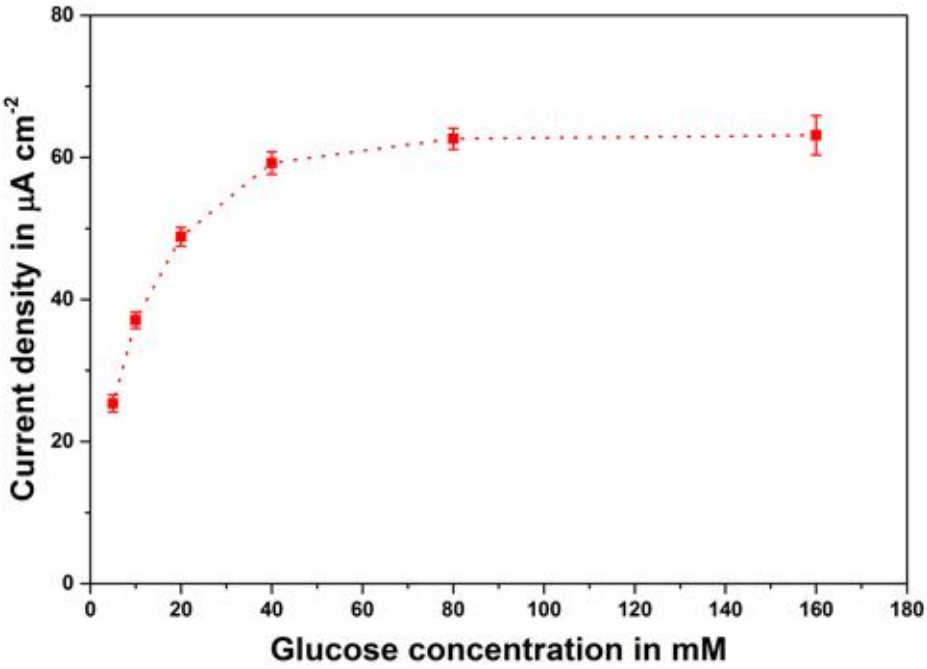

Figure 6.12: *Glucose concentration dependency of the amperometric 2 min stop-flow signals. Error bars show the standard deviation of four parallel measurements.*

6.2.6 Cross-sensitivity

In relation to the microfluidic multiplexed biosensors, the cross-sensitivity between the neighboring channels of the microfluidic network may be a crucial issue. During the applied stop-phase hydrogen peroxide can diffuse back to the next junction point of different channels and thus, induce false test results. Therefore, this effect is to be examined for different stop-flow times.

To mimic the worst case scenario for the evaluation of the cross-sensitivity, it is essential to induce very high signal differences, i.e. H_2O_2 concentration gradient, between the neighboring channels. This is realized here using the avidin-bGOx model assay along with long stop times. For this purpose, signal and blank channels (without any modification) are arranged alternately next to each other. In order to exclude any crosstalk, the blank channels should prove the same signals as measured in 40 mM glucose prior to the assay incubation.

In this context, a 4-channel MultiLab chip is prepared as aforementioned and subsequently measured for different stop-flow durations of 1, 2, 5 and 10 min at a flow rate of 20 µl min^{-1}

per channel. The obtained current densities, as shown in Figure 6.13, for the blank channels are comparable with the previously measured signals in 40 mM glucose in spite of the generated very high signal differences. According to these results, a cross-sensitivity between neighboring channels caused by the H_2O_2 diffusion or back-flow during the stop-phase can be excluded.

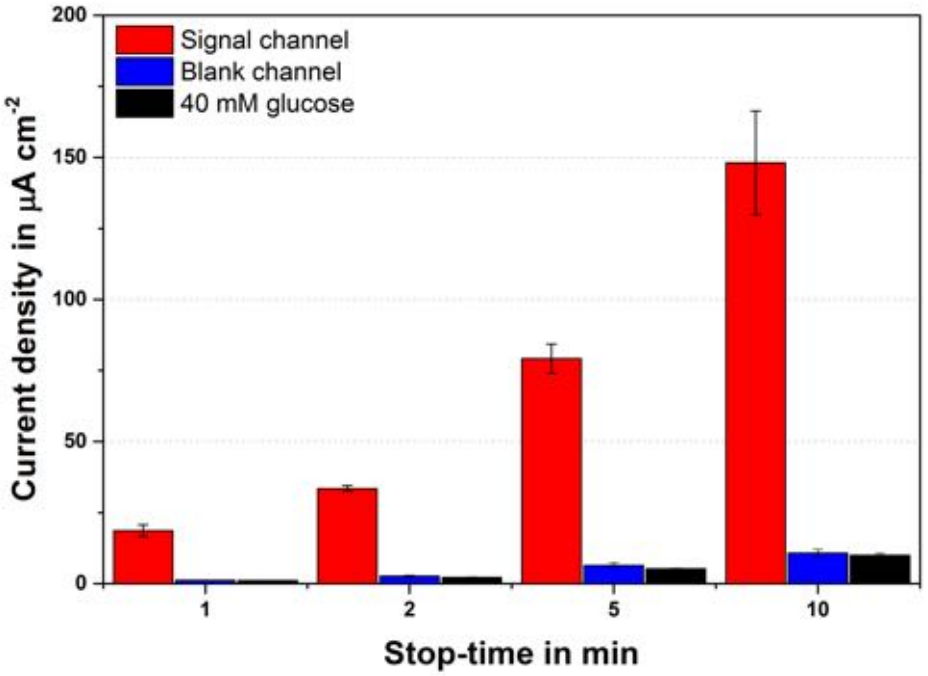

Figure 6.13: *Cross-sensitivity measurement of a MultiLab chip using the avidin-bGOx model assay. Despite induced high signal differences of the neighboring channels, there is almost no influence of these on the measured signals observed. Error bars show the standard deviation of two parallel measurements on a single 4-channel chip.*

7 Results: On-chip antibiotic assay

Preface

This chapter outlines the validation of the developed iLab platform for its assay performance as well as its feasibility for the simultaneous multi-analyte detection in biological fluids on the example of the DNA-based antibiotic assays for tetracycline and pristinamycin. Therefore, a brief introduction of the on-chip antibiotic assay will be given at the beginning followed by the information about the chemicals and methods utilized in this work.

A comprehensive study to optimize different assay parameters is performed. This includes the duration and concentration of each assay component for assay immobilization, and procedure of the sample incubation. Subsequently, calibration curves of both antibiotics in undiluted serum samples are carried out using the optimized assay procedure. Additionally, the proof-of-principle measurements are presented using the common "iLab" and the miniaturized "miLab" microfluidic biosensors to verify the hypothesis introduced in this work and the design rules derived from this.

Finally, the simultaneous detection of different antibiotics from a spiked human plasma is successfully demonstrated in a fast and reproducible manner. Moreover, in order to evaluate the storage conditions and shelf-life of the iLab platform with respect to point-of-care testing, a 3-month study of pre-immobilized microfluidic biosensor chips is given.

The work dealing with the antibiotic assay is realized in close collaboration with the group of Prof. Weber from Centre for Biological Signalling Studies (BIOSS), University of Freiburg.

7.1 DNA-based on-chip antibiotic assay

For the evaluation of the iLab platform regarding its on-chip assay performance as well as its applicability for multiplexing, DNA-based antibiotic assays for tetracycline and pristinamycin are employed. For the integration of the antibiotic assay presented in [28, 34] into the microfluidic chip, several modifications and optimizations had to be employed. A short overview of the adapted assay procedure is provided in this subsection.

To provide an easy and universally applicable biomolecule immobilization on the iLab platform and further to overcome a possible steric hindrance between the components of the assay, adsorption is utilized as an intermediate step for the immobilization of anti-fluorescein

antibodies (spacer) in combination with the bioaffinity immobilization of fluorescein labeled target biomolecules. The working principle as well as the different optimization steps of the DNA-based on-chip antibiotic assay are outlined in Figure 7.1.

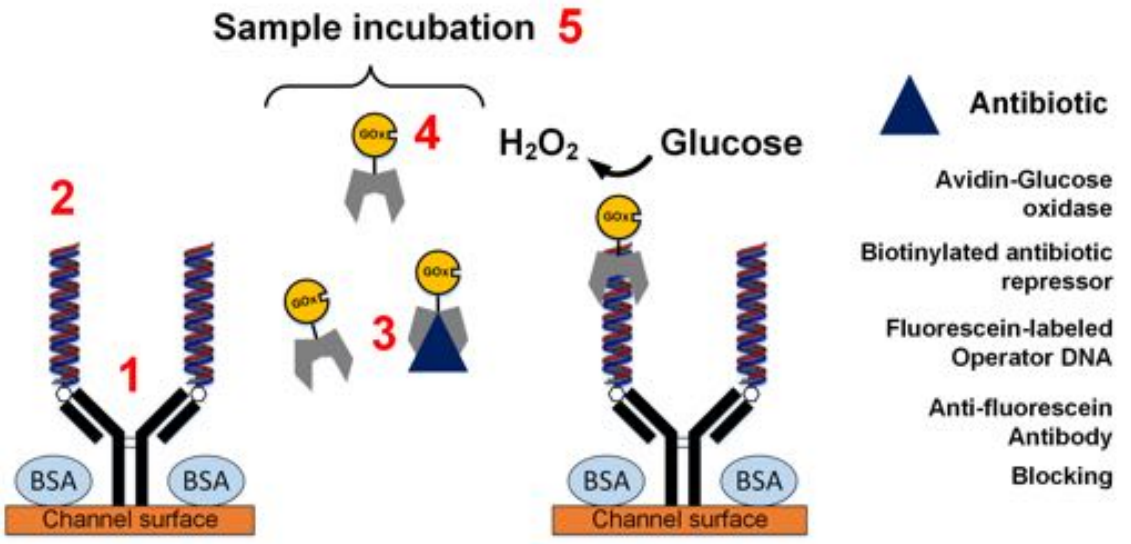

Figure 7.1: *Working principle of the DNA-based antibiotic assays and their main elements. The given numbers depict five different optimization steps: Concentrations of 1) antibody, 2) DNA, 3) biotinylated antibiotic repressor, 4) avidin-GOx and 5) sample incubation including incubation times and number of steps.*

First, the channel surface is functionalized with anti-fluorescein antibodies followed by a subsequent blocking step to exclude any non-specific binding. Secondly, the respective operator DNAs, labeled with fluorescein, are immobilized on the channel surface via adsorbed anti-fluorescein antibodies. Thirdly, the biotinylated antibiotic sensitive repressor proteins are added to the sample and introduced into the immobilization capillary of the microfluidic chip. In the presence of class-specific antibiotics, the antibiotic biosensor protein undergoes a conformational change in its structure and cannot bind to its operator DNA.

Finally, the signal readout is done electrochemically by labeling the biotinylated repressor with the enzyme glucose oxidase via avidin-biotin interaction. This new assay design offers more flexibility and an improvement in total assay times.

7.2 Chemicals and methods

Unless otherwise mentioned, all chemicals and immunoreagents are the same of those used in the previous chapter. In this subsection, the preparation procedure of the fluorescein labeled operator DNAs and the production of the biotinylated repressors for the tetracycline and pristinamycin detection are explained in detail. This work is performed by Claire Chatelle from the group of Prof. Weber from Centre for Biological Signalling Studies (BIOSS), University of Freiburg.

7.2.1 Production and purification of biotinylated repressors

The DNA binding proteins TetR and PIP are produced with a C-terminal Avitag for *in vivo* site-specific biotinylation using the enzyme BirA, followed by a hexahistidine-tag for purification. *E. coli* BL21* (DE3) purchased from Invitrogen, USA are cotransformed with the plasmid pCVC008 for production of a biotinylated TetR (bTetR) protein and pBirA for production of the BirA enzyme. In the case of pristinamycin repressor, *E. coli* BL21* (DE3) pLysS cell are transformed with the plasmid pCVC012 for coexpression of BirA and biotinylated PIP (bPIP).

E. coli cells are grown in Luria Bertani (LB) medium (Becton Dickinson, USA) supplemented with 100 µg ml^{-1} ampicillin and 34 µg ml^{-1} chloramphenicol at 37 °C until a OD_{600} value of 0.6. 50 µM biotin is added to the cell culture medium and the biosensor protein production is induced by 1 mM ß-D-1-thiogalactopyranoside (IPTG) for 4 h at 37 °C for bTetR and overnight at 20 °C for bPIP. Consequently, *E. coli* cells are harvested by centrifugation (6,000 g, 10 min, RT), resuspended in lysis buffer (35 ml per liter initial cell culture volume), containing 50 mM NaH_2PO_4, 300 mM NaCl and 10 mM imidazole, with pH 8.0 and shock-frozen. Cells are then lysed by sonication (60 %, 0.5 s pulse every second for 10 min) and the debris of the *E. coli* cells are eliminated by centrifugation (30,000 g, 30 min, 4 °C). The cleared lysate is loaded onto a gravity flow Ni^{2+}-NTA-agarose Superflow column (10 ml lysate per ml Ni^{2+}-NTA-agarose bead volume, purchased from Qiagen, Germany) followed by different washing steps with 10 column volumes of lysis buffer and 10 column volumes wash buffer (50 mM NaH_2PO_4, 300 mM NaCl and 20 mM imidazole, pH 8.0), and elution with 2 column volumes of elution buffer (50 mM NaH_2PO_4, 300 mM NaCl and 250 mM imidazole, pH 8.0).

The protein concentration is determined by the Bradford method (Bio-Rad, USA) using BSA as standard. Finally, biotinylated proteins are diluted to 1 mg ml^{-1} in elution buffer with 10 % sucrose for protein stabilization, lyophilized and stored at -80 °C. Prior to each experiment the freeze-dried proteins are dissolved in ultra pure water.

7.2.2 Annealing of the fluorescein labeled oligos

Oligonucleotides are purchased from Sigma-Aldrich, Germany. Double-stranded DNA operators TetO and PIR for the binding of the antibiotic repressor proteins TetR and PIP are

produced by mixing the oligos oCVC057 (Fluorescein-5´-gcactccctatcagtgatagagaaacg-3´) and oCVC059 (Fluorescein-5´-gctcgtacaccgtacaagg-3´) with their complementary oligos oCVC049 (5´-cgtttctctatcactgatagggagtgc-3´) and oCVC050 (5´-ccttgtacggtgtacgagc-3´) in equimolar amounts (50 µM of each oligonucleotide) in 1×SSC buffer (containing 15 mM sodium citrate, 150 mM NaCl, at pH 7.0), respectively. For this, the solutions are incubated for 5 min at 95 °C followed by a slow cooling down (2 °C per min) to room temperature.

7.3 On-chip antibiotic assay optimization

This section covers from the optimization of the assay parameters through the proof-of-principle measurements of the claimed hypothesis to the final calibration curves of the both antibiotics on multi-analyte platform. For the basic assay optimization an operator DNA TetO (Fluorescein-5´-gcactccctatcagtgatagagaaacg-3´-Biotin) tagged with biotin as well as fluorescein is employed. Such an approach provides a simplified system with a facile control over the chip performance in comparison with the complete antibiotic assay.

7.3.1 Optimization of the anti-fluorescein antibody concentration

As mentioned in the previous chapter, adsorption of biomolecules is chosen for the functionalization of the biosensor chip. To evaluate its feasibility for the anti-fluorescein antibodies, it is compared with the covalent immobilization by the use of the biotin and fluorescein labeled operator DNA TetO. Similar to Section 6.2.2, the covalent immobilization by means of carboxyl-to-amine crosslinking of the anti-fluorescein antibodies shows overall 36 % higher signals than the adsorption (data not shown). However, the peak current signals of both strategies are again high enough to guarantee an adequate assay performance. Therefore, adsorption is utilized as standard for further measurements.

The first decisive step of the on-chip assay optimization is to establish the optimal antibody concentration required for the surface functionalization of the channel capillary. Therefore, an investigation of the anti-fluorescein antibody concentration is carried out. The on-chip assay preparation begins with the adsorption of the different concentrations of monoclonal anti-fluorescein antibodies IgG CF 488A (Sigma-Aldrich, USA), from 10 µg ml^{-1} up to 100 µg ml^{-1}, on the immobilization capillary for 1 h, followed by a 1 h blocking step with 1 % BSA in PBS. To limit the assay signals only by the antibody concentrations, an excessive TetO concentration of 10 µM is incubated then in the immobilization channel for another hour. At the last step, the bound biotinylated oligos are coupled with 1 µg ml^{-1} avidin-GOx for 15 min.

The results of the different stop-flow measurements, as shown in Figure 7.2, indicate that an increase in the antibody concentrations leads to higher current densities up to a concentration of about 50 µg ml^{-1}. Therefore, this anti-fluorescein antibody concentration has

been selected as the optimum surface coating while maintaining high assay signals along with reasonable reagent costs.

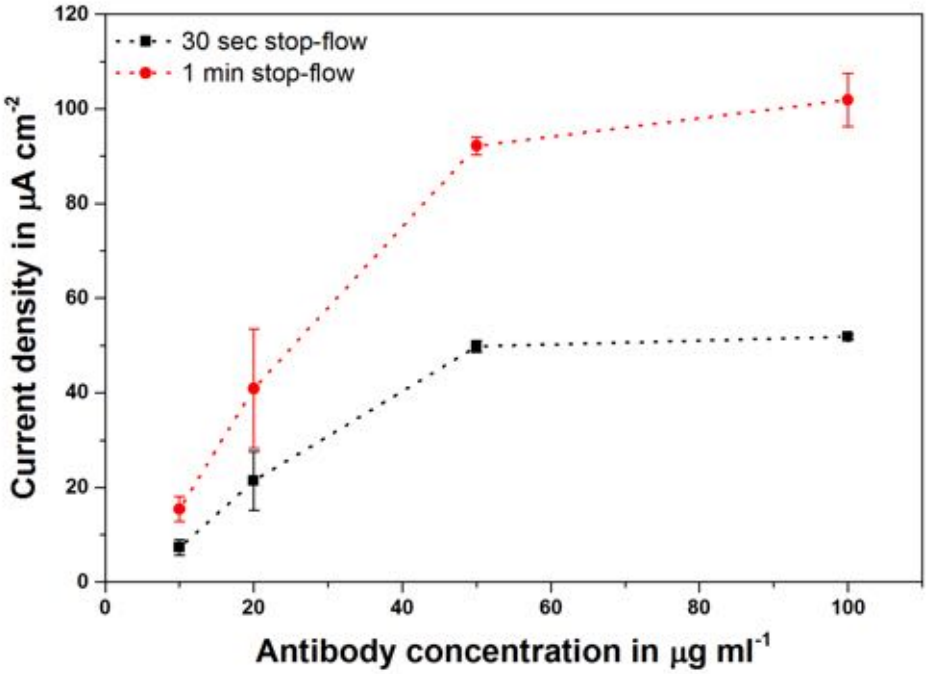

Figure 7.2: *Optimization of anti-fluorescein antibody concentration for different stop-flow times with the amperometric detection. The obtained current signals prove a plateau at a concentration of 50 µg ml^{-1}. Error bars show the standard deviation of two parallel measurements.*

At this point, a brief comparison between the experimentally derived binding capacities of the employed dry film photoresist Pyralux® PC1025 and the geometric estimation of these using the IgG antibodies will be given. The Y-shaped IgG molecule takes up a volume of a lens-shaped spheroid with a diameter d of 15 nm and a thickness t of 3 nm [185]. Assuming their densest monolayer packing, which proves non-quadratic pattern with a factor of $2/\sqrt{3}$, in "upright" or "lying" position (Figure 7.3), the respective the amount Q_{lense} per area is determined by:

$$Q_{lense} = \frac{2}{\sqrt{3}} \cdot \frac{M_w}{N_A} \cdot 10^9 \cdot \begin{cases} 1/td & = 650 \text{ ng cm}^{-2} \text{ at upright position} \\ 1/d^2 & = 130 \text{ ng cm}^{-2} \text{ at lying position} \end{cases} \tag{7.1}$$

where the molecular weight of IgG M_w is 153,000 g mol^{-1}, Avogadro's constant N_A is 6×10^{23} mol^{-1}.

According to the geometrical calculations only, the maximum and minimum amounts of antibodies bound on a solid-phase in a monolayer are 650 and 130 ng cm^{-2}, respectively. A reasonable estimation for the amount of adsorbed antibodies would be equal to 390 ng cm^{-2},

the average value between two maxima. On condition that the proportionality of the molecular weight to volume is given, Q will remain considerably the same for various biomolecules despite of a wide range of their molecular weight. This is caused by the low power relationship between volume and profile area of a molecule.

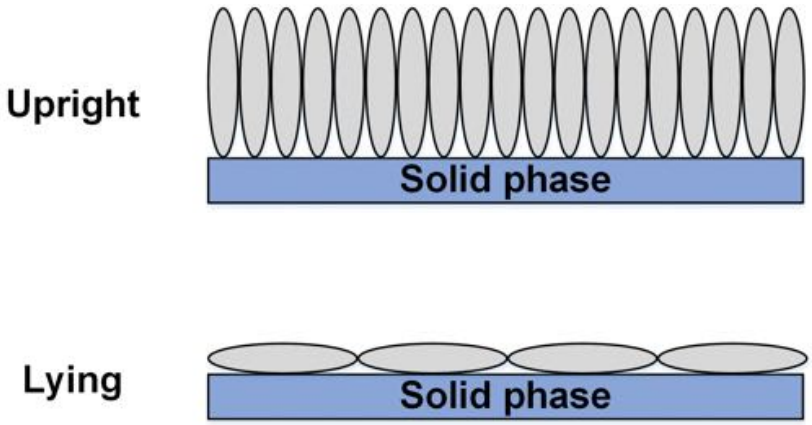

Figure 7.3: *Profiles of the densest IgG monolayers on a solid-phase illustrating the ratio 5:1 between molecules packed in upright and lying position.*

If we assume that the saturation of the channel surface (in this thesis Pyralux® PC1025) with anti-fluorescein antibodies takes place at a concentration between 50 and 100 µg ml^{-1}, the amount of bound antibodies can be found in both cases as 515.9 and 257.94 ng cm^{-2}, respectively. The average value of those, 386.9 ng cm^{-2}, is an appropriate estimate for the amount of adsorbed antibodies and thus, in a perfect agreement with the theoretical estimation.

7.3.2 Optimization of the fluorescein-labeled DNA concentration

Following a bottom to top approach for the assay optimization, the next step is the examination of the fluorescein-labeled DNA concentration. Here, the aforementioned assay procedure is applied with 50 µg ml^{-1} anti-fluorescein antibody, while the concentration of the fluorescein-labeled operator DNA is varied as 10, 5, 1 and 0.1 µM.

As depicted in Figure 7.4, there is no significant difference in the measured current densities subject to the appropriate DNA concentrations. For this reason, a fluorescein-labeled oligonucleotide concentration of 0.1 µM is further used.

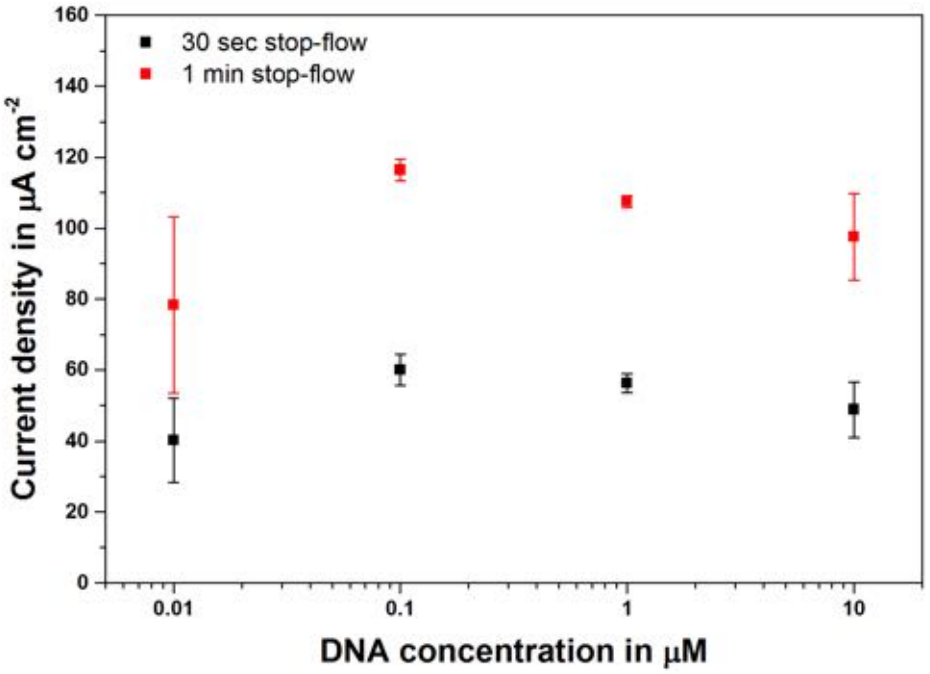

Figure 7.4: *Optimization of the fluorescein-labeled operator DNA concentration using different stop-flow times for the amperometric detection. The measured current densities do not indicate any remarkable difference for the employed DNA concentrations. Error bars show the standard deviation of two parallel measurements.*

7.3.3 Optimization of the GOx concentration

As the next step, the optimization of the enzyme concentration has to be performed for the minimization of the non-specific binding without a loss of sensor sensitivity. For this purpose, different concentrations of avidin-GOx conjugate (2, 1, 0.5 and 0.1 µg ml^{-1}) are employed with the optimized assay protocol comprising 50 µg ml^{-1} anti-fluorescein antibody and 0.1 µM fluorescein-tagged operator DNA.

The amperometric current signals, as depicted in Figure 7.5, present a typical saturation behavior by increasing the enzyme concentration. An avidin-GOx concentration of $1\,\mu g\,ml^{-1}$ is chosen as standard for the antibiotic assay.

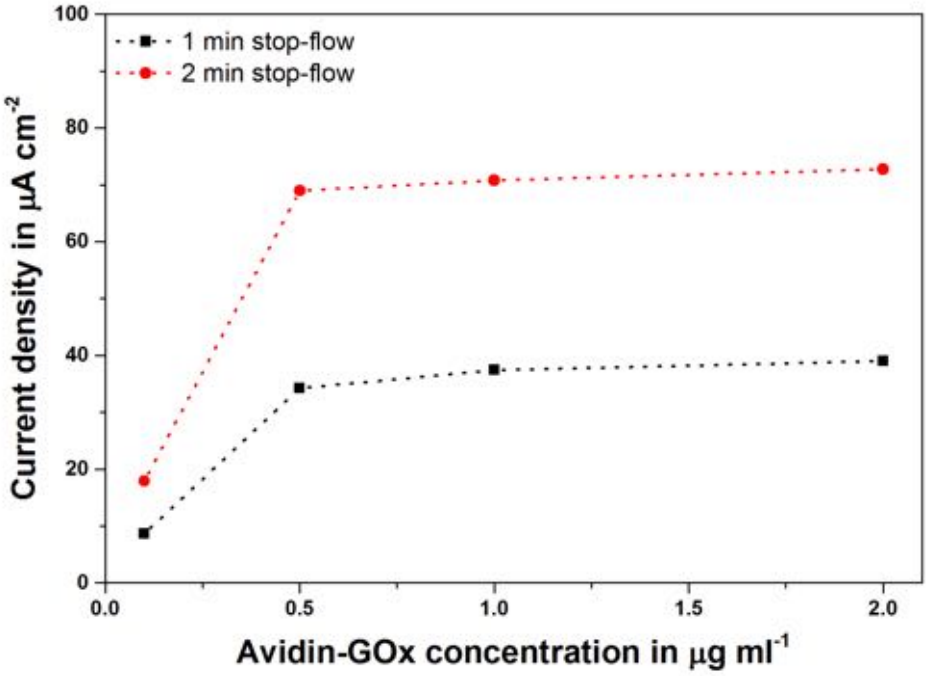

Figure 7.5: *Optimization of the avidin-GOx concentration for different stop-flow times with the amperometric detection. The obtained currents refer a complete signal saturation at a concentration of $1\,\mu g\,ml^{-1}$ avidin-GOx.*

7.3.4 Optimization of the biotinylated repressor concentration

After finalizing the basic characterizations of the on-chip antibiotic assay, complementary optimization steps are examined to improve the assay performance in the following subsections. In this context, the tetracycline assay is employed as the optimization model.

At the first step, the investigation of biotinylated TetR repressor concentration is performed to find out its appropriate amount showing a good signal specificity. Therefore, the signal and background values of the tetracycline assay at different TetR concentrations had to be determined and compared with each other based on the resulting signal-to-background ratios. The signal chips indicate the specific interaction between repressor and operator DNA, while background, i.e. control, chips represent the non-specific binding of the repressor only.

For this purpose, the biosensor chips are immobilized with the optimized assay procedure including the incubation of $50\,\mu g\,ml^{-1}$ anti-fluorescein antibody, 1 % BSA for blocking and

0.1 µM fluorescein-tagged operator DNA, each for 1 h. The control (background) chips are prepared without the operator DNA. Different concentrations of biotinylated TetR (10, 5, 1 and 0.1 µg ml^{-1}) are introduced for 1 h to all biosensor chips in a PBS solution containing 50 mM magnesium chloride ($MgCl_2$). The presence of $MgCl_2$ is essential for the functionality of the DNA-based tetracycline assay. Mg^{2+} binds to TetR and forms a complex. Thus, this enables the release of the repressor from its operator DNAs by modifying their three-dimensional conformation in the presence of tetracyclines [34, 217]. Finally, the bound proteins are labeled with 1 µg ml^{-1} avidin-GOx for 15 min.

The amperometric results measured with the 1 min stop-flow detection are shown in Figure 7.6a. The relation between the measured current densities and the TetR concentration shows a signal saturation at 5 µg ml^{-1}. According to the resulting signal-to-background ratios, as illustrated in Figure 7.6b, 5 and 1 µg ml^{-1} TetR prove a remarkable signal specificity. For the following antibiotic measurements, a TetR concentration of 1 µg ml^{-1} is selected to achieve a good specificity along with a high sensitivity.

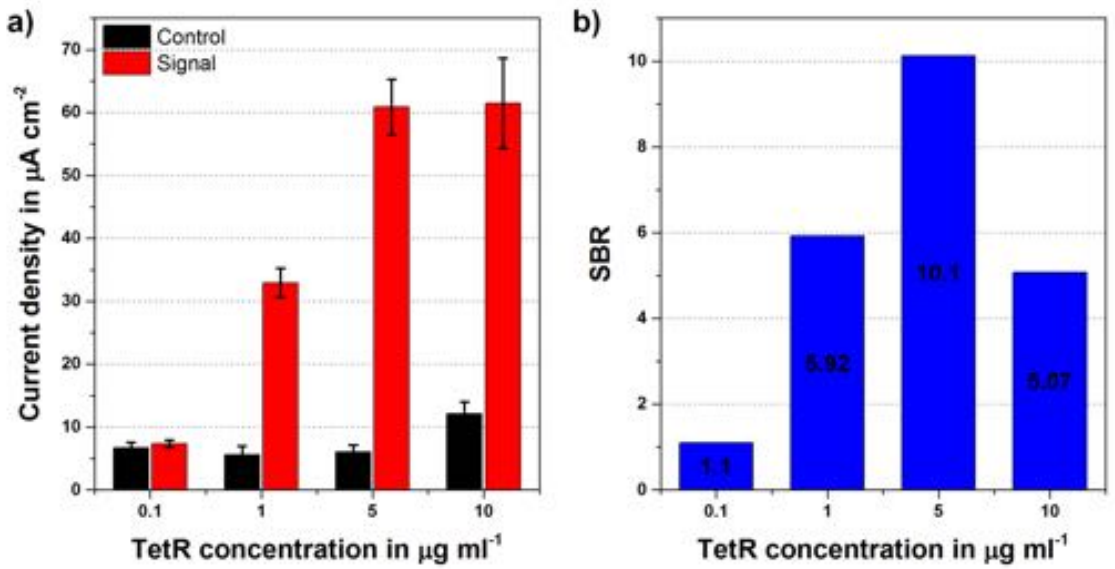

Figure 7.6: *Optimization of biotinylated TetR concentration using the amperometric 1 min stop-flow detection: a) The measured current densities of the signal and control (without the operator DNA) chips. The signal values prove a saturation at a TetR concentration of 5 µg ml^{-1} along with a good signal specificity according to b) the resulting signal-to-background ratios (SBR). To obtain a reasonable trade-off between the specificity and sensitivity 1 µg ml^{-1} is chosen for further measurements. Error bars indicate the standard deviation of two parallel measurements.*

7.3.5 Optimization of the sample incubation procedure

In this part, the sample incubation is optimized in terms of its duration and its process steps. The previously shown results necessitate the repetition of the optimization of TetR

concentration. Consequently, the determination of the optimal PIP concentration for the pristinamycin assay is executed.

7.3.5.1 One-step vs. two-step sample incubation

The initial DNA-based antibiotic assay described in [28, 34] requires a two-step procedure for the incubation of the sample and the enzyme label via antibodies, which results in a complicated assay realization and longer incubation times. In this work, the use of the avidin-biotin interaction for the enzyme labeling gives us the idea of examining the sample incubation process closely. To achieve this, the assessment of the incubation procedure is conducted by comparing the assay performance with an one-step and two-step sample incubation. Herein, a small calibration curve of the tetracycline assay including control, 6.25, 25 and 400 ng ml^{-1} is performed for each sample incubation method.

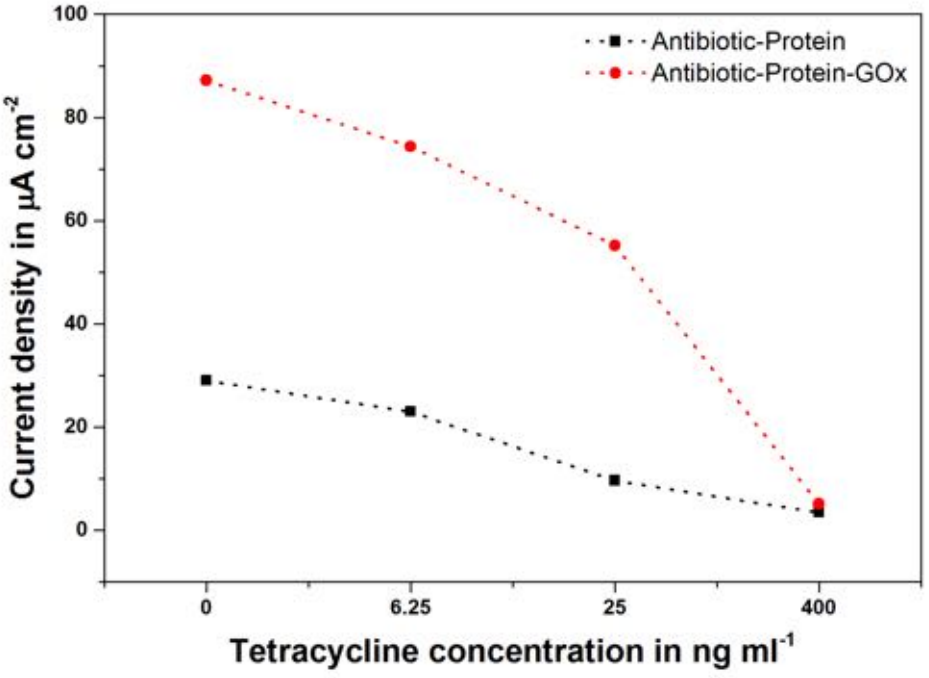

Figure 7.7: *1 min stop-flow measurements illustrating the influence of the one-step vs. two-step sample incubation on the assay performance. According to the small calibration curves of tetracycline, the incubation of the sample with its repressor and the enzyme label GOx in single step leads to three times higher assay signals.*

The biosensor chips are immobilized in accordance with the previously given assay protocol. After the assay preparation, the two-step sample incubation is realized first by the introduction of the different antibiotic concentrations in a protein solution with 1 µg ml^{-1} TetR and then of the 1 µg ml^{-1} avidin-GOx for 15 min. In the case of one-step sample

incubation, different antibiotic calibrators are mixed in a buffer containing both the TetR and the GOx-avidin and immobilized for 15 min in the channel capillary.

The calibration curves of tetracycline resulting from 1 min stop-flow measurements are depicted in Figure 7.7. Surprisingly, the obtained assay signals for the one-step sample incubation are three times higher than the ones of the two-step incubation. This may be arisen from the omitted washing step between the sample and enzyme incubation or a stabilization effect caused by the presence of the enzyme label. Therefore, the one-step sample incubation, comprising the sample (antibiotic), its repressor and the enzyme glucose oxidase, is chosen for the on-chip antibiotic assay.

7.3.5.2 Influence of the sample incubation time

To shorten the sample-to-result times further, the influence of the sample incubation duration on the assay signals is examined. Within this scope, a small calibration curve of tetracycline, as described in the previous section, is carried out for two different incubation times, 5 and 15 min, using the one-step sample incubation.

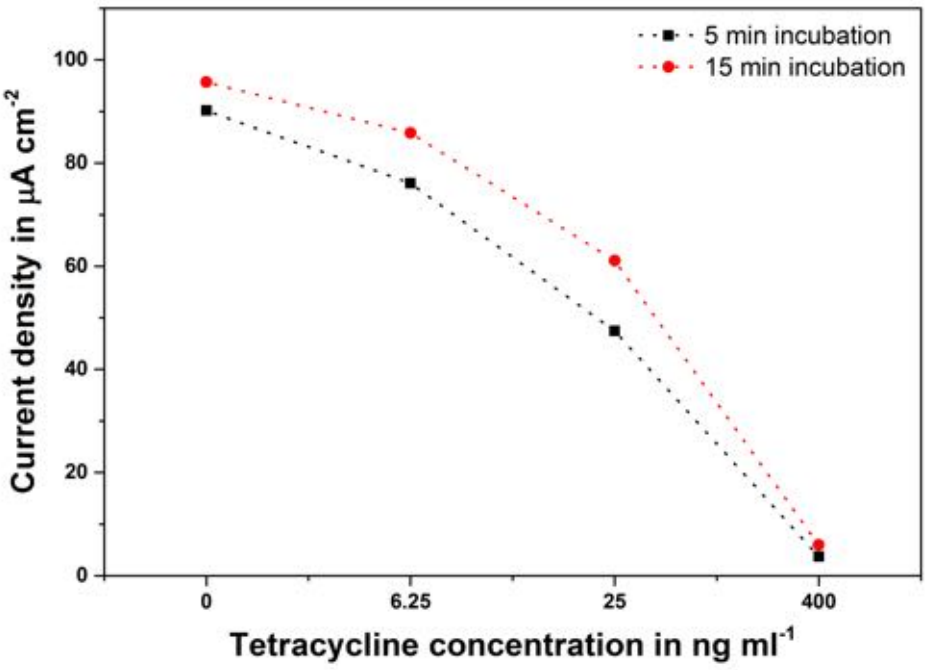

Figure 7.8: *Influence of the sample incubation time on the assay signals for 1 min stop-flow detection. In the case of 5 min sample incubation, the tetracycline assay signals present a slight decrease in the measured current densities while maintaining the assay performance. In order to enable fast sample-to-result times, 5 min sample incubation is chosen as a standard for the on-chip antibiotic assay.*

The influence of the sample incubation time on the tetracycline assay signals measured with 1 min stop-flow detection is represented in Figure 7.8. It can be seen clearly, that the current signals of 5 min sample incubation are slightly lower than 15 min. However, there is no difference between their assay performances. Therefore, the incubation time of the sample is set to 5 min as standard for the on-chip antibiotic assay.

In summary, the duration of the sample incubation is shortened down to five minutes using a single-step procedure, which facilitates fast sample-to-result times with respect to point-of-care testing.

7.3.5.3 Optimization of the biotinylated TetR concentration

The optimizations of the sample incubation procedure lead to the necessity of the repetition of the TetR concentration optimization. For this, again a small tetracycline calibration curve is conducted by the use of two different TetR concentrations, 1 and 0.2 µg ml^{-1}. In this context, different antibiotic concentration are exposed for 5 min into the biosensor chips by means of a single-step incubation.

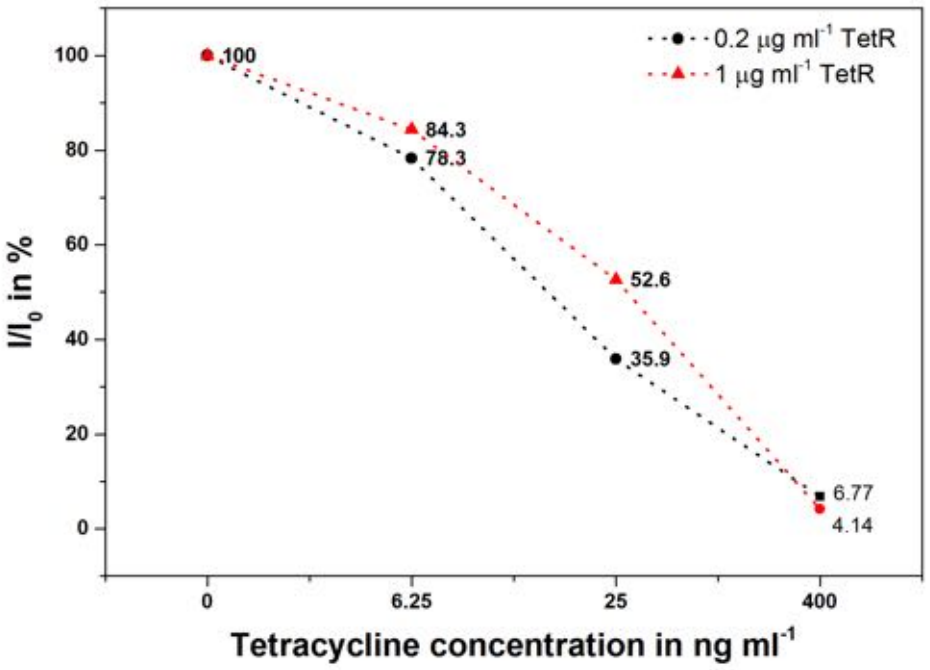

Figure 7.9: *The normalized current signals I/I_0 for 1 min stop-flow detection illustrating the influence of the TetR concentration on the tetracycline assay performance. Decreasing the TetR concentration presents better assay characteristics due to the competitive behavior of the DNA-based antibiotic assay. Hence, a TetR concentration of 0.2 µg ml^{-1} is preferred for the electrochemical tetracycline detection.*

The normalized current signals I/I_0 (given in %) of the tetracycline assay signals are displayed in Figure 7.9 for the applied repressor concentrations. Here, I_0 (zero calibrator) is the amount of the GOx-labeled TetR bound to operator DNAs in the case of the sample without analyte (e.g. antibiotics). Decreasing the TetR concentration provides better assay characteristics, such as high sensitivity due to the competitive nature of the antibiotic assay and enhanced specificity by reducing the background signals, along with reasonable current signals. Thus, $0.2\,\mu g\,ml^{-1}$ TetR is employed for the further on-chip tetracycline measurements.

7.3.5.4 Optimization of the biotinylated PIP concentration

Similar to the optimization of the TetR concentration, the examination of biotinylated PIP repressor concentration are performed to determine its influence on the pristinamycin assay signals. In this sense, different concentrations of biotinylated PIP (5, 2, 1 and $0.2\,\mu g\,ml^{-1}$) are introduced for 1 h to all biosensor chips in a PBS containing 50 mM $MgCl_2$.

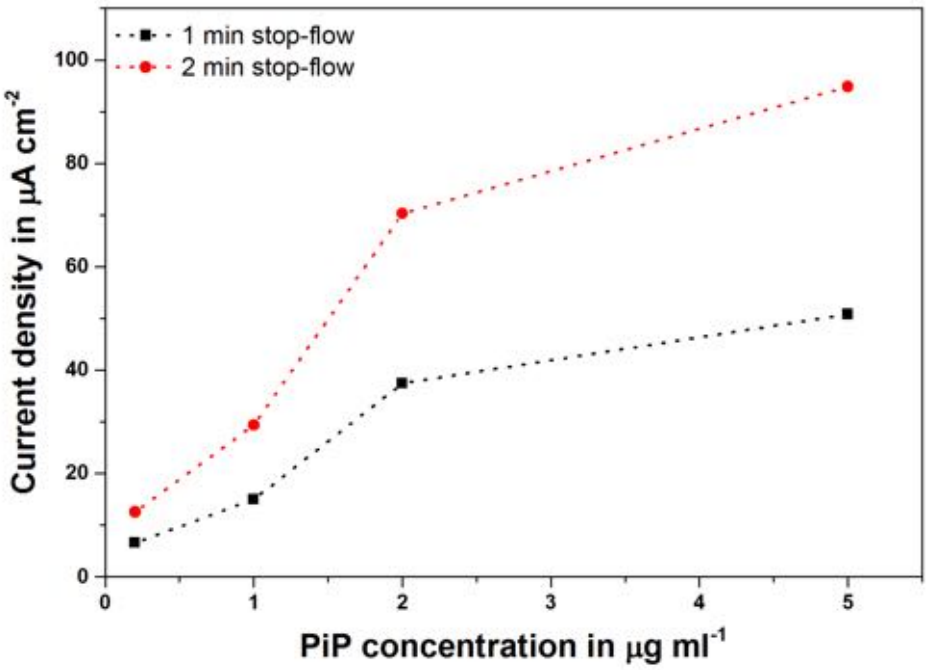

Figure 7.10: *Optimization of biotinylated PIP repressor concentration for the electrochemical detection of pristinamycin. The measured current signals increases by increasing the PIP concentration. The highest value is obtained with $5\,\mu g\,ml^{-1}$ of the repressor. In order to provide sufficiently high signals in the range of tetracycline assay, $2\,\mu g\,ml^{-1}$ PIP is selected.*

The release of PIP repressor from its operator DNA works also in absence of magnesium ions Mg^{2+}. However, magnesium chloride is added into the sample solution in order to

mimic the real measurement conditions for the simultaneous multiplex antibiotic detection. Finally, the bound proteins are labeled with 1 µg ml^{-1} avidin-GOx for 15 min.

The results for the optimization of the biotinylated PIP concentration are depicted in Figure 7.10. The obtained current densities demonstrate a typical saturation behavior with a maximum at a PIP concentration of 5 µg ml^{-1}. To hinder the non-specific binding related to the repressor concentration and to achieve comparable assay signals like tetracycline, 2 µg ml^{-1} PIP is selected for the final pristinamycin assay protocol.

7.3.6 Incubation times of fluorescein-labeled oligos

At the final optimization step of the on-chip antibiotic assay, different incubation times of the fluorescein-labeled oligos are applied employing the optimized assay procedure in order to shorten the total assay times further. For this purpose, at the respective stage the introduction of the operator DNAs to all biosensors is followed for 5, 15, 30 and 60 min.

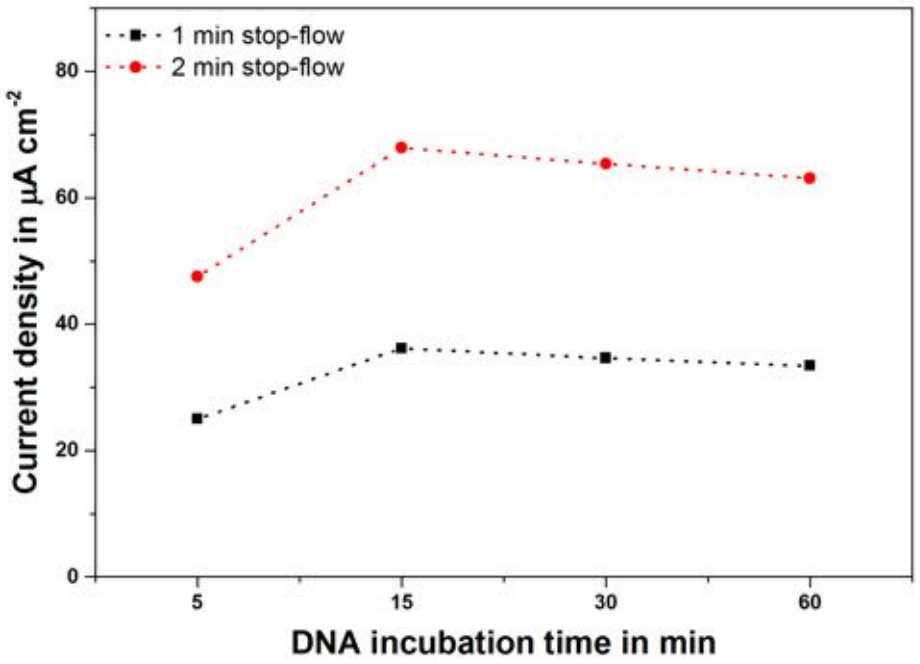

Figure 7.11: *Influence of the DNA incubation times on the assay signals for 1 and 2 min stop-flow measurements. The obtained currents indicate a signal saturation after an incubation time of 15 min for the binding of fluorescein ligand, functionalized at the DNA, in the anti-fluorescein active site of the IgG antibodies.*

Pursuant to measured current signals shown in Figure 7.11 for different stop-flow durations, an incubation time of 15 min is adequate to ensure a complete interaction between the anti-fluorescein antibodies adsorbed on the channel surface and the fluorescein-labeled operator

DNAs. Therefore, the assay protocol for the on-chip antibiotic detection is finalized with the optimized incubation of 15 min for the DNA immobilization.

7.3.7 Proof-of-principle: iLab vs. miLab

The highlight of this thesis is the introduction of the novel design concept based on the claimed hypothesis:

> "The application of the stop-flow technique enables a drastic decrease in the channel geometry of microfluidic biosensors by maintaining their sensitivity and fast quantification independent of the utilized detection technique such as optical or electrochemical."

For the verification of this hypothesis as well as numerical simulations, presented in chapter 4, the proof-of-principle measurements are carried out with the both single-analyte versions of the iLab platform using the optimized on-chip tetracycline assay. Please note that the standard iLab chip has an immobilization channel with a length of 100.8 mm, while the channel length of the miniaturized miLab chip is 16.4 mm only.

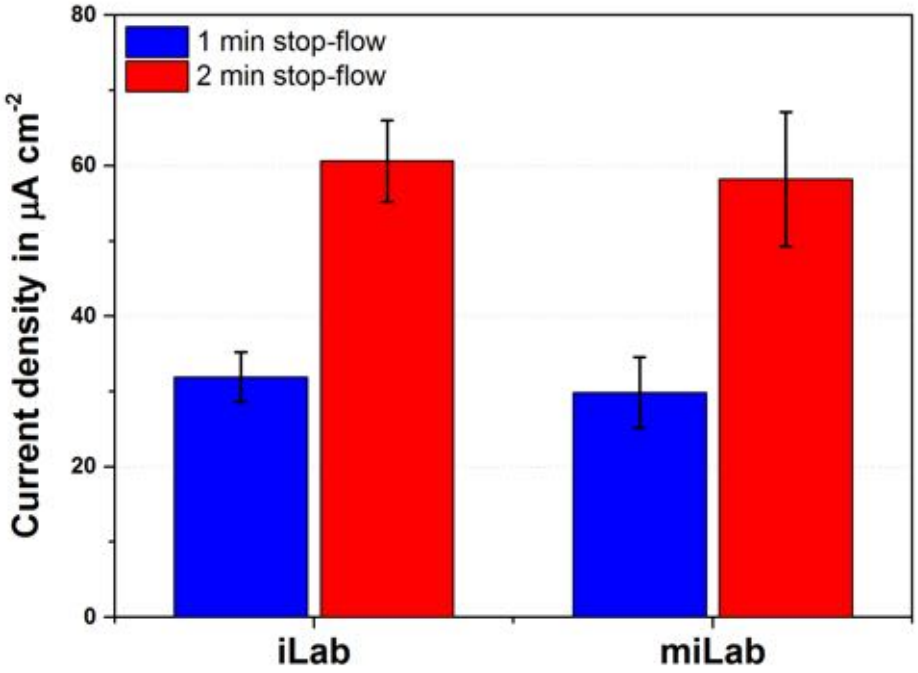

Figure 7.12: *Comparison of the tetracycline assay signals (zero calibrator) obtained from both single-analyte versions of the biosensor platform, iLab vs. miLab. The current peak results of both chip designs match very well with each other in spite of the huge difference in their immobilization capillary lengths. Error bars show the standard deviation of four parallel measurements with reasonable intra-assay CVs of 8.9 % and 15.3 % by 2 min stop-flow measurements for iLab and miLab, respectively.*

The results of the proof-of-principle experiments are illustrated in Figure 7.12. The tetracycline assay signals for zero calibrator are recorded in quadruplicate by stop-flow measurements depicting adequate intra-assay CVs of about 9 % and 15 % for iLab and miLab, or vice versa. As expected from the simulations, the consequent current peaks of both chip designs are almost identical with each other despite the huge difference between their channel lengths. Thus, the proof-of-principle of the postulated hypothesis is demonstrated successfully. Besides, this enables the realization of the multi-analyte approach in cost-effective and compact manner.

7.3.8 Tetracycline & pristinamycin calibration

After the comprehensive study of the assay parameters, the on-chip calibration of both antibiotics are performed over the same concentration range from 1.56 ng ml^{-1} to 1,600 ng ml^{-1} in serum and PBS. For this, different 8-channel MultiLab chips are prepared with either tetracycline or pristinamycin assays using the optimized protocol.

In the first place, 50 µg ml^{-1} monoclonal anti-fluorescein antibody is incubated in all immobilization capillaries for 1 h. After a subsequent blocking step with 1 % BSA in PBS for 1 h, 0.1 µM respective fluorescein labeled operator DNAs, TetO and PIR, encoded for the different antibiotic repressors are introduced for 15 min to all channels, except for the control channel. Between each incubation step, any unbound reagents and biomolecules are removed by washing with 200 µl wash buffer and 100 µl DI-water, introduced from the common outlet to protect the electrochemical cell.

Upon the assay preparation, the different dilutions of particular antibiotics mixed with the protein solution are incubated simultaneously through the individual inlets into all channels for 5 min. The protein solution contains of 1 µg ml^{-1} avidin-GOx, and 0.2 µg ml^{-1} bTetR or 2 µg ml^{-1} bPIP for tetracycline and pristinamycin, respectively. For the calibration in PBS, the protein solution includes additionally 50 mM $MgCl_2$ to modify the three-dimensional conformation of TetR and 1 % BSA to reduce the non-specific binding. Having completed the final washing step with 300 µl wash buffer, the assay signal readout is conducted by the amperometric detection with different stop-flow durations. Standard 4-parameter logistic fit is utilized for curve-fitting analysis.

For the comparison of the results between the developed on-chip tetracycline assay in undiluted serum (red) and in PBS containing 1 % BSA (black), both standard calibration curves are plotted in Figure 7.13. The measured current densities are achieved with 2 min stop-flow measurements using 8-channel MultiLab biosensor chips. The coefficients of variations in multiple assays (inter-assay) are found to be lower than 10 % and $\leq$13 % in serum and in PBS, respectively. The particular assay signals in human plasma exhibit twice higher IC50 value of 48.78 ng ml^{-1} than in PBS with an IC50 value of 22.28 ng ml^{-1}, nevertheless, the slope for both curves are very similar. Besides, the limit of detections are determined by Equation 3.27 for the tetracycline measurements in both samples. Here, a LOD of 6.33 ng ml^{-1} in human plasma and of 5.75 ng ml^{-1} in PBS are calculated, resulting in a dynamic response range up to a tetracycline concentration of 1,600 ng ml^{-1}. The

lowest concentration tested and detected is 1.56 ng ml^{-1} tetracycline with a reasonable CV of 3.14 % for serum and 6.23 % for PBS.

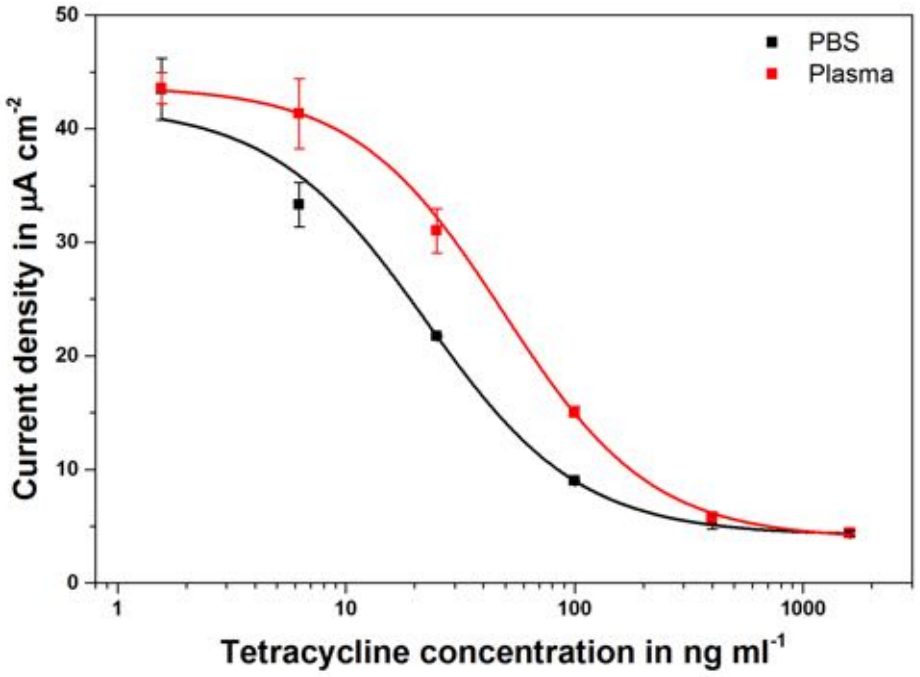

Figure 7.13: *Tetracycline calibration in human plasma (red) and in PBS with 1 % BSA (black) with 4-parameter logistic fit. The current signals are obtained simultaneously from 2 min stop-flow measurements with 8-channel MultiLab chips. Error bars show the standard deviation of three different measurements showing inter-assay CVs of ≤10 % and ≤13 % in plasma and in PBS, respectively.*

In the matter of pristinamycin, the standard calibration curves of the optimized on-chip DNA-based assay in undiluted human serum (red) and in PBS containing 1 % BSA (black) are illustrated in Figure 7.14. Here, the current signals are also recorded by 2 min stop-flow measurements using 8-channel MultiLab chips. The pristinamycin assays are performed in triplicates with reasonable inter-assay CVs of below 10 % for both, serum and PBS.

Unexpectedly, the current densities measured in PBS are almost the half of the ones obtained from human plasma. This decrease in assay signals may be caused by the addition of magnesium chloride, that is employed to ensure the TetR repressor functionality, in the case of PBS. Nevertheless, the resulting parameters for the on-chip pristinamycin assay are as expected. Similar to the on-chip tetracycline calibration, the IC50 value of 29.02 ng ml^{-1} given in serum is higher than the one in PBS of about 18.4 ng ml^{-1}. Furthermore, the slope of the fit curve in plasma is twice as high as in PBS, which results in varying limit of detection values for PBS and serum this time. Regarding the respective 4-parameter logistic fits, a LOD of 9.42 ng ml^{-1} in serum and of 2.4 ng ml^{-1} in PBS are determined with a wide working range up to 1,600 ng ml^{-1} pristinamycin. At this point, the lowest

pristinamycin concentration measured and deduced is 1.56 ng ml^{-1} along with excellent inter-assay CVs of about 1 % for both, serum and PBS.

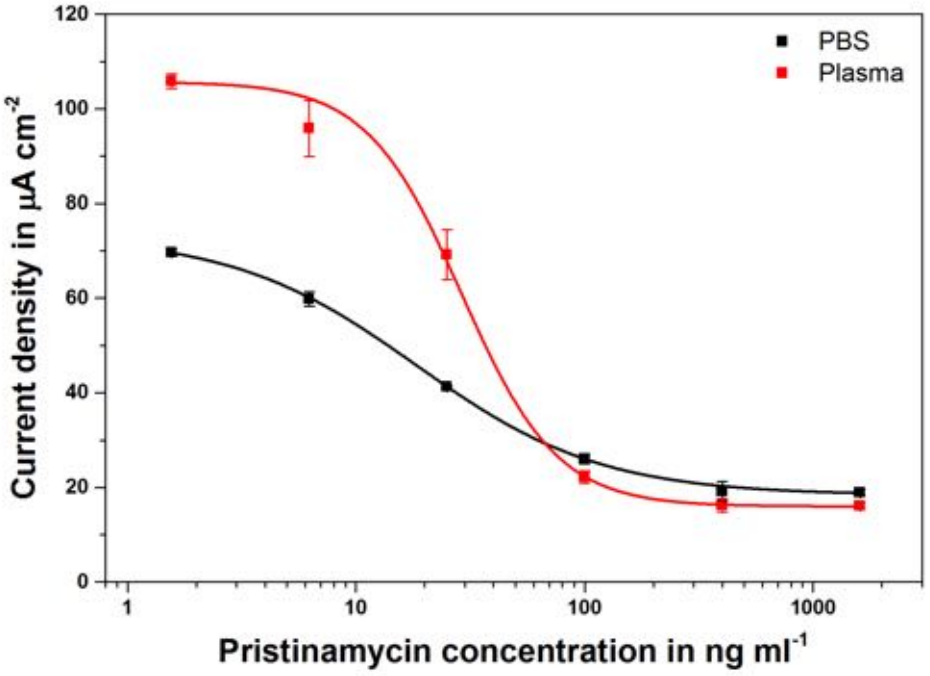

Figure 7.14: *Pristinamycin calibration in human plasma (red) and in PBS containing 1 % BSA (black) with 4-parameter logistic fit. The current signals are obtained simultaneously from 2 min stop-flow measurements with 8-channel MultiLab biosensor chips. Error bars show the standard deviation of three different measurements showing similar inter-assay CVs of below 10 % in both plasma and PBS.*

Important assay parameters for the on-chip detection tetracycline and pristinamycin are summarized in Table 7.1.

Table 7.1: *Important assay parameters of the on-chip antibiotic detection.*

	Tetracycline		**Pristinamycin**	
Parameters	**PBS**	**Plasma**	**PBS**	**Plasma**
IC50 in ng ml^{-1}	22.28	48.78	18.40	29.02
Quality of 4-parametric fit	0.9996	0.9974	0.9996	0.9990
Slope	1.2858	1.3352	1.0739	2.0829
LOD in ng ml^{-1}	5.75	6.33	2.4	9.42
Precision inter-assay (CV) in %	≤ 13	≤ 10	≤ 10	≤ 10

In summary, on-chip antibiotic assay calibrations for the simultaneous detection of tetracycline and pristinamycin are performed successfully in both, human serum and PBS. The on-chip antibiotic assays prove an remarkable diagnostic accuracy with adequate assay performance. Even in undiluted plasma, a detection limit of below 10 ng ml^{-1} for pristinamycin and tetracycline resulting in a wide working range up to 1,600 ng ml^{-1} and inter-assay precisions of about 10 % is achieved. Furthermore, the microfluidic chip platform provides a low consumption of reagent and sample, fast assay preparation times along with a sample-to-result time of only 10 min.

7.4 Simultaneous detection of different antibiotics

One of the main goals of this thesis is the development and the evaluation of an electrochemical microfluidic multiplexed biosensor platform. After the optimization of the assay procedure and the determination of the calibration curves, the simultaneous detection of tetracycline and pristinamycin is performed in a spiked human plasma to verify its feasibility of multiplexing using different analytes this time.

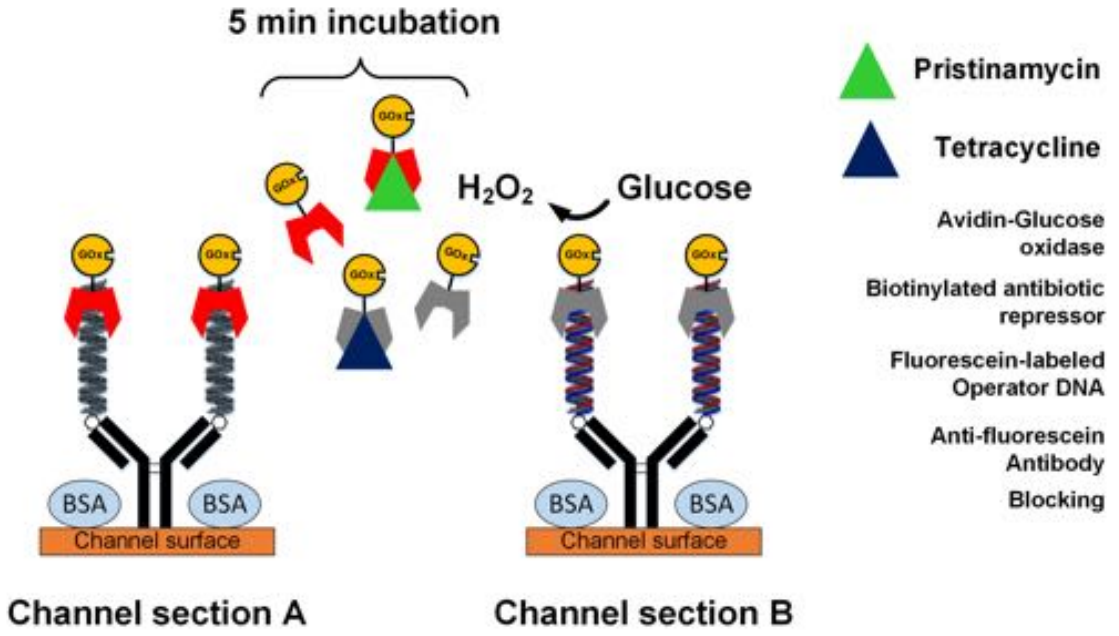

Figure 7.15: *Schematics of the optimized DNA-based antibiotic assay for the simultaneous detection of pristinamycin and tetracycline. The biosensor chip is immobilized with the operator DNA via anti-fluorescein antibody and blocked with 1 % BSA in advance. Only a 5 min single-step sample incubation is sufficient enough for the simultaneous multi-analyte detection.*

For this purpose, alternating channels of the 4-channel MultiLab chips are prepared with either tetracycline or pristinamycin assays. For the measurement, a serum specimen is spiked with 50 ng ml^{-1} tetracycline and 10 ng ml^{-1} pristinamycin. Additionally, the final sample solution contains 1 µg ml^{-1} avidin-GOx, 0.2 µg ml^{-1} and 2 µg ml^{-1} of bTetR and bPIP, respectively. This sample mix is then incubated in all channels for 5 min concurrently. After a subsequent washing, the amperometric signal readout is conducted using a 2 min stop-flow protocol. Schematics of the optimized DNA-based antibiotic assay for the simultaneous antibiotic detection is illustrated in Figure 7.15.

The 2 min stop-flow signals collected by the simultaneous detection of 50 ng ml^{-1} tetracycline and 10 ng ml^{-1} pristinamycin are presented in Figure 7.16 by comparing with the

predicted values from the calibration curves. In order to check the reproducibility of the platform, three different 4-channel measurements are examined each comprising duplicates for every antibiotic (N=3×2).

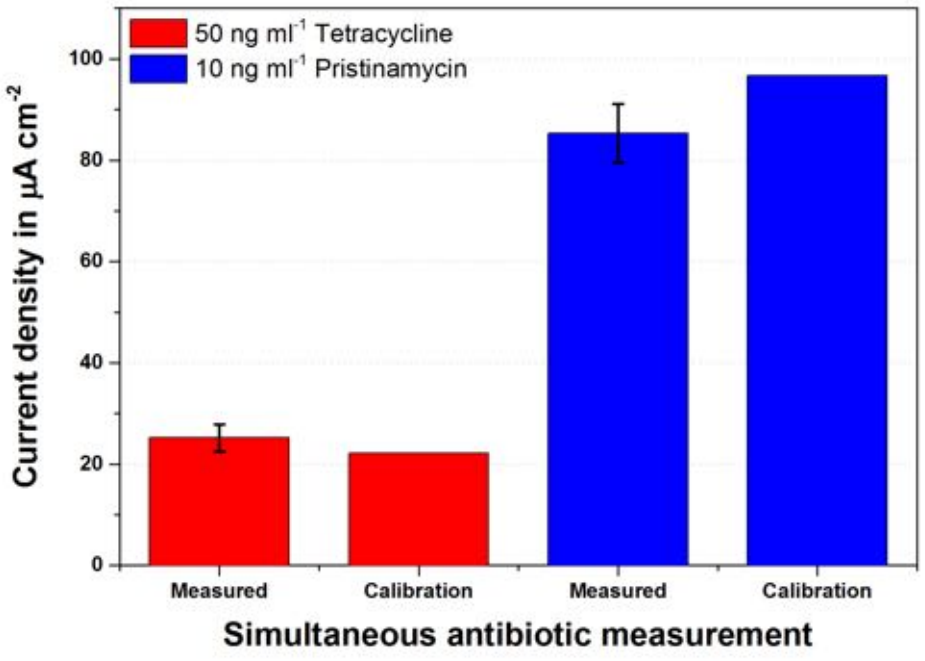

Figure 7.16: *Simultaneous detection of 50 ng ml^{-1} tetracycline and 10 ng ml^{-1} pristinamycin in spiked human plasma using 4-channel MultiLab chips. The current signals obtained from 2 min stop-flow measurements show a good agreement with the respective calibration values for both antibiotics. Error bars show the standard deviation of three different 4-channel measurements in multiple assays (inter-assay) each comprising duplicates for each antibiotic (N=3×2).*

The predicted value for 50 ng ml^{-1} tetracycline is 22.1 µA cm^{-2}, while the measured average current density comes to 25.2±2.67 µA cm^{-2}. For 10 ng ml^{-1} pristinamycin the obtained average current density is 85.32±7.78 µA cm^{-2}, whereas the calibration value is 96.7 µA cm^{-2}. Thus, a good recovery yield between the expected and observed concentrations of both antibiotics is achieved. 50 ng ml^{-1} tetracycline (113.9 % recovery) and 10 ng ml^{-1} pristinamycin (88 % recovery) in spiked serum samples are measured with typical CVs of 11 % and 7 %, or vice versa, in multiple assays (inter-assay).

Compared to its calibration, the tetracycline signal values could arise due to the high concentration of the biotinylated PIP repressor, increasing the overall background (non-specific) signals. In order to avoid any signal effect caused by a possible crosstalk between the components of individual multi-analyte assays, the respective assay calibrations are to be performed either with a sample solution containing all biomolecules or by the determination of the background signals at the same time.

As for pristinamycin, the achieved current densities are slightly lower than expected. This is most probably because of the applied 4-parameter logistic curve, as shown in Figure 7.14. The fit curve differs strongly from the measured values in this concentration region. Despite of these slight differences in the obtained recoveries, the simultaneous detection of two different antibiotics was demonstrated successfully in a sample-to-result time of within 15 min.

7.5 Storage and shelf-life of the biosensors

Other crucial issues for the point-of-care diagnostics are the storage and the shelf-life of the employed biosensors. Herein, the best will be to have a sensor device providing an easy storage (e.g. at RT or +4 °C) along with an extended shelf-life without loosing its sensitivity. In order to validate the storage conditions and shelf-life of the iLab platform, a 3-month survey of pre-immobilized biosensor chips is performed in this thesis.

With this respect, twelve biosensor chips in duplicates are functionalized with Ab-DNA complexes of the tetracycline assay and intermediately blocked with 1 % BSA applying the optimized immobilization procedure. Following 1 min drying using custom-made vacuum pen, the microfluidic chips are sealed airtight together with a desiccant and stored in refrigerator at +4 °C. Prior to each test the chips are incubated with zero calibrator (without sample) and subsequently measured.

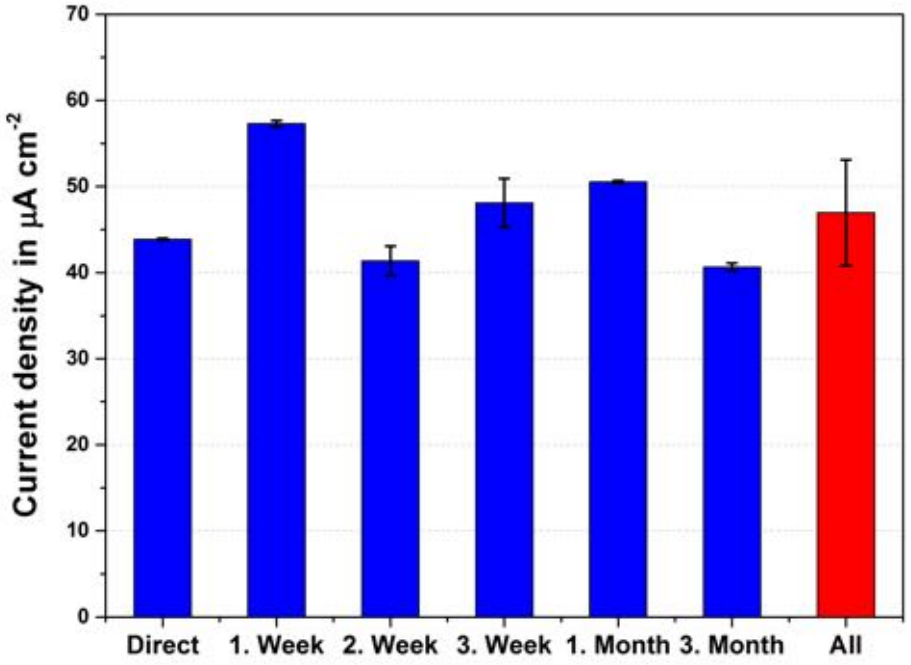

Figure 7.17: *3-Month shelf-life study of the biosensor chips using the tetracycline assay. The microfluidic chips, functionalized with Ab-DNA complexes and intermediately blocked with 1 % BSA, are sealed airtight with a desiccant and stored in refrigerator at +4 °C. Prior to each test the chips are incubated with zero calibrator (without sample) and subsequently measured. Error bars show the standard deviation of two parallel measurements.*

The results of the 3-month shelf-life study of the biosensor chips employing the tetracycline assay is displayed in Figure 7.17. As it is seen, the biosensor chips can easily be stored for longer periods while maintaining their full functionality. Herein, the measured signals

show an excellent reproducibility and precision with a maximum intra-assay CV of 5.8 % and an overall inter-assay CV of 13.1 % after several months.

According to the long-term study, the employed dry film photoresist Pyralux® PC1025 offers outstanding stability for biomolecules with a facile storage. The maximum shelf-life of the microfluidic biosensor tested within the scope of this thesis was three months without any change in its performance assessed directly. Besides, the iLab platform facilitates the simultaneous detection of different sample solutions, e.g. antibiotics in undiluted human plasma, at a desired time for a one-step assay.

8 Conclusion and outlook

This thesis presents the development and application of a low-cost microfluidic biosensor platform for the electrochemical detection of multiplexed assays in clinically relevant samples at the same time. Moreover, a novel design concept including design rules for the microfluidic biosensors using the stop-flow technique has been introduced for the first time.

In the light of this knowledge in combination with different technical measures it was possible to realize the proposed biosensor platform in a low-cost, compact, but still sensitive manner. By means of the advantageous dry film photoresist technology the wafer-level fabrication of the disposable biosensor chips was implemented reproducibly. Subsequently, the performance assessment of the microfluidic multiplexed LOC platform with respect to its electrochemical and biochemical characteristics was accomplished. Furthermore, the established design rules were successfully verified by the proof-of-principle experiments.

Finally, the applicability of the iLab platform for the simultaneous point-of-care testing of multiplex antibiotics in biological fluids is successfully demonstrated in a fast and reproducible manner.

8.1 Design rules for microfluidic biosensors

In this work, different design rules were obtained numerically from the 3D simulations in order to establish a novel design concept for microfluidic LOC platforms using the stop-flow technique. This facilitates the simple and low-cost realization of microfluidic multiplexed biosensors along with a full device performance, including a high sensitivity and fast quantification, independent of the utilized detection method (e.g. electrochemical, optical or calorimetric).

The introduced design rules for microfluidic biosensors are summarized as follows:

1. The length of the immobilization capillary is a key feature for the high sensitivity of microfluidic LOC systems. The application of the stop-flow technique results in a drastic decrease in the channel geometry. By means of the simulation model presented in this work it is possible to determine the optimal length of the immobilization capillary for different channel cross-sections, measurement conditions (e.g. flow rate or stop-time) or even materials.
2. In the case of electrochemical detection, the length of the immobilization section should be at least equal to the size of the working electrode in order to obtain the rectangular-like signals required for the stop-flow measurements.

3. The electrode geometry plays no significant role on the sensor sensitivity of electrochemical LOC platforms employing the stop-flow technique. Yet, it should be designed with the aim of achieving sufficiently high currents as well as low signal-to-noise-ratios for the signal detection.

Finally, the comparison between the simulated and measured stop-flow analysis of a biosensors with optimized design parameters was provided. Both rectangular-shaped signal responses showed a good agreement. As claimed by the hypothesis of this work, the resulting peak widths were almost equal to each other. The slight differences of both signals were most probably caused by the environmental effects such as the compliance of the used silicon tubes.

8.2 Sensor design and fabrication

The thesis encompasses the design through both the fabrication and optimization of the electrochemical biosensors to the final iLab platform. It offers two single-analyte versions, a standard "iLab" and a miniaturized version "miLab", as well as a multi-analyte version "MultiLab" of the dry film photoresist-based microfluidic biosensors.

The employment of the DFR allows facile, high-throughput and low-cost sensor fabrication. The wafer-level implementation of the different biosensor versions was realized in a non-cleanroom setting except the metal deposition. For all lithographic processes of DFRs, low-cost foil masks were applied with a vacuum UV-exposure unit instead of chromium masks and a mask aligner.

For a simple and reliable sensor device different modifications of the previous fabrication method, as presented in [48], were made. Firstly, SU-8 was established as isolation material in lieu of the respective DFR to achieve a well-defined working electrode area. Secondly, the former DFR material Vacrel® 8100 was replaced with Pyralux® PC1025, which provides better chemical stability and better processing. Finally, Ti layer, served as a protective layer for the electrodes during the chip fabrication, was found out to be unnecessary and even disadvantageous and thus, eliminated.

The whole fabrication procedure takes a work-load of about 10 hours, except the hard bake steps and the platinum evaporation, and can be modestly scaled-up. The resulting fabrication costs of the iLab platform are estimated to be below 1 € per channel on the average.

Moreover, the system integration is also decisive for the success of microfluidic biosensor platforms. In this context, the design and fabrication of different custom-made chip holders were successfully demonstrated. They enabled fast and easy fluidic and electrical connection of the single- and multi-analyte versions of the iLab platform with its environment.

8.3 Lab-on-a-chip performance

Prior to the application for point-of-care testing, the performance of the microfluidic multiplexed LOC platform had to be evaluated regarding its electrochemical and biochemical characteristics. The electrochemical characterization started with cyclic voltammetric analysis in order to investigate the electrochemical cell and the oxidation potentials of glucose (substrate) and hydrogen peroxide (analyte). Herein, a superior surface roughness factor of 14.1 was estimated for the platinum electrode on the polyimide substrate, which is twofold higher than the one described by Weltin *et al.* [208] in a similar way. This difference is the result of most probably the optimization of the fabrication procedure, in other words the elimination of the protective titanium layer, which may not be etched completely in hydrofluoric acid.

Furthermore, the theory of the hydrogen peroxide oxidation at platinum electrodes was verified by a cyclic voltammetric study. A working potential of 0.45 V vs. the on-chip Ag/AgCl reference was selected for the electrochemical detection, that enables a diffusion-limited oxidation of hydrogen peroxide and excludes almost any signal effect because of the glucose oxidation at platinum electrodes. Additionally, a chronoamperometric preconditioning protocol comprising an electrode cleaning (50 cycles each with 0.8 V and -0.1 V steps for 5 s) and oxide layer formation at a potential of 0.8 V for 1 min were found to be favorable prior to the amperometric measurement. Consequently, the examination of the performance parameters such as hydrogen peroxide sensitivity and flow rate dependency of the iLab platform were demonstrated. In order to combine high sensitivity with low reagent consumption, a flow rate of 20 µl min^{-1} per channel was chosen as standard. Finally, an average H_2O_2 sensitivity of 21.4 nA mm^{-2} μM^{-1} with a coefficient of variation below 5 % was achieved for the entire iLab platform.

After the electrochemical characterization, the investigation of the immobilization characteristics of the Pyralux® PC 1025, utilized as solid phase material, was performed using an biotin-avidin model assay. For this purpose, different immobilization strategies such as adsorption and covalent immobilization by means of carboxyl-to-amine crosslinking were evaluated. In the case of the covalent immobilization 32 % higher signals than the adsorption along with an improved signal-to-background ratio were achieved. Nevertheless, the measured signals for adsorption were also adequately high for a reasonable assay performance. Therefore, adsorption is selected as standard functionalization strategy.

Furthermore, an optimized assay protocol was achieved with a coating concentration of 100 µg ml^{-1} and an incubation time of 1 h for avidin. To diminish the non-specific interactions of off-target biomolecules, it is found out that the incubation of 1 % BSA for 1 h is the best on-chip blocking strategy for the avidin-GOx enzyme label. To obtain a kinetic limitation of the enzymatic reaction, the substrate concentration was studied. A glucose concentration of 40 mM is chosen for further experiments. Consequently, a cross-sensitivity experiment was performed successfully using MultiLab chips to exclude any crosstalk between neighboring channels caused by the H_2O_2 diffusion or back-flow in the stop-phase.

8.4 On-chip antibiotic assay

Finally, the introduced iLab platform was assessed to determine its assay performance as well as its feasibility for the multiplex antibiotics detection in clinically relevant samples. In this context, DNA-based antibiotic assays for tetracycline and streptogramin were modified and optimized first. For an easy and universally applicable biomolecule immobilization on the iLab platform, the adsorption of anti-fluorescein antibodies was employed as an intermediate immobilization step. Subsequently, the fluorescein tagged target biomolecules were immobilized by bioaffinity layering. Furthermore, such an assay design using an antibody spacer overcomes a possible steric hindrance of the biomolecules. In the following, the optimized incubation protocol of the DNA-based on-chip antibiotic assays is given:

First, the capillary surface is functionalized with 50 µg ml^{-1} anti-fluorescein antibodies for 1 h followed by a subsequent blocking step with 1 % BSA in physiological PBS for 1 h to prevent any non-specific interaction. Consequently, 0.1 µM of fluorescein labeled operator DNAs, TetO and PIR, encoded for the different antibiotic repressors are coupled on the channel surface for 15 min.

Upon the assay preparation, the sample with antibiotics added to the protein solution containing 1 µg ml^{-1} avidin-GOx, and 0.2 µg ml^{-1} or 2 µg ml^{-1} of bTetR and bPIP for tetracycline and pristinamycin, respectively, is incubated into the biosensor chip for only 5 min. After a final washing step with 300 µl wash buffer, the assay signal readout is achieved by the amperometric stop-flow detection within 10 min.

For the verification of the postulated hypothesis, the proof-of-principle measurements were demonstrated successfully using the conventional “iLab” and miniaturized “miLab” chip with a channel length of 100.8 mm and 16.4 mm, or vice versa. In spite of the considerable differences in the channel dimensions, the obtained peak signals were identical. Thus, they facilitate the compact and low-cost implementation of the microfluidic multiplexed biosensors.

Consequently, the on-chip calibration of both antibiotics in human plasma and in PBS were performed by only 2 min stop-flow measurements simultaneously. For tetracycline, a LOD of 6.33 ng ml^{-1} in human plasma and 5.75 ng ml^{-1} in PBS were determined with a wide working range up to 1,600 ng ml^{-1}. The on-chip results performed in multiple assays (inter-assay) show CVs of $\leq$10 % and $\leq$13 % in serum and in PBS, respectively.

In the case of pristinamycin, a LOD of 9.42 ng ml^{-1} in serum and 2.4 ng ml^{-1} in PBS were obtained with a dynamic response range up to 1,600 ng ml^{-1}. Here, on-chip assays were executed in triplicates with appropriate inter-assay CVs of below 10 % for both, serum and PBS. Besides, it was found, that a high concentration of $MgCl_2$ influences the pristinamycin assay signals in PBS.

Upon on-chip assay calibrations, the simultaneous, fast and reliable detection of different antibiotics from a spiked sample with 50 ng ml^{-1} tetracycline and 10 ng ml^{-1} pristinamycin was successfully demonstrated within 15 min. A good spike recovery yield between the predicted and measured concentrations of 50 ng ml^{-1} tetracycline (113.9 % recovery) and

10 ng ml^{-1} pristinamycin (88 % recovery) was achieved in serum samples with inter-assay CVs of 11 % and 7 %, respectively, in multiple assays.

For the comparison between the initial [28, 34] and optimized on-chip DNA-based antibiotic assays, their main features are summarized in Table 8.1. The iLab platform allows the simultaneous point-of-care detection of multiplex antibiotics in a 5 min one-step incubation along with a sensitivity of less than 10 ng ml^{-1} in undiluted human plasma. Furthermore, the on-chip sensing method offers 100-times lower sample/reagent consumption, reduces the total assay time almost in half and performs fast detection within 5 min readout time compared to the conventional techniques.

Table 8.1: *Comparison between the initial [28, 34] and optimized DNA-based antibiotic assays.*

	Initial assay	**Optimized on-chip assay**
Number of steps from sample-to-results	2	1
Sample-to-result time	1 h 30 min	$<$ 15 min
Readout time	10 min	$<$ 5 min
Total assay time	4 h 30 min	2 h 30 min
Sensitivity ng ml^{-1}	$<$ 50	$<$ 10
POC feasibility	no	yes
Multiplexed measurement	not known	yes

In point-of-care testing, the storage and shelf-life of the biosensors play a crucial role. A POC platform should provide a facile storage (e.g. at RT or +4 °C) combined with an extended shelf-life maintaining its sensitivity. For this purpose, the storage conditions and shelf-life of the iLab platform were demonstrated by a 3-month study of the microfluidic chips functionalized with Ab-DNA complexes and intermediately blocked with 1 % BSA. The maximum shelf-life of the biosensors was found to be three months within the scope of this thesis. Herein, the storage of the microfluidic chips was done by sealing airtight together with a desiccant in refrigerator at +4 °C.

8.5 Outlook

The iLab platform targets the point-of-care diagnostics in the first place, yet, owing to its capability for the multiplexing it has a great potential also for the traditional *in vitro* diagnostics. In this regards, it has to be optimized and further developed with respect to high-throughput screening (i.e. the detection of more than 10 parameters). Herein, a novel and facile design idea is introduced at the end of this section.

Our future work regarding the iLab platform encompasses the following issues:

Immobilization techniques: Different immobilization strategies may be further examined to improve the assay performance by increasing the surface activity or to decrease the reagent costs utilized for the surface functionalization. For example, the functionalization of the channel surface can be realized by adsorption of protein G first. This will result in a lower coating concentration of the employed anti-fluorescein antibodies, which are the most expensive assay component and thus, dictate the assay costs. Here, it should be kept in mind that each further incubation step will increase the total preparation time and the complexity of assay.

Application of different bioassays: The iLab platform offers high flexibility in the assay design and thus, facilitates the combination of different assay formats (e.g. competitive or sandwich) as well as of different advanced "omics" techniques (e.g. proteomics, cellomics and genomics) with each other at the same time. For that reason, immunoassays employing different assay formats and/or various combinations of different assay technologies have to be implemented into the microfluidic multiplexed chip and the resulting multiplexing performance should be evaluated. Moreover, the iLab platform might be extended for the detection of additional antibiotics (e.g. penicillins and cephalosporins) in order to cover a wide range of applications.

Nowadays, novel bioassays using non-protein recognition strategy (e.g. miRNA profiling) have drawn great interest for molecular diagnostics. In this regard, the evaluation of the iLab platform for the simultaneous detection of miRNAs in human body fluids will be performed.

Handheld reader: For a point-of-care application, a portable and easy-to-use handheld device is to be developed, which allows simple and fast chip loading together with automated measurement and analyzing procedures. The electrochemical signal readout can be realized by a compact potentiostat with an integrated multiplexer, whereas the microfluidic actuation will be achieved by a micropump or by a pressure controller.

Furthermore, to reduce the complexity of the whole system, it is important to design a disposable microfluidic cartridge comprising the biosensor chip, a waste reservoir and preloaded reagents such as wash buffer or other assay components. For the amperometric measurement, the delivery of the sample and other reagents are provided by pneumatic actuation, performed by the handheld reader, through the microfluidic biosensor chip to a waste reservoir.

Additionally, the immobilization procedures can be automated in order to reduce further the level of complexity of the iLab platform.

The chip design and fabrication: In this work, a novel design concept for the microfluidic biosensors has been presented for the first time, and the resulting sensor device is validated successfully for its applicability for the simultaneous multi-analyte detection. Nevertheless, there is still a need for further optimization in the chip design and fabrication.

In the wafer-level chip fabrication, the most critical step with respect to mass-production is the electrodeposition of the silver/silver chloride onto the reference electrodes because of its limited scaling capacity and the highly hazardous chemicals used. To overcome this limitation, alternative approaches including Ag/AgCl pastes or inks and different materials like platinum [218] will be tested regarding their processing as well as their reference electrode performance.

To enhance the sensitivity of the sensor platform (e.g. in the case of miRNA profiling), the interdigitated electrode arrays (IDAs) will be applied as dual working electrodes together with the so called "redox-cycling" amplification technique. Herein, the electroactive species oxidized at one finger electrode, generator, diffuses most likely to the neighboring finger electrode, collector, polarized to a potential enabling a reduction process, where it is reduced again back to the initial form. Thus, this results in an electrochemical amplification of both the generator and collector current signals. Primarily, the gap between the finger electrodes determines the amplification factor [219, 220].

In close corporation with Vorarlberg University of Applied Sciences, Austria a simple, low-cost and lift-off free fabrication approach for periodic structures with adjustable nanometer gaps for IDAs is introduced for the first time. Partel *et al.* [220] demonstrated with the invented fabrication technique an amplification factor of 116 using the gold IDAs with 160 nm electrode gap. This proves the great potential of such an approach and is the highest amplification factor achieved by redox cycling so far, to the best of our knowledge.

Moreover, carbon-based materials such as boron doped diamond or graphene can be utilized as working electrode material due to their excellent electrochemical properties including low capacitive currents, wide potential window and chemical inertness [221].

Acknowledgments

First of all, I would like to thank **Prof. Gerald Urban** for the acceptance and supervision of this thesis. I appreciate his scientific knowledge and experience which leads me through the way. His trust in me from the beginning reflected on me as self confidence in my studies and in my life. Besides, his sense of justice encourages me always to undertake new responsibilities that will help me to build my career further. I felt his support in every aspect, especially in my hard times.

I also want to thank **Prof. Wilfried Weber** for accepting to be the 2nd referee of this thesis and for his valuable advices in a gentle way.

I would like to specially thank you, **André Kling**. It was a real pleasure having you as my first student co-worker. In the course of the time we have learned a lot together and mutually. Unfortunately, it was not always easy for you to be the first one, but always fun for me. For sure, you contribute a lot to the milestone of this work with your great assistance through numerous experiments, and writing process standing by me in all issues without any complaints. Thank you for being there not only as supportive colleague but also as a close friend.

The whole story began on the day we met each other while I was looking with one of my friend for a student co-worker job. It was really lucky of me to have the chance working for you, **Jochen Kieninger**. In ten years, I have learned a lot from you both in academic and private life and further, we became close friends. You were always one of the great supporter of this thesis with your knowledge and to-the-point solutions. Thank you for always being there!

Although you were the last one that joined us, **Claire Chatelle**, your contribution to this work can not be underestimated. Your great effort and goal-oriented approach helped me a lot, especially on issues regarding biology and biochemistry. Thanks to your great sense of responsibility, you never left me in the lurch. It is always my pleasure to work with you and hopefully we will continue our pleasant collaboration in the future.

I warmly thank you, **Stefan Partel**, my "loyal project partner" without any project and funding! Hopefully, we will be "awarded" soon for our effective collaboration of many years. I think this cooperation could not remain so long, if we were not so close in the meantime. Working with you is really enjoyable. Moreover, your encouragement, motivation and belief in what we do is always exciting and inspiration for me.

I remember your first day at our chair in my group, **Mr. Lucas Armbrecht**! Such an enthusiastic, sophisticate and hardworking student! You are always willing to learn new

things and have self discipline to achieve your goals. Although I went “crazy” from time to time because of your stubbornness (!), I should confess, this helped me a lot somehow. Apart from this, your contribution to this work is unquestionable. I wish you good luck out there for your dissertation.

My long-term roommate **Andreas Weltin**; I spent more time with you than my wife at home! Although we never worked officially in a common project, yet we have “common” obsessions such as a clean and a neat office. I enjoy our discussions about technical and non-technical issues. Without your contribution, it might not be possible to employ such remarkable solutions in this work. Thank you for your support!

A special acknowledgment should be made to **Prof. Jürgen Heinze** for his great support and valuable advices, especially in the field of electrochemistry. It was a great pleasure for me having the chance to work with him.

Additionally, I would like to thank my ex-colleague **Josef Horàk** for his help in biology and biochemistry, as well as for the close friendship through the years. We had always enjoyable time. Special thanks go to **Elmar Laubender** for his contribution to my basic knowledge in electrochemistry and of course for the great time together. The work dealing with the scanning electrochemical microscope is a deep passion and I am very happy to share this feeling with you. **Barbara Enderle** deserves a special acknowledgment and many thanks for providing unwavering support and assistance all the time. Her full engagement along with her good mood was always a great motivation for me. Let the sunshine in!

I want to thank my thesis students **Rabih Ktaich** and **Edvina Qelibari** for their great work and wonderful time together. They had also a serious impact on this thesis. Many sincere thanks to **Johannes Huber** and **Richard Bruch** for proof reading of this work. Furthermore, I would like to thank all the past and present colleagues at the Laboratory for Sensors who supported me during this thesis and contributed to the great working atmosphere: **Kuppusamy Aravindalochanan**, **Hüseyin Bakırcı**, **Michael Bergmann**, **Uwe Bieser**, **Hubert Flamm**, **Loic Ledernez**, **Fethi Olcaytuğ**, **Olena Yurchenko**.

I would like to mention my close childhood friends, especially **Ahmet Utku Alp**, **Taylan Can**, **Umutay Sarıgül** and **Derya Yavuz**. Thanks to your great support in my difficult times not only in Turkey but also in Germany, I was able to overcome those difficulties as smoothly as it was possible. I know that you are always there for me!

Finally, I wholeheartedly thank my parents, **Idil Zaimoğlu** and **Ersin Dinçer** (May he rest in peace), for their tremendous support and love without any expectations. Above all, I thank my mother for encouraging me to revial my own potential, for never judging my decisions but always supporting me without any hesitations. I felt always very lucky to have such a brave woman as my mother. I love you mom.

Last but not least, I would like to thank my adorable wife, my best friend and my hard-working colleague **Bilge Nur Dincer**. Without your great support and endless faith in me all the time, it would not have been possible to get through every trial and tribulation along this long journey. From now on, a new life begins for us. Let us enjoy it! I love you **Bilge Nur**.

References

[1] Fu, E.; Yager, P.; Floriano, P. N.; Christodoulides, N. and McDevitt, J. T., Perspective on diagnostics for global health. *IEEE Pulse* **2011**, 2(6), 40–50.

[2] Yager, P.; Edwards, T.; Fu, E.; Helton, K.; Nelson, K.; Tam, M. R. and Weigl, B. H., Microfluidic diagnostic technologies for global public health. *Nature* **2006**, 442(7101), 412–418.

[3] Yager, P.; Domingo, G. J. and Gerdes, J., Point-of-care diagnostics for global health. *Annual Review of Biomedical Engineering* **2008**, 10(1), 107–144.

[4] Spindel, S. and Sapsford, K. E., Evaluation of optical detection platforms for multiplexed detection of proteins and the need for point-of-care biosensors for clinical use. *Sensors* **2014**, 14(12), 22313–22341.

[5] Luppa, P. B.; Müller, C.; Schlichtiger, A. and Schlebusch, H., Point-of-care testing (POCT): Current techniques and future perspectives. *TrAC Trends in Analytical Chemistry* **2011**, 30(6), 887–898.

[6] Jung, W.; Han, J.; Choi, J.-W. and Ahn, C. H., Point-of-care testing (POCT) diagnostic systems using microfluidic lab-on-a-chip technologies. *Microelectronic Engineering* **2015**, 132, 46–57.

[7] Gauglitz, G., Point-of-care platforms. *Annual Review of Analytical Chemistry* **2014**, 7(1), 297–315.

[8] Haeberle, S. and Zengerle, R., Microfluidic platforms for lab-on-a-chip applications. *Lab on a Chip* **2007**, 7(9), 1094–1110.

[9] Sackmann, E. K.; Fulton, A. L. and Beebe, D. J., The present and future role of microfluidics in biomedical research. *Nature* **2014**, 507(7491), 181–189.

[10] Mohammed, M.-I. and Desmulliez, M. P. Y., Lab-on-a-chip based immunosensor principles and technologies for the detection of cardiac biomarkers: A review. *Lab on a Chip* **2011**, 11(4), 569–595.

[11] Whitesides, G. M., The origins and the future of microfluidics. *Nature* **2006**, 442(7101), 368–373.

[12] Ng, A. H. C.; Uddayasankar, U. and Wheeler, A. R., Immunoassays in microfluidic systems. *Analytical and Bioanalytical Chemistry* **2010**, 397(3), 991–1007.

[13] Han, K. N.; Li, C. A. and Seong, G. H., Microfluidic chips for immunoassays. *Annual Review of Analytical Chemistry* **2013**, 6, 119–141.

[14] Chin, C. D.; Linder, V. and Sia, S. K., Lab-on-a-chip devices for global health: Past studies and future opportunities. *Lab on a Chip* **2007**, 7(1), 41–57.

[15] Bange, A.; Halsall, H. B. and Heineman, W. R., Microfluidic immunosensor systems. *Biosensors and Bioelectronics* **2005**, 20(12), 2488–2503.

[16] Dittrich, P. S. and Manz, A., Lab-on-a-chip: Microfluidics in drug discovery. *Nature Reviews Drug Discovery* **2006**, 5(3), 210–218.

[17] Nahavandi, S.; Baratchi, S.; Soffe, R.; Tang, S.-Y.; Nahavandi, S.; Mitchell, A. and Khoshmanesh, K., Microfluidic platforms for biomarker analysis. *Lab on a Chip* **2014**, 14(9), 1496–1514.

[18] Bruus, H., *Theoretical microfluidics*. Oxford University Press, Oxford, **2008**.

[19] Manz, A.; Graber, N. and Widmer, H., Miniaturized total chemical analysis systems: A novel concept for chemical sensing. *Sensors and Actuators B: Chemical* **1990**, 1(1-6), 244–248.

[20] Hervás, M.; López, M. A. and Escarpa, A., Electrochemical immunosensing on board microfluidic chip platforms. *TrAC Trends in Analytical Chemistry* **2012**, 31, 109–128.

[21] Edwards, R., *Immunodiagnostics: A practical approach*. Oxford University Press, New York, **1999**.

[22] Vaidya, S. V. and Bonventre, J. V., *Biomarkers: In medicine, drug discovery, and environmental health*. John Wiley & Sons, Inc., New Jersey, **2010**.

[23] Ekins, R. P. and Chu, F. W., Multianalyte immunoassay. *Journal of Pharmaceutical and Biomedical Analysis* **1989**, 7(2), 155–168.

[24] Yan, X.; Li, H.; Yan, Y. and Su, X., Developments in pesticide analysis by multianalyte immunoassays: A review. *Analytical Methods* **2014**, 6(11), 3543–3554.

[25] Wild, D., *The immunoassay handbook*. 4th ed., Elsevier Inc., New York, **2013**.

[26] Rusling, J. F., Multiplexed electrochemical protein detection and translation to personalized cancer diagnostics. *Analytical Chemistry* **2013**, 85(11), 5304–5310.

[27] Kingsmore, S. F., Multiplexed protein measurement: Technologies and applications of protein and antibody arrays. *Nature Reviews Drug Discovery* **2006**, 5(4), 310–321.

[28] Weber, C. C.; Link, N.; Fux, C.; Zisch, A. H.; Weber, W. and Fussenegger, M., Broad-spectrum protein biosensors for class-specific detection of antibiotics. *Biotechnology and Bioengineering* **2005**, 89(1), 9–17.

[29] Lannigan, F. J., Combating antibiotic resistance. *Clinical Otolaryngology and Allied Sciences* **2004**, 29(3), 284–287.

[30] Centers for Disease Control and Prevention, *National strategy for combating antibiotic resistant bacteria*. Tech. Rep. September, **2014**, URL `http://www.cdc.gov/drugresistance/pdf/carb{_}national{_}strategy.pdf`.

[31] World Health Organization, Fact sheet Nr. 194 - Antimicrobial resistance. **2015**, URL `http://www.who.int/mediacentre/factsheets/fs194/en/`.

[32] Hughes, D., Microbial genetics: Exploiting genomics, genetics and chemistry to combat antibiotic resistance. *Nature Reviews Genetics* **2003**, 4(6), 432–441.

[33] O'Neill, J., *Securing new drugs for future generations: The pipeline of antibiotics.* May, **2015**.

[34] Link, N.; Weber, W. and Fussenegger, M., A novel generic dipstick-based technology for rapid and precise detection of tetracycline, streptogramin and macrolide antibiotics in food samples. *Journal of Biotechnology* **2007**, 128(3), 668–680.

[35] Kling, J., Moving diagnostics from the bench to the bedside. *Nature Biotechnology* **2006**, 24(8), 891–893.

[36] Nyholm, L., Electrochemical techniques for lab-on-a-chip applications. *The Analyst* **2005**, 130(5), 599–605.

[37] Wang, J., *Analytical electrochemistry.* 3rd ed., John Wiley & Sons, Inc., New Jersey, **2006**.

[38] Bard, A. J. and Faulkner, L. R., *Electrochemical methods: Fundamentals and applications.* 2nd ed., John Wiley & Sons, Inc., New Jersey, **2001**.

[39] Kling, A.; Dincer, C.; Armbrecht, L.; Horak, J.; Kieninger, J. and Urban, G., Electrochemical microfluidic platform for simultaneous multi-analyte detection. *Procedia Engineering* **2015**, 120, 916–919.

[40] Armbrecht, L.; Dincer, C.; Kling, A.; Horak, J.; Kieninger, J. and Urban, G., Self-assembled magnetic bead chains for sensitivity enhancement of microfluidic electrochemical biosensor platforms. *Lab on a Chip* **2015**, 15(22), 4314–4321.

[41] Araz, M. K.; Tentori, A. M. and Herr, A. E., Microfluidic multiplexing in bioanalyses. *Journal of Laboratory Automation* **2013**, 18(5), 350–366.

[42] Wan, Y.; Su, Y.; Zhu, X.; Liu, G. and Fan, C., Development of electrochemical immunosensors towards point of care diagnostics. *Biosensors and Bioelectronics* **2013**, 47, 1–11.

[43] Foudeh, A. M.; Fatanat Didar, T.; Veres, T. and Tabrizian, M., Microfluidic designs and techniques using lab-on-a-chip devices for pathogen detection for point-of-care diagnostics. *Lab on a Chip* **2012**, 12(18), 3249–3266.

[44] Ling, M. M.; Ricks, C. and Lea, P., Multiplexing molecular diagnostics and immunoassays using emerging microarray technologies. *Expert Review of Molecular Diagnostics* **2007**, 7(1), 87–98.

[45] Joos, T. O.; Stoll, D. and Templin, M. F., Miniaturised multiplexed immunoassays. *Current opinion in chemical biology* **2002**, 6(1), 76–80.

[46] Díaz-González, M.; Muñoz-Berbel, X.; Jiménez-Jorquera, C.; Baldi, A. and Fernández-Sánchez, C., Diagnostics using multiplexed electrochemical readout devices. *Electroanalysis* **2014**, 26(6), 1154–1170.

[47] Chin, C. D.; Linder, V. and Sia, S. K., Commercialization of microfluidic point-of-care diagnostic devices. *Lab on a Chip* **2012**, 12(12), 2118–2134.

[48] Horak, J.; Dincer, C.; Bakirci, H. and Urban, G., A disposable dry film photoresist-based microcapillary immunosensor chip for rapid detection of Epstein-Barr virus infection. *Sensors and Actuators B: Chemical* **2014**, 191, 813–820.

[49] Horak, J.; Dincer, C.; Bakirci, H. and Urban, G., Sensitive, rapid and quantitative detection of substance P in serum samples using an integrated microfluidic immunochip. *Biosensors and Bioelectronics* **2014**, 58, 186–192.

[50] Horak, J.; Dincer, C.; Qelibari, E.; Bakirci, H. and Urban, G., Polymer-modified microfluidic immunochip for enhanced electrochemical detection of troponin I. *Sensors and Actuators B: Chemical* **2015**, 209, 478–485.

[51] Riebeseel, K.; Enderle, B.; Jobst, G.; Urban, G. and Moser, I., BioMEMS for the electrochemical detection of troponin I. *5th IEEE Conference on Sensors* **2006**, 160–161.

[52] Abbott Point of Care, Inc., *The i-STAT system: Comprehensive point-of-care testing.*

[53] Apple, F. S.; Murakami, M. M.; Christenson, R. H.; Campbell, J. L.; Miller, C. J.; Hock, K. G. and Scott, M. G., Analytical performance of the i-STAT cardiac troponin I assay. *Clinica Chimica Acta* **2004**, 345(1-2), 123–127.

[54] Peled, N., Design and implementation of a microchemistry analyzer. *Pure and Applied Chemistry* **1996**, 68(10), 1837–1841.

[55] Gordon, J. and Michel, G., Discerning trends in multiplex immunoassay technology with potential for resource-limited settings. *Clinical Chemistry* **2012**, 58(4), 690–698.

[56] Ko, Y.-J.; Maeng, J.-H.; Ahn, Y.; Hwang, S. Y.; Cho, N.-G. and Lee, S.-H., Microchip-based multiplex electro-immunosensing system for the detection of cancer biomarkers. *Electrophoresis* **2008**, 29(16), 3466–3476.

[57] Fu, Q.; Zhu, J. and Van Eyk, J. E., Comparison of Multiplex Immunoassay Platforms. *Clinical Chemistry* **2010**, 56(2), 314–318.

[58] Clark, T. J.; McPherson, P. H. and Buechler, K. F., The Triage cardiac panel. *Point of Care: The Journal of Near-Patient Testing & Technology* **2002**, 1(1), 42–46.

[59] Buechler, K. F.; Moi, S.; Noar, B.; McGrath, D.; Villela, J.; Clancy, M.; Shenhav, A.; Colleymore, A.; Valkirs, G. and Lee, T., Simultaneous detection of seven drugs of abuse by the Triage™ panel for drugs of abuse. *Clinical Chemistry* **1992**, 38(9), 1678–1684.

[60] Apple, F. S.; Christenson, R. H.; Valdes, R.; Andriak, A. J.; Berg, A.; Duh, S. H.; Feng, Y. J.; Jortani, S. A.; Johnson, N. A.; Koplen, B.; Mascotti, K. and Wu, A. H., Simultaneous rapid measurement of whole blood myoglobin, creatine kinase MB, and cardiac troponin I by the triage cardiac panel for detection of myocardial infarction. *Clinical Chemistry* **1999**, 45(2), 199–205.

[61] Taranova, N.; Berlina, A.; Zherdev, A. and Dzantiev, B., Traffic light immunochromatographic test based on multicolor quantum dots for the simultaneous detection of several antibiotics in milk. *Biosensors and Bioelectronics* **2015**, 63, 255–261.

[62] Martinez, A. W.; Phillips, S. T. and Whitesides, G. M., Three-dimensional microfluidic devices fabricated in layered paper and tape. *Proceedings of the National Academy of Sciences* **2008**, 105(50), 19606–19611.

[63] Rolland, J. P. and Mourey, D. A., Paper as a novel material platform for devices. *MRS Bulletin* **2013**, 38(4), 299–305.

[64] Ge, L.; Yan, J.; Song, X.; Yan, M.; Ge, S. and Yu, J., Three-dimensional paper-based electrochemiluminescence immunodevice for multiplexed measurement of biomarkers and point-of-care testing. *Biomaterials* **2012**, 33(4), 1024–1031.

[65] Dungchai, W.; Chailapakul, O. and Henry, C. S., Electrochemical detection for paper-based microfluidics. *Analytical Chemistry* **2009**, 81(14), 5821–5826.

[66] Martinez, A. W.; Phillips, S. T.; Carrilho, E.; Thomas, S. W.; Sindi, H. and Whitesides, G. M., Simple telemedicine for developing regions: Camera phones and paper-based microfluidic devices for real-time, off-site diagnosis. *Analytical Chemistry* **2008**, 80(10), 3699–3707.

[67] Cheng, C.-M.; Martinez, A. W.; Gong, J.; Mace, C. R.; Phillips, S. T.; Carrilho, E.; Mirica, K. A. and Whitesides, G. M., Paper-Based ELISA. *Angewandte Chemie* **2010**, 122(28), 4881–4884.

[68] Pollock, N. R.; Rolland, J. P.; Kumar, S.; Beattie, P. D.; Jain, S.; Noubary, F.; Wong, V. L.; Pohlmann, R. A.; Ryan, U. S. and Whitesides, G. M., A paper-based multiplexed transaminase test for low-cost, point-of-care liver function testing. *Science Translational Medicine* **2012**, 4(152), 152ra129.

[69] Vella, S. J.; Beattie, P.; Cademartiri, R.; Laromaine, A.; Martinez, A. W.; Phillips, S. T.; Mirica, K. A. and Whitesides, G. M., Measuring markers of liver function using a micropatterned paper device designed for blood from a fingerstick. *Analytical Chemistry* **2012**, 84(6), 2883–2891.

[70] Talapatra, A.; Rouse, R. and Hardiman, G., Protein microarrays: Challenges and promises. *Pharmacogenomics* **2002**, 3(4), 527–536.

[71] Dill, K.; Montgomery, D. D.; Ghindilis, A. L.; Schwarzkopf, K. R.; Ragsdale, S. R. and Oleinikov, A. V., Immunoassays based on electrochemical detection using microelectrode arrays. *Biosensors and Bioelectronics* **2004**, 20(4), 736–742.

[72] Roth, K. M.; Peyvan, K.; Schwarzkopf, K. R. and Ghindilis, A., Electrochemical detection of short DNA oligomer hybridization using the CombiMatrix ElectraSense microarray reader. *Electroanalysis* **2006**, 18(19-20), 1982–1988.

[73] Ghindilis, A. L.; Smith, M. W.; Schwarzkopf, K. R.; Roth, K. M.; Peyvan, K.; Munro, S. B.; Lodes, M. J.; Stöver, A. G.; Bernards, K.; Dill, K. and McShea, A., CombiMatrix oligonucleotide arrays: Genotyping and gene expression assays employing electrochemical detection. *Biosensors and Bioelectronics* **2007**, 22(9-10), 1853–1860.

[74] Hornauer, H.; Klause, U. and Müller, H. J., IMPACT - Eine Protein-Array Technologie für die diagnostische Anwendung der Zukunft. *Biospektrum Special: Proteomics in der molekularen Medizin* **2004**, 564–565.

[75] Claudon, A.; Vergnaud, P.; Valverde, C.; Mayr, A.; Klause, U. and Garnero, P., New automated multiplex assay for bone turnover markers in osteoporosis. *Clinical Chemistry* **2008**, 54(9), 1554–1563.

[76] Chandra, P. E.; Sokolove, J.; Hipp, B. G.; Lindstrom, T. M.; Elder, J. T.; Reveille, J. D.; Eberl, H.; Klause, U. and Robinson, W. H., Novel multiplex technology for diagnostic characterization of rheumatoid arthritis. *Arthritis Research & Therapy* **2011**, 13(3), R102.

[77] Bernard, A.; Michel, B. and Delamarche, E., Micromosaic Immunoassays. *Analytical Chemistry* **2001**, 73(1), 8–12.

[78] Ligler, F. S.; Taitt, C. R.; Shriver-Lake, L. C.; Sapsford, K. E.; Shubin, Y. and Golden, J. P., Array biosensor for detection of toxins. *Analytical and Bioanalytical Chemistry* **2003**, 377(3), 469–477.

[79] Endo, T.; Kerman, K.; Nagatani, N.; Hiepa, H. M.; Kim, D. K.; Yonezawa, Y.; Nakano, K. and Tamiya, E., Multiple label-free detection of antigen-antibody reaction using localized surface plasmon resonance-based core-shell structured nanoparticle layer nanochip. *Analytical Chemistry* **2006**, 78(18), 6465–6475.

[80] Aćimović, S. S.; Ortega, M. A.; Sanz, V.; Berthelot, J.; Garcia-Cordero, J. L.; Renger, J.; Maerkl, S. J.; Kreuzer, M. P. and Quidant, R., LSPR chip for parallel, rapid, and sensitive detection of cancer markers in serum. *Nano Letters* **2014**, 14(5), 2636–2641.

[81] Heinze, J., Ultramicroelectrodes in electrochemistry. *Angewandte Chemie International Edition* **1993**, 32(9), 1268–1288.

[82] Skládal, P. and Kaláb, T., A multichannel immunochemical sensor for determination of 2,4-dichlorophenoxyacetic acid. *Analytica Chimica Acta* **1995**, 316, 73–78.

[83] Kojima, K.; Hiratsuka, A.; Suzuki, H.; Yano, K.; Ikebukuro, K. and Karube, I., Electrochemical protein chip with arrayed immunosensors with antibodies immobilized in a plasma-polymerized film. *Analytical Chemistry* **2003**, 75(5), 1116–1122.

[84] Los, M.; Los, J.; Blohm, L.; Spillner, E.; Grunwald, T.; Albers, J.; Hintsche, R. and Wegrzyn, G., Rapid detection of viruses using electrical biochips and anti-virion sera. *Letters in Applied Microbiology* **2005**, 40(6), 479–485.

[85] Pavlovic, E.; Lai, R. Y.; Wu, T. T.; Ferguson, B. S.; Sun, R.; Plaxco, K. W. and Soh, H. T., Microfluidic device architecture for electrochemical patterning and detection of multiple DNA sequences. *Langmuir* **2008**, 24(3), 1102–1107.

[86] Wilson, M. S. and Nie, W., Multiplex measurement of seven tumor markers using an electrochemical protein chip. *Analytical Chemistry* **2006**, 78(18), 6476–6483.

[87] Wilson, M. S. and Nie, W., electrochemical multianalyte immunoassays using an array-based sensor. *Analytical Chemistry* **2006**, 78(8), 2507–2513.

[88] Ricci, F.; Adornetto, G. and Palleschi, G., A review of experimental aspects of electrochemical immunosensors. *Electrochimica Acta* **2012**, 84, 74–83.

[89] Henry, O. Y.; Fragoso, A.; Beni, V.; Laboria, N.; Sánchez, J. L. A.; Latta, D.; Von Germar, F.; Drese, K.; Katakis, I. and O'Sullivan, C. K., Design and testing of a packaged microfluidic cell for the multiplexed electrochemical detection of cancer markers. *Electrophoresis* **2009**, 30, 3398–3405.

[90] Albers, J.; Grunwald, T.; Nebling, E.; Piechotta, G. and Hintsche, R., Electrical biochip technology: A tool for microarrays and continuous monitoring. *Analytical and Bioanalytical Chemistry* **2003**, 377(3), 521–527.

[91] Elsholz, B.; Nitsche, A.; Achenbach, J.; Ellerbrok, H.; Blohm, L.; Albers, J.; Pauli, G.; Hintsche, R. and Wörl, R., Electrical microarrays for highly sensitive detection of multiplex PCR products from biological agents. *Biosensors and Bioelectronics* **2009**, 24(6), 1737–1743.

[92] Schumacher, S.; Nestler, J.; Otto, T.; Wegener, M.; Ehrentreich-Förster, E.; Michel, D.; Wunderlich, K.; Palzer, S.; Sohn, K.; Weber, A.; Burgard, M.; Grzesiak, A.; Teichert, A.; Brandenburg, A.; Koger, B.; Albers, J.; Nebling, E. and Bier, F. F., Highly-integrated lab-on-chip system for point-of-care multiparameter analysis. *Lab on a Chip* **2012**, 12(3), 464–473.

[93] Cagnin, S.; Caraballo, M.; Guiducci, C.; Martini, P.; Ross, M.; SantaAna, M.; Danley, D.; West, T. and Lanfranchi, G., Overview of Electrochemical DNA Biosensors: New Approaches to Detect the Expression of Life. *Sensors* **2009**, 9(4), 3122–3148.

[94] Sato, K.; Yamanaka, M.; Takahashi, H.; Tokeshi, M.; Kimura, H. and Kitamori, T., Microchip-based immunoassay system with branching multichannels for simultaneous determination of interferon-gamma. *Electrophoresis* **2002**, 23(5), 734–739.

[95] Godin, J.; Chen, C.-H.; Cho, S. H.; Qiao, W.; Tsai, F. and Lo, Y.-H., Microfluidics and photonics for Bio-System-on-a-Chip: A review of advancements in technology towards a microfluidic flow cytometry chip. *Journal of Biophotonics* **2008**, 1(5), 355–376.

[96] Ateya, D. A.; Erickson, J. S.; Howell, P. B.; Hilliard, L. R.; Golden, J. P. and Ligler, F. S., The good, the bad, and the tiny: A review of microflow cytometry. *Analytical and Bioanalytical Chemistry* **2008**, 391(5), 1485–1498.

[97] Dunbar, S. A., Applications of Luminex® xMAP™ technology for rapid, high-throughput multiplexed nucleic acid detection. *Clinica Chimica Acta* **2006**, 363(1-2), 71–82.

[98] Dunbar, S. A. and Jacobson, J. W., Parallel processing in microbiology: Detection of infectious pathogens by Luminex xMAP multiplexed suspension array technology. *Clinical Microbiology Newsletter* **2007**, 29(11), 79–86.

[99] Hashemi, N.; Erickson, J. S.; Golden, J. P. and Ligler, F. S., Optofluidic characterization of marine algae using a microflow cytometer. *Biomicrofluidics* **2011**, 5(3), 032009.

[100] Shriver-Lake, L. C.; Golden, J.; Bracaglia, L. and Ligler, F. S., Simultaneous assay for ten bacteria and toxins in spiked clinical samples using a microflow cytometer. *Analytical and Bioanalytical Chemistry* **2013**, 405(16), 5611–5614.

[101] Strohmeier, O.; Keller, M.; Schwemmer, F.; Zehnle, S.; Mark, D.; von Stetten, F.; Zengerle, R. and Paust, N., Centrifugal microfluidic platforms: Advanced unit operations and applications. *Chemical Society Reviews* **2015**, 44(17), 6187–6229.

[102] Andreasen, S. Z.; Kwasny, D.; Amato, L.; Brøgger, A. L.; Bosco, F. G.; Andersen, K. B.; Svendsen, W. E. and Boisen, A., Integrating electrochemical detection with centrifugal microfluidics for real-time and fully automated sample testing. *RSC Advances* **2015**, 5(22), 17187–17193.

[103] Li, T.; Fan, Y.; Cheng, Y. and Yang, J., An electrochemical lab-on-a-CD system for parallel whole blood analysis. *Lab on a Chip* **2013**, 13, 2634–2640.

[104] Honda, N., Simultaneous Multiple Immunoassays in a Compact Disc-Shaped Microfluidic Device Based on Centrifugal Force. *Clinical Chemistry* **2005**, 51(10), 1955–1961.

[105] Inganäs, M.; Dérand, H.; Eckersten, A.; Ekstrand, G.; Honerud, A.-K.; Jesson, G.; Thorsén, G.; Söderman, T. and Andersson, P., Integrated microfluidic compact disc device with potential use in both centralized and point-of-care laboratory settings. *Clinical Chemistry* **2005**, 51(10), 1985–1987.

[106] Tang, D.; Hou, L.; Niessner, R.; Xu, M.; Gao, Z. and Knopp, D., Multiplexed electrochemical immunoassay of biomarkers using metal sulfide quantum dot nanolabels and trifunctionalized magnetic beads. *Biosensors and Bioelectronics* **2013**, 46, 37–43.

[107] Dill, K.; Ghindilis, A. and Schwarzkopf, K., Multiplexed analyte and oligonucleotide detection on microarrays using several redox enzymes in conjunction with electrochemical detection. *Lab on a Chip* **2006**, 6(8), 1052–1055.

[108] Feng, L.-N.; Bian, Z.-P.; Peng, J.; Jiang, F.; Yang, G.-H.; Zhu, Y.-D.; Yang, D.; Jiang, L.-P. and Zhu, J.-J., Ultrasensitive multianalyte electrochemical immunoassay based on metal ion functionalized titanium phosphate nanospheres. *Analytical Chemistry* **2012**, 84(18), 7810–7815.

[109] Tang, J.; Tang, D.; Niessner, R.; Chen, G. and Knopp, D., Magneto-controlled graphene immunosensing platform for simultaneous multiplexed electrochemical immunoassay using distinguishable signal tags. *Analytical Chemistry* **2011**, 83(13), 5407–5414.

[110] Wang, J.; Liu, G. and Merkoçi, A., Electrochemical coding technology for simultaneous detection of multiple DNA targets. *Journal of the American Chemical Society* **2003**, 125(11), 3214–3215.

[111] Kong, F.-Y.; Xu, B.-Y.; Xu, J.-J. and Chen, H.-Y., Simultaneous electrochemical immunoassay using CdS-DNA and PbS-DNA nanochains as labels. *Biosensors and Bioelectronics* **2013**, 39(1), 177–182.

[112] Thorsen, T.; Maerkl, S. J. and Quake, S. R., Microfluidic large-scale integration. *Science* **2002**, 298(5593), 580–584.

[113] Melin, J. and Quake, S. R., Microfluidic large-scale integration: The evolution of design rules for biological automation. *Annual Review of Biophysics and Biomolecular Structure* **2007**, 36(1), 213–231.

[114] Dong, H.; Li, C.-M.; Zhang, Y.-F.; Cao, X.-D. and Gan, Y., Screen-printed microfluidic device for electrochemical immunoassay. *Lab on a Chip* **2007**, 7, 1752–1758.

[115] Lawi, W.; Wiita, C.; Snyder, S. T.; Wei, F.; Wong, D.; Wong, P. K.; Liao, J. C.; Haake, D. and Gau, V., A microfluidic cartridge system for multiplexed clinical analysis. *Journal of Laboratory Automation* **2009**, 14(6), 407–412.

[116] McDonald, J. C. and Whitesides, G. M., Poly(dimethylsiloxane) as a material for fabricating microfluidic devices. *Accounts of Chemical Research* **2002**, 35(7), 491–499.

[117] Au, A. K.; Lai, H.; Utela, B. R. and Folch, A., Microvalves and micropumps for bioMEMS. *Micromachines* **2011**, 2(4), 179–220.

[118] Kong, J.; Jiang, L.; Su, X.; Qin, J.; Du, Y. and Lin, B. *Lab on a Chip* (11), 1541–1547.

[119] Shao, G.; Wang, J.; Li, Z.; Saraf, L.; Wang, W. and Lin, Y., Poly(dimethylsiloxane) microchip-based immunoassay with multiple reaction zones: Toward on-chip multiplex detection platform. *Sensors and Actuators B: Chemical* **2011**, 159(1), 44–50.

[120] Wu, A. R.; Kawahara, T. L. A.; Rapicavoli, N. A.; van Riggelen, J.; Shroff, E. H.; Xu, L.; Felsher, D. W.; Chang, H. Y. and Quake, S. R., High throughput automated chromatin immunoprecipitation as a platform for drug screening and antibody validation. *Lab on a Chip* **2012**, 12(12), 2190–2198.

[121] Skelley, A. M.; Scherer, J. R.; Aubrey, A. D.; Grover, W. H.; Ivester, R. H. C.; Ehrenfreund, P.; Grunthaner, F. J.; Bada, J. L. and Mathies, R. A., Development and evaluation of a microdevice for amino acid biomarker detection and analysis on Mars. *Proceedings of the National Academy of Sciences* **2005**, 102(4), 1041–1046.

[122] Kalisky, T. and Quake, S. R., Single-cell genomics. *Nature Methods* **2011**, 8(4), 311–314.

[123] Chin, C. D.; Laksanasopin, T.; Cheung, Y. K.; Steinmiller, D.; Linder, V.; Parsa, H.; Wang, J.; Moore, H.; Rouse, R.; Umviligihozo, G.; Karita, E.; Mwambarangwe, L.; Braunstein, S. L.; van de Wijgert, J.; Sahabo, R.; Justman, J. E.; El-Sadr, W. and Sia, S. K., Microfluidics-based diagnostics of infectious diseases in the developing world. *Nature Medicine* **2011**, 17(8), 1015–1019.

[124] Chin, C. D.; Cheung, Y. K.; Laksanasopin, T.; Modena, M. M.; Chin, S. Y.; Sridhara, A. A.; Steinmiller, D.; Linder, V.; Mushingantahe, J.; Umviligihozo, G.; Karita, E.; Mwambarangwe, L.; Braunstein, S. L.; van de Wijgert, J.; Sahabo, R.; Justman, J. E.; El-Sadr, W. and Sia, S. K., Mobile Device for Disease Diagnosis and Data Tracking in Resource-Limited Settings. *Clinical Chemistry* **2013**, 59(4), 629–640.

[125] Lafleur, L.; Stevens, D.; McKenzie, K.; Ramachandran, S.; Spicar-Mihalic, P.; Singhal, M.; Arjyal, A.; Osborn, J.; Kauffman, P.; Yager, P. and Lutz, B., Progress toward multiplexed sample-to-result detection in low resource settings using microfluidic immunoassay cards. *Lab on a Chip* **2012**, 12(6), 1119–1127.

[126] Stevens, D. Y.; Petri, C. R.; Osborn, J. L.; Spicar-Mihalic, P.; McKenzie, K. G. and Yager, P., Enabling a microfluidic immunoassay for the developing world by integration of on-card dry reagent storage. *Lab on a Chip* **2008**, 8(12), 2038–2045.

[127] Hu, W.; Lu, Z.; Liu, Y.; Chen, T.; Zhou, X. and Li, C. M., A portable flow-through fluorescent immunoassay lab-on-a-chip device using ZnO nanorod-decorated glass capillaries. *Lab on a Chip* **2013**, 13(9), 1797–1802.

[128] Moreira, N. H.; de Jesus de Almeida, A. L.; de Oliveira Piazzeta, M. H.; de Jesus, D. P.; Deblire, A.; Gobbi, Â. L. and Fracassi da Silva, J. A., Fabrication of a multichannel PDMS-glass analytical microsystem with integrated electrodes for amperometric detection. *Lab on a Chip* **2009**, 9(1), 115–121.

[129] Rossier, J. S.; Baranek, S.; Morier, P.; Vollet, C.; Vulliet, F.; Dechastonay, Y. and Reymond, F., GRAVI: Robotized microfluidics for fast and automated immunoassays in low volume. *Journal of Laboratory Automation* **2008**, 13(6), 322–329.

[130] Rossier, J. S.; Vollet, C.; Carnal, A.; Lagger, G.; Gobry, V.; Girault, H. H.; Michel, P. and Reymond, F., Plasma etched polymer microelectrochemical systems. *Lab on a Chip* **2002**, 2(3), 145–150.

[131] Hoegger, D.; Morier, P.; Vollet, C.; Heini, D.; Reymond, F. and Rossier, J. S., Disposable microfluidic ELISA for the rapid determination of folic acid content in food products. *Analytical and Bioanalytical Chemistry* **2006**, 387(1), 267–275.

[132] Kwakye, S.; Goral, V. N. and Baeumner, A. J., Electrochemical microfluidic biosensor for nucleic acid detection with integrated minipotentiostat. *Biosensors and Bioelectronics* **2006**, 21(12), 2217–2223.

[133] Bagotsky, V. S., *Fundamentals of electrochemistry*. 2nd ed., John Wiley & Sons, Inc., New Jersey, **2006**.

[134] Brett, C. M. A. and Brett, A. M. O., *Electrochemistry: Principles, methods, and applications*. 2nd ed., Oxford University Press, Oxford, **1994**.

[135] Lambrechts, M. and Sansen, W., *Biosensors: Microelectrochemical devices*. 1st ed., Taylor and Francis Group, Bristol, **1992**.

[136] Hamann, C. H. and Vielstich, W., *Elektrochemie*. Wiley-VCH, Weinheim, **1998**.

[137] Zoski, C. G., *Handbook of electrochemistry*. 1st ed., Elsevier B.V., Amsterdam, **2007**.

[138] Ives, D. J. G. and Janz, G. J., *Reference electrodes, theory and practice*. Academic Press, New York, **1961**.

[139] Mroz, A.; Borchardt, M.; Diekmann, C.; Cammann, K.; Knoll, M. and Dumschat, C., Disposable reference electrode. *The Analyst* **1998**, 123(6), 1373–1376.

[140] Nann, T. and Urban, G., A new dynamic hydrogen reference electrode for applications in thin-film sensor systems. *Sensors and Actuators B: Chemical* **2000**, 70(1-3), 188–195.

[141] Angerstein-Kozlowska, H.; Conway, B. and Sharp, W., The real condition of electrochemically oxidized platinum surfaces. *Journal of Electroanalytical Chemistry and Interfacial Electrochemistry* **1973**, 43(1), 9–36.

[142] Doña Rodríguez, J. M.; Herrera Melián, J. A. and Pérez Peña, J., Determination of the real surface area of Pt electrodes by hydrogen adsorption using cyclic voltammetry. *Journal of Chemical Education* **2000**, 77(9), 1195–1197.

[143] Aschauer, E.; Fasching, R.; Varahram, M.; Jobst, G.; Urban, G.; Nicolussi, G.; Husinsky, W.; Friedbacher, G. and Grasserbauer, M., Surface modification of platinum thin film electrodes towards a defined roughness and microsporosity. *Journal of Electroanalytical Chemistry* **1997**, 426(1-2), 157–165.

[144] Biegler, T.; Rand, D. and Woods, R., Limiting oxygen coverage on platinized platinum; relevance to determination of real platinum area by hydrogen adsorption. *Journal of Electroanalytical Chemistry and Interfacial Electrochemistry* **1971**, 29(2), 269–277.

[145] Jerkiewicz, G.; Vatankhah, G.; Lessard, J.; Soriaga, M. P. and Park, Y. S., Surface-oxide growth at platinum electrodes in aqueous H_2SO_4, reexamination of its mechanism through combined cyclic-voltammetry, electrochemical quartz-crystal nanobalance, and Auger electron spectroscopy measurements. *Electrochimica Acta* **2004**, 49(9-10), 1451–1459.

[146] Hall, S. B.; Khudaish, E. A. and Hart, A. L., Electrochemical oxidation of hydrogen peroxide at platinum electrodes. Part IV: Phosphate buffer dependence. *Electrochimica Acta* **1999**, 44(25), 4573–4582.

[147] Lingane, J. J. and Lingane, P. J., Chronopotentiometry of hydrogen peroxide with a platinum wire electrode. *Journal of Electroanalytical Chemistry* **1963**, 5(6), 411–419.

[148] Prabhu, V. G.; Zarapkar, L. R. and Dhaneshwar, R. G., Electrochemical studies of hydrogen peroxide at a platinum disc electrode. *Electrochimica Acta* **1981**, 26(6), 725–729.

[149] Hickling, A. and Wilson, W. H., The anodic decomposition of hydrogen peroxide. *Journal of the Electrochemical Society* **1951**, 98(11), 425–433.

[150] Luppa, P. B.; Sokoll, L. J. and Chan, D. W., Immunosensors - Principles and applications to clinical chemistry. *Clinica Chimica Acta* **2001**, 314(1-2), 1–26.

[151] Findlay, J. W. A.; Smith, W. C.; Lee, J. W.; Nordblom, G. D.; Das, I.; Desilva, B. S.; Khan, M. N. and Bowsher, R. R., Validation of immunoassays for bioanalysis: A pharmaceutical industry perspective. *Journal of Pharmaceutical and Biomedical Analysis* **2000**, 21(6), 1249–1273.

[152] Yakovleva, J. and Emnéus, J., Electrochemical immunoassays. In *Bioelectrochemistry: Fundamentals, experimental techniques and applications*, edited by P. N. Bartlett, 1st ed., John Wiley & Sons, Inc., Chichester, **2008**, 377–410.

[153] Revoltella, R. P.; Laricchia Robbio, L. and Liedberg, B., Comparison of conventional immunoassays (RIA, ELISA) with surface plasmon resonance for pesticide detection and monitoring. *Biotherapy* **1998**, 11(2-3), 135–145.

[154] Gosling, J. P., A decade of development in immunoassay methodology. *Clinical Chemistry* **1990**, 36(8), 1408–1427.

[155] Ronkainen-Matsuno, N. J.; Thomas, J. H.; Halsall, H. B. and Heineman, W. R., Electrochemical immunoassay moving into the fast lane. *TrAC Trends in Analytical Chemistry* **2002**, 21(4), 213–225.

[156] Warsinke, A.; Benkert, A. and Scheller, F. W., Electrochemical immunoassays. *Fresenius' Journal of Analytical Chemistry* **2000**, 366(6-7), 622–634.

[157] Coons, A. H.; Creech, H. J. and Jones, R. N., Immunological properties of an antibody containing a fluorescent group. *Experimental Biology and Medicine* **1941**, 47(2), 200–202.

[158] Yalow, R. S. and Berson, S. A., Assay of plasma insulin in human subjects by immunological methods. *Nature* **1959**, 184, 1648–1649.

[159] Yalow, R. S. and Berson, S. A., Immunoassay of endogenous plasma insulin in man. *The Journal of clinical investigation* **1960**, 39, 1157–1175.

[160] Ekins, R. P., The estimation of thyroxine in human plasma by an electrophoretic technique. *Clinica Chimica Acta* **1960**, 5, 453–459.

[161] Christopoulos, T. K. and Diamandis, E. P., *Immunoassay.* 1st ed., Academic Press, San Diego, **1996**.

[162] Engvall, E. and Perlmann, P., Enzyme-linked immunosorbent assay (ELISA) quantitative assay of immunoglobulin G. *Immunochemistry* **1971**, 8(9), 871–874.

[163] Rocco, R. M., *Landmark papers in clinical chemistry.* 1st ed., Elsevier B.V., Amsterdam, **2006**.

[164] Avrameas, S. and Uriel, J., Method of antigen and antibody labelling with enzymes and its immunodiffusion application. *Comptes Rendus Hebdomadaires des Seances de L'academie des Sciences. Serie D: Sciences Naturelles* **1966**, 262(24), 2543–2545.

[165] Nakane, P. K. and Pierce, G. B., Enzyme-labeled antibodies: Preparation and application for the localization of antigens. *The Journal of Histochemistry and Cytochemistry* **1966**, 14(12), 929–931.

[166] Sever, J. L., Application of a microtechnique to viral serological investigations. *Journal of Immunology* **1962**, 88, 320–329.

[167] Takatsy, G., The use of spiral loops in serological and virological micro-methods. *Acta Microbiologica et Immunologica Hungarica* **2003**, 50(4), 369–383.

[168] Catt, K. and Tregear, G. W., Solid-phase radioimmunoassay in antibody-coated tubes. *Science* **1967**, 158(808), 1570–1572.

[169] Van Weemen, B. and Schuurs, A. H. W. M., Immunoassay using antigen-enzyme conjugates. *FEBS Letters* **1971**, 15(3), 232–236.

[170] Engvall, E., The ELISA, Enzyme-linked immunosorbent assay. *Clinical Chemistry* **2010**, 56(2), 319–320.

[171] O'Kennedy, R.; Byrne, M.; O'Fagain, C. and Berns, G., Experimental section: A review of enzyme-immunoassay and a description of a competitive enzyme-linked immunosorbent assay for the detection of immunoglobulin concentrations. *Biochemical Education* **1990**, 18(3), 136–140.

[172] Aydin, S., A short history, principles, and types of ELISA, and our laboratory experience with peptide-protein analyses using ELISA. *Peptides* **2015**, 72, 4–15.

[173] Lindström, P. and Wager, O., IgG autoantibody to human serum albumin studied by the ELISA-technique. *Scandinavian Journal of Immunology* **1978**, 7(5), 419–425.

[174] Yorde, D. E.; Sasse, E. A. and Wang, T. Y., Competitive enzyme linked immunoassay with use of soluble enzyme-antibody immune complexes for labeling. I. Measurement of human choriogonadotropin. *Clinical Chemistry* **1976**, 22(8), 1372–1377.

[175] Nelson, M. A.; Reiter, W. S. and Hage, D. S., Chromatographic competitive binding immunoassays: A comparison of the sequential and simultaneous injection methods. *Biomedical Chromatography* **2003**, 17(2-3), 188–200.

[176] Kato, K.; Hamaguchi, Y.; Okawa, S.; Ishikawa, E. and Kobayashi, K., Use of rabbit antibody IgG bound onto plain and aminoalkylsilyl glass surface for the enzyme-linked sandwich immunoassay. *Journal of Biochemistry* **1977**, 82(1), 261–266.

[177] Rusmini, F.; Zhong, Z. and Feijen, J., Protein immobilization strategies for protein biochips. *Biomacromolecules* **2007**, 8(6), 1775–1789.

[178] Kim, D. and Herr, A. E., Protein immobilization techniques for microfluidic assays. *Biomicrofluidics* **2013**, 7(4), 041501.

[179] Sam, S.; Touahir, L.; Salvador Andresa, J.; Allongue, P.; Chazalviel, J.-N.; Gouget-Laemmel, A. C.; Henry de Villeneuve, C.; Moraillon, A.; Ozanam, F.; Gabouze, N. and Djebbar, S., Semiquantitative study of the EDC-NHS activation of acid terminal groups at modified porous silicon surfaces. *Langmuir* **2010**, 26(2), 809–814.

[180] Wang, C.; Yan, Q.; Liu, H.-B.; Zhou, X.-H. and Xiao, S.-J., Different EDC-NHS activation mechanisms between PAA and PMAA brushes and the following amidation reactions. *Langmuir* **2011**, 27(19), 12058–12068.

[181] Staros, J. V.; Wright, R. W. and Swingle, D. M., Enhancement by N-hydroxysulfosuccinimide of water-soluble carbodiimide-mediated coupling reactions. *Analytical Biochemistry* **1986**, 156(1), 220–222.

[182] Bogdanov, A.; Klibanov, A. and Torchilin, V., Protein immobilization on the surface of liposomes via carbodiimide activation in the presence of N-hydroxysulfosuccinimide. *FEBS Letters* **1988**, 231(2), 381–384.

[183] Thermo Fisher Scientific Inc., *NHS & Sulfo-NHS: Instructions*. **2009**.

[184] Janeway, C. A.; Travers, J. P.; Walport, M. and Shlomchik, M. J., *Immunobiology: The immune system in health and disease*. 5th ed., Garland science, New York, **2001**.

[185] Esser, P., *Application note 6: Principles in adsorption to polystyrene*. Thermo Fisher Scientific Inc., **2010**.

[186] Köhler, G. and Milstein, C., Continuous cultures of fused cells secreting antibody of predefined specificity. *Nature* **1975**, 256(5517), 495–497.

[187] Shrestha, D.; Bagosi, A.; Szöllősi, J. and Jenei, A., Comparative study of the three different fluorophore antibody conjugation strategies. *Analytical and Bioanalytical Chemistry* **2012**, 404(5), 1449–1463.

[188] Urban, G., *BioMEMS*. 1st ed., Springer, Dordrecht, **2006**.

[189] Ziegler, A.; Koch, A.; Krockenberger, K. and Grosshennig, A., Personalized medicine using DNA biomarkers: A review. *Human Genetics* **2012**, 131(10), 1627–1638.

[190] Gossen, M. and Bujard, H., Tight control of gene expression in mammalian cells by tetracycline-responsive promoters. *Proceedings of the National Academy of Sciences* **1992**, 89(12), 5547–5551.

[191] Menzel, A.; Gübeli, R. J.; Güder, F.; Weber, W. and Zacharias, M., Detection of real-time dynamics of drug-target interactions by ultralong nanowalls. *Lab on a Chip* **2013**, 13(21), 4173–4179.

[192] Moina, C. and Ybarra, G., Fundamentals and applications of immunosensors. In *Advances in Immunoassay Technology*, edited by N. H. L. Chiu, 1st ed., InTech, **2012**.

[193] Findlay, J. W. A. and Dillard, R. F., Appropriate calibration curve fitting in ligand binding assays. *The AAPS Journal* **2007**, 9(2), E260–E267.

[194] DeSilva, B.; Smith, W.; Weiner, R.; Kelley, M.; Smolec, J.; Lee, B.; Khan, M.; Tacey, R.; Hill, H. and Celniker, A., Recommendations for the bioanalytical method validation of ligand-binding assays to support pharmacokinetic assessments of macromolecules. *Pharmaceutical Research* **2003**, 20(11), 1885–1900.

[195] Gottschalk, P. G. and Dunn, J. R., The five-parameter logistic: A characterization and comparison with the four-parameter logistic. *Analytical Biochemistry* **2005**, 343(1), 54–65.

[196] International Conference on Harmonisation of Technical Requirements for Registration of Pharmaceuticals for Human Use, *Validation of analytical procedures: Text and methodology*. **2005**.

[197] R&D Systems Tools for Cell Biology Research™, *ELISA reference guide & catalog*. **2010**.

[198] Thermo Fisher Scientific Inc., *Tech tip #58: Spike-and-recovery and linearity-of-dilution assessment*. **2007**.

[199] Oh, K. W.; Lee, K.; Ahn, B. and Furlani, E. P., Design of pressure-driven microfluidic networks using electric circuit analogy. *Lab on a Chip* **2012**, 12(3), 515–545.

[200] Hauke, G., *An introduction to fluid mechanics and transport phenomena*, vol. 86 of *Fluid mechanics and its applications*. Springer, New York, **2008**.

[201] Davies, M. J.; Marques, M. P. C. and Radhakrishnan, A. N. P., Microfluidics theory in practice. In *Microfuidics in detection science: Lab-on-a-chip technologies*, 5, Royal Society of Chemistry, Cambridge, **2015**, 29–60.

[202] Wang, K. and Fatoyinbo, H. O., Digital microfluidics. In *Microfuidics in detection science: Lab-on-a-chip technologies*, 1st ed., 5, Royal Society of Chemistry, Cambridge, **2015**, 84–135.

[203] Yang, L.-J.; Yao, T.-J. and Tai, Y.-C., The marching velocity of the capillary meniscus in a microchannel. *Journal of Micromechanics and Microengineering* **2004**, 14(2), 220–225.

[204] Armbrecht, L.; Dincer, C.; Kling, A.; Horak, J.; Kieninger, J. and Urban, G., Signal amplification using magnetic bead chains in microfluidic electrochemical biosensors. *18th International Conference on Solid-State Sensors, Actuators and Microsystems - TRANSDUCERS* **2015**, 1601–1604.

[205] Biomedicals MP, LLC., *Product data sheet of glucose oxidase from Aspergillus Niger*. URL `http://www4.mpbio.com/ecom/docs/proddata.nsf/03d5991c3a7e7f0d8525792e00243e31/ecc46dafecee584f852568da00749533`.

[206] Shaw, J. M.; Gelorme, J. D.; LaBianca, N. C.; Conley, W. E. and Holmes, S. J., Negative photoresists for optical lithography. *IBM Journal of Research and Development* **1997**, 41(1.2), 81–94.

[207] DuPont Electronic Technologies, *General processing guidelines of DuPont™ Pyralux® PC 1000*. **2012**.

[208] Weltin, A., *Multiparametric, flexible microsensors for in vivo application*. Ph.D. thesis, University of Freiburg, **2015**.

[209] DuPont Electronic Technologies, *Technical data sheet of DuPont™ Pyralux® AP*. **2012**.

[210] Kieninger, J., *Electrochemical microsensor system for cell culture monitoring*. Ph.D. thesis, University of Freiburg, **2011**.

[211] Frey, O.; Holtzman, T.; McNamara, R. M.; Theobald, D. E. H.; van der Wal, P. D.; de Rooij, N. F.; Dalley, J. W. and Koudelka-Hep, M., Enzyme-based choline and l-glutamate biosensor electrodes on silicon microprobe arrays. *Biosensors and Bioelectronics* **2010**, 26(2), 477–484.

[212] de Mele, M.; Videla, H. and Arvía, A., The electrooxidation of glucose on platinum electrodes in buffered media. *Bioelectrochemistry and Bioenergetics* **1983**, 10(2-3), 239–249.

[213] Wilde, C. P. and Zhang, M., Oxidation of glucose at electrodeposited platinum electrodes in alkaline solution. *Journal of the Chemical Society* **1993**, 89(2), 241–255.

[214] Ramachandran, S.; Fontanille, P.; Pandey, A. and Larroche, C., Gluconic acid: Properties, applications and microbial production. *Food Technology and Biotechnology* **2006**, 44(2), 185–195.

[215] Dirkx, J. M. H. and van der Baan, H. S., The oxidation of glucose with platinum on carbon as catalyst. *Journal of Catalysis* **1981**, 67(1), 1–13.

[216] Balbuena, P. B. and Gubbins, K. E., Theoretical interpretation of adsorption behavior of simple fluids in slit pores. *Langmuir* **1993**, 9(7), 1801–1814.

[217] Orth, P.; Schnappinger, D.; Hillen, W.; Saenger, W. and Hinrichs, W., Structural basis of gene regulation by the tetracycline inducible Tet repressor-operator system. *Nature Structural Biology* **2000**, 7(3), 215–219.

[218] Kasem, K. K. and Jones, S., Platinum as a reference electrode in electrochemical measurements. *Platinum Metals Review* **2008**, 52(2), 100–106.

[219] Partel, S.; Kasemann, S.; Choleva, P.; Dincer, C.; Kieninger, J. and Urban, G., Novel fabrication process for sub-micron interdigitated electrode arrays for highly

sensitive electrochemical detection. *Sensors and Actuators B: Chemical* **2014**, 205, 193–198.

[220] Partel, S.; Dincer, C.; Kasemann, S.; Kieninger, J.; Edlinger, J. and Urban, G., Lift-off free fabrication approach for periodic structures with tunable nano gaps for interdigitated electrode arrays. *ACS Nano* **2015**, DOI:10.1021/acsnano.5b06405.

[221] Dincer, C.; Ktaich, R.; Laubender, E.; Hees, J.; Kieninger, J.; Nebel, C. E.; Heinze, J. and Urban, G. A., Nanocrystalline boron-doped diamond nanoelectrode arrays for ultrasensitive dopamine detection. *Electrochimica Acta* **2015**, 185, 101–106.

Nomenclature

ν	Average velocity
A	Electrode area
a_{Ox}	Activity coefficients of the oxidized species in mol l^{-1}
a_{Red}	Activity coefficients of the reduced species in mol l^{-1}
C_D	Double layer capacity
E_0	Standard potential of the electrode
F	Faraday constant, F = 96,487 As mol^{-1}
F_c	Fragment crystallisable
F_{ab}	Fragment antigen binding
H_C	Heavy chain
I	Current
J	Flow
j_c	Double layer current density
k_a	Association rate constant in M^{-1} s^{-1}
k_d	Dissociation rate constant in s^{-1}
K_{eq}	Equilibrium constant
L_C	Light chain
Q	Charge
R	Universal gas constant, R = 8.314 J K^{-1} mol^{-1}
R_C	Internal resistance of a potentiostat
T	Kelvin temperature

U	Potential
µFN	Microfluidic network
µPAD	Microfluidic paper-based analytical device
µTAS	Miniaturized total analysis systems
AFP	R-fetoprotein
Ag	Silver
AgCl	Silver chloride
AIDS	Acquired immune deficiency syndrome
ALT	Alanine aminotransferase
AP	Alkaline phosphatase
AST	Aspartate aminotransferase
Au	Gold
BSA	Bovine serum albumin
CA125	Carcinoma antigen 125
CA199	Carcinoma antigen 199
CAP	Chloramphenicol
CCD	Charge coupled device
CCL18	Chemokine (C-C motif) ligand 18
CDR	Complementarity-determining region
CdS	Cadmium sulfide
CE	Counter electrode
CEA	Carcinoembryonic antigen
CMOS	Complementary metal oxide semiconductor
COC	Cyclic olefin copolymer
CR	Current range

CRP	C-reactive protein
cTnI	Cardiac troponin I
CV	Coefficient of variation
DFR	Dry-film photoresist
DI-water	Deionized water
DNA	Deoxyribonucleic acid
EA	Ethanolamine
ECL	Electrochemiluminescence
EDC	N-ethyl-N´-(3-(dimethylamino)propyl)carbodiiimide
EIA	Enzyme immunoassay
EIS	Electrochemical immunosensors
ELISA	Enzyme linked immunosorbent assay
FEM	Finite element method
FIA	Flow injection analysis
FITC	Fluorescein isothiocyanate
GOx	Glucose oxidase
H_2	Hydrogen gas
H_2O_2	Hydrogen peroxide
H_2SO_4	Sulfric acid
HCG	Human chorionic gonadotropin
HCl	Hydrogen chloride
HIV	Human immunodeficiency virus
HPLC	High-performance liquid chromatography
HRP	Horseradish peroxidase
IDA	Interdigitated electrode arrays

Ig	Immunoglobulin
IPTG	ß-D-1-thiogalactopyranoside
IVDs	*In vitro* diagnostics
KCl	Kalium chloride
LB	Luria Bertani
LOC	Lab-on-a-chip
LOD	Limit of detection
LOQ	Limit of quantification
LSPR	Localized surface plasmon resonance
MAI	Multi-analyte immunoassay
MEA	Microelectrode array
MEMS	Micro-electromechanical systems
MES	4-morpholinoethanesulfonic acid
$MgCl_2$	Magnesium chloride
MIA	Micromosaic immunoassay
miRNA	micro RNA
mLSI	Microfluidic large-scale integration
n	Number of electrons
Na_2CO_3	Sodium carbonate
NaCl	Sodium chloride
NHE	Normal hydrogen electrode
NHS	N-hydroxysuccinimide
OCP	Open circuit potential
OD	Optical density
OFL	Ofloxacin

Ox	Oxidized form of the redox couple
PBS	Phosphate buffered saline
PbS	Lead sulfide
PCB	Printed circuit board
PDF	Pressure-driven flow
PDMS	Polydimethylsiloxane
PET	Polyethyene terephtalate
PI	Polyimide
POCT	Point-of-care testing
PSA	Prostate specific antigen
Pt	Platinum
PVD	Physical vapor deposition
QDs	Quantum dots
RE	Reference electrode
Red	Reduced form of the redox couple
RIA	Radioimmunoassay
SBR	Signal-to-background ratio
SCE	Saturated calomel electrode
SD	Standard deviation
SEM	Scaning electron microscope
SHE	Standard hydrogen electrode
SNR	Signal-to-noise ratio
SPR	Surface plasmon resonance
STM	Streptomycin
Ti	Titanium

TIRF	Total internal reflectance fluorescence
UV	Ultraviolet
VLSI	Very-large-scale integration
WE	Working electrode
WHO	World Health Organisation
ZnO	Zinc oxide
ZnS	Zinc sulfide
ß-gal	Beta galactosidase